# ABSTRACT

Title of Document: DEVELOPMENT OF AN ADVANCED HEAT EXCHANGER MODEL FOR STEADY STATE AND FROSTING CONDITIONS

Varun Singh
Doctor of Philosophy, 2009

Directed By: Reinhard Radermacher, Professor
Department of Mechanical Engineering

Air-to-refrigerant fin-and-tube heat exchangers are a key component in the heating, air conditioning and refrigeration industry. Considering their dominance, the industry has focused immensely on employing computer modeling in their design and development. Recently, advances in manufacturing capabilities, heat exchanger technology coupled with the move towards new environment-friendly refrigerants provide unprecedented challenges for designers and opportunities for researchers. In addition, the field of Computational Fluid Dynamics (CFD) has assumed a greater role in the design of heat exchangers.

This research presents the development of an advanced heat exchanger model and design tool which aims to provide greater accuracy, design flexibility and unparalleled capabilities compared to existing heat exchanger models. The heat exchanger model developed here achieves the following.

- Account for tube-to-tube conduction along fins, which is known to degrade the performance of heat exchangers, especially in carbon dioxide gas coolers

- Study and develop heat exchangers with arbitrary fin sheets, which meet performance as well as packaging goals with minimal consumption of resources
- Allow engineers to integrate CFD results for air flow through a heat exchanger, which the modeling tool employs to develop its air propagation sequence leading to improved accuracy over existing models which assume normal air flow propagation
- Function in a quasi-steady state mode for the purpose of simulating frost accumulation and growth on heat exchangers, and completely simulate local heat transfer degradation, as well as blockage of flow passage on air side

Additionally, the heat exchanger model was used to investigate gains that are enabled due to the presence of cut fins in carbon dioxide gas coolers and develop design guidelines for engineers. Finally, this dissertation analyzes the implications of minimum entropy generation on heat exchanger performance criteria of heat capacity and pressure drop, as well as evaluates the ability of entropy generation minimization as a design objective. This also serves as the first step toward an expert knowledge-based system for guiding engineers towards better designs, during the process of heat exchanger design.

# DEVELOPMENT OF AN ADVANCED HEAT EXCHANGER MODEL FOR STEADY STATE AND FROSTING CONDITIONS

By

Varun Singh

Dissertation submitted to the Faculty of the Graduate School of the
University of Maryland, College Park, in partial fulfillment
of the requirements for the degree of
Doctor of Philosophy
2009

Advisory Committee:

Dr. Reinhard Radermacher, Chair
Dr. Jungho Kim
Dr. Tien-Mo Shih
Dr. Bao Yang
Dr. Gary Pertmer (Dean's Representative)

© Copyright by
Varun Singh
2009

# DEDICATION

*To my grandparents.*

*Without their infinite wisdom, no one in my family would have had the opportunity to pursue the best education possible*

ACKNOWLEDGEMENTS

I am deeply indebted to my advisor, Dr. Radermacher, for giving me the opportunity to conduct research at Center for Environmental Energy Engineering (CEEE). I came in as a student interested in obtaining a Ph.D. but through his guidance and advice, today I am a researcher interested in finding solutions to engineering problems. I am also grateful to my dissertation committee members, Dr. Kim, Dr. Shih, Dr. Yang and Dr. Pertmer for their time and effort in making this dissertation more valuable to the engineering and scientific community.

I would like to offer a special note of thanks for Vikrant Aute who taught me the importance of meeting (or beating) deadlines and getting things done "ASAP". I would also like to thank Jon Winkler who was always a nudge away and was a tremendous help throughout my stay at CEEE, especially during the early days when he acted as an interlocutor between Vikrant and me. In addition, I would like to thank Omar Abdelaziz (who I christened "NOmar" for his scientific skepticism) who ensured that I was thorough in my research findings and provided data to test some features of the model developed here. Finally, I would like to thank Paul Kalinowski who was a reliable friend and spotter at the gym, and ensured that the 250+ pound barbell never got close to crushing me.

The models presented in the thesis would not be useful without the substantial experimental data made available for purposes of validation by Dr. Xudong Wang (now at AHRI) and Jan Muehlbauer at CEEE, and Dr. Hyunyoung Kim at Daikin's Environmental Technologies Laboratory. I am indebted to these gentlemen for their

cooperation. In addition, I would like to recognize all CEEE sponsors for their constructive feedback during all stages of this thesis.

I would like to thank my brother for being a source of inspiration. I would like to thank Sonal for being a constant source of support and sanity through some of the most trying periods of my research. Finally, I am grateful to my parents for their patience and encouragement. They have played roles of teachers, friends and above all, parents better than I could have asked for or deserved.

TABLE OF CONTENTS

Nomenclature ..... xv

Chapter 1. Introduction ..... 1

1.1 Air to Refrigerant Heat Exchangers ..... 1
1.1.1 Types of Air-to-refrigerant heat exchangers ..... 1
1.1.2 Application of tube-and-fin heat exchangers ..... 1
1.1.3 Fin Types for Fin-and-Tube Heat Exchangers ..... 4
1.2 Modeling of Heat Exchangers ..... 5
1.3 Literature Review ..... 8
1.3.1 Heat Exchanger Models ..... 8
1.3.2 Effect of Heat Conduction on Heat Exchanger Performance ..... 12
1.3.3 Heat Exchanger Design Optimization ..... 13
1.3.4 Arbitrary Fin Sheet Heat Exchangers ..... 14
1.3.5 Air Flow Maldistribution in Heat Exchangers ..... 15
1.3.6 CFD in Heat Exchangers ..... 16
1.3.7 Models for Frost Accumulation ..... 18
1.3.8 Design of Heat Exchanger using Irreversibility Analysis ..... 21
1.3.9 Summary of Background and Gaps ..... 24
1.4 Research Objectives ..... 26
1.5 Completed Tasks / Thesis Organization ..... 28
1.5.1 Model for Tube-to-Tube Conduction in Fin-and-Tube Heat Exchangers . 28
1.5.2 Modeling of Fin-and-Tube Heat Exchangers with Arbitrary Fin Sheet .... 29
1.5.3 CFD-Based Air Propagation in Fin-and-Tube Heat Exchangers ..... 29
1.5.4 Frost Growth and Accumulation in Fin-and-Tube Heat Exchangers ..... 30
1.5.5 Investigation of Entropy Generation Analysis in Heat Exchanger Design 31

Chapter 2. Modeling of Tube-to-Tube Conduction in Fin-and-Tube Heat Exchangers 32

2.1.1 Modeling Approach ..... 32
2.1.2 Modeling Assumptions ..... 33
2.1.3 Computational Grid ..... 35
2.1.4 Solution Methodology ..... 36
2.1.5 Sub-divided Segment with Heat Conduction ..... 42
2.1.6 Simulation Study ..... 48
2.1.7 Comparison of “thermal resistance model” and “heat conduction model” 52
2.1.8 Evaluation of Neighboring Tube Selection for Inline Coils ..... 55
2.2 Validation against Experimental Data ..... 59
2.2.1 Experiments by Jin et al. ..... 59
2.2.2 Experiments by Zilio et al. ..... 62
2.3 Conclusions ..... 65

Chapter 3. Effect of cut fins on gas cooler performance ..... 67

3.1 Study of Cut Fins ..... 67
3.2 Effect of Configuration ..... 68
3.2.1 Configuration 1 ..... 69
3.2.2 Configuration 2 ..... 73
3.2.3 Comparing configuration 1 and configuration 2 ..... 74
3.3 Effect on fin material savings ..... 75
3.4 Effect on evaporator inlet quality ..... 76
3.5 Effect of Cut Length Constraint ..... 77
3.6 Conclusions ..... 80

Chapter 4. Modeling of Fin-and-Tube Heat Exchangers with Arbitrary Fin Sheet 82

4.1.1 Heat Exchanger with Arbitrary Fin Sheet ..... 82
4.1.2 Modeling Approach ..... 84
4.1.3 Modeling Assumptions ..... 86
4.1.4 Air Side Propagation ..... 87
4.1.5 Simulation Study ..... 90
4.2 Validation against Experimental Data ..... 97
4.2.1 Heat Exchanger Description ..... 98
4.2.2 Transformation for Modeling ..... 100
4.3 Conclusions ..... 102

Chapter 5. Modeling of Fin-and-Tube Heat Exchanger using CFD-based Air Propagation 104

5.1.1 Processing Heat Exchanger Geometry Data ..... 104
5.1.2 Processing CFD Data ..... 108
5.2 Validation ..... 113
5.3 CFD Simulation ..... 117
5.4 Results and Validations ..... 122
5.5 Conclusions ..... 133

Chapter 6. Modeling of Frost Growth and Accumulation in Fin-and-Tube Heat Exchangers 136

6.1.1 Modeling Assumptions ..... 136
6.1.2 Solution Methodology ..... 136
6.2 Validation ..... 141
6.2.1 Validation results ..... 144
6.3 Model Verification and Capabilities ..... 147
6.4 Conclusions ..... 151

Chapter 7. Investigation of Entropy Generation Minimization in Heat Exchanger Design 153

7.1.1 Entropy Generation ..... 153
7.1.2 Effect of Wall-Fluid ΔT on Number of Entropy Generation Units ..... 154
7.1.3 Entropy Generation Units and Heat Exchanger Performance ..... 155
7.2 Optimization Study ..... 160
7.2.1 Hot Water Coil ..... 161
7.2.2 Condenser ..... 163
7.3 Conclusions ..... 166

Chapter 8. Design Guidelines for Engineers ..... 168

Chapter 9. Summary and conclusions ..... 173

9.1 Modeling of Tube-to-Tube Conduction in Fin-and-Tube Heat Exchangers .. 173
9.2 Effect of Fin Cuts on Gas Cooler Performance ..... 174
9.3 Modeling of Fin-and-Tube Heat Exchanger with Arbitrary Fin Sheet ..... 174
9.4 Modeling of Fin-and-Tube Heat Exchanger using CFD-based Air Propagation ..... 175
9.5 Modeling of Frost Growth and Accumulation in Fin-and-Tube Heat Exchangers ..... 176
9.6 Investigation of Entropy Generation Minimization in Heat Exchanger Design ..... 177

Chapter 10. List of major contributions and future work ..... 178

10.1 Major Contributions ..... 178
10.2 List of Publications ..... 179
10.3 Future Work ..... 181

Chapter 11. Appendices ..... 183

11.1 Appendix A: Introduction to Modeling ..... 183
11.1.1 Definition ..... 183
11.1.2 Motivation for modeling ..... 183
11.1.3 Steps in modeling ..... 183
11.2 Appendix B: Genetic Algorithms ..... 185
11.2.1 Representing a solution ..... 186
11.2.2 Assigning fitness to a Solution ..... 187
11.2.3 Reproduction operator ..... 187
11.2.4 Crossover operator ..... 187
11.2.5 Mutation operator ..... 188
11.3 Appendix C: Correlation Applicability Range ..... 189

11.4 Appendix D: Implementation of Alternative Dehumidification Method ..... 193

Chapter 12. REFERENCES ..... 194

# LIST OF TABLES

Table 1.1: Classification of air to refrigerant heat exchangers ..... 1
Table 2.1: Specifications of 2-tube evaporator and correlations used ..... 44
Table 2.2: Specification of two tube water heat exchanger ..... 51
Table 2.3: Specifications of 3bank-9tube water heat exchanger ..... 54
Table 2.4: Specifications of inline water coil and correlations employed ..... 57
Table 2.5: Geometric specifications and correlations used for Jin et al heat exchanger ..... 59
Table 2.6: Test cases for Jin et al experiments ..... 60
Table 2.7: Test conditions for Zilio *et al.* experiment ..... 62
Table 4.1: Overall specification of test heat exchanger ..... 90
Table 4.2: Control volumes separated by discontinuous fins ..... 91
Table 4.3: Control volumes used to model hypothetical heat exchanger (all dimensions in m) ..... 91
Table 4.4: Geometric details of the R410A test condenser ..... 99
Table 4.5: Test conditions for R410A condenser ..... 99
Table 5.1: Heat exchanger specifications and correlations used ..... 116
Table 5.2: Test conditions for the heat exchanger ..... 117
Table 5.3: Source tubes (src) and their % contribution of air mass flow rate for each tube, using 3D-CFD data ..... 128
Table 6.1: Heat exchanger specifications and correlations employed for validation 142
Table 7.1: Problem formulation ..... 160
Table 7.2: Specifications of the hot water coil ..... 161
Table 7.3: Geometry specifications for condenser ..... 163
Table 11.1: Air side correlations applicability range ..... 189
Table 11.2: Two-phase heat transfer correlation applicability range ..... 190
Table 11.3: Two phase pressure drop correlation applicability range ..... 192

# LIST OF FIGURES

Figure 1.1: Sample product range and packaging of fin-and-tube heat exchangers (Courtesy: Carrier Corporation) ..... 2
Figure 1.2: Sample round-tube and wire-fin heat exchangers ..... 3
Figure 1.3: Round-tube and spine-fin heat exchangers, courtesy of the Trane Company ..... 3
Figure 1.4: Commonly used fin types in air-to-refrigerant heat exchangers ..... 5
Figure 1.5: Gaps in research and development of models for air-to-refrigerant fin-and-tube heat exchangers ..... 26
Figure 1.6: Illustration for feature comparison of desired heat exchanger model and existing heat exchanger models ..... 28
Figure 2.1: Dimensions and boundary conditions used in the modeling approach to account for tube-to-tube conduction in fin-and-tube heat exchangers ..... 35
Figure 2.2: (a) Equivalent resistance diagram ignoring fin conduction used by most existing models, (b) actual resistance diagram with tube-to-tube conduction and (c) modified resistance diagram after combining primary and secondary heat transfer areas through fin efficiency ..... 38
Figure 2.3: Solution methodologies for the "thermal resistance model" and the "heat conduction model" ..... 39
Figure 2.4: Unknowns and equations for the “heat conduction model” ..... 41
Figure 2.5: Unknowns and equations for "thermal resistance model" ..... 42
Figure 2.6: Temperatures, lengths and phases involved in the sub dividable segment implementation ..... 43
Figure 2.7: Illustration to show cut fins in the new model’s equivalent resistance diagram ..... 44
Figure 2.8: Verification of sub-divided segment method for the temperature linked equation based model through comparison of superheated and two-phase region lengths for the new model and Jiang et al’s model ..... 45
Figure 2.9: Comparison of sub-divided lengths for Jiang et al's model and the new Singh et al's model ..... 46
Figure 2.10: Comparison of heat capacity predicted by Jiang et al. and the new model of Singh et al. ..... 47
Figure 2.11: Comparison of length of superheated region for Singh et al's model with and without conduction, to verify the effect of tube-to-tube conduction ..... 48
Figure 2.12: Outline of problem used to test effect of air side heat transfer coefficient on temperature distribution on the fin surface ..... 49
Figure 2.13: Temperature distribution on the fin surface. Air heat transfer coefficient increases from $10 Wm^{-2}K^{-1}$ to $10000\ Wm^{-2}K^{-1}$ from top left to top right, and top to bottom. All temperatures are in K ..... 50
Figure 2.14: Dependence of the new model on number of segments ..... 52
Figure 2.15: Schematic of heat exchanger used to compare "thermal resistance model" and "heat conduction model" with simulation time ..... 53
Figure 2.16: Temperature profile of refrigerant in flow direction to show the equivalence of “heat conduction model” and “thermal resistance model” with suitable multipliers ..... 55

Figure 2.17: (a) Inline water coil chosen to study effect of neighboring tube selection, (b) temperature distribution when "heat conduction model" is employed, (c) maximum four neighbors possible for "thermal resistance model" and (d) maximum eight neighbors possible for “thermal resistance model” ..... 56
Figure 2.18: Comparison of water temperature profiles for "heat conduction" and "thermal resistance" models with four and eight neighbors ..... 58
Figure 2.19: (a) Schematic of the gas cooler tested by Jin at al., (b) results of Jiang et al. validation (c) results of the new model validation, comparison of measured tube-bend temperatures against (d) Jiang et al. and the (e) new model, and (e, f) refrigerant temperature profiles compared against measured profiles for two representative cases ..... 61
Figure 2.20: (a) Schematic of the heat exchanger texted by Zilio *et al.*, (b) comparison of measured heat capacities and values predicted by Zilio *et al.* and the new model, comparison of measured and predicted tube bend temperatures by (c) Zilio *et al.* and (d) for the new model. (e) and (f) show the comparison of refrigerant temperature flow profile for two representative cases ..... 64
Figure 3.1: (a) Gas cooler with continuous fins, (b) cuts made in configuration 1 and (c) cuts made in configuration 2 ..... 68
Figure 3.2: Gain in heat capacity, over baseline, for Configuration 1 for (a) 38 $gs^{-1}$ and (b) 76 $gs^{-1}$ ..... 70
Figure 3.3: Two cases compared to understand diminishing gain after 12 cuts for cuts 1-18 ..... 71
Figure 3.4: (a) Comparison of temperature profile for case 1 and case 12 and (b) zoomed into the last 20% of the circuit to highlight the difference; (c) comparison of temperature profile for case 12 and case 18 and (d) zoomed into the last 20% of the circuit to highlight the difference, and (e) heat gained by refrigerant, air and segment (due to conduction) in the last heat exchanger segment ..... 73
Figure 3.5: Gain in heat capacity, over baseline, for Configuration 2 for (a) 38 $gs^{-1}$ and (b) 76 $gs^{-1}$ ..... 74
Figure 3.6: Comparison of configuration 1 and configuration 2 for refrigerant flow rates of (a) 38 $gs^{-1}$ and (b) 76 $gs^{-1}$ ..... 75
Figure 3.7: The % reduction in fin material used for refrigerant flow rate of (a) 38 $gs^{-1}$ and (b) 76 $gs^{-1}$ ..... 75
Figure 3.8: Gain in evaporator inlet quality at 7.2 °C evaporating temperature for refrigerant mass flow rates of (a) 38 $gs^{-1}$ and (b) 76 $gs^{-1}$ ..... 76
Figure 3.9: Fin cut locations determined by the MOGA for (a) 25%, (b) 50% and (c) 75% cut length constraint; modified fin cuts based on feasibility of implementation for (d) 25%, (e) 50% and (f) 75% cut length constraint. ..... 78
Figure 3.10: Normalized heat capacity of the baseline continuous case, 3 MOGA results and 3 MOGA-modified cases ..... 79
Figure 3.11: Heat gained by the refrigerant in each tube before and after fin cuts were placed for (a) 25%, (b) 50% and (c) 75% cut length constraint ..... 80
Figure 4.1: (a) Standard staggered configuration for a fin-and-tube heat exchanger and (b) arbitrary fin sheet for fin-and-tube heat exchanger ..... 82
Figure 4.2 Information obtained by processing Cartesian grids using heat exchanger specifications..... 86

Figure 4.3: Methodology for obtaining weights for mixing of air stream ..... 88
Figure 4.4: Schematic to explain air propagation through heat exchanger..... 89
Figure 4.5: Air mass flow rate initialization for test case ..... 92
Figure 4.6: Water and wall temperature in water flow direction (a) and difference in water and wall temperature averaged for each tube (b) ..... 94
Figure 4.7: Temperature distribution on arbitrary fin sheet and corresponding wall temperatures ..... 96
Figure 4.8: Air temperature distribution at the exit of test coil ..... 97
Figure 4.9: R410A condenser used to validate arbitrary fin sheet heat exchanger model..... 98
Figure 4.10: (a) Actual R410A condenser and (b) transformation of the original geometry for modeling..... 100
Figure 4.11: Air velocity distribution on R410A condenser coil face ..... 101
Figure 4.12: Validation results for R410A condenser ..... 101
Figure 5.1: Sample A-Coil ..... 105
Figure 5.2: Methodology for processing heat exchanger geometry data..... 107
Figure 5.3: Definitions for heat exchanger grid parameters ..... 108
Figure 5.4: Clustering of points in an unstructured CFD mesh can lead often lead to inaccurate interpolated variables..... 110
Figure 5.5: Shortcomings of lack of directional information in inverse distance averaging..... 111
Figure 5.6: CFD data processing methodologies for (a) 2D-CFD data and (b) 3D-CFD data ..... 113
Figure 5.7: A-shaped coil tested by Wang *et al.* (2009) ..... 114
Figure 5.8: Circuitry of the heat exchanger tested..... 115
Figure 5.9: (a) Problem description, (b) 2D computational domain and (c) 3D computational domain..... 120
Figure 5.10: 2D computational domain with a magnified view showing the finer grid resolution near the wall to capture high gradients in flow variables ..... 121
Figure 5.11: (a) 2D-CFD mesh used to simulate the air flow over the heat exchanger. (b) Velocity vectors in the computational domain, and (c) shows the comparison of interpolated u (x-component) of the velocity on the coil face ..... 122
Figure 5.12: CFD mesh (a) at the centerplane, or the mid-plane between two fins, and the velocity vectors (b) at the centerplane, and (c) shows the comparison of interpolated u velocities at the center inlet plane with the 3D-CFD results. Figures (d) thourgh (f) show the same quantities 6.9e-3 mm from the wall ..... 124
Figure 5.13: Comparison of 3D-CFD velocities at the centerline at (a) the plane of entry , planes after (b) 1st and (c) 2nd banks, and (d)the plane of exit, and u-velocity profiles (e-h) at 6.9μm from the fin at the same planes as (a) through (d) ..... 125
Figure 5.14: Total air mass flow rate (a) into the heat exchanger and (b) out of the heat exchanger ..... 126
Figure 5.15: Air velocity vectors for tube 19, with arrows showing control volumes contributing air flow to tube 19 ..... 129
Figure 5.16: Air velocity vectors for tube 1, with arrows showing control volumes contributing air flow to tube 1 ..... 130

Figure 5.17: Air velocity vectors for tube 37, with arrows showing control volumes contributing air flow to tube 37 including entrainment of exit flow..... 130
Figure 5.18: (a) Comparison of predicted heat laod with measured heat capacity and (b) refrigerant mass flow rate distribution through the three circuits ..... 132
Figure 5.19: (a) Coil circuitry of the left bank , (b) the 3D-CFD velocity vectors (ms-1) at the center line, and (c) the % heat capacity contribution of each tube to the total heat exchanger heat capacity ..... 133
Figure 6.1: Equivalent resistance diagram for frosting conditions (a), and simplified diagram (b) after ignoring frost layer, indicated by blue lines in (a), present on fins ..... 137
Figure 6.2: Unknowns and equations associated with the frost growth model ..... 138
Figure 6.3: Solution methodology for heat exchanger frost growth model..... 139
Figure 6.4: End view of the R-22 evaporator used to validate frost growth model.. 141
Figure 6.5: Polynomial curve fit of the inlet air flow rate of 210 cfm used for the simulation..... 143
Figure 6.6: Linear curve fit of air flow rate of 240 cfm used for the simulation..... 143
Figure 6.7: Effect of time step on frost density prediction on Tube 28 illustrates time step independence ..... 144
Figure 6.8: (a) Comparison of simulated and measured sensible and latent heat capacity, (b) comparison of simulation and experimental outlet superheat, (c) comparison of outlet air temperature at the top of the coil and (d) the bottom of the coil..... 144
Figure 6.9: (a) Comparison of simulated and measured sensible and latent heat capacity, (b) comparison of simulation and experimental outlet superheat, (c) comparison of outlet air temperature at the top of the coil and (d) the bottom of the coil..... 145
Figure 6.10: Plots showing growth of frost layer through tubes (a) 1 to 4, (b) 5 to 8, (c) 9 to 12, (d) 13 to 16, (e) 17 to 20, (f) 21 to 24 and (g) 25 to 28. ..... 148
Figure 6.11: % blockage of free flow area for all tubes at the end of the frost period ..... 149
Figure 6.12: Plots showing time response of tube wall (W) and frost surface (F) temperatures through tubes (a) 1 to 4, (b) 5 to 8, (c) 9 to 12, (d) 13 to 16, (e) 17 to 20, (f) 21 to 24 and (g) 25 to 28. ..... 150
Figure 6.13: Plots showing time response of frost density through tubes (a) 1 to 4, (b) 5 to 8, (c) 9 to 12, (d) 13 to 16, (e) 17 to 20, (f) 21 to 24 and (g) 25 to 28. ..... 151
Figure 7.1: Schematic of entropy generation and optimum point of operation. ..... 154
Figure 7.2: Condenser/Evaporator coil used in entropy study..... 155
Figure 7.3: Water coil used in entropy study..... 156
Figure 7.4: Effect of varying tube length for R134a condenser on entropy generation, heat capacity and refrigerant pressure drop ..... 157
Figure 7.5: Effect of varying tube length for R134a evaporator on entropy generation, heat capacity and refrigerant pressure drop ..... 157
Figure 7.6: Effect of varying tube length for a chilled water coil on entropy generation, heat capacity and refrigerant pressure drop ..... 157
Figure 7.7: Effect of varying tube length for hot water coil on entropy generation, heat capacity and refrigerant pressure drop ..... 158

Figure 7.8: Effect of varying fin density for R134a condenser on entropy generation a, heat capacity and air pressure drop ..... 158
Figure 7.9: Effect of varying fin density for R134a evaporator on entropy generation a, heat capacity and air pressure drop ..... 159
Figure 7.10: Effect of varying fin density for a chilled water coil on entropy generation a, heat capacity and air pressure drop ..... 159
Figure 7.11: Effect of varying fin density for hot water coil on entropy generation a, heat capacity and air pressure drop ..... 159
Figure 7.12: Optimization results for (a) Problem A and (b) for Problem B..... 162
Figure 7.13: Comparison of unique points in solution spaces of problems A and B, in terms of heat load per unit pressure drop ..... 163
Figure 7.14: Comparison of solution spaces of problem A and problem B for R134a condenser ..... 164
Figure 7.15: Points chosen to study the cause of divergence of results between problem A and problem B for condenser..... 165
Figure 7.16: Entropy generation profile for two design points from problem A and problem B for R134a condenser ..... 166
Figure 8.1: Comparison of air flow maldistribution as predicted using 2D-CFD and 3D-CFD..... 170
Figure 8.2: Comparison of refrigerant mass flow rate predicted by the heat exchanger model, when 2D-CFD and 3D-CFD were used for air flow simulation..... 171
Figure 11.1: Steps involved in modeling ..... 184
Figure 11.2: Optimization problem for design optimization of a fin and tube heat exchanger ..... 186
Figure 11.3: Concatenated bit strings which represent one complete design ..... 186
Figure 11.4: Crossover and mutation operations in GAs..... 188
Figure 11.5: Working principle of a genetic algorithm ..... 188
Figure 11.6: (a) Existing dehumidification method based on enthalpy potential method and (b) alternative dehumidification method based on Domanski's (1999) formulation..... 193

NOMENCLATURE

| | |
|---|---|
| A | Area,$m^2$ |
| c | Specific heat, $Jkg^{-1}K^{-1}$ |
| d | Diameter, mm, in, m |
| D | diffusion coefficient of water vapor in air, $m^2/s$ |
| dS | rate of specific entropy generation, W/mKkg |
| g | acceleration due to gravity, $m/s^2$ |
| h | Specific enthalpy, J kg-1, Height of A-Coil heat exchanger, m |
| k | Thermal conductivity, $Wm^{-1}K^{-1}$ |
| L | Length of segment, Length of region, Length of A-Coil heat exchanger ,m |
| $\dot{m}$ | Mass flow rate, $kghr^{-1}$, $gsec^{-1}$ |
| N | number of units |
| nFin | Number of fins per segment length |
| nMax | maximum number of neighboring tubes |
| NTU | Number of transfer units |
| $\dot{Q}$ | Heat transfer rate, W |
| R,r | prescribed distance, m |
| T | Temperature, °C, K |
| th | Fin thickness, mm |
| U | Heat transfer coefficient , $Wm^{-2}K^{-1}$ |
| U | Overall heat transfer coefficienct, $Wm^{-2}K^{-1}$ |
| u,v | x- and y-velocity |

| | |
|---|---|
| W | width of A-coil heat exchanger, m |
| xCFD,yCFD | x,y locations on CFD mesh |

**Subscripts**

| | |
|---|---|
| A | Air |
| *d* | Diffusion |
| *F* | Fin, Frost |
| *i* | Inner, Inlet |
| *o* | Outer, Outlet |
| *p* | Constant pressure, Primary |
| *r, ref* | Refrigerant |
| *s* | Entropy generation |
| *W* | Wall |
| $\Delta T_{1,r(a)}$ | $T_{r(a),i} - T_{w,i(o)}$ |
| $\Delta T_{2,r(a)}$ | $Tr_{(a),o} - T_{w,i(o)}$ |

**Greek Symbols**

| | |
|---|---|
| $\mu$ | dynamic viscosity, $Ns/m^2$ |
| $\delta$ | thickness, m |
| $\varepsilon$ | effectiveness, frost porosity |
| $\eta$ | Fin efficiency |
| $\rho$ | Density, $kgm^{-3}$ |
| $\tau$ | Sheer stress, $N/m^2$ |

**Abbreviations**

| | |
|---|---|
| 2D | two dimensional |
| 3D | three dimensional |
| CFD | Computational fluid dynamics |
| DES | Detached eddy simulation |
| DP | Drop in pressure |
| FPI | Fins per inch |
| HTC | Heat transfer coefficient |
| HX | Heat Exchanger |
| LES | Large eddy simulation |
| MFR | mass flow rate |
| MOGA | Multi objective genetic algorithm |
| RANS | Reynolds averaged navier stokes |
| RNG | Re-normalization group |
| RSM | Reynolds stress model |
| SRC | Source tube control volume |
| SST | Shear stress transport |

# CHAPTER 1. INTRODUCTION

## 1.1 Air to Refrigerant Heat Exchangers

Air-to-refrigerant heat exchangers are an integral part of all refrigeration, air conditioning and heat pumping equipment. This section discusses their basic classifications, basis for classification and applications.

### 1.1.1 Types of Air-to-refrigerant heat exchangers

The two common types of air to refrigerant heat exchangers are fin and tube heat exchangers and microchannel heat exchangers. While the basis of classification of heat exchangers is subjective and dependent on several parameters, namely type of fluid, operating conditions; the classification of air-to-refrigerant heat exchangers into the two categories is based on hydraulic diameter (Kandlikar and Grande, 2002), as shown in Table 1.1.

**Table 1.1: Classification of air to refrigerant heat exchangers**

| Channel Type | Hydraulic Diameter |
|---|---|
| Conventional | $D_h > 3mm$ |
| Minichannels | $D_h$ between 3mm and 200µm |
| Microchannels | $D_h$ between 200µm and 10µm |
| Transitional Channels | $D_h$ between 10µm and 0.1µm |
| Nanochannels | $D_h < 0.1$ µm |

### 1.1.2 Application of tube-and-fin heat exchangers

Fin-and-tube heat exchangers are amongst the most common type of air-to-refrigerant heat exchangers used by the industry. They are preferred because of their superior performance, ease of manufacturing and proven reliability. In fact, even with the recent advances in so-called microchannel heat exchangers, industry trends show

that several heat exchanger manufacturers still prefer the fin-and-tube heat exchangers, albeit with tubes of smaller diameters. They are commonly employed in stationary as well as mobile applications.

Round-tube and plate fin type fin-and-tube heat exchangers are commonly used in condensers, evaporators and sensible fluid coils in all heating, ventilation, air conditioning and refrigeration equipment. They are also used in various different configurations, such A-coils and slanted I coils; as well as in cooling towers and outdoor condensing units. Figure 1.1 shows a sample product range of fin-and-tube heat exchangers, courtesy of Carrier Corporation.

**Figure 1.1: Sample product range and packaging of fin-and-tube heat exchangers (Courtesy: Carrier Corporation)**

Round-tube and wire-fin heat exchangers, shown in Figure 1.2, are used as condensers in domestic refrigerators and freezers. Air side heat transfer in wire-fin coils is characterized by natural convection and they are relatively inexpensive to manufacture.

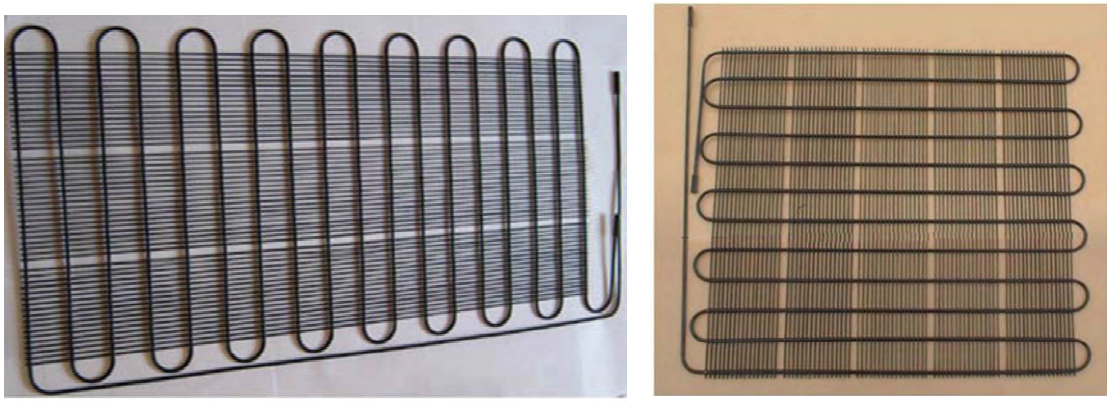

**Figure 1.2: Sample round-tube and wire-fin heat exchangers**

Round-tube and spine-fin heat exchangers, shown in Figure 1.3, are used in outdoor condensing units. They are characterized by high fin efficiency, large fin areas and significant pressure drop.

**Figure 1.3: Round-tube and spine-fin heat exchangers, courtesy of the Trane Company**

It is evident that depending upon the application, they are either employed to condition the air to a desired state (e.g., in evaporators, indoor units, fan coil units) or

use air as a source to condition the refrigerant to a desired state point (condensers, outdoor units). Typically, the resistance to heat transfer is much higher on the air side than the refrigerant side. Therefore, design rules require the area for heat transfer on air side to be enhanced using secondary surfaces, called fins.

### 1.1.3 Fin Types for Fin-and-Tube Heat Exchangers

All air to refrigerant heat exchangers employ several different kinds of fin types, depending on desired objectives and constraints. Some of the criteria determining the fin type are heat transfer characteristics, pressure drop characteristics, condensate retention, heat transfer area desired, volume constraints, manufacturing constraints, fouling constraints, amongst others. Figure 1.4 shows the commonly used fin types.

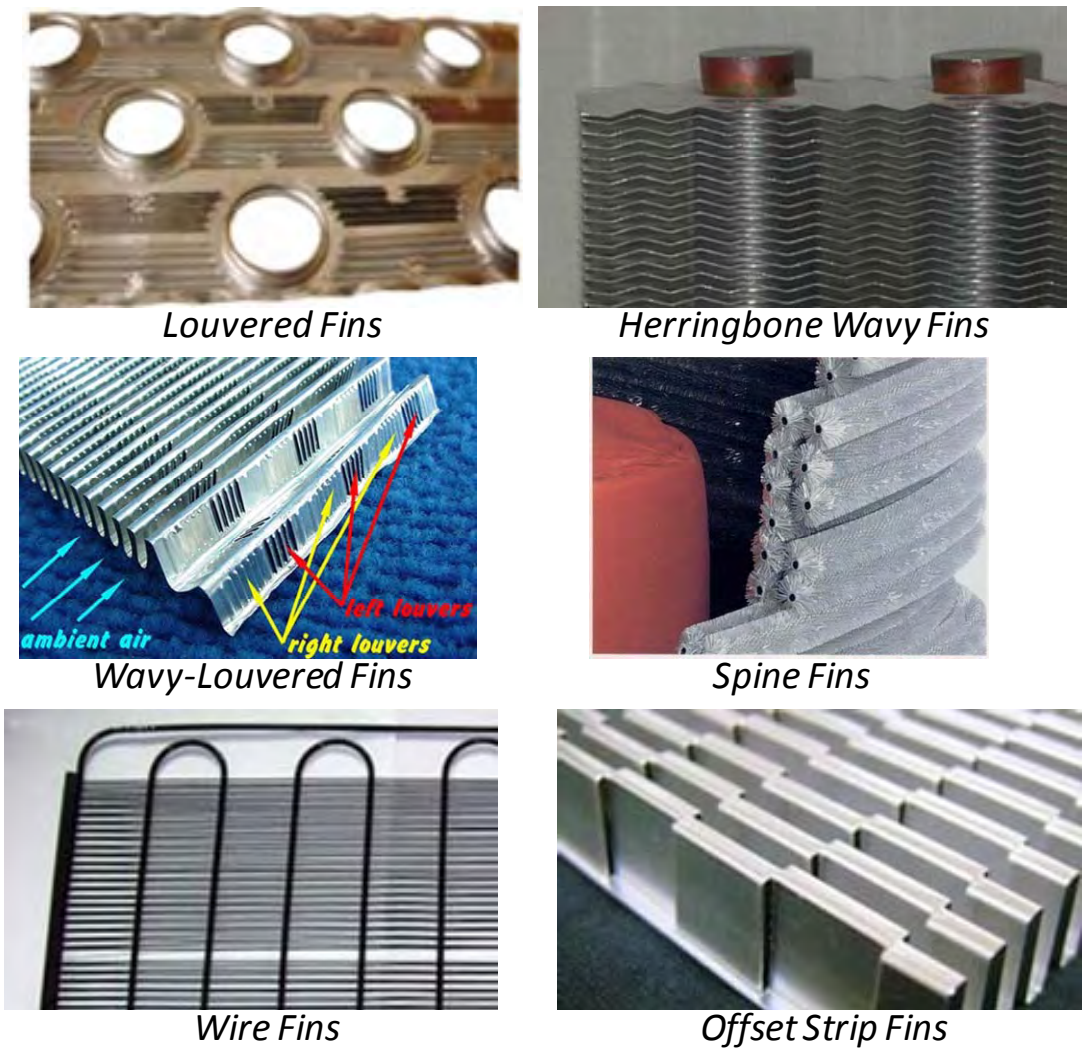


**Figure 1.4: Commonly used fin types in air-to-refrigerant heat exchangers**

## 1.2 Modeling of Heat Exchangers

Computer modeling is now an indispensable cog in the wheel of modern heat exchanger design and development [see Appendix A]. With increased reliance on heat exchanger simulations, development of advanced heat exchanger models is both a challenge and a research opportunity. The importance of modeling and systematic design only grows with increasing cost of raw materials and a need for more efficient products. Development of an advanced heat exchanger model will facilitate engineers

and industry in meeting their objectives of improved performance and reduced consumption of raw materials, while migrating towards newer and environmentally safer refrigerants.

There are several distributed heat exchanger models, both steady state and transient, in literature. The focus of this research is on steady state models and frost growth models for fin-and-tube heat exchangers. Most of the existing heat exchanger models are based on an array of assumptions which are aimed at a) ignoring less important phenomena, b) ignoring capabilities that are not desirable and c) skillfully simplifying complicated phenomena with minimum impact on accuracy, amongst others.

Tube-to-tube conduction across fins in fin-and-tube heat exchangers falls under the first category. Due to temperature gradients between different tubes in a fin-and-tube heat exchanger shown in Figure 1.1, heat conducts across these tubes through fins. At the time of development of most heat exchanger models, this phenomenon was ignored because it was considered less important. The primary reason for this was the fact that most evaporating and condensing applications have close to constant wall temperatures and low fin densities. Resurgence of carbon dioxide as a refrigerant in transcritical cycles where supercritical heat rejection involves a significant drop in refrigerant temperature, which leads to degraded heat exchanger performance due to tube-to-tube conduction, as well as manufacturing of fins with very small fin spacing (~1mm), has ensured that tube-to-tube conduction must be incorporated in modeling of a fin-and-tube heat exchanger. Further, due to the lack of a model capable of simulating tube-to-tube conduction, the potential gains

if tubes could be insulated from each other via cut fins have not been studied and quantified systematically.

Development of a model capable of simulating a heat exchanger with arbitrary fin sheets or varying geometric parameters falls under the second category. Increasing efficiency standards and depleting resources have motivated engineers to explore design variation within a heat exchanger to ensure that the design exploits local variations in refrigerant properties as well as air side characteristics. Such a design is specially motivated by condensers, evaporators and gas coolers where research has shown that local heat transfer coefficient and pressure drop varies significantly through the heat exchanger. In the absence of modern efficiency standards, coupled with sufficient resources and lack of scientific knowledge of regimes of heat transfer and pressure drop during phase change processes, a model capable of geometric variations within a heat exchanger was not desirable. However, in the current scientific environment, such a model assumes great importance in ensuring rapid advancement of heat exchanger technology.

The assumption of normal air flow through the heat exchanger falls under the third category. This phenomenon was ignored by most heat exchanger models because simulating air flow was deemed to be outside the domain of heat exchanger modeling. However, with increasing use of CFD codes and software for simulating complex air flow over a heat exchanger, it is desirable that a heat exchanger model be capable of using the results from CFD simulation of air flow through the heat exchanger.

In terms of transient processes, a frosting evaporator operates unsteadily during the period of frost growth and accumulation on the heat exchanger surface. Existing frost models focus on growth of frost and ignore the accompanying changes in refrigerant state and properties. An advanced heat exchanger model would address frost growth and accompanying changes in refrigerant as well as air side performance in an integrated manner to facilitate the design of better evaporators under frosting conditions.

While there has been comprehensive research in the area of irreversibility or entropy generation analysis for heat exchangers, there is little understanding of what minimum irreversibility implies in terms of generally accepted heat exchanger design objectives of maximum heat capacity and minimum pressure drop. One of the reasons behind this lack of understanding is that researchers working in the area of irreversibility analysis have focused on theoretical quantification of irreversibility. Distributed heat exchanger models can aid in better understanding of irreversibility-based criteria in design of heat exchangers for single phase as well as two-phase flows, and ultimately, determine the usefulness of such criteria for the purpose of heat exchanger design.

## 1.3 Literature Review

### 1.3.1 Heat Exchanger Models

Use of simulations and models for studying heat exchangers traces its history several decades back when scientists and researchers first started developing models for heat transfer. Amongst the earliest simulations of a heat exchanger, Hermann (1962) developed an electronic analog computer flow chart to set up a steam generation process in a heat exchanger, which was a major component in a steam-

power system. The rapid development of electronic computers led the heat transfer community to realize the vast potential of computers in the study of heat transfer. In a prescient paper titled "A Bright Future for Computers in Heat Transfer", Katz and Briggs (1965) outlined areas showing budding use of computers at the time, including development of correlations, solving fundamental equations and optimizing heat exchanger designs. Since then, the field has matured and today, there are several heat exchanger models and tools in the literature used to model both steady state and transient behavior of heat exchangers, which have been validated against experimental results.

Rossi and Braun (1995) presented a heat exchanger model which is part of ACMODEL (Shen*, et al.*,2004) vapor compression cycle simulation tool. This heat exchanger model is based on the Effectiveness-NTU (ε-NTU) (Shah and Mueller, 1985) approach, and used correlations to obtain required coefficients for heat transfer, pressure drop, void fraction etc. Domanski (2003, 1999) presented a public-domain heat exchanger design and simulation tool, EVAP-COND. It is based on the model developed by Lee and Domanski (1997) which followed a tube-by-tube approach for modeling heat transfer. EVAP-COND offers many features like refrigerant maldistribution through circuits of different lengths and one-dimensional air flow maldistribution. Jiang *et al.* (2006) presented a model based on segment-by-segment approach for modeling heat transfer. In this model, each tube is divided into several segments. This allows the user to model two-dimensional air flow maldistribution on coil face. There are many features that both these tools offer (Domanski,1999; Jiang, *et al.*,2006). However, these models ignored the phenomena of heat conduction

through fins in fin-and-tube heat exchangers, which can significantly (10-20% of overall heat capacity) (Zilio*, et al.*, 2007) degrade the heat exchanger performance in some applications. Liu *et al.* (2004) developed a general steady state model for a fin and tube heat exchanger based on graph theory. Their model accounts for refrigerant distribution through a flexible circuitry arrangement and accounts for heat conduction between tubes as well. Their approach is not based on the ε-NTU method. Rather, they apply conservation of energy to a given control volume, starting with guessed outlet states for air and refrigerant as well as guessed wall temperatures. In an iterative process for every control volume of the heat exchanger, wall temperature, outlet refrigerant state, and outlet air state are obtained such that energy is conserved for the control volume. Their tube-by-tube model assumes that a tube can have at most four neighbors, even for staggered configurations. Further, in a given tube, there can be a considerable change in wall temperature, which can only be captured by a model that further divides a tube into several smaller control volumes. Their model also doesn't provide sufficient rationale for such and other assumptions made in their model, and they don't show any results to compare heat exchanger performance between continuous and discontinuous fins. The model proposed here accounts for above-mentioned weaknesses, and also implements an iteration-free energy-conservation approach for a given control volume. Liang *et al.* (2001) studied the effect of refrigerant circuitry on evaporator performance through numerical modeling. They developed a distributed simulation model for predicting the steady state operation of an R-134a evaporator coil. Oliet *et al.* (2002) carried out a numerical simulation of the dehumidification on tube-and-fin heat exchangers and suggested

modeling strategies. They suggest three different strategies, QUICKchess, BASICchess and ADVANCEDchess, all of them were aimed at accurately solving the dehumidification process. ADVANCEDchess model accounts for tube-to-tube heat transfer in calculating temperatures on a discretized two-dimensional fin surface, which is used to accurately obtain heat transfer to air through convection, details of liquid film formation and actual fin efficiencies. These discretized quantities are lumped into macro volumes formed by fin and tube and applied to relevant equations at that level. Lee and Domanski (1997) suggested a model to account for heat conduction through fins. This model is capable of accounting for tube-to-tube conduction in a tube-by-tube heat exchanger model. In this model, the heat transfer to air and refrigerant is calculated using the ε-NTU approach for every tube in the heat exchanger. On the second iteration, using wall temperatures obtained from the first iteration, and first order neighboring tubes around the current tube being calculated, heat transfer due to conduction is obtained as follows:

$$\left(Q_r\right)_j^i = \left(Q_a\right)_j^i + \left(\sum_n \left(Q_f\right)_j^{i-1}\right) \tag{1.1}$$

Where *i* is the current iteration step, *i-1* is the previous iteration step and *j* is the current tube. This approach assumes that the temperature profiles of the two fluids used for developing the ε-NTU formulation relationship is valid, in the presence of conduction through the fin. However, Shah and Sekulic (2003) show that development of ε-NTU relationship assumes all heat from one fluid is exchanged with the other (i.e., no fin conduction). Further, the approach of Lee and Domanski (1997) lacks robustness, particularly around the pinch-off region, as mentioned by Payne and Domanski (2003). All the above mentioned heat exchanger models (with

or without the capability to model tube-to-tube heat conduction through fins) do not have the ability to simulate partially discontinuous fins.

1.3.2 Effect of Heat Conduction on Heat Exchanger Performance

Degradation of heat exchanger performance due to heat conduction has been studied by several researchers. Researchers have studied the degradation of performance of regenerators due to longitudinal conduction ((Bahnke and Howard,1964; McQuiston and Parker,1994; Mondt,1979; Yuan and Kou, 1998) for several decades now. Chiou (1978) presented a study of thermal performance deterioration of cross flow heat exchangers due to two-dimensional longitudinal heat conduction through the heat exchanger walls in the direction of fluid flows. The first patent for fin-and-tube heat exchangers was issued in 1925 (Cox, 1925), though studies of performance degradation due to fin conduction didn't appear till much later. This was probably because initial applications, heat transfer fluids and circuit arrangements weren't expected to show significant performance degradation due to heat conduction between tubes. Heun and Crawford (1994) performed analytical study of the effects of longitudinal fin conduction on multi-pass cross-counter flow single-depth-row heat exchanger. They assumed the fins to have one-dimensional temperature distributions, and solve them using a system of non-dimensional differentials equations. They showed degradation in heat exchanger performance for large ratios of air-side conductance to air heat capacity and small thermal resistance of the fin section. Romero-Mendez *et al.* (1997) developed an analytical model for studying the effect of tube-to-tube conduction through fins for a single row heat exchanger. They identified five dimensionless parameters, and showed the effect of various heat exchanger parameters on heat capacity degradation. They showed

degradation of up to 20% for cases with tube-to-tube conduction. Their analysis showed the importance of distribution of areas in a heat exchanger. Payne and Domanski (2003) showed significant loss of superheat and capacity in an evaporator with continuous fins when compared to a similar heat exchanger with discontinuous fins. Jin *et al.* (2004) tested a carbon dioxide gas cooler for 36 different test conditions, and modeled the heat exchanger using the model developed by Jiang *et al.* (2006). The refrigerant temperature profile through the heat exchanger showed a significant difference between the predicted and experimental results. Zilio *et al.* (2007) showed that carbon dioxide supercritical heat exchangers with discontinuous fins (where fins between tubes are cut to insulate tubes from each other) showed a higher heat capacity than heat exchangers with continuous fins, for same heat exchangers, and refrigerant and air inlet parameters. It must be noted that the fins were louvered in their study, and cutting fins didn't contribute to any additional air side enhancement.

### 1.3.3 Heat Exchanger Design Optimization

In this work, the heat exchanger model is used to systematically study the effect of cut fins on heat exchanger performance. To investigate the optimal location of fin cuts, given a constraint on total fin cut length, the heat exchanger model is coupled with an optimization algorithm. Bennett *et al.* (1994) were amongst the first to apply multi-variable optimization to a heat exchanger design problem. They minimized the cost of a run-around heat exchanger subject to several constraints using gradient based optimization. Litinetski and Abramzon (1998) used an adaptive random search algorithm to optimize a compact heat exchanger. Genetic algorithms [See Appendix C] have been widely used in design optimization of a wide variety of

heat exchangers. Quiepo *et al*. (1994) applied it to optimize a device for electronics cooling. Schmit *et al.* (1996) applied GAs to design a high intensity cooler. Aute *et al.* (2004) applied multi-objective genetic algorithms to optimize the design of a condenser. Ozkol and Komurgoz (2005) employed a genetic algorithm to optimize the geormetry of a heat exchanger core. Peng and Ling (2008) applied genetic algorithms to minimize the volume and operating cost of a plate-fin heat exchanger. Cavazzuti and Corticelli (2008) carried out optimization of enhanced surfaces of heat exchangers for maximum heat transfer and minimum pressure drop using genetic algorithms coupled with a CFD solver. The surfaces were automatically generated and parameterized using Bezier curves. Most recently, Abdelaziz (2009) applied approximation assisted genetic algorithms for design of a novel heat exchanger.

### 1.3.4 Arbitrary Fin Sheet Heat Exchangers

Most physical prototypes of heat exchangers have several uniform parameters within a heat exchanger like tubes per bank (also known as tubes per row), tube pitch (step and row pitch), tube diameter, tube location, rectangular footprint etc. However, there has been a recent development towards moving away from such uniformities in a heat exchanger. These modifications in design are aimed at not only improving the refrigerant side performance, but also reduce the air side resistance, which is usually the dominant thermal resistance to heat transfer in an air to refrigerant heat exchanger. The motivation for these new developments is improved performance due to better circuiting and air flow, compact design and packaging aspects. Such heat exchangers can have variable tube diameters, tube locations, tube pitches, tubes per bank and non-rectangular footprint with internal and external jagged edges. Further, tubes can also be selectively insulated from tube-to-tube conduction through cuts

made in the fin sheet. Researchers have developed heat exchangers with certain non-uniformities to exploit the opportunities offered by these non-uniformities. Fin-and-tube heat exchangers used in freezers often have variable tube diameters and non-uniform fin spacing throughout the heat exchanger. This is done to ensure the heat exchanger doesn't get blocked rapidly due to frost formation, and it reduces the number of defrost cycles required. Researchers have published heat exchanger models that account for variable fin spacing (Jiang*, et al.*,2006, Yang*, et al.*,2006b). Yang *et al.* (2006a) optimized the fin spacing of a frost fin-and-tube evaporator to increase the operational time of the coil between defrost cycles, and to increase the performance of the coil. Other variations, like variable tube diameters and locations, in design of a heat exchanger have also been explored by certain heat exchanger manufacturers (Mitsubishi Electric, 2008).

### 1.3.5 Air Flow Maldistribution in Heat Exchangers

Most heat exchanger models surveyed assume air is flowing perpendicular to the tube banks throughout the coil. Chwalowski *et al.* (1989) studied the suitability of the simplified perpendicular air flow assumption for evaporator computer models. They conducted smoke tests through heat exchangers to observe stream lines within the heat exchanger, for V-coils (Chwalowski's preferred term for A-coils) and I shaped coil (single slab of an A-coil). The V coils and the I-coils were tested for different inclination angles, and the experiments showed that overall capacity was dependent on the coil position. Chwalowski *et al.* concluded that if one section of the heat exchanger is starving, and the other flooding, it will degrade the capacity of the heat exchanger. Fagan (1980) showed that maldistribution exceeding 50% of the average coil face velocity can degrade the capacity of a heat exchanger by as much as

20%. Chwalowski *et al.* suggested employing a non-uniform air velocity profile on the face of the coil, as a better option than assuming uniform air velocity profile. Heat exchanger model of Domanski (1999) is capable to taking a one-dimensional air velocity profile on the coil face, where as the model of Jiang *et al.* (2006) can take a two dimensional air velocity profile on the face of the coil. Both the models have been validated for A-shaped coils, with suitable correction factors. While the ability to use non-uniform air velocity profiles is a step forward, it still can not account for the complex paths through which air flows inside the coil. Domanski and Yashar (2007) carried out a systematic circuitry optimization of an A-coil using Domanski's heat exchanger model, assuming perpendicular air propagation through the coil. While this represents a significant contribution in terms of circuitry optimization, the uncertainty associated with the simplified air flow assumption can potentially undermine real-world applicability of their results.

### 1.3.6 CFD in Heat Exchangers

As mentioned earlier, the rise of computing power has led to a surge in CFD studies of heat exchangers. While CFD is widely used to study heat exchangers in entirety, as well as studies of individual fluid streams; it is important review the application of CFD to studies of air side performance of heat exchangers. Sunden (2007) reviewed the use of CFD in research and design of heat exchangers. The author concluded that CFD is most commonly used in visualizing complex flow patterns in novel heat exchanger geometries. Quite often, justifiable simplifications are applied to reduce the computational burden of conduction CFD studies. These simplifications include ignoring edge effects and utilizing structural symmetry and periodic flow, amongst others.

Given Sunden's (2007) conclusions, it is not surprising that the body of work in using CFD to evaluate heat transfer and pressure drop coefficients is large, and continuous to grow with increasing computing power. Zhang and Dahl (2000) used CFD to evaluate heat transfer and pressure drop characteristics of smooth wavy fin-and-tube heat exchangers. The authors conducted full-3D simulation of heat exchangers including accounting for conduction between tubes, and the results showed good agreement with measured values of j and f factors. Perrotin and Clodic (2003) used CFD to study heat transfer characteristics of louvered fin and tube heat exchangers. There are several such studies in the literature and the above just provide a very short cross section of the literature. Kramer and Eitel (2003) applied full scale CFD and 1D system simulation to design of a high end cooling components for automotive applications. CFD was used to detailed optimization of all thermodynamic characteristics of the heat exchangers and 1-D simulation for the evaluation of such a heat exchanger in its entire cooling environment (i.e. vehicle simulation). This technique was applied to the product development process to increase quality as well as reduce development time. Abdelaziz (2009) conducted a multi-dimensional multi-scale simulation of novel heat exchanger geometries and combined it with an effectiveness-NTU based heat exchanger model to evaluate heat exchanger performance. The focus of CFD in this work was on evaluation of heat transfer and pressure drop performance of heat exchangers. In the literature reviewed, there were no studies of CFD to evaluate air propagation paths in a heat exchanger, followed by the use of the obtained propagation sequence in a control-volume based heat exchanger model.

### 1.3.7 Models for Frost Accumulation

Frost formation on cold surfaces has been of great interest to the refrigeration and heat pump engineering community. Formation of frost on a heat exchanger surface results in:

a) Reduction on heat transfer rate due to fouling characteristics of frost development

b) Blockage of air flow passages through the heat exchanger

c) Degradation in capacity of the equipment which is typically rated at dry condition

These considerations often dictate the design of equipment which is designed to operate, at some point in its life cycle, under frosting conditions. Frost growth and accumulation often governs the size of equipment, the control of energy-intensive defrosting cycles, removal of large amounts of condensate in a short period of time, etc.

Growth of frost on heat transfer surfaces has been widely studied by physicists and engineers alike. Literature on frost growth and accumulation can be broadly categorized into three categories:

a) Investigation of frost incipience and frost crystal morphology

b) Study of frost properties, like conductivity and density etc., on various surface geometries like flat plates, cylinders etc., for various flow conditions

c) Theoretical and computational analysis of frost growth on performance of heat transfer surfaces

While this research concerns itself primarily with the third category, namely modeling of frost growth on fin-and-tube heat exchangers, it requires an understanding and review of research on fundamental frost properties.

As frost forms on a surface, there are two critical properties that determine its effect on performance of heat transfer equipment, frost density and frost thermal conductivity. Though authors studied ways of mitigating frost before him (Brosky (1926) suggested blowing hot air through a mine shaft to prevent frost formation), Schropp (1935) was amongst the first to study frost formation and its detrimental effects on heat transfer. Besides him, several others proposed correlations between frost density and conductivity and they have been summarized by O'Neal and Tree (1985). There was significant variation in these correlations, and the data showed sizeable scatter. Also, most of the correlations failed to capture the effect of temperature at which frost was formed. Recent work on frost density and conductivity correlation development, reviewed by Irragory *et al.* (2004), takes into account effect of surface and air temperatures, and provides different correlations for different conditions. Their work formed a valuable resource in choosing the correct correlations for frost conductivity for the numerical model proposed in this thesis.

To increase the ability to predict, and therefore, control, the formation of frost, several numerical models have been proposed. Most of the research has been focused on developing frost growth models for different surfaces, like parallel plates. Sami and Duong (1989) proposed an explicit equation for vapor diffusion rate combined with mass and energy balance integral equations to obtain rate of frost growth on parallel plates. Cheng and Cheng (2001) combined an integral approach for the heat

and mass transfer over the frost layer with the equation of average frost density (based on temperature) to obtain the frost growth rate. The primary purpose of this thesis is to develop a frost growth model with application to fin and tube heat exchangers. For discussion on various methods of simulating frost growth on parallel plates, the reader is referred to (Iragorry, *et al.*, 2004)

Seker *et al.* (2004b) proposed a frost accumulation model for fin-and-tube evaporators where they analyzed heat and mass transfer characteristics numerically. The authors assumed constant evaporating temperature, and did not carry out refrigerant side modeling. On the air side, they assumed potentials only with air inlet temperature, and such assumptions can, not only lead to over-prediction of heat capacity but all temperature cross over, thereby violating the second law of thermodynamics. In a follow-up paper containing the validation of the model (Seker, *et al.*,2004a), the authors validated key quantities, like overall UA of the heat exchanger and air side pressure drop. While this is significant, quantities like degradation of overall heat capacity, superheat and outlet temperatures are equally important, especially when a frost evaporator is operating in a vapor compression system.

In a series of publications, Chen *et al.* (Chen, *et al.*,2003, Chen, *et al.*,2000a, Chen, *et al.*,2000b) developed and validated a numerical model to predict degradation of air side heat capacity, as well as degradation in air pressure drop due to blocking of air flow passages. Their model assumed constant air flow rate, and constant heat exchanger surface temperature. This assumption is not valid in most frost evaporators due to the presence of the superheated region where the refrigerant temperature rises

about the saturation temperature. In addition, such a model can not accurately predict the spatial distribution of frost accurately since it depends greatly on refrigerant side conditions.

Yang *et al.* (2006c) developed a model for simulating the performance of a fin-and-tube heat exchanger under frosting conditions. While this model simulated refrigerant side conditions, it treated tube and fin surfaces separately with tube and fin surfaces having different temperatures. In addition, their modeling used inlet air as well as refrigerant temperatures to evaluate heat transfer from the air as well as refrigerant, as opposed to a potential dependent upon inlet and outlet temperatures as well as neighboring tube temperatures, which exert influence through conduction. Typically, the influence of tube-to-tube conduction is negligible, a comprehensive frost model must be capable of accounting for this phenomena. Finally, while their model is developed with the capability to simulate refrigerant side, it was validated using total heat capacity and frost mass accumulated. There was no validation of air or refrigerant outlet conditions.

### 1.3.8 Design of Heat Exchanger using Irreversibility Analysis

A heat exchanger is usually characterized by two types of thermodynamic losses. First of these two losses is associated with the heat transfer across a finite temperature difference. The second loss is due to pressure drop in a heat exchanger. The irreversibility loss associated with heat transfer across a finite temperature difference can be mitigated by increasing the heat transfer flow area and reducing the local temperature difference through enhancements. However, increasing the flow area can lead to greater overall frictional loss and higher pressure drop, and the irreversibility loss due to pressure drop increases. This shows that these two losses are

mutually conflicting. Also, this points to the existence of an "optimum" heat exchanger design where these two losses are minimized. Ideally, a heat exchanger should be designed to work in the neighborhood of this optimum.

Ever since Clausius (1851) proposed the concept of irreversibility, there has been abundant work, though mostly analytical in nature, in the area of irreversibility analysis and its application to designing heat exchangers. This has led to several concepts for quantifying irreversibility. Entropy generation minimization was first proposed by McClintock (1951) who developed equations for optimum design of fluid passages for a heat exchanger based on minimum entropy production. Since then, a lot of research has been carried out in the area of thermodynamic optimization using irreversibility analysis. Bejan (Bejan, 1977; Bejan, 1978) examined the coupling losses due to heat transfer across a finite temperature difference and frictional pressure drop. He proposed the use of number of entropy generation units, $N_S$ as a basic parameter in describing heat exchanger performance. Poulikakos and Bejan (1982) established the theoretical framework for the minimization of entropy generation for extended surfaces (fins). The authors developed an entropy generation rate formula for a general fin, and then applied the analytical methods and graphical results developed as a result, for selecting optimum dimensions of fins. Aceves-Saborio *et al.* (1989)extended this method to incorporate the irreversibility associated with material of construction. Entropy generation minimization has been to optimizing a cross flow heat exchangers as well (Ogulata*, et al.*, 2000; Ogulata and Doba,1998). However, they didn't study heat transfer, pressure drop and cost of material used in the optimum heat exchangers. Witte and Shamsundar (1983)

proposed a thermodynamic efficiency concept for heat exchange devices. The efficiency was written in terms of mean absolute temperatures of the two fluids and the appropriate environment temperature. The authors applied the concept to typical heat exchange cases to demonstrate its usefulness.

Several authors (Auracher,1984; Cornelissen and Hirs,1999; Cornelissen and Hirs,1997) have outlined the theory of framing heat transfer and pressure drop losses in a heat exchanger, in the form of exergy. This requires assumption of a reference temperature, which Auracher recognizes as a weakness because of its arbitrary nature. The concept of exergy minimization has also been extended to include the lifecycle of heat exchangers as well as other thermal systems (Cornelissen and Hirs, 1999). Sekulic (1986) defined enthalpy exchange irreversibility norm (EEIN) as a measure of internal heat exchanger irreversibilities. Aceves-Saborio *et al.* extended the entropy generation minimization method to account for exergy of the material of construction. Sekulic (Sekulic, 1990) proposed a second law quality of a heat exchange process in heat exchanger analysis. However, the contribution of fluid friction was ignored. DeJong *et al.* (1997) developed an entropy-based method for air side analysis of heat exchangers, but refrigerant side analysis was not considered. Park and Jacobi (2003) compared the performance of flat tube and round tube heat exchangers using a second-law based performance evaluation criteria. All of these studies cited involve an analytical approach to heat exchanger analysis and design. Considering the analytical nature, all of these studies considered applicability of entropy generation minimization to single phase flow, where heat transfer is always sensible, i.e., it is always accompanied by change in temperature of the fluids. In addition, none of the

studies reviewed commented on the usability of entropy generated in a heat exchanger, or heat transfer process, as an optimization objective where real-world constraints like cost and heat capacity dictate heat exchanger design.

### 1.3.9 Summary of Background and Gaps

While modeling of air-to-refrigerant fin-and-tube heat exchangers is a mature field, literature survey suggests there are significant gaps as shown in Figure 1.5, and the emerging need for new capabilities which needs to be addressed. The phenomena of heat conduction between tubes in fin-and-tube heat exchangers can cause significant degradation in heat exchanger performance, and none of the models reviewed account for this phenomena. Further, current heat exchanger models assume repeatable patterns in heat exchanger geometry and design. While this might be an optimum under ideal conditions, in reality refrigerant and air side heat transfer and pressure drop characteristics are not uniform throughout the heat exchanger. Literature survey shows that these characteristics are strongly influenced by local conditions, like local tube diameters, local tube spacing, etc. Current heat exchanger models do not empower researchers to fully explore the opportunities available by varying geometrical parameters locally within a heat exchanger. The advent of computational fluid dynamics provides enormous opportunity for improving heat exchanger design through better quantitative analysis of air flow over the heat exchanger, particularly for heat exchangers with complex air flow patterns like recirculation zones. However, full CFD simulation of an entire heat exchanger is computational expensive, and not conducive to heat exchanger design. This opens up an area of immense opportunity where CFD simulations can complement heat exchanger models through a hybridized approach, where CFD results are adapted for

heat exchanger models to improve their accuracy, without any additional computational cost, with the exception of a single CFD run and pre-processing of CFD results. Current heat exchanger models do not utilize CFD and this greatly hinders their accuracy, as well as potential. Modeling of frost growth and accumulation on heat exchangers has received relatively less attention than steady-state modeling. Most frost development models for fin-and-tube heat exchangers assume constant wall temperatures, and ignore the refrigerant side modeling. The models that incorporate refrigerant side do so in a simplified manner. Further, none of the models present validations of refrigerant side results, which are of tremendous importance for the system-level performance of the heat exchanger. There is a clear need for a heat exchanger model that not only addresses the abovementioned weaknesses, but also provides the necessary tools to heat exchanger designers to fully explore all possible design improvements.

Another area of vast research has been irreversibility analysis of heat exchangers. While, minimization of irreversibility analysis is often touted as a thermodynamic objective when it comes to designing heat exchangers, most of the rationale behind this is based on theoretical calculations. While such research enhances fundamental understanding of heat exchanger thermodynamics, it is imperative to understand its importance and applicability to heat exchangers, especially relative to well-established performance measures like maximization of heat capacity and minimization of pressure drop.

| Authors (Year) | Steady State | Refrigerant modeled | Equations | Correlation Based | Fin Conduction | Airside CFD Integration | Arbitrary Fin Sheet | Frost Model | Irreversibility Analysis |
|---|---|---|---|---|---|---|---|---|---|
| Rossi et al. (1995) | ✓ | ✓ | e-NTU | ✓ | | | | | |
| Domanski (1999) | ✓ | ✓ | e-NTU | ✓ | Not robust | | Plugged tubes | | |
| Liang et al. (2001) | ✓ | ✓ | e-NTU | ✓ | | | | | |
| Oliet et al. (2002) | ✓ | ✓ | UA-LMTD | ✓ | Only for fin efficiency | | | | |
| Liu et al. (2004) | ✓ | ✓ | UA-LMTD | ✓ | No results shown | | | | |
| Jiang et al. (2006) | ✓ | ✓ | e-NTU | ✓ | | At coil entrance | Plugged tubes, fin spacing | | |
| Chen et al. (2003) | | | UA-$T_{in}$ | ✓ | | | | ✓ | |
| Seker et al. (2004) | | | UA-$T_{mean}$ | ✓ | | | | ✓ | |
| Yang et al. (2006) | | | UA-$T_{in}$ | ✓ | | | Fin spacing | ✓ | |

**Figure 1.5: Gaps in research and development of models for air-to-refrigerant fin-and-tube heat exchangers**

With these gaps, and a greater need than ever before for efficient heat exchangers that perform better and consume less resources, it is highly desirable for the research community to further advance development of heat exchanger models that are robust, accurate, computationally inexpensive, and complement peripheral advancements to ensure continued improvements in heat exchanger technology.

## 1.4 Research Objectives

This dissertation concerns itself with steady state and transient modeling of fin-and-tube air-to-refrigerant heat exchangers. The emphasis of the thesis is two-pronged: the introduction of new flexibility to heat exchanger simulation and design, and the investigation and integration of a nascent expert system that guides the designer to better solutions. Both involve the development of an advanced heat exchanger simulation tool with the following capabilities:

- Tube-to-tube heat conduction across fins. This model is used to develop understanding of effect of fin cuts on enhancing carbon dioxide gas cooler performance
- User-defined tube diameters and locations, number of tubes per bank, location of fin cuts (discontinuous fins) within heat exchanger, fin density through-out the heat exchanger, non-rectangular fin sheet
- Ability to adapt air flow distribution from CFD results for heat exchanger simulations in order to account for air mal-distribution inside the coil
- Model for frost accumulation and growth

Secondly, it investigates entropy generation analysis for design of fin-and-tube heat exchangers with a focus on the following:

- Ability to find optimum size of a given parameter for minimum irreversibility losses
- Ability of entropy generation to replace conventional heat exchanger design objective like heat capacity, and associated merits and demerits

The goals of the thesis are summed up in Figure 1.6.

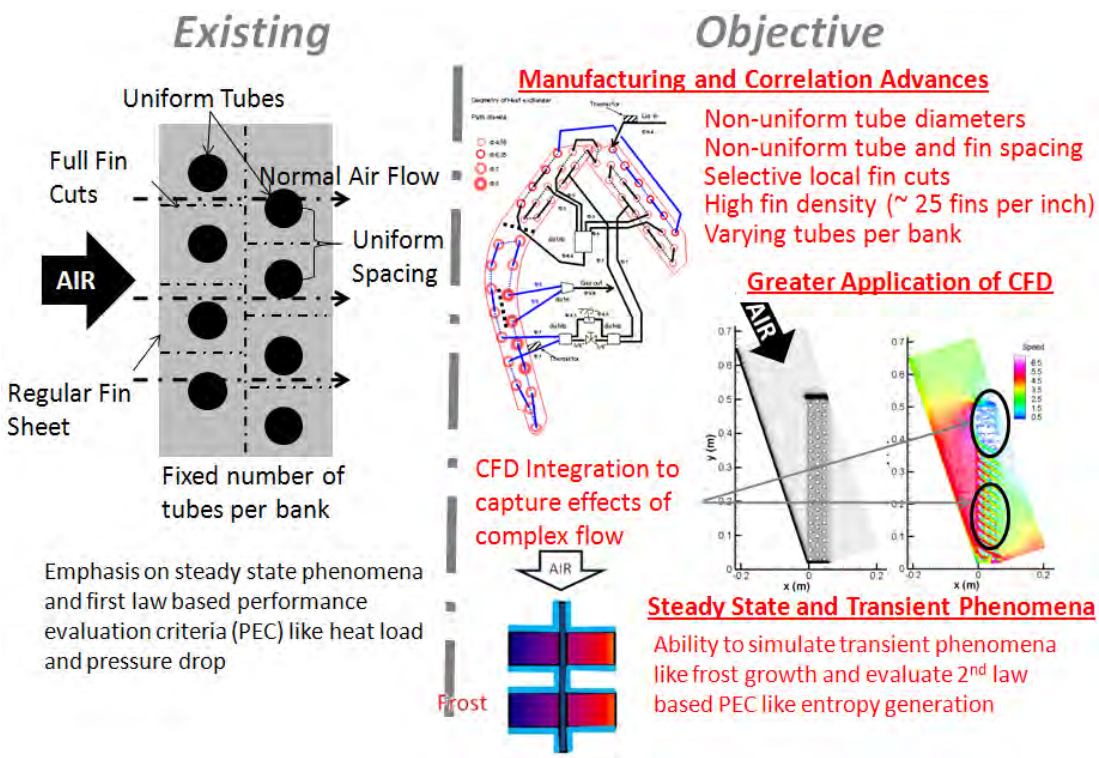


**Figure 1.6: Illustration for feature comparison of desired heat exchanger model and existing heat exchanger models**

## 1.5 Completed Tasks / Thesis Organization

Given the outline of research, this thesis is split into smaller research sections which result in the advanced heat exchanger model.

### 1.5.1 Model for Tube-to-Tube Conduction in Fin-and-Tube Heat Exchangers

There are several models for simulating steady state operation of fin-and-tube heat exchangers in literature. However, most of them ignore tube-to-tube conduction through fins. The models that incorporate tube-to-tube conduction do not address the phenomena fundamentally, through wall-temperature linked equations. Instead, the existing models adapt existing formulations to account for fin conduction, which can lead to unstable solution procedures (Lee and Domanski, 1997), as described in Section 1.3.1.

Chapter 2 describes the newly developed model based on wall-temperature linked equations to simulate the steady state operation of a fin-and-tube air to refrigerant heat exchanger, which accounts for conduction between tubes through fins. Chapter 3 discusses the results of the investigation into the effects of cut fins on performance of carbon dioxide gas coolers.

### 1.5.2 Modeling of Fin-and-Tube Heat Exchangers with Arbitrary Fin Sheet

Most existing fin-and-tube heat exchangers have uniform geometric parameters as well as configurations. However, there has been a recent move towards varying geometric parameters within a heat exchanger, like tube diameters, tube pitches, tube locations, etc. This is aimed at ensuring that the heat exchanger meets optimum performance as well as packaging objectives. Currently, there are no heat exchanger models in literature that are capable of simulating such heat exchangers.

Chapter 4 describes the new heat exchanger model capable of simulating a heat exchanger with varying geometric configurations, namely tube diameters, tubes per bank, non-rectangular footprint, internal jagged edges as well as variable fin cut locations, is developed.

### 1.5.3 CFD-Based Air Propagation in Fin-and-Tube Heat Exchangers

All heat exchanger models reviewed here assume air flow to be perpendicular to the tube banks of a fin-and-tube heat exchanger, and assume air flow to be unidirectional, from one bank to the next. Some heat exchanger models account for maldistribution of air flow on the face of the heat exchanger. However, these models assume air flow profile to propagate as is, through the heat exchanger. These assumptions might hold true if the general direction of flow of air is perpendicular to the heat exchanger core. However, one of the most commonly used configurations of

fin-and-tube heat exchangers in the air conditioning and heat pump systems, has one or two fin-and-tube heat exchanger cores arranged such that main air flow is not perpendicular to the heat exchanger slab(s). This leads to fairly complex air flow through the heat exchanger where air propagates across banks and tubes within the same bank. Also, CFD results show pockets of recirculation within the heat exchanger, and outflow gets entrained into these zones of recirculation, re-entering the heat exchanger through the exit face (Domanski and Yashar, 2007; Abdelaziz*, et al.*,2008).

Chapter 5 describes the new heat exchanger model with CFD-based air propagation is developed. This model combines the strengths of CFD simulation and distributed heat exchanger model, to increase the accuracy of heat exchanger models in terms of overall as well as tube wise results.

### 1.5.4 Frost Growth and Accumulation in Fin-and-Tube Heat Exchangers

While there are several frost growth models in literature, there are only a handful of heat exchanger frost growth models. Heat exchanger frost growth models also have varying degrees of simplifying assumptions ranging from constant wall temperature to separate analysis for tubes and fins. Also, none of the models were validated against refrigerant conditions at the evaporator outlet, which is critical for a heat exchanger which is always operating in a vapor compression system.

Chapter 6 describes a quasi-steady state heat exchanger model developed for simulating frost accumulation and growth. The model is capable of modeling frost growth and accompanying degradation in heat exchanger performance including blocking of flow passages on air side, degradation of refrigerant super heat and degradation of air outlet conditions.

### 1.5.5 Investigation of Entropy Generation Analysis in Heat Exchanger Design

The concept of irreversibility losses and analysis has been studied thoroughly over the past several decades. Most of these studies have been aimed at theoretical quantification of irreversibility losses. Several authors have proposed measures of quantifying irreversibility losses in heat exchangers. However, most of these studies have been confined to single phase fluids. In addition, there has been little research in evaluating irreversibility or entropy generation minimization as a substantive objective for heat exchanger design.

Chapter 7 evaluates entropy generation minimization using a heat exchanger model in terms of existing heat exchanger design objectives of heat capacity and pressure drop. Further, entropy generation minimization is employed as an objective in heat exchanger design, and optimum designs generated are compared against designs obtained by using heat capacity as an objective.

# CHAPTER 2. MODELING OF TUBE-TO-TUBE CONDUCTION IN FIN-AND-TUBE HEAT EXCHANGERS

The model proposed in this thesis is based on the solution methodology implemented by Jiang et al. (2006), for a segmented heat exchanger modeling tool.

## 2.1.1 Modeling Approach

This model was developed to provide the greatest generality and flexibility in designing and simulating air-to-refrigerant heat exchangers. It is based on a detailed numerical model of thermal and fluid flow phenomena integrated with comprehensive working fluid libraries, correlations for heat transfer, pressure drop etc. and optimized numerical libraries. Its graphical interface offers ease of circuitry design, input and output of data, choice of fin types and refrigerants, parametric study and optimization capability. Jiang et al.'s modeling approach is introduced here. The primary focus of this paper is to introduce a model for fin conduction. Therefore, the reader is referred to the original publication for further detail about Jiang et al.'s model.

To allow generalized circuitry, Jiang et al. utilize a junction-tube connectivity matrix. Such a matrix allows for the tracking of refrigerant flow from inlet(s) of the coil to the outlet(s). This allows multiple circuits within a heat exchanger with merging and splitting of circuits. Mass flow rates through different circuits are solved to ensure pressure drop through different sub-circuit lengths, of a given circuit are equal. To account for non-uniform distribution of air flow at coil entrance, as well as varying transport and thermal properties and coefficients, each finned-tube macro volume is divided into segments, which are numbered in direction of refrigerant flow.

Each segment of the heat exchanger is treated as a discrete unit of heat transfer. Air velocities are propagated through successive banks of the heat exchanger, as they

are on the face of the coil. The presence of thermal resistance can be accounted for through a fouling resistance term. However, the model disregards conduction of heat through finned plates between tubes.

For modeling the refrigerant side heat transfer, the ε-NTU method is used for each segment. When the heat transfer surface temperature is below the dew point temperature of air stream, some moisture condenses out and latent heat transfer occurs. For dehumidification calculation, the method based on enthalpy potential proposed by McQuiston and Parker (1994) is used. For modeling air side, mass energy and humidity is conserved as air propagates through heat exchanger segments. Air side pressure drop is calculated using applicable correlations [See Appendix C] depending upon various geometric and flow parameters.

Jiang *et al.* implemented a sub-divided segment approach that allows the heat exchanger to be modeled as a tube-by-tube model (one segment per tube) without significant loss in accuracy of the results. This subdivided segment model establishes, iteratively, the length of different phases if there are one or more phase changes within a segment.

### 2.1.2 Modeling Assumptions

To develop a heat exchanger modeling and design tool capable of accounting for tube-to-tube conduction, two models have been proposed here. Both the models have different assumptions.

The assumptions of the first model are as follows:

1) While obtaining heat conducted from one tube to another, this model ignores the effect of air side heat transfer coefficient. This assumption is shown to be an acceptable simplification.

2) The model assumes that a given tube interacts only with its immediate neighbors as far as conduction is concerned. To obtain the heat conducted between neighboring tubes, Fourier's law of conduction (Incropera and DeWitt, 1996) is applied. Figure 2.1(a) shows a tube and its nearest neighbors and characteristic dimensions used to calculating heat transfer due to conduction. The method for obtaining characteristic dimensions and neighboring tubes is explained in the grid generation section. Because of this assumption, this model is henceforth referred to as the "thermal resistance model".

The assumptions for the second model are as follows:

1) The air side heat transfer coefficient and air temperature while obtaining conductive heat transfer between tubes is assumed to be the same as the segment to which the fin section is associated. Figure 2.1(b) shows the scatter plot of fin sections that are associated to tubes based on nearest distance calculation.

2) The heat exchanger profile is overlaid on a two-dimensional Cartesian grid and knowledge about the geometry is added to the grid. This information is used to obtain the amount of heat conducted in or out of a tube segment. Because the two-dimensional heat diffusion equation is solved in this model, it is henceforth referred to as the "heat conduction model".

3) The Cartesian grid employed in the "heat conduction" model to calculate temperature distribution over the fin surface approximates the circumference of the tube as a multi-sided polygon. While this

approximation has negligible effect on the temperature distribution when grid resolution is sufficient, use of body fitted co-ordinates will reduce the need to high grid refinement as well as the associated computational burden (Chu, 1971; Oliet *et al.*, 2009)

The "thermal resistance model" and the "heat conduction model" are compared in section 2.1.7. The "thermal resistance model" is computationally inexpensive, though the "heat conduction model" is more accurate. Through use of suitable multipliers, it is shown that the "thermal resistance model" is equivalent to "heat conduction model".

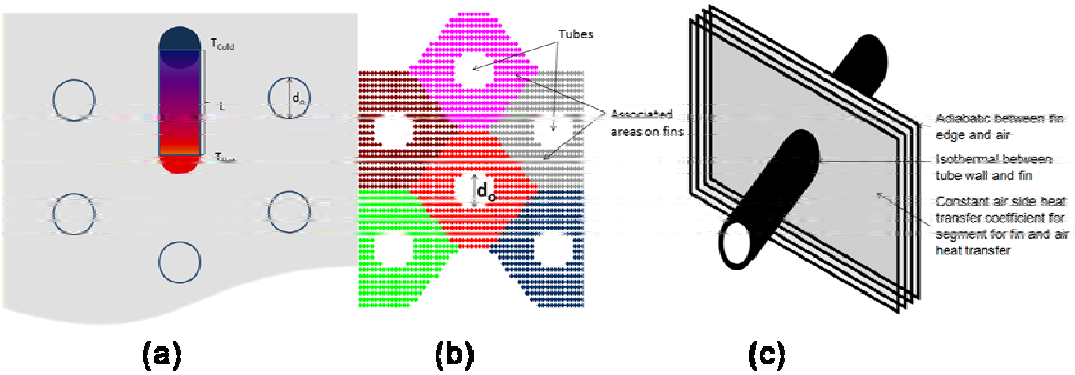


**Figure 2.1: Dimensions and boundary conditions used in the modeling approach to account for tube-to-tube conduction in fin-and-tube heat exchangers**

2.1.3 Computational Grid

A two dimensional Cartesian grid is created to provide useful information to both the resistance and conduction models, using suitable grid spacing defined by number of x and y grid points per unit horizontal and vertical spacing respectively. Using a nearest-distance calculation, each grid point is associated with a tube segment as shown in Figure 2.1 (b). By processing this information and refrigerant flow direction in a tube, the nearest neighbors of a given tube segment are obtained.

The “thermal resistance model” uses this information to obtain the nearest neighbors of a given tube. Further, this grid is used to obtain the distance between neighboring tubes. Tube outer diameter is used as the characteristic width for conduction between tubes. Using the mathematical statement for Fourier’s law of conduction, heat transferred between tubes is obtained.

The “heat conduction model” solves the steady state heat diffusion equation on the entire fin surface. The heat diffusion equation, shown in equation (2.1) is solved numerically using the Gauss Seidel successive iteration scheme (Kreyszig, 2005) which can unconditionally solve diagonally-dominant matrices.

$$\frac{\partial}{\partial x}\left(k\frac{\partial T}{\partial x}\right)+\frac{\partial}{\partial y}\left(k\frac{\partial T}{\partial y}\right)+S(T-T_{air})=0 \tag{2.1}$$

The boundary condition between the tube wall and fin is considered to be isothermal as shown in Figure 2.1(c), and at the same temperature as the tube outer wall temperature. The wall temperature is obtained by the segment heat transfer model. The heat conducted in or out of a given tube segment is obtained through the gradients in temperature across the given associated fin areas as shown in Figure 2.1(b). The fin edge is considered to be an adiabatic boundary ignoring the heat flux transferred through it. The surface of the fin itself is treated as a constant flux boundary condition with the relevant air temperature and air heat transfer coefficient.

### 2.1.4 Solution Methodology

ε-NTU equations are widely used for modeling heat transfer. For a cross flow, mixed-mixed flow configuration, these equations are obtained by integrating the energy conservation equations for a discretized control volume. Lee and Domanski

(1997) accounted for fin conduction by adding an additional conduction term in the ε-NTU model. They calculated air side heat capacity based on the ε-NTU approach. Using wall temperatures of the neighboring tubes and applying Fourier's law of conduction for a rectangular slab (with width equal to tube outer diameter), they obtain heat conducted into or out of the given control volume. Using the heat conducted and air side heat capacity, the refrigerant side heat capacity is obtained. However, the ε-NTU approach, based on its premise, ignores any heat flux coming in or leaving the control volume besides the two fluid streams. The equivalent thermal resistance diagram without any heat conduction is shown in Figure 2.2(a). However, with fin conduction, the overall equivalent resistance diagram is modified and changes to the one shown in Figure 2.2(b). This implies that the overall UA equation on which ε-NTU method is based is not valid for current model.

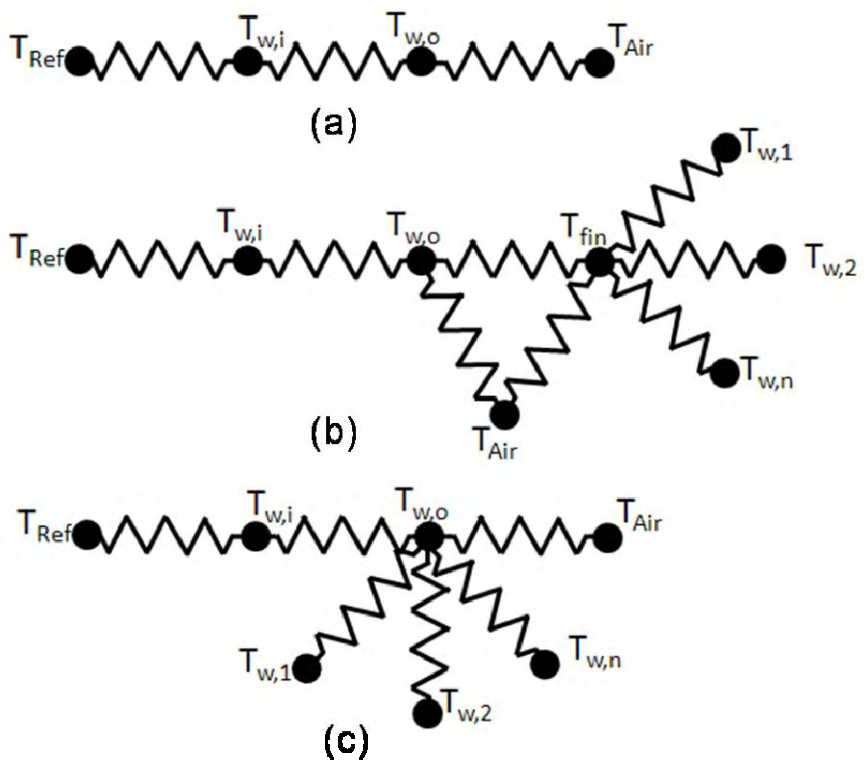


**Figure 2.2: (a) Equivalent resistance diagram ignoring fin conduction used by most existing models, (b) actual resistance diagram with tube-to-tube conduction and (c) modified resistance diagram after combining primary and secondary heat transfer areas through fin efficiency**

Further, though the approach of Lee and Domanski can be shown to work in most situations, the model fails when temperatures pinch off (Payne and Domanski, 1997). The neighboring wall temperatures used to obtain fin conduction lag the current iteration step. When refrigerant and air temperatures pinch off, and refrigerant outlet condition is updated based on neighboring wall temperatures from previous iteration, it can lead to violation of second law with refrigerant and air temperatures crossing. This prevents the model from being unconditionally stable.

In the model developed here, the equivalent thermal resistance diagram shown in Figure 2.2(b) is further simplified and fin temperature is combined with wall temperature through the use of fin efficiency as shown in Figure 2.2(c). This ensures

that the numerical model represents the physics more accurately than the ε-NTU model. Further, the solution methodologies shown in Figure 2.3(a) and Figure 2.3(b) avoid the lag in iteration step by solving for all temperatures simultaneously, making the model unconditionally stable.

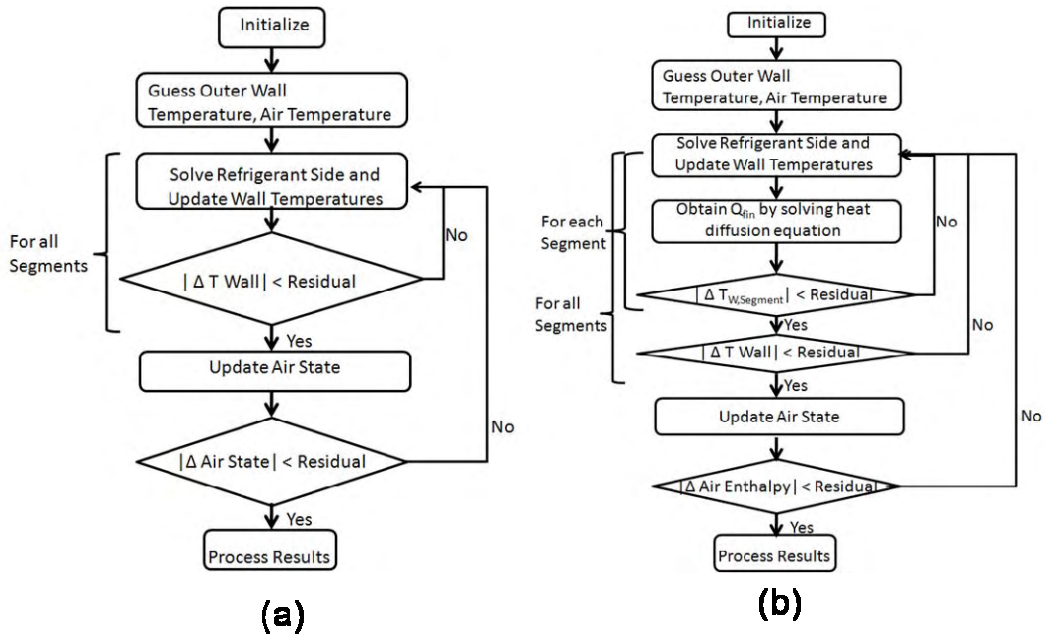


**Figure 2.3: Solution methodologies for the "thermal resistance model" and the "heat conduction model"**

The refrigerant side is modeled with discretized control volumes, formed by segments, and equations for conservation of energy are applied. The following equations are used for solving the refrigerant side in the “thermal resistance model”. The four unknowns are refrigerant and air outlet states, $h_{out}$, $T_{air,out}$, and the inner and outer wall temperatures, $T_{w,i}$ and $T_{w,o}$.

Equation (2.2) defines the heat transfer from the refrigerant to inner wall.

$$m_{ref,in}(h_{in} - h_{out}) = U_{ref} A_{in} \frac{(\Delta T_{1,r} - \Delta T_{2,r})}{\ln \frac{\Delta T_{1,r}}{\Delta T_{2,r}}} \tag{2.2}$$

Equation (2.3) defines the heat transferred from the inner wall to the outer wall through conduction.

$$U_{ref} A_{in} \frac{(\Delta T_{1,r} - \Delta T_{2,r})}{\ln \frac{\Delta T_{1,r}}{\Delta T_{2,r}}} = \frac{2\pi kL}{\ln(d_o / d_i)} (Tw_i - Tw_o) \tag{2.3}$$

Equation (2.4) defines the heat transferred from the outer wall to air and to the neighboring tubes due to conduction through fins. The authors decided not to apply the correction factor on Log Mean Temperature Difference (LMTD) method, F, for cross flow heat exchangers because the current method yielded excellent comparison with ε-NTU approach, as shown in section 2.1.6.2 .

$$\begin{aligned} \frac{2\pi kL}{\ln(d_o / d_i)} (Tw_o - Tw_i) = {} & U_{air} A_P \frac{(\Delta T_{1,a} - \Delta T_{2,a})}{\ln \frac{\Delta T_{1,a}}{\Delta T_{2,a}}} \\ & + U_{air} \eta_{fin} A_S \frac{(\Delta T_{1,a} - \Delta T_{2,a})}{\ln \frac{\Delta T_{1,a}}{\Delta T_{2,a}}} \\ & + \sum_{n=1}^{nMax} k \times d_o \times th \times nFin \times \frac{(Tw_n - Tw_o)}{\left| R_0 - R_n \right|} \end{aligned} \tag{2.4}$$

where nMax is the maximum number of neighbors for the given tube and *R* is the location of tubes on a two-dimensional grid (Tube 0 is the current tube). The last term in Equation (2.4) represents the conduction heat transfer to the current tube from neighboring tubes where n is the number of neighbors. It should be noted that this equation can be extended to account for longitudinal conduction along the tube as well by including the wall temperatures of upstream and downstream segments. In the "heat conduction model", this term is replaced by $Q_{fin}$ which is a function of outer wall temperatures of all tubes, air temperatures and air side heat transfer coefficient besides material and geometry parameters.

Temperature difference between the outer wall and air is assumed to be logarithmic as well, and the heat transfer is defined by Equation(2.5).

$$m_{air} c_{p,air} (T_{air,in} - T_{air,out}) = U_{air} \left(A_P + \eta A_S\right) \frac{(\Delta T_{1,a} - \Delta T_{2,a})}{\ln \frac{\Delta T_{1,a}}{\Delta T_{2,a}}} \quad (2.5)$$

where $A_P$ is the primary heat transfer area on the air side, and $A_S$ is the secondary heat transfer area on the air side. The equations and associated unknowns for the "heat conduction model" are shown in Figure 2.4.

$$\begin{Bmatrix} T_{a,o} \\ T_{w,i} \\ T_{w,o} \\ h_{out} \end{Bmatrix} \quad \begin{Bmatrix} m_{ref,in}(h_{in} - h_{out}) = U_{ref} A_{in} \frac{(\Delta T_{1,r} - \Delta T_{2,r})}{\ln \frac{\Delta T_{1,r}}{\Delta T_{2,r}}} \\ U_{ref} A_{in} \frac{(\Delta T_{1,r} - \Delta T_{2,r})}{\ln \frac{\Delta T_{1,r}}{\Delta T_{2,r}}} = \frac{2\pi kL}{\ln(d_o/d_i)} (Tw_i - Tw_o) \\ \frac{2\pi kL}{\ln(d_o/d_i)} (Tw_o - Tw_i) = U_{air} A_P \frac{(\Delta T_{1,a} - \Delta T_{2,a})}{\ln \frac{\Delta T_{1,a}}{\Delta T_{2,a}}} \\ \qquad + U_{air} \eta_{fin} A_S \frac{(\Delta T_{1,a} - \Delta T_{2,a})}{\ln \frac{\Delta T_{1,a}}{\Delta T_{2,a}}} + Q_{Cond} \\ m_{air} c_{p,air} (T_{air,in} - T_{air,out}) = U_{air} \left(A_P + \eta A_S\right) \frac{(\Delta T_{1,a} - \Delta T_{2,a})}{\ln \frac{\Delta T_{1,a}}{\Delta T_{2,a}}} \end{Bmatrix}$$

**Figure 2.4: Unknowns and equations for the "heat conduction model"**

The equations and associated unknowns for the "thermal resistance model" are shown in Figure 2.5.

$$\begin{Bmatrix} T_{a,o} \\ T_{w,i} \\ T_{w,o} \\ h_{out} \end{Bmatrix} \quad \begin{Bmatrix} m_{ref,in}(h_{in} - h_{out}) = U_{ref} A_{in} \dfrac{(\Delta T_{1,r} - \Delta T_{2,r})}{\ln \dfrac{\Delta T_{1,r}}{\Delta T_{2,r}}} \\ U_{ref} A_{in} \dfrac{(\Delta T_{1,r} - \Delta T_{2,r})}{\ln \dfrac{\Delta T_{1,r}}{\Delta T_{2,r}}} = \dfrac{2\pi kL}{\ln(d_o/d_i)}(Tw_i - Tw_o) \\ \dfrac{2\pi kL}{\ln(d_o/d_i)}(Tw_o - Tw_i) = U_{air} A_P \dfrac{(\Delta T_{1,a} - \Delta T_{2,a})}{\ln \dfrac{\Delta T_{1,a}}{\Delta T_{2,a}}} \\ \qquad + U_{air} \eta_{fin} A_S \dfrac{(\Delta T_{1,a} - \Delta T_{2,a})}{\ln \dfrac{\Delta T_{1,a}}{\Delta T_{2,a}}} \\ \qquad + \sum_{n=1}^{nMax} k \times d_o \times th \times nFin \times \dfrac{(Tw_n - Tw_o)}{\left| R_0 - R_n \right|} \\ m_{air} c_{p,air}(T_{air,in} - T_{air,out}) = U_{air}\left(A_P + \eta A_S\right) \dfrac{(\Delta T_{1,a} - \Delta T_{2,a})}{\ln \dfrac{\Delta T_{1,a}}{\Delta T_{2,a}}} \end{Bmatrix}$$

**Figure 2.5: Unknowns and equations for "thermal resistance model"**

2.1.5 Sub-divided Segment with Heat Conduction

The solution approach for handling a segment with phase change is the same as that of Jiang et al. and the reader is referred to the original paper for a detailed explanation. However, when fin conduction is accounted for, the wall temperatures within a segment that is subdivided are different for the subdivided zones. This is hardly surprising as varying heat transfer coefficients of different phases lead to different wall temperatures. While accounting for fin conduction, the various wall temperatures within a segment are used while obtaining the corresponding conduction heat transfer for that particular segment as illustrated in Figure 2.6.

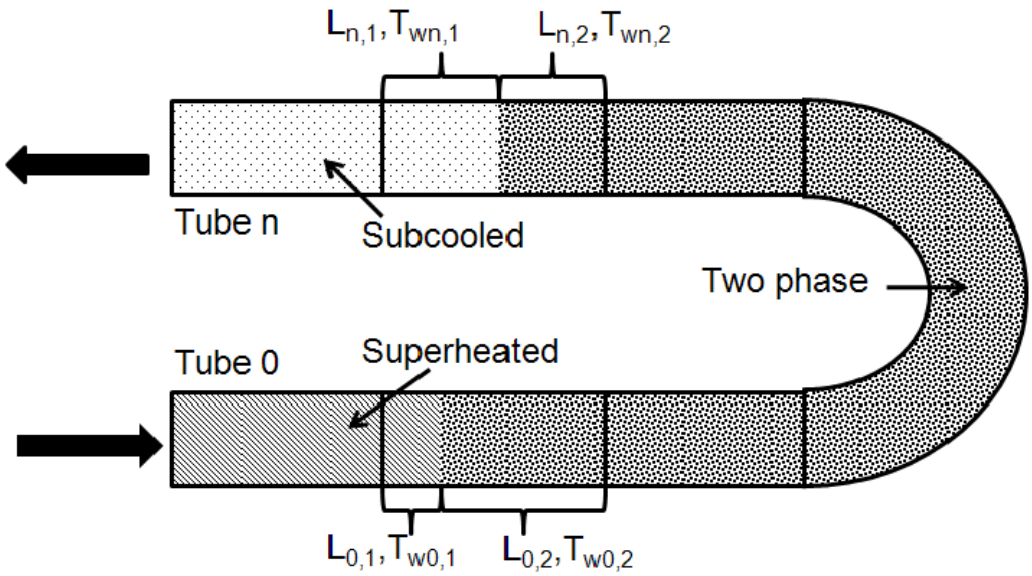


**Figure 2.6: Temperatures, lengths and phases involved in the sub dividable segment implementation**

Tube n and Tube 0 are neighbors and the segments where the phase changes occur are connected through fins. The heat conduction for tube 0, through fins, is described in Equations (2.6) and(2.7).

$$Q_{fin,1} = f(T_{w0,1} - T_{wn,1}, L_{0,1}) \tag{2.6}$$

$$Q_{fin,2} = f(T_{w0,2} - T_{wn,1}, L_{0,2} - L_{n,2}) + f(T_{w0,2} - T_{wn,2}, L_{n,2}) \tag{2.7}$$

*2.1.5.1 Verification of sub-divided segment method*

To verify the subdivided segment method, a hypothetical 2 tube evaporator was modeled. The specifications of the evaporator are given in Table 2.1.

**Table 2.1: Specifications of 2-tube evaporator and correlations used**

| Parameters | | | Correlations | |
|---|---|---|---|---|
| Number of Segments | 10 | --- | Air Side HTC | Kim-Youn-Webb |
| Tube Configuration | Staggered | | Refrigerant Side HTC - Liquid | Dittus-Boelter |
| Number of Tubes Per Bank | 2 | --- | Refrigerant Side HTC - Two Phase | Dobson |
| Number of Tube Banks | 1 | --- | Refrigerant Side HTC - Vapor | Dittus-Boelter |
| Tube Length | 10.0 | m | | |
| Tube OD | 0.01 | m | Air Side DP | Kim-Youn-Webb |
| Tube Thickness | 0.33 | mm | Refrigerant Side DP - Liquid | Blasius |
| Tube Vertical Spacing | 1 | in | Refrigerant Side DP - Two Phase | Friedel |
| Tube Horizontal Spacing | 0.75 | in | Refrigerant Side DP - Vapor | Blasius |
| FPI | 20 | fpi | | |
| Fin Thickness | 0.005 | in | | |
| Fin Type | Flat | --- | | |
| Coil Face Air Velocity | 4.0 | $ms^{-1}$ | | |

The sub-divided segment method developed here is based on wall-temperature linked equations. The result yielded by this method, assuming all cut fins, as shown in Figure 2.7, must match those predicted by Jiang et al's Effectiveness-NTU based method.

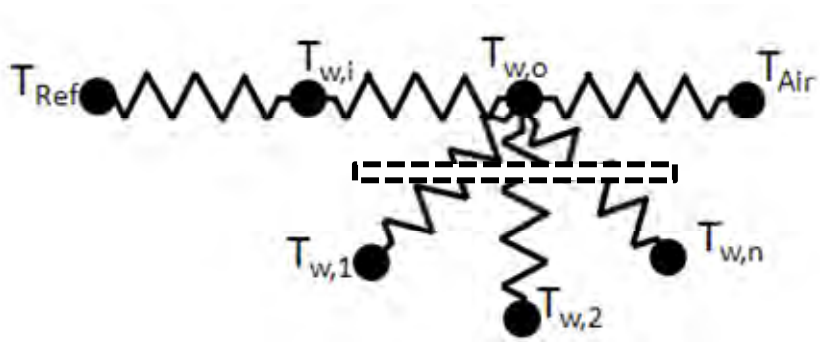


**Figure 2.7: Illustration to show cut fins in the new model's equivalent resistance diagram**

With varying outlet superheat, the results show that the % difference length stays within 2.5% of the lengths predicted by Jiang et al., as shown in Figure 2.8.

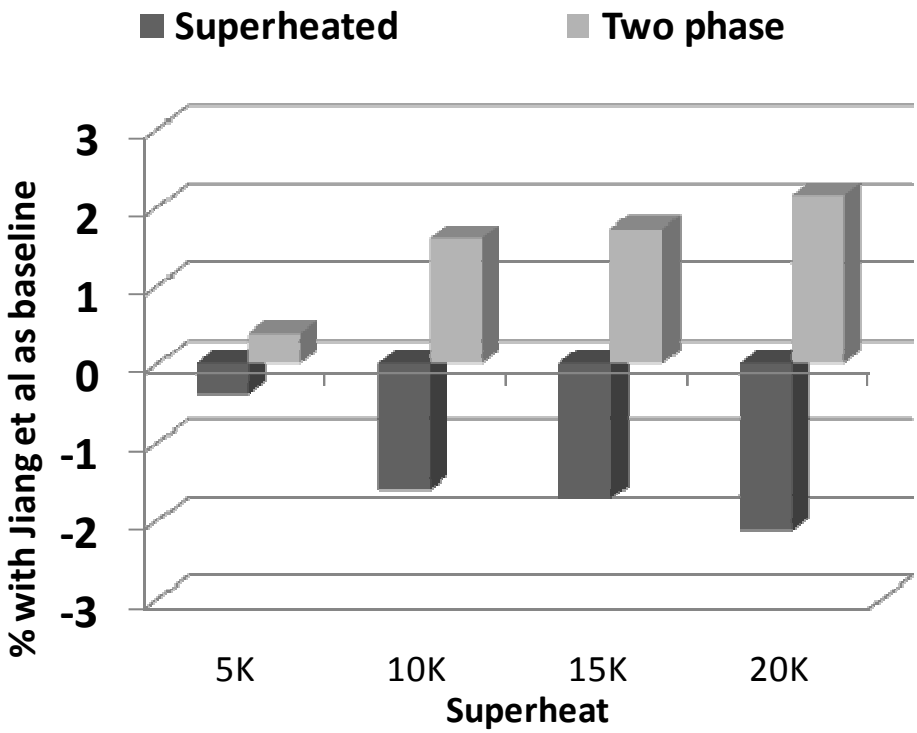


**Figure 2.8: Verification of sub-divided segment method for the temperature linked equation based model through comparison of superheated and two-phase region lengths for the new model and Jiang et al's model**

The comparison of actual lengths is shown in Figure 2.9.

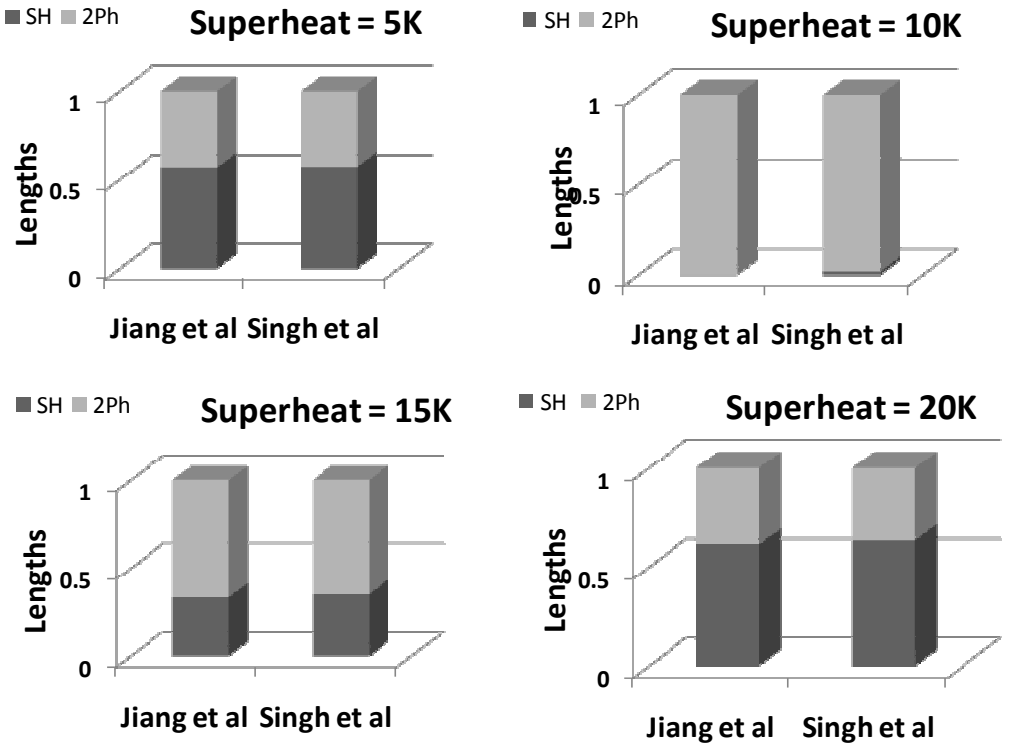


**Figure 2.9: Comparison of sub-divided lengths for Jiang et al's model and the new Singh et al's model**

Finally, to verify the newly developed sub-divided segment method, the overall heat capacity comparison between Jiang *et al.* and Singh *et al.* (2008) is shown in Figure 2.10.

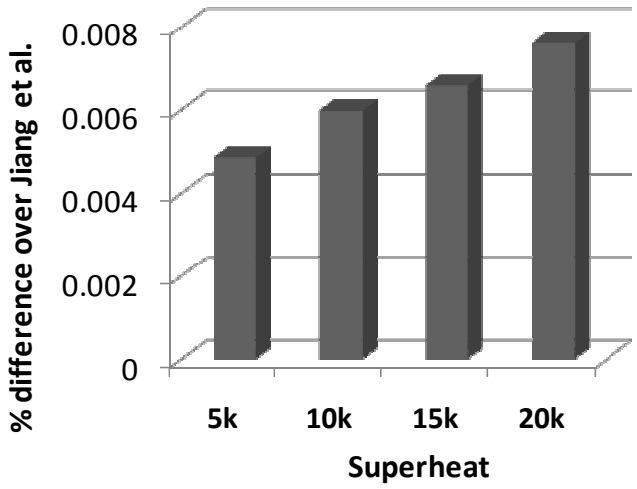


**Figure 2.10: Comparison of heat capacity predicted by Jiang et al. and the new model of Singh et al.**

As a next step, to verify the effect of tube-to-tube conduction, Figure 2.11 shows its effect on tube-to-tube conduction of individual phases within the subdivided segment. The refrigerant mass flow rate is fixed such that the desired superheat is obtained for the Singh et al model with tubes insulated, i.e. no tube-to-tube conduction via fins. This implies that the due to performance degradation, the evaporator does not attain the desired superheat for the same mass flow rate when tube-to-tube conduction is enabled. As evident from the figure, the length of the superheated region when conduction is accounted for is less than its value when tubes are considered insulated from each other. This occurs because the superheated region is able to conduct heat away from itself towards the two-phase region via fins, leading to diminished superheated length. This phenomenon was also shown experimentally by Lee and Domanski (1997).

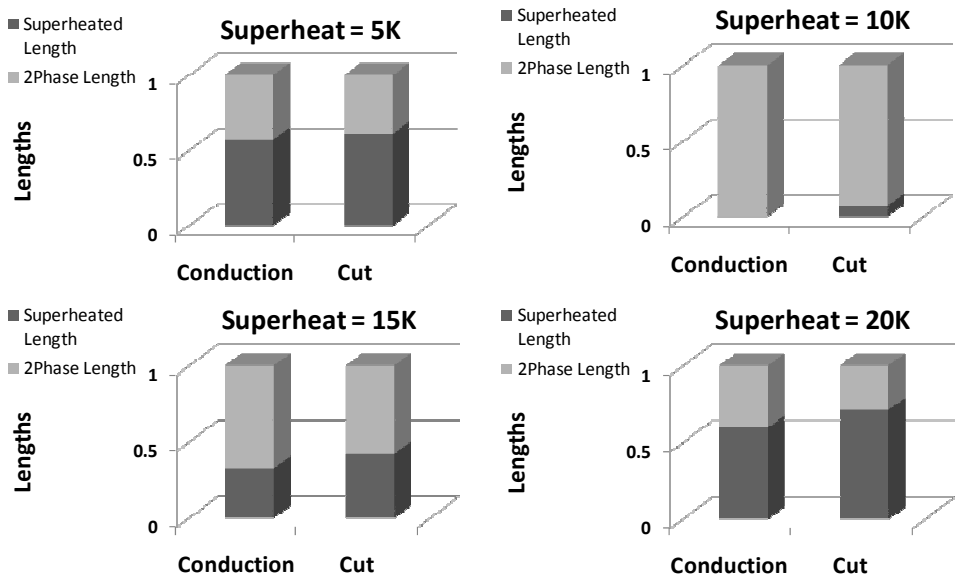


**Figure 2.11: Comparison of length of superheated region for Singh et al's model with and without conduction, to verify the effect of tube-to-tube conduction**

## 2.1.6 Simulation Study

The new models ("thermal resistance" and "heat conduction") are compared against Jiang *et al.*'s model. This is an important step in verifying the new models because Jiang *et al.*'s model has been widely validated against experimental data. Because the equations for refrigerant side heat transfer model simplify to being the same for both "thermal resistance" and "heat conduction" models in the absence of conduction, for the purpose of verification, they are referred to as the "new model".

### *2.1.6.1 Effect of Air Heat Transfer Coefficient on Fin Temperature Distribution*

To analyze the effect of air side heat transfer coefficient on the temperature distribution, the following two-dimensional problem was set up. As shown in Figure 2.12, a rectangular surface 20 mm by 14 mm with a surface thermal conductivity of 237 $Wm^{-1}K^{-1}$ was created. On this surface, at halfway along the height, and at x locations of 0.5 cm and 1.5 cm, two hollow circles of diameter 4mm were created.

These circles were set as being isothermal, and at 400 and 300K. The edge of the rectangular surface is treated as adiabatic. The surface itself is considered as constant flux boundary with air temperature fixed at 293K. The two dimensional steady state heat diffusion equation is solved to obtain the temperature distribution on the surface was calculated for varying air heat transfer coefficient (Patankar, 1980). Figure 2.13(a) shows the temperature distribution along the section Y'-Y' from Figure 5. Figure 2.13(b) shows the temperature distribution over the entire surface for increasing air heat transfer coefficient.

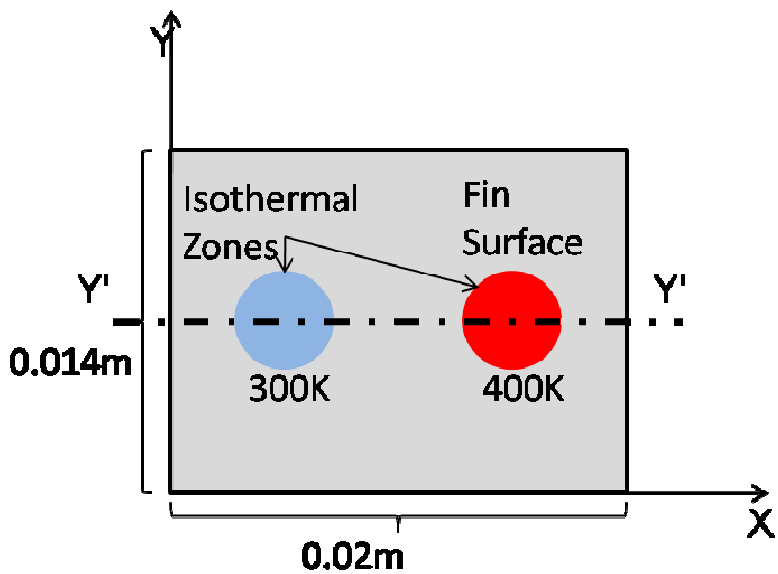


**Figure 2.12: Outline of problem used to test effect of air side heat transfer coefficient on temperature distribution on the fin surface**

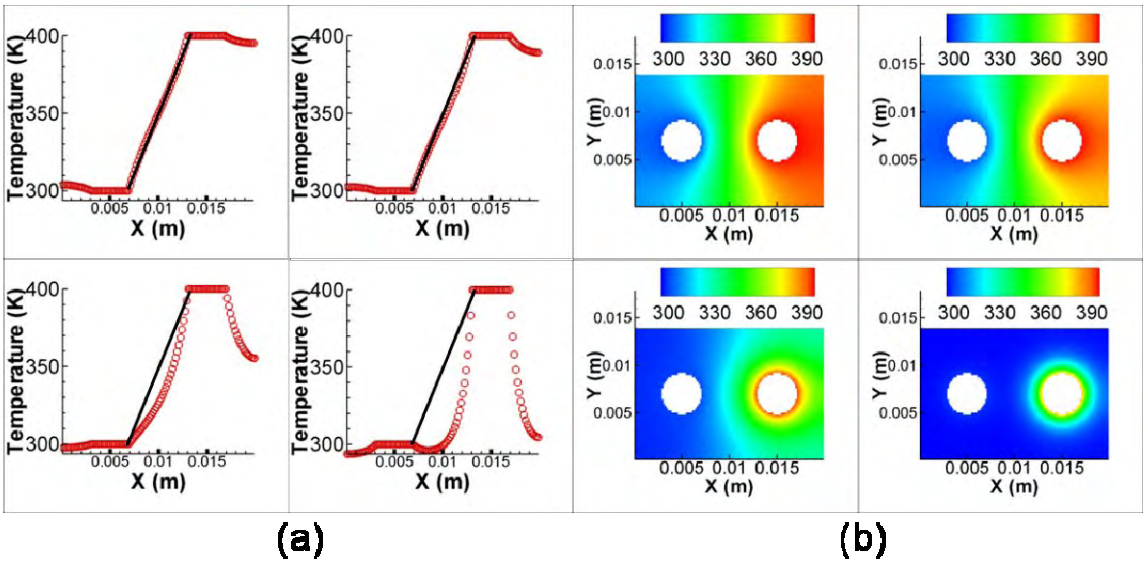


**Figure 2.13: Temperature distribution on the fin surface. Air heat transfer coefficient increases from 10Wm$^{-2}$K$^{-1}$ to 10000 Wm$^{-2}$K$^{-1}$ from top left to top right, and top to bottom. All temperatures are in K**

The air heat transfer coefficients are increased from 10 Wm$^{-2}$K$^{-1}$ up to 10,000 Wm$^{-2}$K$^{-1}$. Comparing the actual temperature profile with the superimposed linear profile shows that up to 100 Wm$^{-2}$K$^{-1}$, the linear profile closely matches the actual profile. At 1000 Wm$^{-2}$K$^{-1}$, the temperature profile deviates from linear and at 10,000 Wm$^{-2}$K$^{-1}$, the temperature of the fin at the point equidistant from the two isothermal zones drops to a minimum, leading to no heat conduction between the two zones. The air heat transfer coefficients of the order of 1000 Wm$^{-2}$K$^{-1}$ are rare in more tube-and-fin heat transfer calculations (Kays and London,1998), and the temperature drop of 100K is also higher than what is usually seen between neighboring tubes, even in high temperature applications such as $CO_2$ gas coolers(Hwang, *et al.*,2007, Brown, *et al.*,2002, Groll and Kim,2007). This analysis shows that ignoring air side heat transfer from the fin surface for conduction calculation, as is done in the resistance model, is acceptable.

*2.1.6.2 Segment Independence*

The ε-NTU method is based on analytically integrating the temperature profiles of two fluids over a given area to obtain the heat capacity. However, in the current approach, the governing equations are discretized and solved, as is. This can lead to a dependence of heat capacity on segment length if the segment length is too large. Therefore, the new model was tested against Jiang *et al.* model for a simple two tube water-to-air heat exchanger shown in Figure 2.14(a). The specifications of the heat exchanger are given in Table 2.2.

**Table 2.2: Specification of two tube water heat exchanger**

| Parameters | | | Correlations | |
|---|---|---|---|---|
| Number of Segments | Variable | — | Air Side HTC | Kim-Youn-Webb |
| Tube Configuration | Inline | | Refrigerant Side HTC - Liquid | Dittus-Boelter |
| Number of Tubes Per Bank | 2 | — | Refrigerant Side HTC - Two Phase | Dobson |
| Number of Tube Banks | 1 | — | Refrigerant Side HTC - Vapor | Dittus-Boelter |
| Tube Length | 10.0 | m | | |
| Tube OD | 0.01 | m | Air Side DP | Kim-Youn-Webb |
| Tube Thickness | 0.33 | mm | Refrigerant Side DP - Liquid | Blasius |
| Tube Vertical Spacing | 1 | in | Refrigerant Side DP - Two Phase | Friedel |
| Tube Horizontal Spacing | 0.75 | in | Refrigerant Side DP - Vapor | Blasius |
| FPI | 20 | fpi | | |
| Fin Thickness | 0.005 | in | | |
| Fin Type | Flat | — | | |
| Coil Face Air Velocity | 4.0 | $ms^{-1}$ | | |

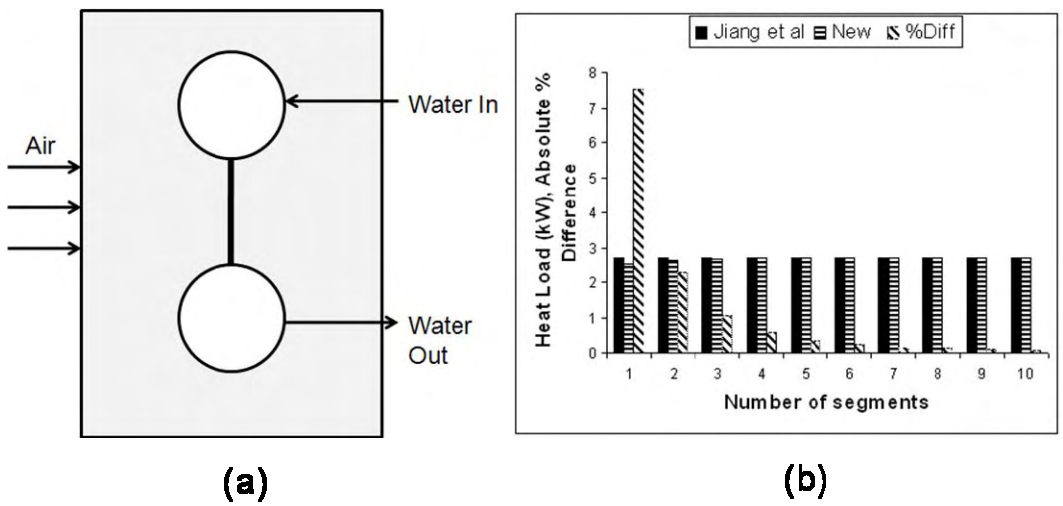


**Figure 2.14: Dependence of the new model on number of segments**

For calculating air side heat transfer coefficient and pressure drop, correlation proposed by Kim et al. (Kim, *et al.*,1999) was used. For calculating water heat transfer coefficient and pressure drop, correlations proposed by Dittus and Boelter (Dittus and Boelter,1985) and Blasius (Schlichting and Gersten,2000) were used, respectively.

The results, shown in Figure 2.14(b), reveal that with the increasing number of segments, the difference between heat capacity predicted by Jiang *et al.*'s model and the new model diminish to well within ±0.05% for 10 segments. This proves the segment independence of the new model when a sufficient number of segments are used.

2.1.7 Comparison of "thermal resistance model" and "heat conduction model"

The "thermal resistance model" uses Fourier's law of conduction to obtain the heat transfer between tubes, while the "heat conduction model" solves the heat diffusion equation with air as a source/sink to obtain heat transfer between tubes. To prove that the two yield the same result, with multipliers for the "thermal resistance

model" across tube rows and within tube rows, a hot water heat exchanger (Figure 2.15) with the specifications mentioned in Table 2.3 was modeled. These multipliers are dependent on several factors, some of which are as follows:

a) Type of fin enhancement (Slit, Louver etc)

b) Ratio of row and tube pitch to tube outer diameters

The water mass flow rate was 20 gm $sec^{-1}$ with an inlet pressure and temperature of 0.35 MPa and 51.85°C, respectively. The air inlet pressure was 1 atm and 25 °C and 50% relative humidity. These conditions were chosen to highlight the effect of heat transfer between tubes on overall heat exchanger performance, as well as the effect of the two different approaches on overall heat capacity and wall temperature profile.

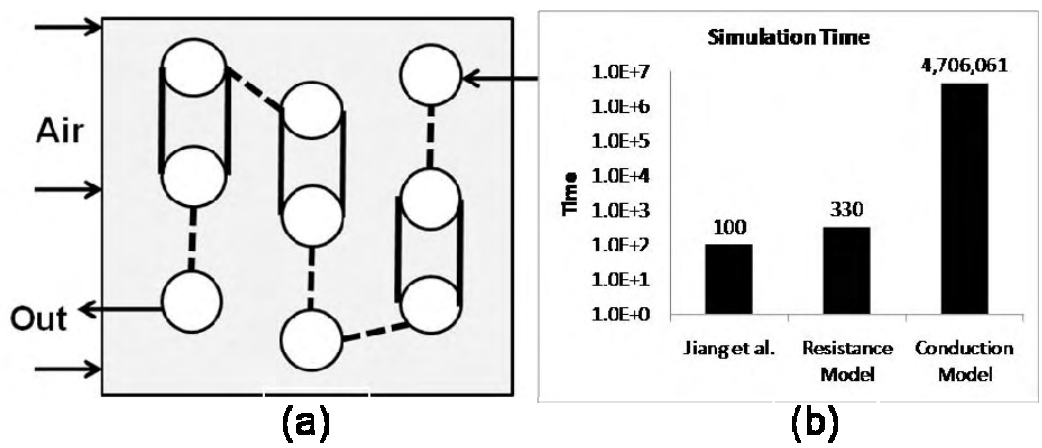


**Figure 2.15: Schematic of heat exchanger used to compare "thermal resistance model" and "heat conduction model" with simulation time**

**Table 2.3: Specifications of 3bank-9tube water heat exchanger**

| Parameters | | | Correlations | |
|---|---|---|---|---|
| Number of Segments | 10 | — | Air Side HTC | Kim-Youn-Webb |
| Tube Configuration | Staggered | | Refrigerant Side HTC - Liquid | Dittus-Boelter |
| Number of Tubes Per Bank | 3 | — | Refrigerant Side HTC - Two Phase | Dobson |
| Number of Tube Banks | 3 | — | Refrigerant Side HTC - Vapor | Dittus-Boelter |
| Tube Length | 1.0 | m | | |
| Tube OD | 0.01 | m | Air Side DP | Kim-Youn-Webb |
| Tube Thickness | 1.0 | mm | Refrigerant Side DP - Liquid | Blasius |
| Tube Vertical Spacing | 1 | in | Refrigerant Side DP - Two Phase | Friedel |
| Tube Horizontal Spacing | 0.8 | in | Refrigerant Side DP - Vapor | Blasius |
| FPI | 15 | fpi | | |
| Fin Thickness | 0.005 | in | | |
| Fin Type | Flat | — | | |
| Coil Face Air Velocity | 2.0 | $ms^{-1}$ | | |

To compare the two solvers, tube wall temperature is calculated at the last segment of every tube in the refrigerant flow direction. The results (Figure 2.16(a)) clearly show that while the "thermal resistance model" captures the trend in wall temperature accurately, it is unable to capture the true effect of heat conduction on the overall coil performance with all temperatures agreeing within ±1.6°C. However, with multipliers of 2.0 for transverse conduction, and 2.2 for longitudinal conduction, all temperatures agree within ±0.7°C. The results are shown in Figure 2.16(b). As shown in Figure 2.15(b), the "thermal resistance model" is much less computationally expensive than the "heat conduction model". Further, the computational time for Jiang et al. model and the "thermal resistance model" are comparable, which is valuable in a rapid design environment. This is an additional benefit that motivated this comparison.

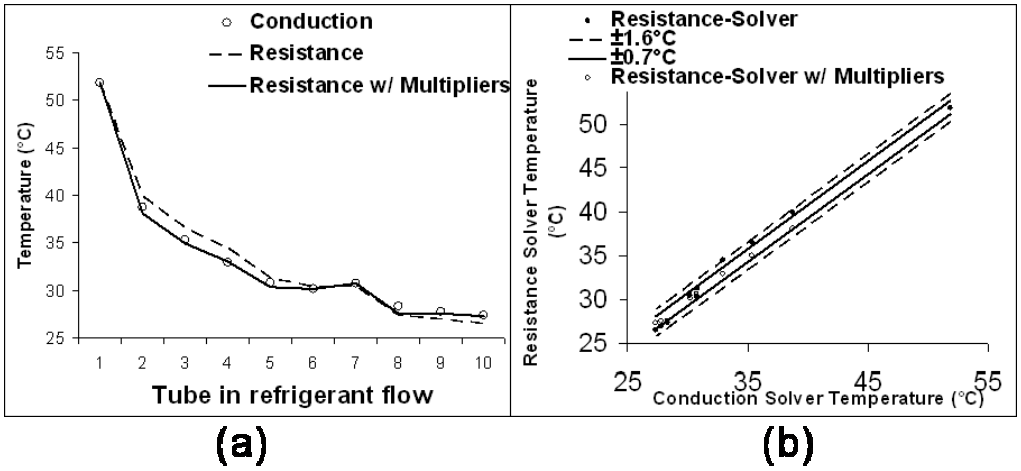


**Figure 2.16: Temperature profile of refrigerant in flow direction to show the equivalence of "heat conduction model" and "thermal resistance model" with suitable multipliers**

2.1.8 Evaluation of Neighboring Tube Selection for Inline Coils

One of the common configurations of fin-and-tube heat exchangers is an inline configuration, as shown in Figure 2.17 (a). The model developed here assumes that the maximum number of neighbors possible for any given tube for an inline configuration for the "thermal resistance model" is four, based on the nearest distance function qualification, as shown in Figure 2.17 (c). However, depending on the ratio of vertical and horizontal spacing, the number of effective neighbors can be eight, as shown in Figure 2.17 (d).

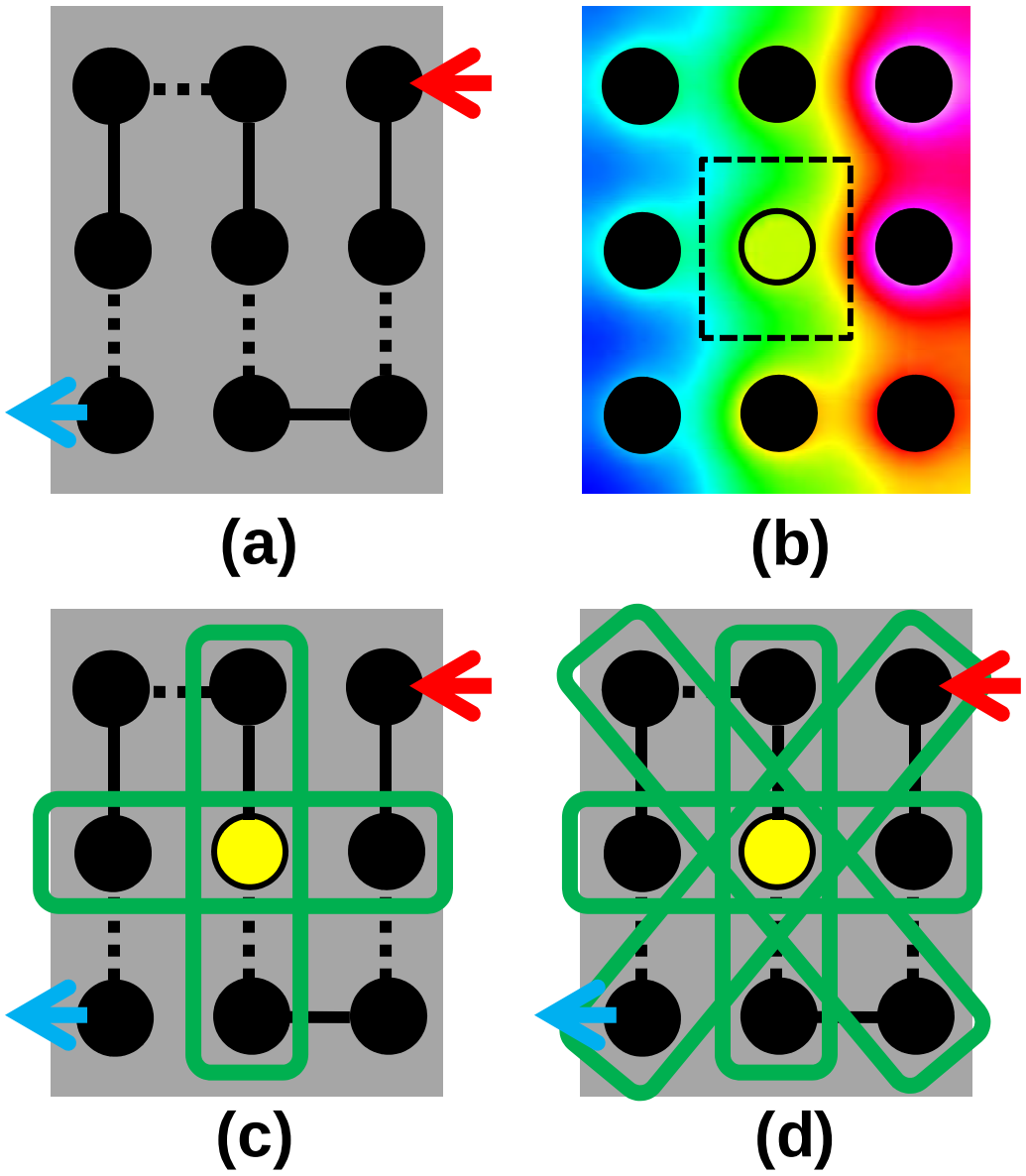


**Figure 2.17: (a) Inline water coil chosen to study effect of neighboring tube selection, (b) temperature distribution when "heat conduction model" is employed, (c) maximum four neighbors possible for "thermal resistance model" and (d) maximum eight neighbors possible for "thermal resistance model"**

To evaluate the impact of choosing eight neighbors, an inline water coil was simulated. Specifications of the coil are given in Table 2.4.

**Table 2.4: Specifications of inline water coil and correlations employed**

| Parameters | | | Correlations | |
|---|---|---|---|---|
| Number of Segments | 10 | --- | Air Side HTC | Kim-Youn-Webb |
| Tube Configuration | Inline | | Refrigerant Side HTC - Liquid | Dittus-Boelter |
| Number of Tubes Per Bank | 3 | --- | Refrigerant Side HTC - Two Phase | Dobson |
| Number of Tube Banks | 3 | --- | Refrigerant Side HTC - Vapor | Dittus-Boelter |
| Tube Length | 1.0 | m | | |
| Tube OD | 0.01 | m | Air Side DP | Kim-Youn-Webb |
| Tube Thickness | 1.0 | mm | Refrigerant Side DP - Liquid | Blasius |
| Tube Vertical Spacing | 1 | in | Refrigerant Side DP - Two Phase | Friedel |
| Tube Horizontal Spacing | 0.8 | in | Refrigerant Side DP - Vapor | Blasius |
| FPI | 15 | fpi | | |
| Fin Thickness | 0.005 | in | | |
| Fin Type | Flat | --- | | |
| Coil Face Air Velocity | 2.0 | $ms^{-1}$ | | |

The results of the analysis shown in Figure 2.18 (a) and (b) compare the water temperature profiles through the length of the heat exchanger, in water flow direction from the start tube to the end tube.

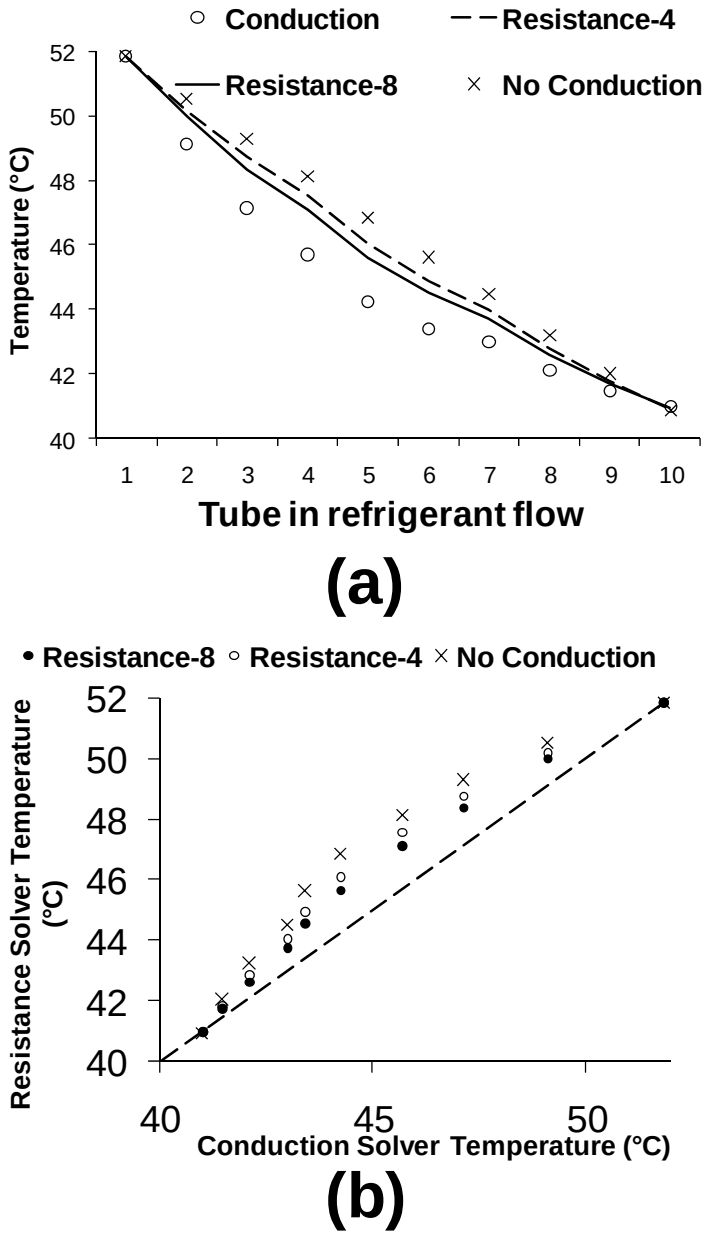


**Figure 2.18: Comparison of water temperature profiles for "heat conduction" and "thermal resistance" models with four and eight neighbors**

The results clearly show that the temperature profile when eight neighbors are selected provides a more accurate performance than four neighbors, when evaluated against the benchmark “heat conduction solver”.

## 2.2 Validation against Experimental Data

To validate the "thermal resistance model", two sets of experimental data were used:

1) Experiments conducted by Jin *et al.* (2004)

2) Experiments conducted by Zilio *et al.* (2007)

### 2.2.1 Experiments by Jin et al.

Jin *et al.* tested a carbon dioxide gas cooler at 36 different test conditions. The heat exchange process in this gas cooler occurred in the supercritical region. The specifications of the gas cooler are shown in Table 2.5.

**Table 2.5: Geometric specifications and correlations used for Jin et al heat exchanger**

| Parameters | | | Correlations | |
|---|---|---|---|---|
| Number of Segments | 10 | — | Air Side HTC | Wang-Lee |
| Tube Configuration | Staggered | | Refrigerant Side HTC - Liquid | Gnielinski |
| Number of Tubes Per Bank | 18 | — | Refrigerant Side HTC - Two Phase | Dobson |
| Number of Tube Banks | 3 | — | Refrigerant Side HTC - Vapor | Gnielinski |
| Tube Length | 0.61 | m | | |
| Tube OD | 0.0084 | m | Air Side DP | Wang-Lee |
| Tube Thickness | 0.406 | mm | Refrigerant Side DP - Liquid | Blasius |
| Tube Vertical Spacing | 1 | in | Refrigerant Side DP - Two Phase | Friedel |
| Tube Horizontal Spacing | 0.625 | in | Refrigerant Side DP - Vapor | Blasius |
| FPI | 17 | fpi | | |
| Fin Thickness | 0.0043 | in | | |
| Fin Type | Slit | — | | |
| Coil Face Air Velocity | variable | $ms^{-1}$ | | |

Figure 2.19 (a) shows the schematic of the heat exchanger with thermocouple locations. Table 2.6 shows the test conditions for the experiments. The accuracy of the T type Copper-Constantan thermocouples employed was ±0.2°C.

**Table 2.6: Test cases for Jin et al experiments**

| No | Inlet Air Temp [°F (°C)] | Ref MFR [lbmin$^{-1}$ (gs$^{-1}$)] | Inlet Pressure [psia (MPa)] | Air Frontal Velocity [fpm (ms$^{-1}$)] |
|---|---|---|---|---|
| 1 | 85 (29.4) | 5 (38) | 1,300 (9.0) | 200, 400, 600 (1.0, 2.0, 3.0 ) |
| 2 | | | 1,450 (10.0) | 200, 400, 600 (1.0, 2.0, 3.0 ) |
| 3 | | | 1,600 (11.0) | 200, 400, 600 (1.0, 2.0, 3.0 ) |
| 4 | | 10 (76) | 1,300 (9.0) | 200, 400, 600 (1.0, 2.0, 3.0 ) |
| 5 | | | 1,450 (10.0) | 200, 400, 600 (1.0, 2.0, 3.0 ) |
| 6 | | | 1,600 (11.0) | 200, 400, 600 (1.0, 2.0, 3.0 ) |
| 7 | 95 ( 35) | 5 (38) | 1,300 (9.0) | 200, 400, 600 (1.0, 2.0, 3.0 ) |
| 8 | | | 1,450 (10.0) | 200, 400, 600 (1.0, 2.0, 3.0 ) |
| 9 | | | 1,600 (11.0) | 200, 400, 600 (1.0, 2.0, 3.0 ) |
| 10 | | 10 (76) | 1,300 (9.0) | 200, 400, 600 (1.0, 2.0, 3.0 ) |
| 11 | | | 1,450 (10.0) | 200, 400, 600 (1.0, 2.0, 3.0 ) |
| 12 | | | 1,600 (11.0) | 200, 400, 600 (1.0, 2.0, 3.0 ) |

For modeling this gas cooler, the air side heat transfer coefficient was obtained using the correlation proposed by Wang and Lee (2001) for slit fins. Carbon Dioxide heat transfer and pressure drop were calculated using correlations proposed by Gnielinski (1976) and Blasius (Schlichting and Gersten, 2000), respectively.

Figure 2.19(b) shows the overall heat capacity comparison for Jin et al. model and measured values and Figure 2.19(c) show the overall heat capacity comparison of "thermal resistance model" and predicted values. The predicted heat capacity for the "thermal resistance model" agrees within ±3% of the experimental values. This is better than the overall predicted heat capacity for the Jiang *et al.* model which is ±5% within the experimental values. The experimental heat capacity was calculated as the average of refrigerant side capacity and air side capacity.

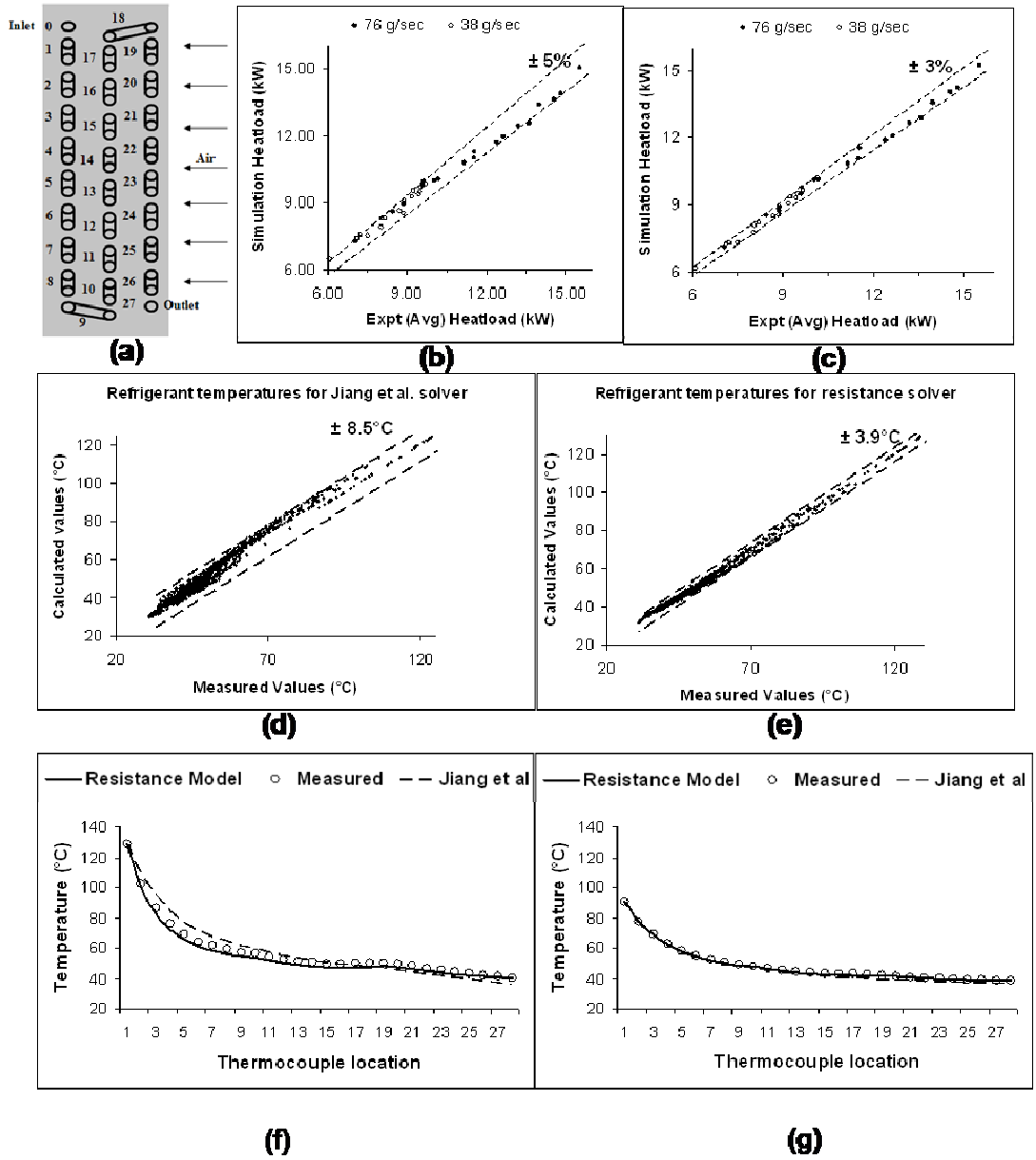


**Figure 2.19: (a) Schematic of the gas cooler tested by Jin at al., (b) results of Jiang et al. validation (c) results of the new model validation, comparison of measured tube-bend temperatures against (d) Jiang et al. and the (e) new model, and (e, f) refrigerant temperature profiles compared against measured profiles for two representative cases**

The refrigerant temperature distribution for the two models, i.e. "thermal resistance model" and Jiang *et al.* model, is shown in Figure 2.19(d) and Figure 2.19(e). It is evident from these distributions that the "thermal resistance model" predicts all temperatures accurately within ±3.3°C, whereas the Jiang *et al.* model

predicts temperatures within ±8.5°C. Figure 2.19(f) and Figure 2.19(g) show the temperature profile for "thermal resistance model" compared with the temperature profile for Jiang *et al.* model for the highest and the lowest average temperature difference between calculated and measured values. The highest error between measured and the predicted refrigerant temperature using resistance solver is 3.9°C (Case 4, in Table 2.6, with face velocity of 2.0 m $sec^{-1}$). The highest error between measured and predicted refrigerant temperature using Jiang *et al.* model is 8.5°C (Case 3, in Table 2.6, with face velocity 1.0 m $sec^{-1}$). These profiles clearly show that the "thermal resistance model" follows the refrigerant temperature profile more accurately than the Jiang *et al.* model which ignores fin conduction.

2.2.2 Experiments by Zilio et al.

Zilio *et al.* (2007) tested two different gas coolers, with continuous and discontinuous (cut) fins, with two different circuit arrangements. Figure 2.20(a) shows one of the arrangements with cuts separating tubes. For other circuit arrangements, the reader is referred to Zilio *et al.* Gas cooler B had the same circuit arrangement as gas cooler A; however, the banks were separated through discontinuous fins. The heat exchangers were tested at three different conditions shown in Table 2.7. The refrigerant temperature is measured at the U-bends at 15 different locations along the refrigerant flow direction, for the upper circuit only.

**Table 2.7: Test conditions for Zilio *et al.* experiment**

| No | Air Frontal Velocity [$ms^{-1}$] | Ref MFR [$kghr^{-1}$)] | $CO_2$ Inlet Pressure [MPa] | $CO_2$ Inlet Temperature [°C] | Air Inlet Temperature [°C] |
|---|---|---|---|---|---|
| 1 | 1.6 | 169.0 | 7.911 | 87.0 | 20.3 |
| 2 | 1.6 | 167.1 | 8.599 | 97.6 | 21.5 |
| 3 | 1.6 | 166.4 | 9.102 | 107.8 | 23.0 |

The numerical model proposed in Zilio *et al.* is unable to predict the measured refrigerant temperature profile of the three gas coolers. In fact, for all the three gas coolers, their model predicts the same overall heat capacity and temperature profile because it does not account for fin conduction, as shown in their results. The "thermal resistance model" and Zilio *et al.* model predict the heat capacity within ±5% of the experimental value as shown in Figure 2.20(b). In the absence of pressure drop data and other factors like effectiveness of fin cuts in insulating tube banks, the difference between predicted and measured values is difficult to reduce. As shown in Figure 2.20(c) and Figure 2.20(d), the "thermal resistance model" is able to predict refrigerant temperature profile within ±8.5°C, which is a significant improvement over Zilio *et al.*'s model.

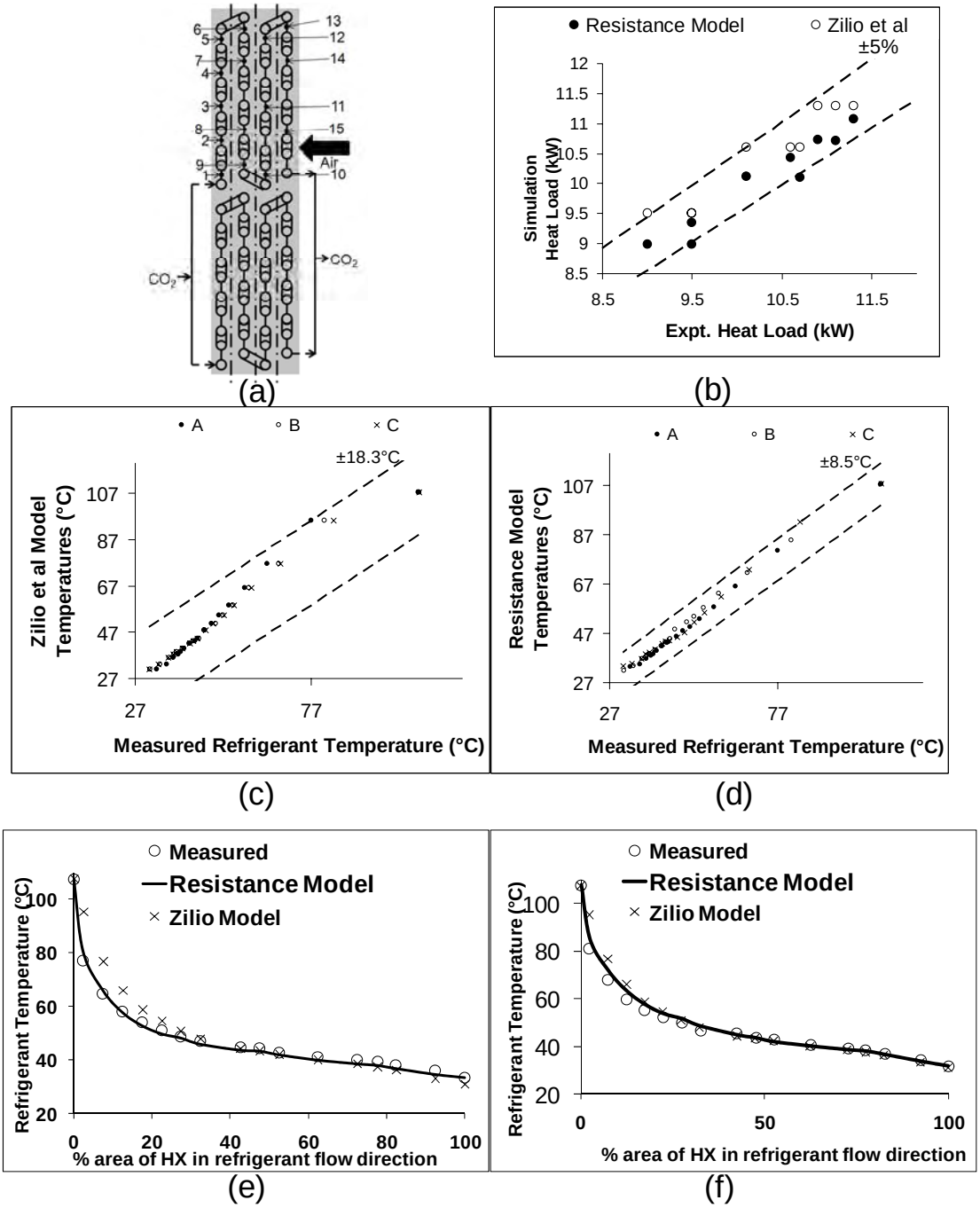


**Figure 2.20: (a) Schematic of the heat exchanger texted by Zilio *et al.*, (b) comparison of measured heat capacities and values predicted by Zilio *et al.* and the new model, comparison of measured and predicted tube bend temperatures by (c) Zilio *et al.* and (d) for the new model. (e) and (f) show the comparison of refrigerant temperature flow profile for two representative cases**

## 2.3 Conclusions

Two segment-by-segment models that account for fin conduction, the "thermal resistance model" and the "heat conduction model", for refrigerant to air heat transfer in fin-and-tube heat exchangers are introduced. The "thermal resistance model", as well as the "heat conduction model", is capable of accounting for heat transfer between tubes through the fins. The "thermal resistance model" uses Fourier's law of conduction to obtain the heat transferred between neighboring tubes in a heat exchanger, whereas the "heat conduction model" solves the two-dimensional heat diffusion equation on the fin surface to obtain heat transfer between tubes. The "thermal resistance model" ignores air heat transfer coefficient. However, it is shown that, with reasonable values (current air-conditioning and refrigeration applications) of air side heat transfer coefficients, it does not have a significant effect on the temperature distribution on the fin surface. It is shown that the heat exchanger performance predicted by the "thermal resistance model" is equivalent to the prediction of the "heat conduction model", after using suitable multipliers for tube-to-tube conduction. However, more analysis needs to be done to analytically obtain these multipliers. The proposed models are validated against two sets of experimental data. The "thermal resistance model" is able to predict the overall heat capacity for experiments conducted by Jin *et al.* within ±3%. It predicts temperatures at 27 tube locations for 36 different test cases within ±3.3°C of the measured values. For experiments conducted by Zilio *et al.*, the "thermal resistance model" predicts all heat capacities within ±5%. All the measured temperatures were predicted within ±8.5°C. The "heat conduction model", which solves the two-dimensional steady state heat diffusion equation, offers greater accuracy in obtaining tube-to-tube heat transfer due

to conduction but it is significantly computational slower than the “thermal resistance model”, which obtains the heat transferred due to conduction using Fourier’s law of heat conduction.

Analysis of experiments of Jin *et al.* shows that the average difference between the bend temperature predicted by Jiang *et al.* model and “thermal resistance model” is 2.8 °C. It is evident that the larger difference in temperature profile between Jiang *et al.* model and “thermal resistance model”, through the heat exchanger is indicative of larger effect of fin conduction. Upon investigation, it was found that 11 out of 36 cases had a difference larger than 2.8°C. All these cases had air velocity less than 1.0 $ms^{-1}$. This suggests that low air speed in the current application accelerates the performance degradation of the gas cooler.

# CHAPTER 3. EFFECT OF CUT FINS ON GAS COOLER PERFORMANCE

Literature shows that presence of tube-to-tube conduction diminishes the performance of fin-and-tube heat exchangers, primarily in gas coolers and evaporators. However, there is little work done to quantify the benefits of cut fins on performance of fin-and-tube heat exchangers. In addition to lack of quantification of various performance benefits of using cut fins in fin-and-tube heat exchangers, there are no design guidelines on location of fin cuts on a fin and tube heat exchanger, given constraints on total length of the cut.

## 3.1 Study of Cut Fins

This study, aimed at quantifying the benefits of cut fins, is structured in four parts aimed at understanding different aspects of cut fins on gas cooler performance

a) Effect of configuration: This is aimed at providing an understanding of the effect of sequence of cuts transverse to the air flow direction on the heat exchanger heat capacity.

b) Effect on fin material savings: The aim of this study is to evaluate the fin material savings after making all possible fin cuts, given a target heat capacity.

c) Effect on evaporator inlet quality: Most gas coolers operate in a vapor compression system, and the aim of this study is to understand the gain in evaporator inlet quality due to enhanced gas cooler performance when all banks are insulated from each other using fin cuts. This provides a much-prized system context to improvements in gas cooler performance.

d) Effect of cut length constraint: The aim of this study is to understand the optimum location of fin cuts perpendicular to air flow direction, given the maximum allowed cut length, for maximum gain in heat capacity over the baseline continuous fin case.

### 3.2 Effect of Configuration

To study the effect of cuts on overall performance of the gas cooler, two configurations of cuts were chosen. The configuration, or the sequence in which fins are cut to separate tubes, directly influences the degree of performance enhancement of the gas cooler. The configurations chosen for this study are shown in Figure 3.1

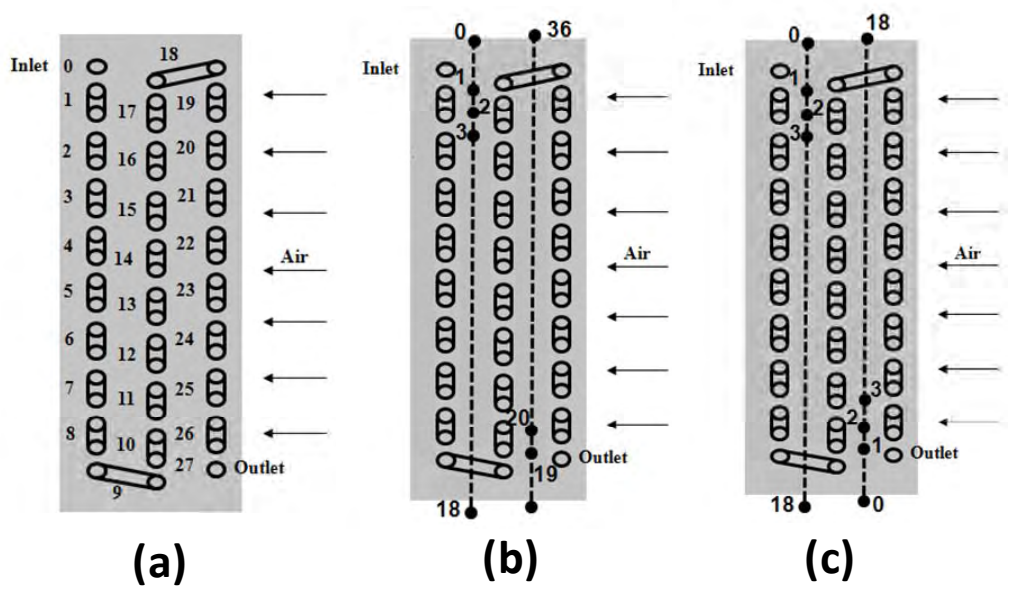


**Figure 3.1: (a) Gas cooler with continuous fins, (b) cuts made in configuration 1 and (c) cuts made in configuration 2**

Figure 3.1(a) shows the baseline case with continuous fins. The first configuration, in Figure 3.1(b), shows that a total of 36 different cut sizes were simulated for all 36 test cases. Cut 0-1 was the first cut, 0-2 being the second and so

on till 18, till one bank was completely insulated. Similarly, cut in the second bank were initiated from bottom to top, all the way until the three tube banks were insulated from each other.

The second configuration, in Figure 3.1(c), shows that a total of 18 different cut sizes were simulated for all 36 test cases. Cut 0-1 was the first cut, which was initiated on both the banks with intent to insulate the tubes with the highest temperature gradient. This was carried on incrementally till cut 0-18, which is identical to 0-36 state of configuration 1.

The underlying reason for selecting these two configurations was separation of the highest temperature tubes through discontinuous fins. The highest temperature gradient between tubes leads to the highest heat transfer due to tube-to-tube conduction, and this leads to significant performance degradation.

The results for studies on the two configurations are presented in the following sections. Firstly, the two configurations are analyzed independently, and effect of changing air speed is presented. This is followed by the comparison of the two configurations in terms of performance enhancement as a function of length of the cut.

### 3.2.1 Configuration 1

To understand the performance response of the heat exchanger to different air velocities, average percent gain in heat capacity, over baseline, was plotted for all three different velocities on $1ms^{-1}$, $2ms^{-1}$ and $3ms^{-1}$. The results, shown in Figure 3.2, indicate that the gain in heat capacity is higher for 38 $gs^{-1}$ refrigerant mass flow rate than 76 $gs^{-1}$ mass flow rate. Results also show that the lowest air velocity test cases

gain the most over base heat capacity for test conditions where mass flow rate for refrigerant is 38gs$^{-1}$. However, for 76 gs$^{-1}$, the heat capacity gain for the lowest air velocity test condition is higher than other cases for the first 18 cuts. However, after cuts ranging from 19-36, the overall heat capacity gain for air velocities 2 ms$^{-1}$ and 3ms$^{-1}$ is higher than the gain for 1ms$^{-1}$.

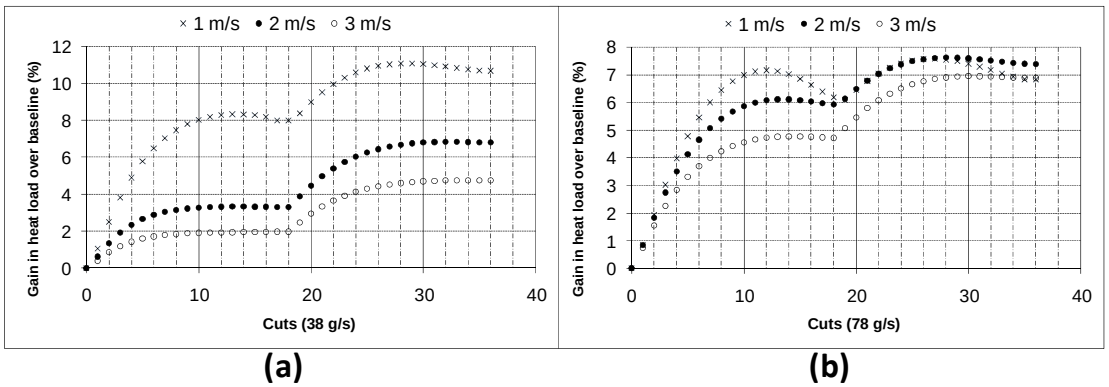


**Figure 3.2: Gain in heat capacity, over baseline, for Configuration 1 for (a) 38 gs$^{-1}$ and (b) 76 gs$^{-1}$**

It must be noted that for the test case with 76 gs$^{-1}$ mass flow rate with 1ms$^{-1}$ air velocity, the overall heat capacity gain due to cuts ranging from 1-18 peaks at 12 cuts and then diminishes. To better understand this phenomena, the heat exchanger temperature profiles of case with 12 cuts is compared that with 18 cuts, and the case with 1 cut is compared to the case with 12 cuts, as shown in Figure 3.3.

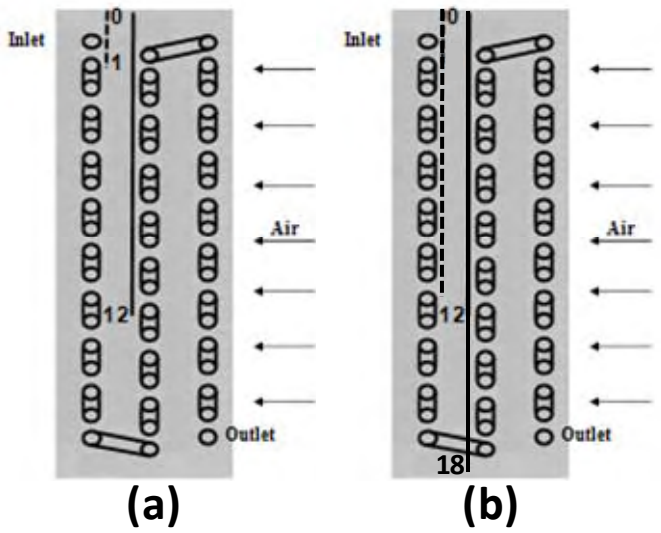


**Figure 3.3: Two cases compared to understand diminishing gain after 12 cuts for cuts 1-18**

Upon comparing the refrigerant temperature profiles for case with 1 cut and 12 cuts, in Figure 3.4(a) and (b), it is seen that the refrigerant temperature drops rapidly for the case with 1 cut in the first 40% of the heat exchanger area due to heat conduction through the fin, but thereafter, the refrigerant temperature increases due to the same phenomena. For case with 12 cuts, the heat conduction doesn't influence the latter part of the heat exchanger, leading to a steady drop in refrigerant temperature. It should be noted that the drop in the last 20% of the heat exchanger length is more significant for case with 1 cut than the case with 12 cuts.

However, for case 12 and case 18 (Figure 3.4 (c) and (d)), the comparison shows that the refrigerant temperature of the case with 12 cuts increases in the last 5 % of the heat exchanger. This is due to the neighboring bank temperature being higher for case 12 than for case 18, which leads to heat conducted to the last 5% of the heat exchanger. Air at $1ms^{-1}$ doesn't have enough heat capacity to remove that excess heat leading to lower heat capacity for case 18.

This phenomenon is explained in Figure 3.4(e), where heat conducted due to fins, heat gained by refrigerant and heat gain by air, are shown for the last segment of the heat exchanger. A positive value of heat indicates that the refrigerant ($Q_{Ref}$), air ($Q_{Air}$) and segment due to conduction ($Q_{Fin}$) are gaining heat, whereas negative value implies the opposite. It should be noted that the air side heat capacity of the last segment is nearly the same for all three cases but the heat conducted by fins is markedly different, as is the refrigerant heat capacity. $Q_{Fin}$ is the highest for case 18 which has the highest temperature gradient with the neighboring tube, followed by case 12 and case 1. Since the air side heat capacities are nearly same, due to same air inlet state in all three cases, and nearly same refrigerant temperature, the refrigerant heat capacity ($Q_{Ref}$) compensates for the difference between $Q_{Fin}$ and $Q_{Air}$, maintaining the energy balance in the segment. This validates the refrigerant temperature behavior in the last 20% of the heat exchanger length for cases 1, 12 and 18, and explains the degrading performance of the heat exchanger from cut 12 to cut 18.

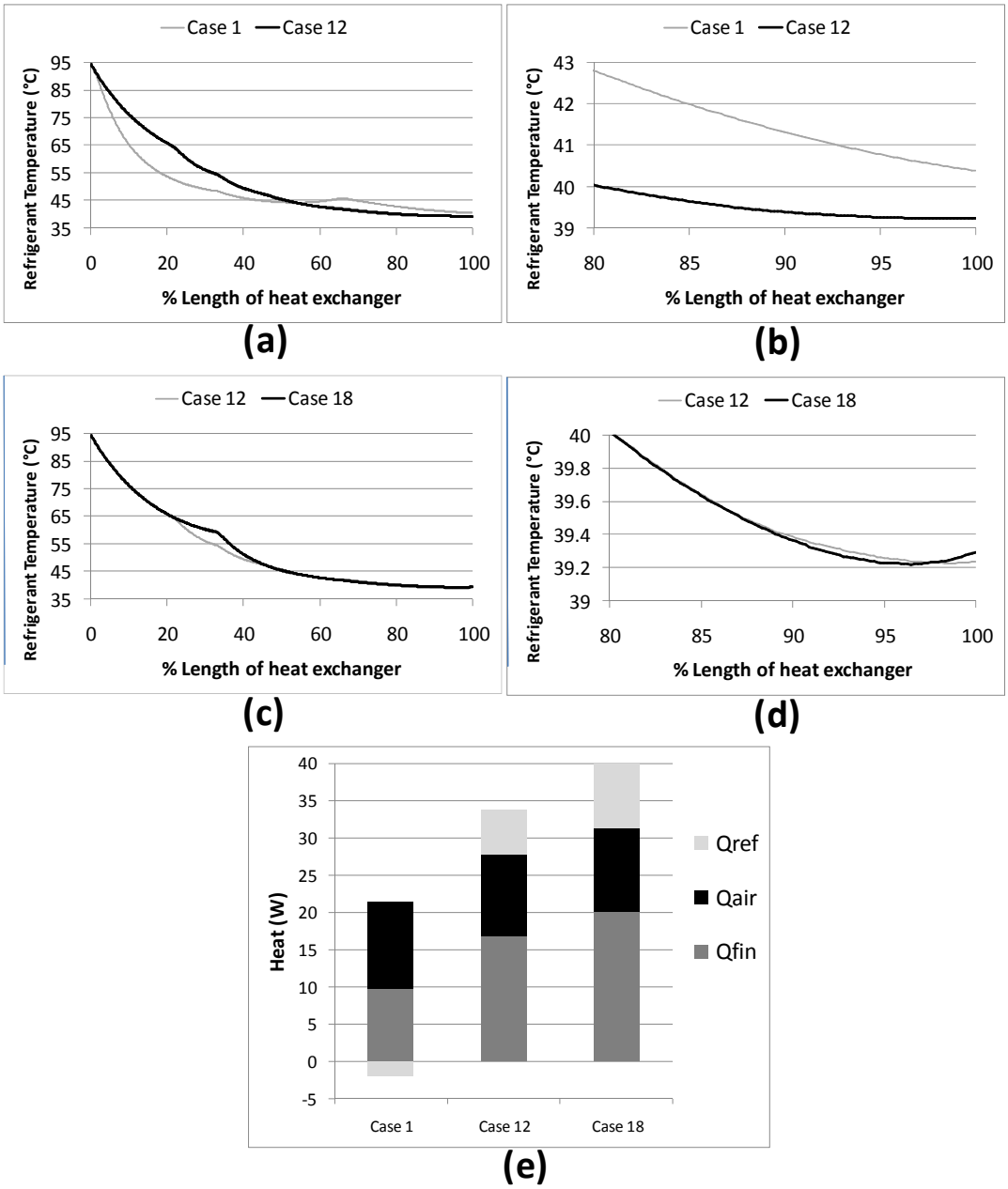


**Figure 3.4: (a) Comparison of temperature profile for case 1 and case 12 and (b) zoomed into the last 20% of the circuit to highlight the difference; (c) comparison of temperature profile for case 12 and case 18 and (d) zoomed into the last 20% of the circuit to highlight the difference, and (e) heat gained by refrigerant, air and segment (due to conduction) in the last heat exchanger segment**

### 3.2.2 Configuration 2

For configuration 2, there are a total of 18 incremental cuts with both the slabs being cut simultaneously as shown in Figure 3.1(c). When gain in heat capacity is

compared, in Figure 3.5 (a) and (b), the maximum gain is for the lowest air velocity test conditions for 38gs$^{-1}$ test cases. However for refrigerant mass flow rate 76gs$^{-1}$, all three air velocity test cases (1ms$^{-1}$, 2ms$^{-1}$, 3 ms$^{-1}$) show a comparable gain in heat capacity. Similar to the configuration 1, for refrigerant mass flow rate 76 gs$^{-1}$ and 38 gs$^{-1}$, and air velocity 1ms$^{-1}$, after a certain number of cuts, any further cuts lead to a diminishing gain in heat capacity.

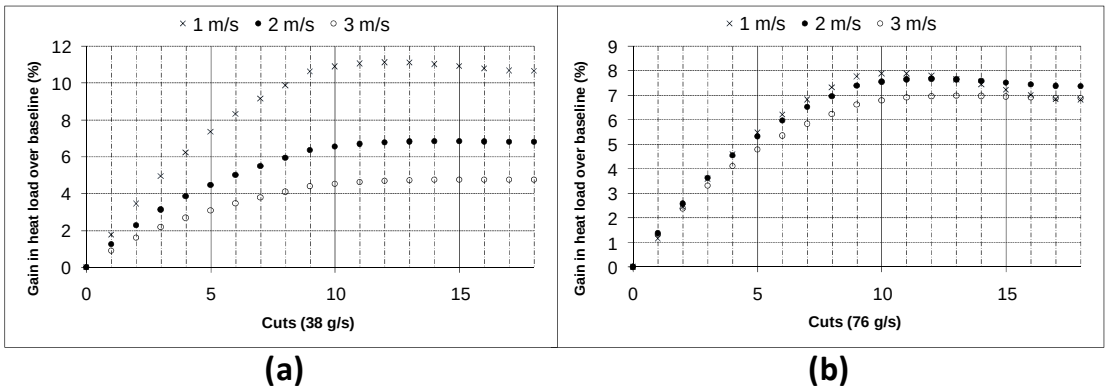


**(a)** **(b)**

**Figure 3.5: Gain in heat capacity, over baseline, for Configuration 2 for (a) 38 gs$^{-1}$ and (b) 76 gs$^{-1}$**

3.2.3 Comparing configuration 1 and configuration 2

To highlight the significance of location of cut in addition to the length of cut, along with the dependence of refrigerant flow rate and conditions, the average gain in heat capacity for all three velocity test conditions (1ms$^{-1}$, 2ms$^{-1}$, 3 ms$^{-1}$) is compared for non-dimensionalized cut length for 38gs$^{-1}$ and 76 gs$^{-1}$ refrigerant mass flow rate test conditions. From Figure 3.6(a), it is evident that if only up to 36% of the heat exchanger can be cut, configuration 1 gives greater gain than configuration 2 for 38gs$^{-1}$ refrigerant mass flow rate. For cut length between 36% and 80%, configuration 2 provides greater heat capacity gain than configuration 1. For 76 gs$^{-1}$ mass flow rate test conditions, the heat capacity gain in configuration 2 is higher than configuration 1

if the cut length is between 20% and 80%, as shown in Figure 3.6(b). For all other cut lengths, the gain in heat capacity from the two configurations is similar.

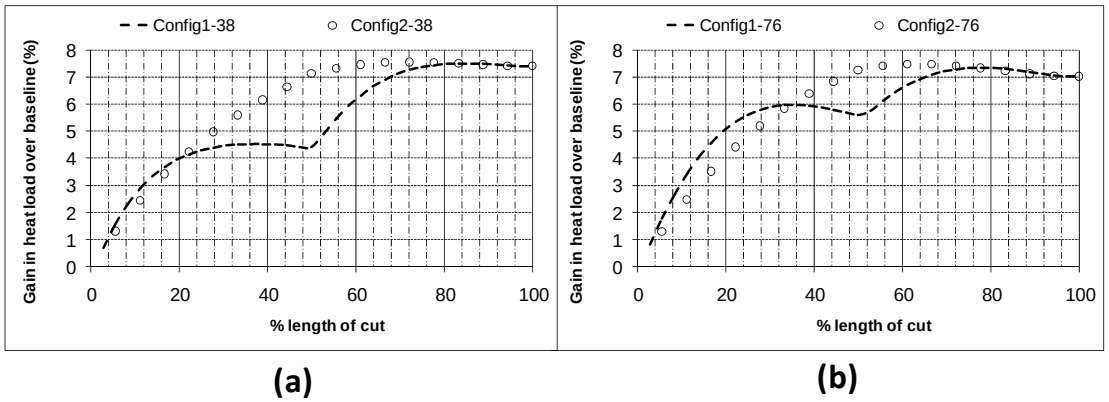


**Figure 3.6: Comparison of configuration 1 and configuration 2 for refrigerant flow rates of (a) 38 $gs^{-1}$ and (b) 76 $gs^{-1}$**

## 3.3 Effect on fin material savings

Considering the enhancement in the gas cooler heat capacity after fin cuts, it is important to understand the savings in fin material, given a target heat capacity. This converse problem comprises of fixing a heat capacity, and using Singh *et al.*'s (2008) model to simulate the test cases by varying the fin density from 8 to 20 fins per inch. The study was not extended beyond 20 fins per inch to avoid the pinch off point of heat exchanger performance.

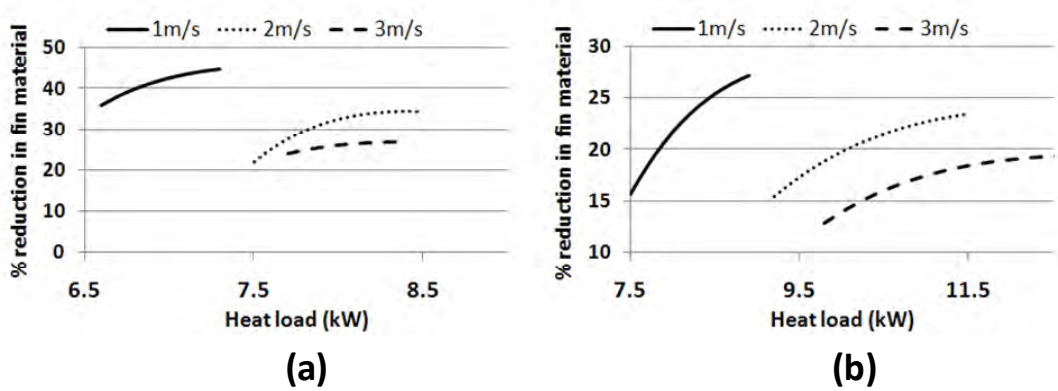


**Figure 3.7: The % reduction in fin material used for refrigerant flow rate of (a) 38 $gs^{-1}$ and (b) 76 $gs^{-1}$**

It can be seen that the reduction in fin material for 38 $gs^{-1}$ refrigerant mass flow rate are greater than 76 $gs^{-1}$. For a given mass flow rate, the savings are the greatest for the lower air speeds, and reduce with increasing air speed. Additionally, the gain in savings in fin material diminishes with increasing fins density.

### 3.4 Effect on evaporator inlet quality

Assuming an evaporator inlet temperature of 7.2 °C, the effect of enhanced gas cooler performance on the evaporator inlet quality was analyzed. Results are shown in Figure 3.8.

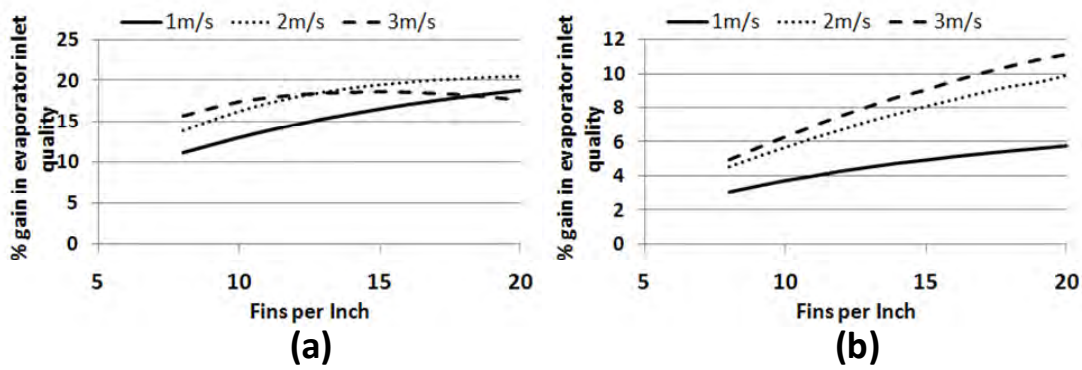


**Figure 3.8: Gain in evaporator inlet quality at 7.2 °C evaporating temperature for refrigerant mass flow rates of (a) 38 $gs^{-1}$ and (b) 76 $gs^{-1}$**

It can be seen that the gains in evaporator inlet quality for 38 $gs^{-1}$ mass flow rate are higher than 76 $gs^{-1}$, in general. For a constant refrigerant mass flow rate, the % gains are the lowest for lowest air speeds and increase with increasing air speeds. However, as the gas cooler gets closer to its pinch-off region, the gains start diminishing as can be seen in Figure 3.8(a). This is because the gas cooler with discontinuous fins pinches off at lower fins per inch than the gas cooler with continuous fins.

### 3.5 Effect of Cut Length Constraint

In this study, the fin cut length separating tube banks (or rows) was restricted to 25%, 50% and 75% of total fin cut length available. Following this constraint, the a multi-objective genetic algorithm (MOGA) was employed to maximize the heat capacity of the gas cooler by cutting the fin sheets as long as the length of all cuts didn't exceed the given length constraint. Considering the similarity of response of all 36 cases to fin cuts for configurations 1 and 2 owing to the common circuitry, one test case is chosen for this analysis. The test case is

Air speed: $1 ms^{-1}$

Refrigerant mass flow rate: $38 gs^{-1}$

Air temperature: 29.4 °C

Refrigerant pressure: 9 MPa

Results from the MOGA are summarized in Figure 3.9 (a) through (c).Owing to a lack of a constraint in the optimization problem to ensure "contiguous cuts", the optimizer cut fins in a non-contiguous manner. Due to this, the cuts were modified to be contiguous as shown in Figure 3.9 (d) through (f) while still maintaining the cut length constraints of 25%, 50% and 75% of total fin cut length available. To further emphasize the minor nature of the modifications made to the MOGA results, normalized heat capacity of all cases is shown in Figure 3.10.

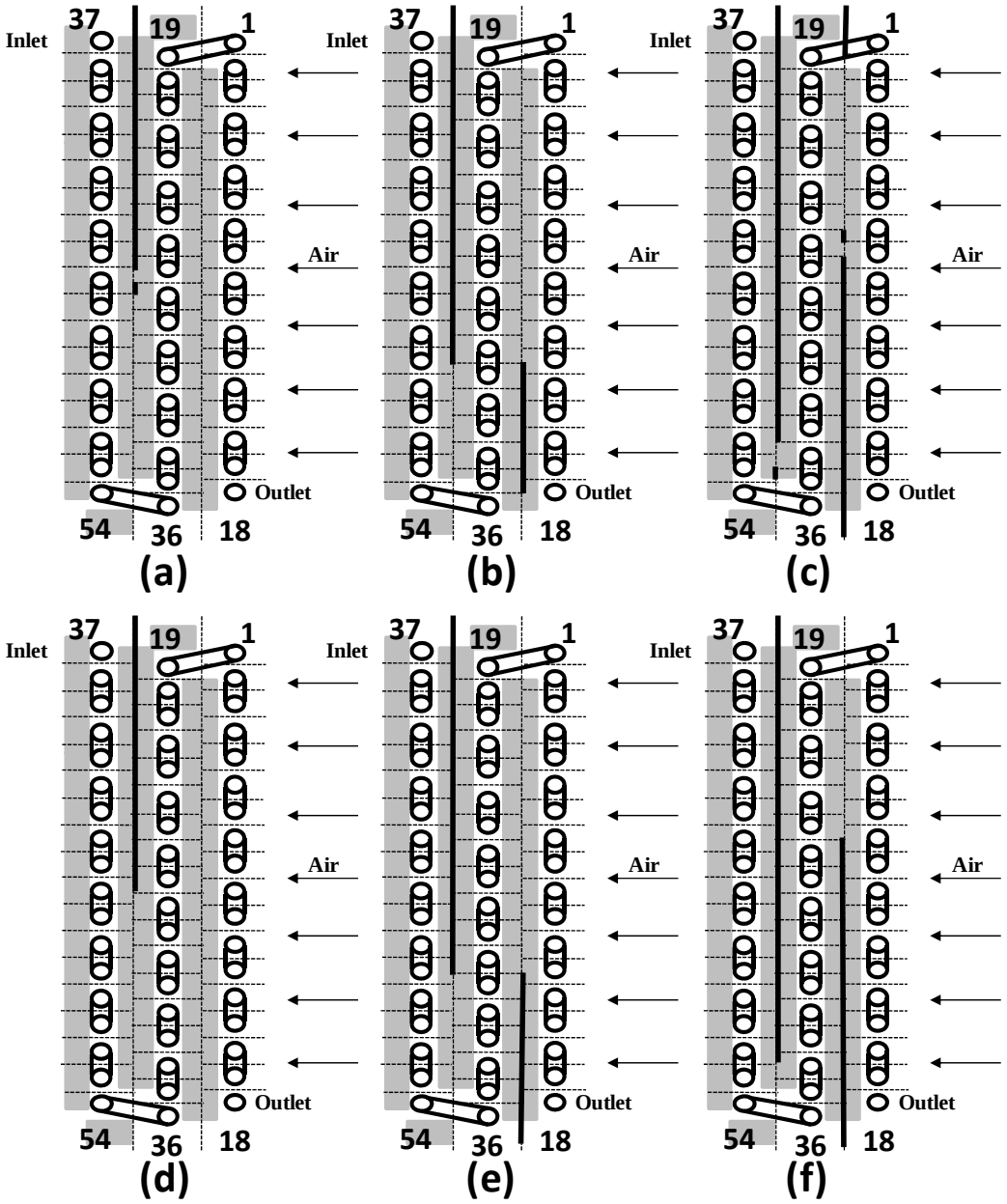


**Figure 3.9: Fin cut locations determined by the MOGA for (a) 25%, (b) 50% and (c) 75% cut length constraint; modified fin cuts based on feasibility of implementation for (d) 25%, (e) 50% and (f) 75% cut length constraint.**

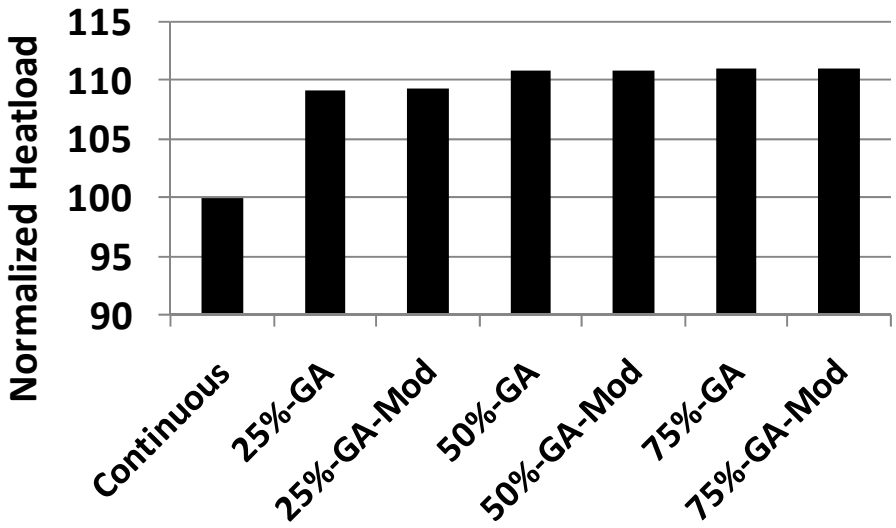


**Figure 3.10: Normalized heat capacity of the baseline continuous case, 3 MOGA results and 3 MOGA-modified cases**

To develop a phenomenological understanding of the fin cut locations, the heat gained by the refrigerant in each tube was studied. This follows from the original objective which was to maximize the refrigerant heat capacity in the gas cooler. Figure 3.11 compares the heat gained by the refrigerant for the continuous baseline case with the three cut length constraint cases. It is evident that for all three cases, the cuts are preferentially placed by the optimizer in a manner that ensures the refrigerant doesn't gain heat in any of the tubes. The locations where the most heat is gained by the refrigerant are amongst the first to be insulated via a fin cut. The heat gained or lost by the refrigerant is determined by an energy balance on the air side, the refrigerant side and the heat transferred through the fins.

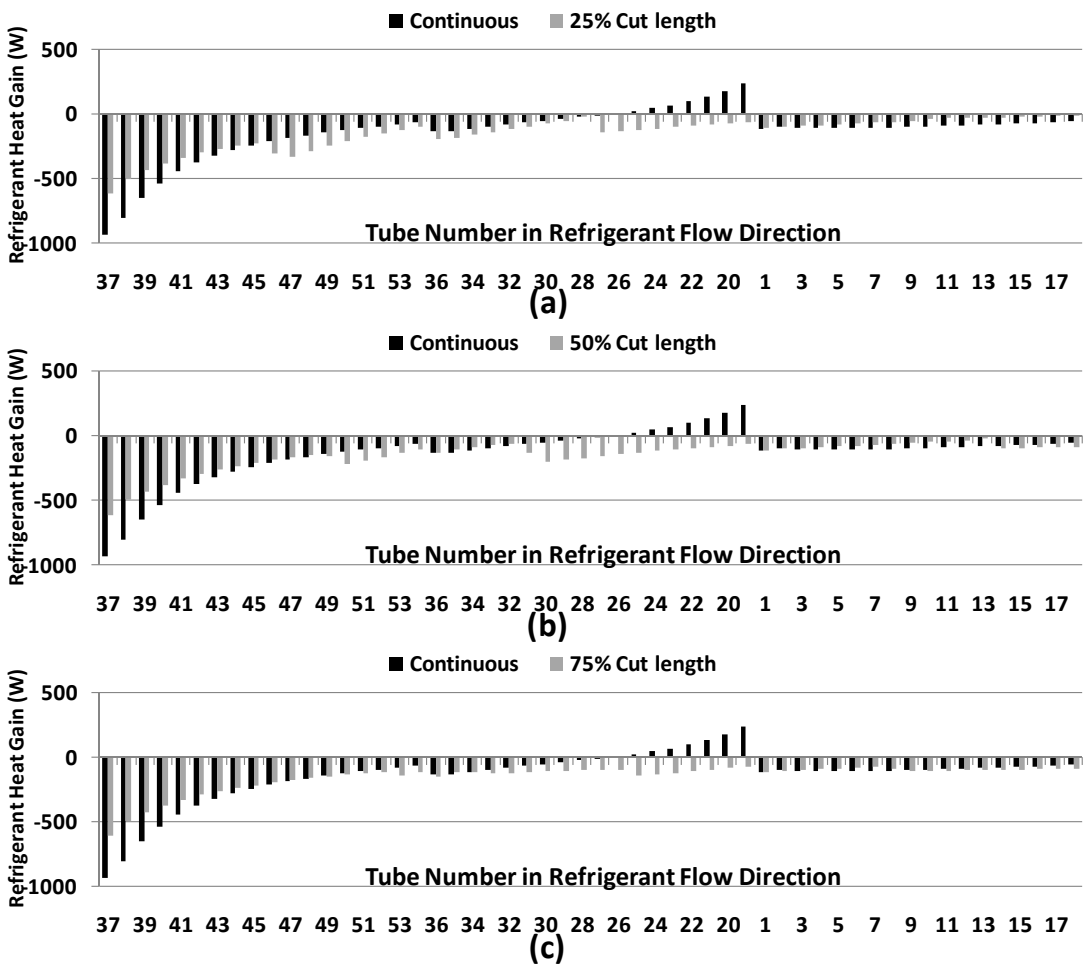


**Figure 3.11: Heat gained by the refrigerant in each tube before and after fin cuts were placed for (a) 25%, (b) 50% and (c) 75% cut length constraint**

## 3.6 Conclusions

Using a validated heat exchanger model capable of simulating cut and continuous fins, the improvement in heat exchanger performance due to discontinuous fins is shown using several wide ranging criteria. To understand effect of cut configurations, two different configurations of cut patterns were studied. It is shown that with increasing cut length, the gain in heat capacity increases in most cases. It was shown that for certain test conditions, the gain in heat capacity can be up to 12% over the baseline. In terms of fin material savings, at lower heat capacities, lower refrigerant

and air flow rates, the fin material savings due to the presence of fin cuts can be as high as 45%. Fin material savings are lower at higher air speeds for a given refrigerant mass flow rate, and for a given air speed, lower for higher refrigerant flow rates. For the same heat capacity and constant refrigerant flow rate, the fin material savings are higher for lower air speeds, and decrease with increasing air speed. In terms of evaporator inlet quality, the gains in quality are uniformly higher for lower refrigerant flow rates than those for higher refrigerant flow rates, with % gain in quality as high as 20%. For a given refrigerant flow rate, the gains are higher for higher air speeds, and reduce for lower air speeds. The gains start diminishing with increasing fins per inch, as the specific cases start to approach the pinch-off point. Finally, studies with a fin cut length constraint in place show that, in order to maximize heat capacity, it is suggested that cuts be placed preferentially at locations that ensure the refrigerant doesn't gain heat. While this might seem trivial, the refrigerant heat capacity is a function of heat transfer due to fin conduction as well as air side heat transfer, both of which together influence the refrigerant side heat capacity.

# CHAPTER 4. MODELING OF FIN-AND-TUBE HEAT EXCHANGERS WITH ARBITRARY FIN SHEET

## 4.1.1 Heat Exchanger with Arbitrary Fin Sheet

Most existing fin-and-tube heat exchangers have standard tube configurations like inline or staggered with uniform tube sizes, tube pitches, tube locations and a rectangular footprint, as shown in Figure 4.1(a).

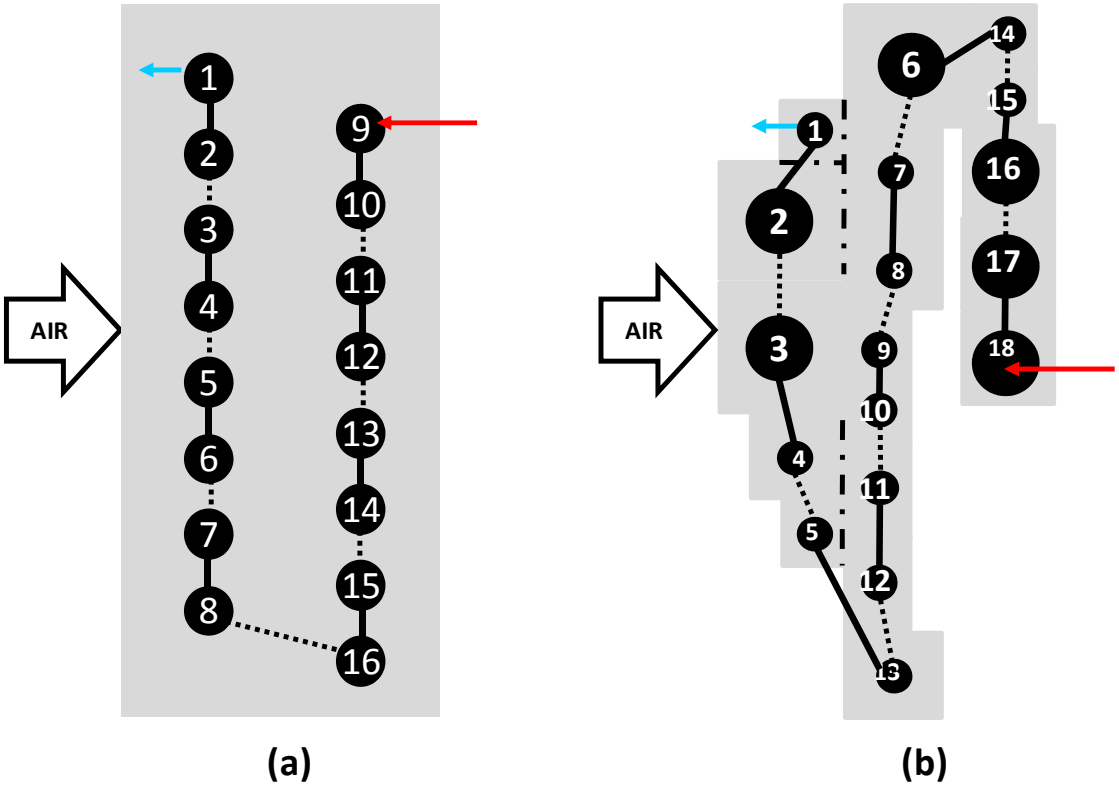


**Figure 4.1: (a) Standard staggered configuration for a fin-and-tube heat exchanger and (b) arbitrary fin sheet for fin-and-tube heat exchanger**

This is dictated by several aspects, which include ease of manufacturing and familiarity with the design process, in general. However, restricting the design to such uniformity often doesn't push the limits of what can be achieved in terms of performance by adapting the coil design to flow conditions of refrigerant and air side

as well as envelope constraints. There are several degrees of freedom which can be exploited to improve the design of a fin-and-tube heat exchanger such as:

1) Tube size: Recent studies have led to a better understanding of the dependence of refrigerant flow regimes during evaporation or condensation on heat transfer coefficients and pressure drop (Cheng, *et al.*,2008). These flow regimes have a strong correlation with the refrigerant mass flux through a tube. This knowledge empowers engineers to incorporate different tube sizes to maximize heat transfer coefficients while minimizing pressure drop.

2) Tube pitch: Air flowing into a heat exchanger can have significant maldistribution due to several factors like location of fan or conditions downstream of the heat exchanger. This maldistribution implies that tube pitches and locations inside a heat exchanger need to be designed so as to maximize the air side performance, i.e., increase overall UA while maintaining the air side pressure drop within acceptable limits.

These are only a few opportunities available in terms of optimizing the design of a fin-and-tube heat exchanger. Ultimately, the basis of such increased design flexibility with an "arbitrary fin sheet" is to provide optimum conditions for heat transfer, while minimizing pressure drop.

To facilitate the design process, it is imperative to have a design-simulation tool which can model a heat exchanger with arbitrary fin sheet. Such a model should have the capability of modeling a fin-and-tube heat exchanger with, all or some, of the following characteristics, as shown in Figure 4.1(b).

1) Variable tube diameters: This feature allows an engineer to change the mass flux per tube to obtain flow regime conducive to efficient heat transfer and reduced pressure drop.

2) Variable tubes per bank, tube pitches and tube locations: This feature allows the engineer to essentially break free from the concept of tube banks. One tube can be in several banks simultaneously, in terms of how the air propagates through the heat exchanger.

3) Non-rectangular footprint: This feature allows an engineer to design a heat exchanger tailored for highly restrictive footprints and spaces.

4) Internal jagged edges: This facilitates an engineer in "wrapping" a coil around a fan, leading to a more integrated and compact fan-coil unit.

5) Variable fin cut locations: This feature further allows a user in preventing losses associated with tube-to-tube conduction on a selective basis. Singh *et al.* (2008a) showed the influence of selective cuts on a fin-and-tube heat exchanger performance.

These capabilities provide significant challenges to the modeling approach of conventional heat exchangers, especially in the way air flow is modeled.

4.1.2 Modeling Approach

The modeling approach on the refrigerant side is similar to the heat exchanger model presented in 2.1.1. The modeling of arbitrary fin sheet heat exchanger is based on that approach.

There are two significant modeling challenges posed by arbitrary fin sheets.

1) Due to the lack of pattern in terms of tube locations, sizes, pitches, etc.; the model must allow detailed heat exchanger specification. Further, fin-tubes control volumes interact with their neighbors through air propagation and tube-to-tube heat conduction, as shown in Figure 4.2. In the schematic, tube 4 has only one air side neighbor which is tube 1, whereas it has three conduction neighbors, tubes 3, 5 and 6.
2) Arbitrary fin sheets lead to arbitrary staggering of fin-tube control volumes with respect to each other. For standard (non-arbitrary) tube configurations, air flow rate can be propagated through the heat exchanger in a repeatable pattern for all fin-tube control volumes. However, in an arbitrary fin sheet, this is not the case. For instance, as shown in Figure 4.2, tube 5 is downstream from tube 1 and tube 2, and will receive air in different amounts, whereas tube 4 is downstream of tube 1 and will receive all its air from tube 1.

Addressing these two challenges requires a Cartesian grid on which the fin sheet is modeled, along with algorithms to process information for air propagation and heat conduction.

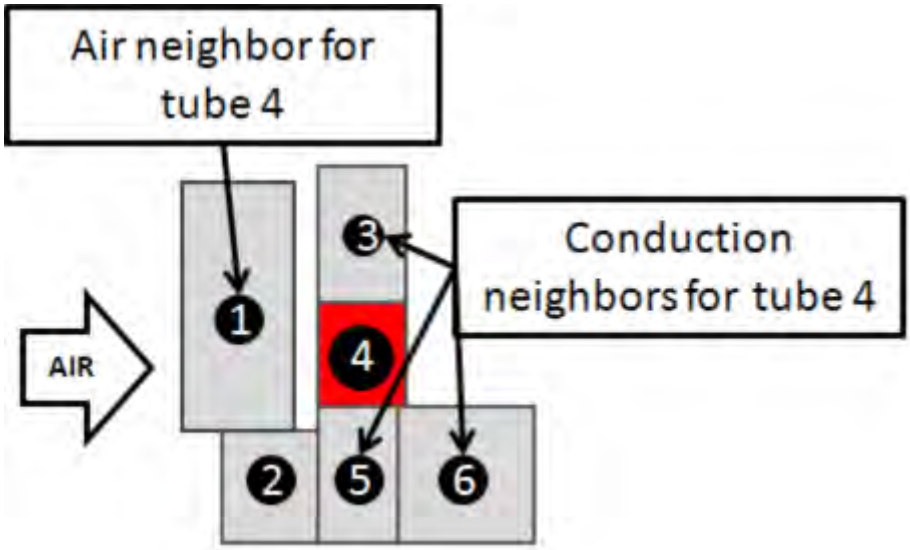


**Figure 4.2 Information obtained by processing Cartesian grids using heat exchanger specifications**

Prior to discussion of the algorithms, it is important to discuss relevant assumptions.

4.1.3 Modeling Assumptions

The assumptions of the model are as follows:

1) Air is assumed to propagate perpendicularly through the heat exchanger. Arbitrary tube arrangement of the kind shown in schematics in this paper, can lead to significant maldistribution inside the coil. However, physical prototypes, like the one validated here, do not have such highly arbitrary tube arrangements or sizes, and it can be assumed that air flows perpendicularly through the coil.

2) As air propagates through a coil, it mixes thoroughly in a fin-and-tube control volume before heat transfer occurs.

Air side heat transfer coefficients and pressure drop values are obtained through existing correlations which are applied on a segment by segment basis.

### 4.1.4 Air Side Propagation

The heat exchanger model requires that air is propagated through a heat exchanger. For a standard configuration, this is a fairly direct and mathematically, uncomplicated. For an inline configuration, air state is propagated downstream, as is, to the logical downstream control volume. For staggered configurations, air state from two upstream control volumes is mixed equally, and propagated to the control volume downstream. Clearly, in the case of an arbitrary fin sheet, either of the two above-stated laws cannot be applied.

To implement air side propagation, a mixing law weighted by the interacting face areas of different control volumes was developed. This concept decomposes to one dimensional problem where only edges interact because in the tube-wise direction, all control volumes have the same dimension, i.e. segment length. The weighted averages for the mixing law was obtained using the methodology explain in Figure 4.3.

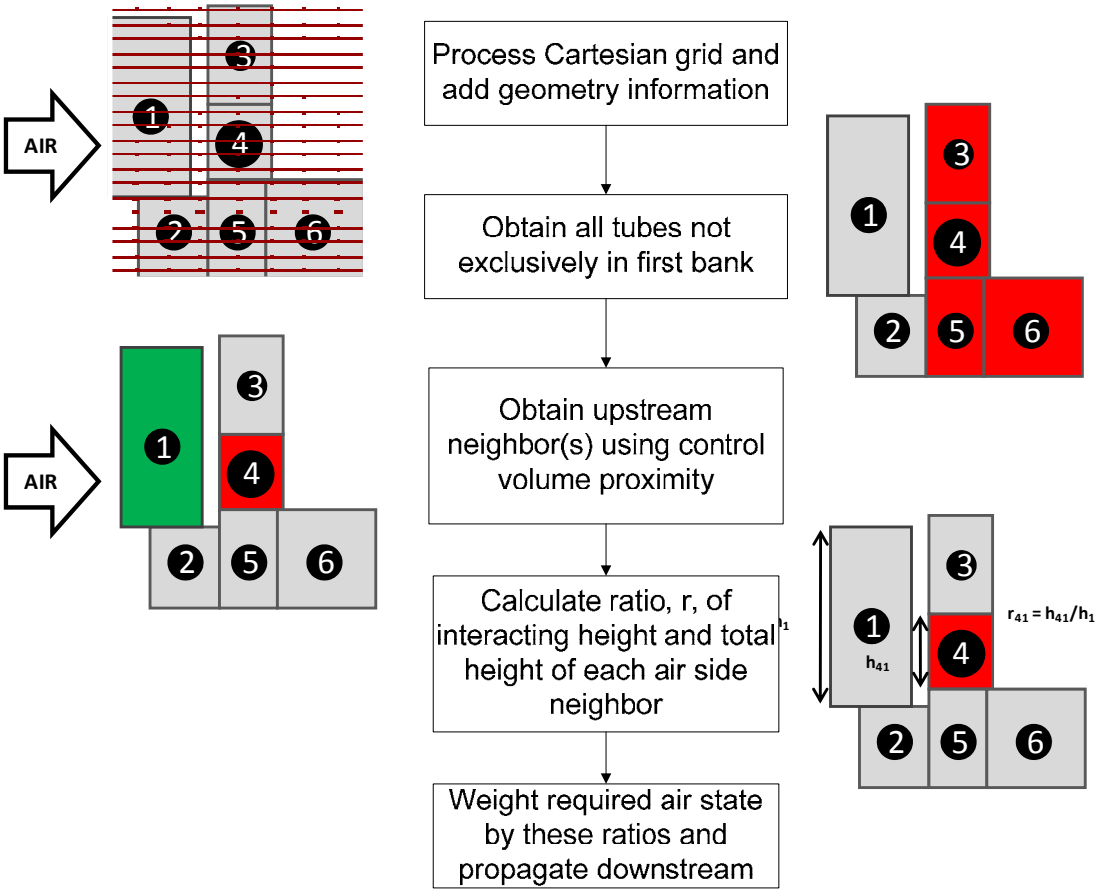


**Figure 4.3: Methodology for obtaining weights for mixing of air stream**

This is further explained using Figure 4.4.

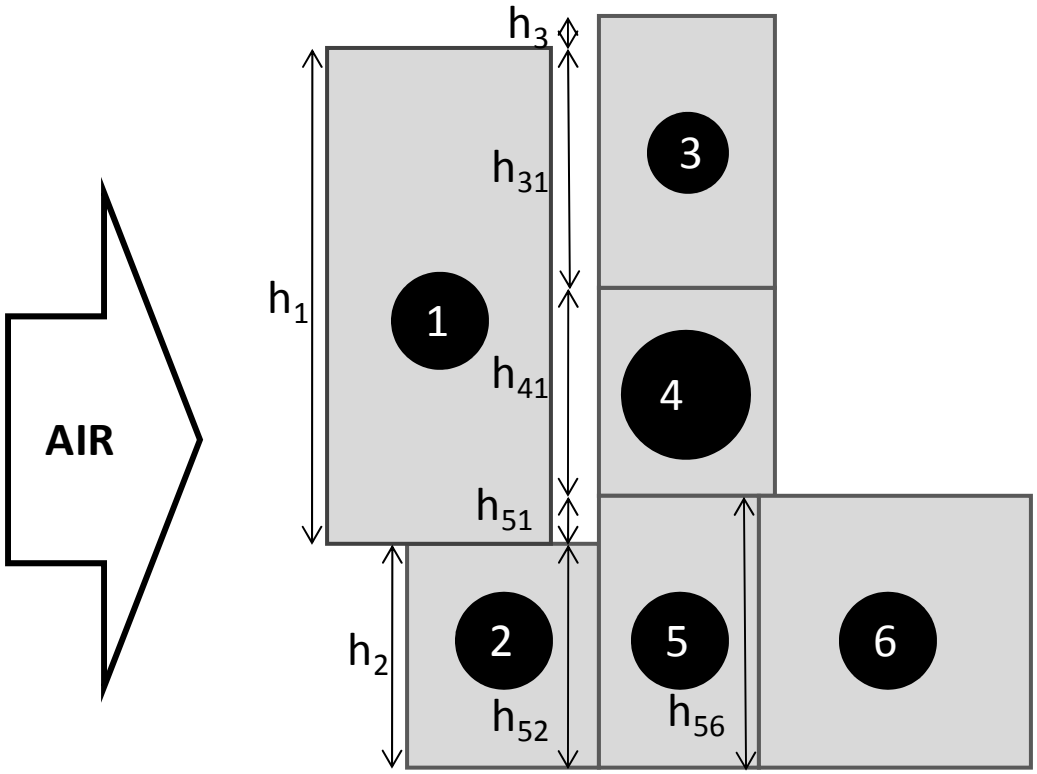


**Figure 4.4: Schematic to explain air propagation through heat exchanger**

Let the mass flow rate entering the exposed faces of tube-1 be $mf_1$, tube-2 be $mf_2$ and tube-3 be $mf_3$. Applying weighted mixing laws based on methodology shown in equation (4.1) will lead to the following mass flow rates for control volumes that are not exclusively part of the heat exchanger face.

$$
\begin{aligned}
m_3 &= mf_3 + \frac{mf_1 \cdot h_{31}}{h_1} \\
m_4 &= \frac{mf_1 \cdot h_{41}}{h_1} \\
m_5 &= \frac{mf_1 \cdot h_{51}}{h_1} + \frac{mf_2 \cdot h_{52}}{h_2} \\
m_5 &= \frac{m_5 \cdot h_{56}}{h_5}
\end{aligned}
\tag{4.1}
$$

4.1.5 Simulation Study

To completely understand the challenges and the entire range of capabilities of the heat exchanger model for arbitrary fin sheet fin-and-tube heat exchanger, a simulation study was carried out exploring one specific example.

*4.1.5.1 Description of Coil used for Simulation Study*

As described earlier, for modeling purposes, an arbitrary fin heat exchanger is assembled using control volumes for each tube. The test (different from the experimental coil) coil is a hot water coil, shown in Figure 4.1(b), while the overall specifications for the heat exchanger are shown in Table 4.1.

**Table 4.1: Overall specification of test heat exchanger**

| Parameters | | | Correlations | |
|---|---|---|---|---|
| Number of Segments | 10 | --- | Air Side HTC | Kim-Youn-Webb |
| Tube Length | 0.61 | m | Air Side DP | Kim-Youn-Webb |
| Tube Thickness | 0.3 | mm | Refrigerant Side HTC - Liquid | Gnielinski |
| FPI | 15 | fpi | Refrigerant Side DP - Liquid | Churchill |
| Fin Thickness | 0.0043 | in | | |
| Fin Type | Plain | --- | | |

Table 4.2 lists control volumes that are separated by discontinuous fins or fin cuts.

**Table 4.2: Control volumes separated by discontinuous fins**

| Control Volume 1 | Control Volume 2 |
|---|---|
| 1 | 6 |
| 1 | 7 |
| 1 | 2 |
| 2 | 7 |
| 2 | 8 |
| 4 | 10 |
| 4 | 11 |
| 5 | 11 |
| 5 | 12 |

The specifications of each control volume at shown in Table 4.3.

**Table 4.3: Control volumes used to model hypothetical heat exchanger (all dimensions in m)**

| Tube Number | Tube Inner Diameter | Center x co-ordinate | Center y co-ordinate | Control volume width | Control volume height |
|---|---|---|---|---|---|
| 1 | 0.005 | 0.015 | 0.020 | 0.01 | 0.01 |
| 2 | 0.01 | 0.010 | 0.035 | 0.02 | 0.02 |
| 3 | 0.01 | 0.010 | 0.055 | 0.02 | 0.02 |
| 4 | 0.005 | 0.013 | 0.073 | 0.015 | 0.015 |
| 5 | 0.005 | 0.015 | 0.085 | 0.01 | 0.01 |
| 6 | 0.01 | 0.030 | 0.010 | 0.02 | 0.02 |
| 7 | 0.005 | 0.028 | 0.028 | 0.015 | 0.015 |
| 8 | 0.005 | 0.028 | 0.043 | 0.015 | 0.015 |
| 9 | 0.005 | 0.025 | 0.055 | 0.01 | 0.01 |
| 10 | 0.005 | 0.025 | 0.065 | 0.01 | 0.01 |
| 11 | 0.005 | 0.025 | 0.078 | 0.015 | 0.01 |
| 12 | 0.005 | 0.025 | 0.093 | 0.015 | 0.01 |
| 13 | 0.005 | 0.028 | 0.108 | 0.015 | 0.015 |
| 14 | 0.005 | 0.045 | 0.005 | 0.01 | 0.01 |
| 15 | 0.005 | 0.045 | 0.015 | 0.01 | 0.01 |
| 16 | 0.01 | 0.045 | 0.028 | 0.015 | 0.015 |
| 17 | 0.01 | 0.045 | 0.043 | 0.015 | 0.015 |
| 18 | 0.01 | 0.045 | 0.058 | 0.015 | 0.015 |

Air inlet condition was set to be 293.15 K with 50% relative humidity. Air inlet velocity was given a one-dimensional, i.e. height-wise maldistribution, such that air mass flow rate entering each control volume exposed on the heat exchanger face received 28.0 $gs^{-1}$ of air, as shown in Figure 4.5: Air mass flow rate initialization for test case Figure 4.5(a). This led to a total air mass flow rate of 224 $gs^{-1}$. This velocity profile was chosen to display the capability of the heat exchanger model in accounting for velocity maldistribution. Further, this is also used to compare analytical air mass flow rate propagation with grid based air mass flow rate propagation in Figure 4.5 (b).

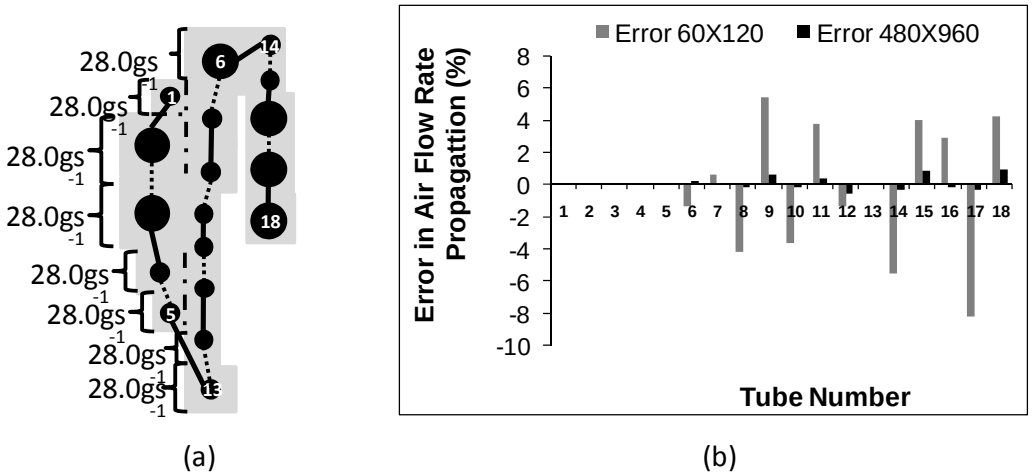


**Figure 4.5: Air mass flow rate initialization for test case**

*4.1.5.2 Analysis of Grid-Based Calculations*

Whenever spatial discretization is employed, it comes with the cost of grid dependence of all associated variables. For the test case, the variables dependent on grid spacing are:

1) Tube-to-tube heat transfer due to conduction

2) Air propagation

Grid dependence of tube-to-tube heat transfer was addressed in (Singh*, et al.*,2008b) where the "heat conduction model" was introduced. In this section, we will focus on grid dependence of air propagation.

Conservation of air mass flow rate is absolutely critical to any heat exchanger model. Therefore, it is imperative that dependence of air propagation on grid density is investigated. In order to study this, an air mass flow rate of 28 $gs^{-1}$ was set to all exposed "face" areas of the test heat exchanger as shown in Figure 4.5(a).

Using geometric calculations, analytical mass flow rates for all tubes downstream of the face were calculated and compared with two different grid densities, 60 by 120 and 480 by 960. Figure 4.5(b) shows the percent error due to the two grid sizes when compared to an analytical propagation scheme. Errors for tubes 1 through 5 are zero because they use initialized air flow rates, as is. This is because these tubes are exclusively on the face, and don't use the model's propagation scheme. For the tubes downstream, the error for the coarser grid is for individual control volumes and it lies between -8% and +6%. Though, due to the nature of the grid based propagation scheme, the average error per control volume is -0.26%. In terms of overall mass conservation, however, the total error is 0.023%. The error for the finer grid for individual control volumes lies well within ±1 % and the average error per control volume is +0.09%. The error in overall mass conservation is 0.02%.

This study shows that overall mass flow rate for both coarse and fine grids is conserved acceptably; the error for individual control volumes for coarse grid is higher and requires the use of fine grids. It must also be mentioned by extent of grid refinement is determined by the ratio of the heights of two interacting control

volumes, where ratios much greater than or much less than 1.0 requiring greater grid refinement.

*4.1.5.3 Result of Simulation Study*

The test coil was simulated using the "heat conduction model" which allows the engineer to study temperature distribution over the entire fin sheet, using widely used correlations for heat transfer and pressure drop (Kim*, et al.*,1999, Schlichting and Gersten,2000, Gnielinski,1976). Figure 4.6(a) shows the average water temperature and the tube wall temperature per tube, in the direction of water flow through the heat exchanger. It is interesting to note, in Figure 4.6(b), that the difference between water temperature and wall temperature changes for every tube. This is dependent on factors such as state of the air, conduction to neighboring tubes and heat transfer areas of control volumes associated with tubes. Based on the fundamental law of heat transfer, the difference between wall and water temperature will be proportional to the heat transfer from water to wall, or vice versa.

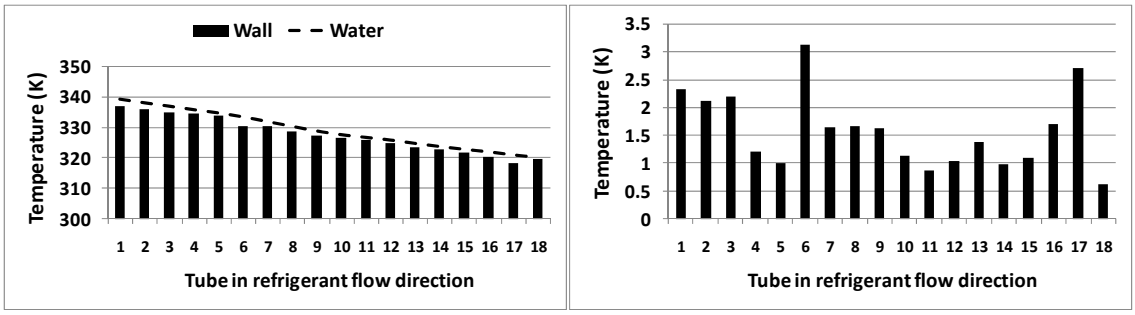


**(a)** **(b)**

**Figure 4.6: Water and wall temperature in water flow direction (a) and difference in water and wall temperature averaged for each tube (b)**

Figure 4.7 shows the temperature distribution on the fin corresponding to the set of control volumes at furthest depth into the page, corresponding to Figure 4.1(b).

It is interesting to note that while the wall temperature continues to drop in refrigerant flow direction, in general, it is seen to increase going from tube 6 to tube 7 (number 6 to 7 in refrigerant flow direction) and tube 2 to tube 1 (number 17 to 18 in refrigerant flow direction). This can be attributed to several factors such as neighboring wall temperatures, state of incoming air, heat transfer areas etc. The advanced heat exchanger model allows an engineer to study factors such as temperature distribution, effect of discontinuous fins in much greater detail than existing models.

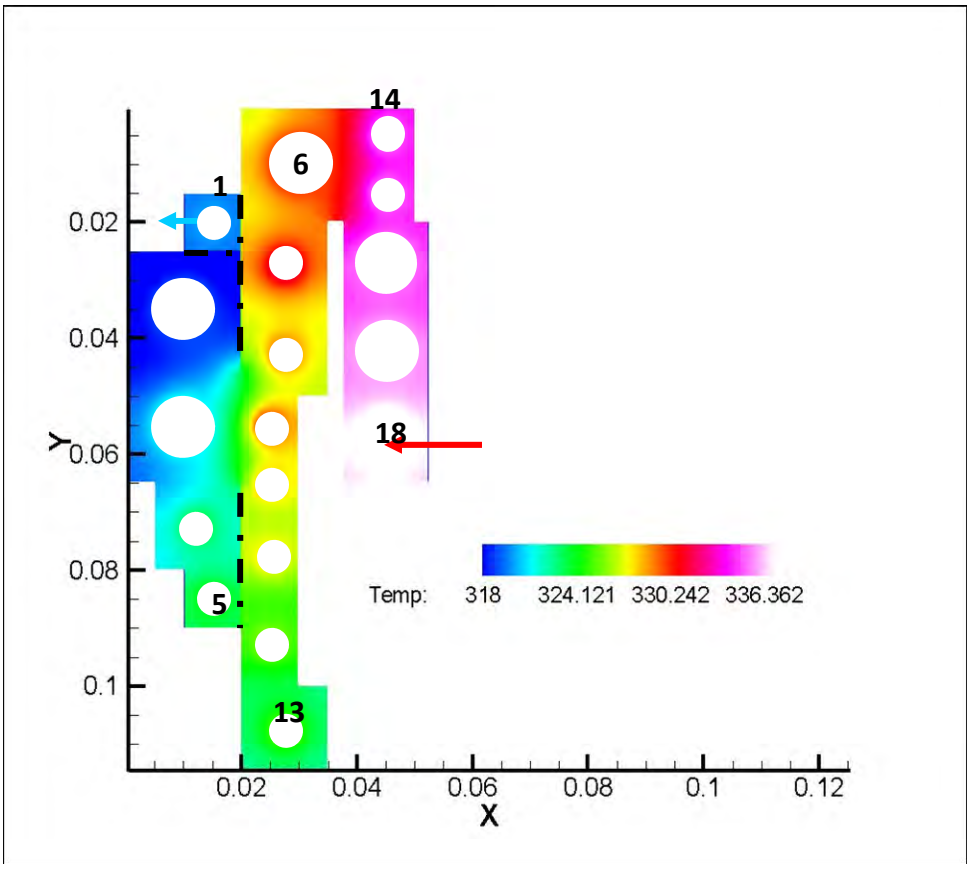


(a)

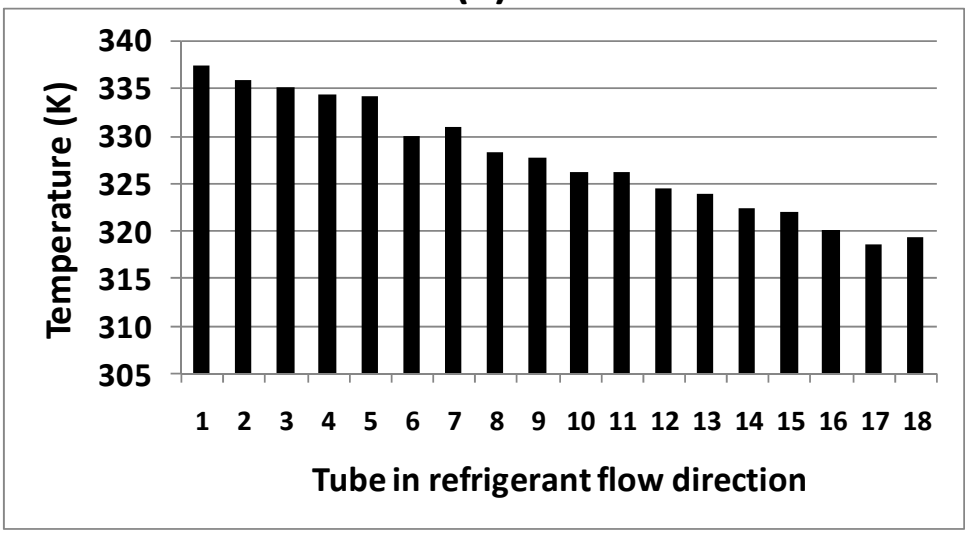


(b)

**Figure 4.7: Temperature distribution on arbitrary fin sheet and corresponding wall temperatures**

Figure 4.8 shows the air temperature distribution at the exit of the heat exchanger, on a tube-by-tube basis, which clearly reflects the arbitrary nature of the coil. Numbers on the y-axis from 1 through 9 represent tubes 14 through 18 and tubes 10 through 13 which form the coil's exit face or "last bank". Air gains the most heat as it passes through the thickest part of the coil, while it is least heated as it passes through the narrowest part of the coil. Details of this nature provide the capability of tailoring the heat exchanger geometry to desired outlet air temperature profile, a capability which most existing heat exchanger models won't facilitate.

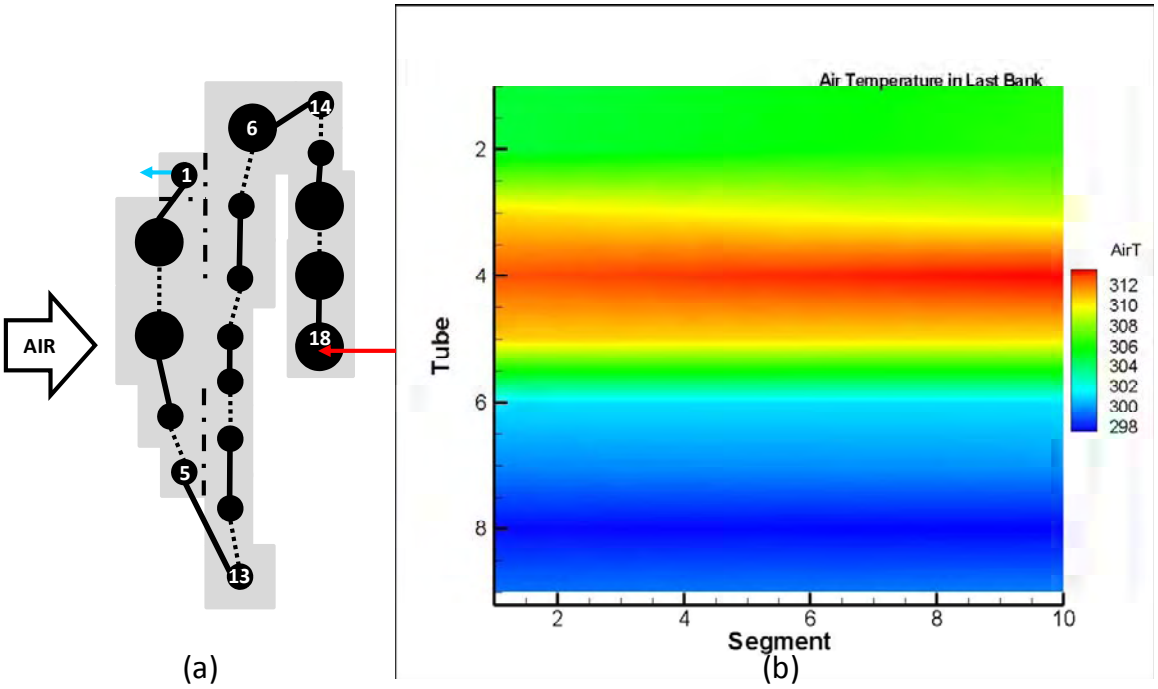


**Figure 4.8: Air temperature distribution at the exit of test coil**

## 4.2 Validation against Experimental Data

The model developed here was validated against data collected through experiments conducted by the authors at an industrial laboratory.

4.2.1 Heat Exchanger Description

Experiments were carried out on an R410A fin-and-tube condenser shown in Figure 4.9.

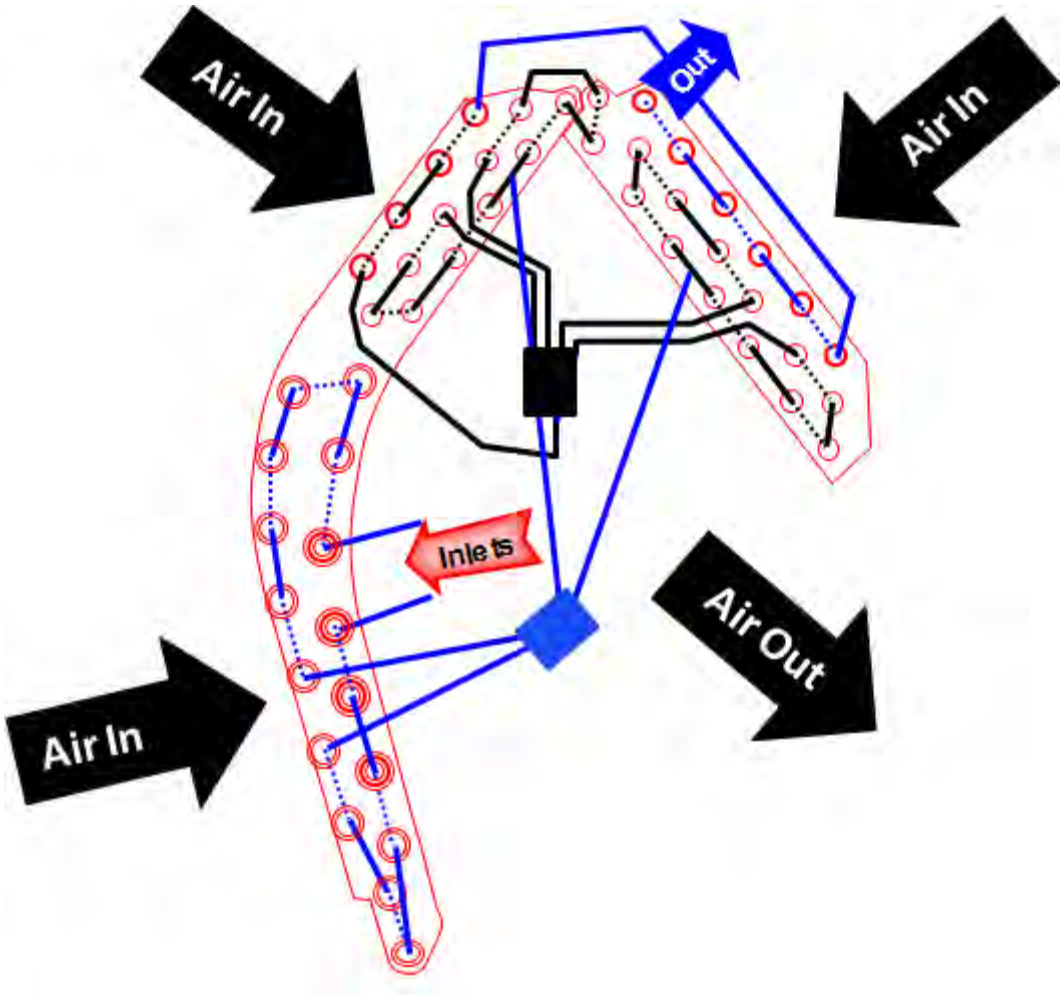


**Figure 4.9: R410A condenser used to validate arbitrary fin sheet heat exchanger model**

The heat exchanger consists of two de-superheating circuits that split into four circuits aimed at phase change and all circuits merge into a single sub-cooling circuit. The geometry details for the heat exchanger are shown in Table 4.4. The condenser had plain fins and smooth round tubes.

**Table 4.4: Geometric details of the R410A test condenser**

| Parameter | Range | Unit |
|---|---|---|
| Tube length | 0.67 | m |
| Fin thickness | 0.1 | mm |
| Fin pitch | 1.0 | mm |
| Frontal area | 0.2184 | $m^2$ |
| Tube diameters | 4.76, 6.35, 7.0, 8.0 | mm |

The heat exchanger was tested at 8 different mass flow rates shown in Table 4.5.

**Table 4.5: Test conditions for R410A condenser**

| Parameter | Range | Unit |
|---|---|---|
| Air flow rate | 14.6 | $m^3$/min |
| Air inlet dry bulb temp. | 20 | °C |
| Air inlet wet bulb temp. | 15 | °C |
| R410A pressure in | 1.85 | MPa |
| Flow rate | 39-54 | kg/hr |
| R410A temperature in | 40.5 | °C |
| R410A temperature sat. | 31.3 | °C |

The following features of the proposed model were used:(a) Variable tube diameters, (b)Variable tubes per bank, (c)Variable tube pitches, (d)One dimensional air maldistribution on coil face and (e) jagged external and internal edges (non-rectangular footprint)

Tube-to-tube conduction plays a significant role, mainly in gas coolers and evaporators as described in Lee and Domanski (1997), Jin *et al.* (2004) and Zilio (2007). Considering that this was an R410A condenser, heat conduction between tubes was ignored in the model.

4.2.2 Transformation for Modeling

The condenser can be considered as being made of three different slabs, A, B and C. The air volume flow rates and velocity profiles for the three slabs were measured. Based on the fact that air follows the path of least pressure drop (Chwalowski *et al.*, 1989; Domanski and Yashar, 2007), it is assumed that air flows perpendicularly through the three slabs. This allows the adaptation of the actual heat exchanger into a modified geometry as shown in Figure 4.10 (a) and (b).

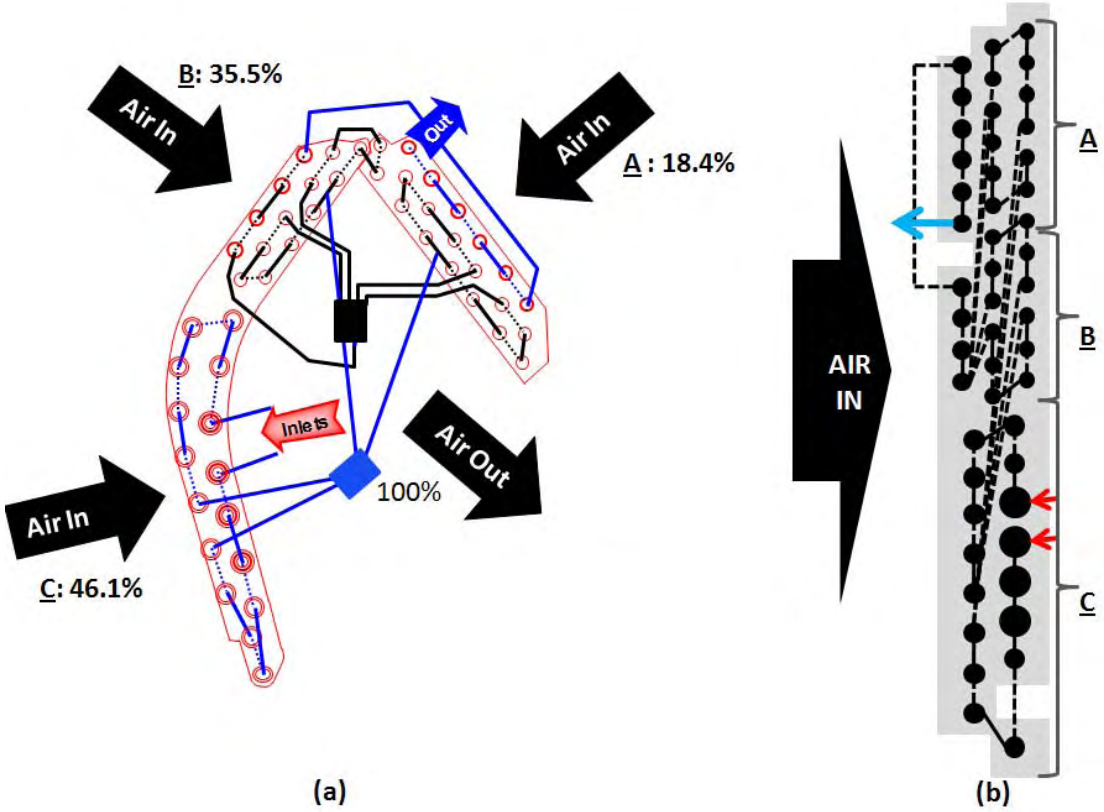


**Figure 4.10: (a) Actual R410A condenser and (b) transformation of the original geometry for modeling**

The air velocity distribution was obtained through actual measurement, and used as input to the model, as shown in Figure 4.11.

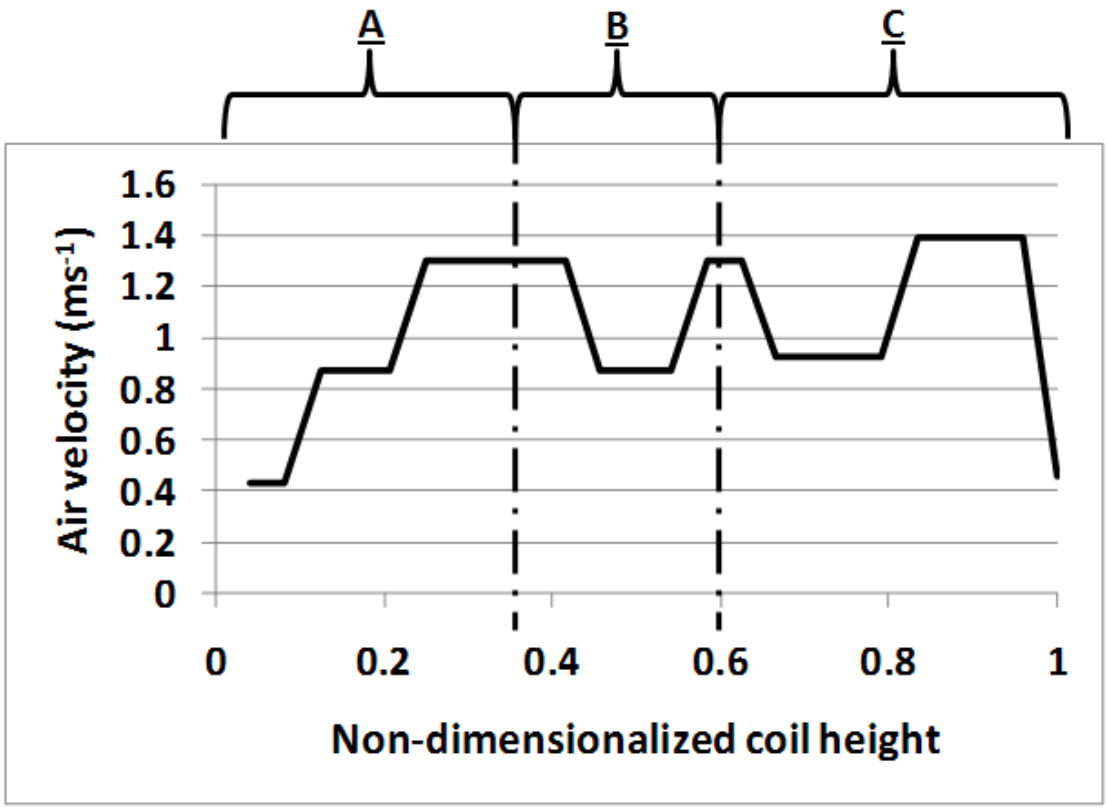


**Figure 4.11: Air velocity distribution on R410A condenser coil face**

Air heat transfer coefficients were obtained by applying standard correlations (Kim *et al.*, 1999) on a slab-wise basis, considering slabs A, B and C within themselves have standard staggered fin-and-tube configurations.

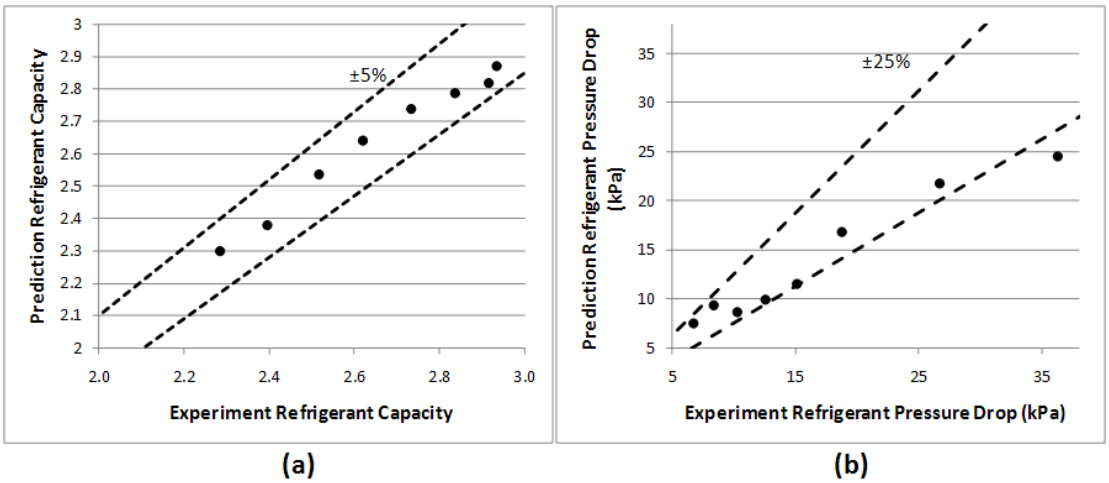


**Figure 4.12: Validation results for R410A condenser**

Validation results are shown in Figure 4.12. Overall heat capacity agrees well within ±5%. 7 out of 8 points on refrigerant side pressure drop agree within ±25%.

### 4.3 Conclusions

A new heat exchanger model for fin-and-tube air-to-refrigerant heat exchangers with arbitrary fin sheets was developed. This model is capable of accounting for several varying parameters, such as tube diameters, tube locations, tube pitches, and internal as well as external jagged edges, variable number of tubes per bank and variable location of fin cuts. A new grid based air propagation algorithm is introduced. The model was validated against experiments, and heat capacity prediction was found to be within ±5% of measured values. The overall pressure drop for 7 out of 8 cases was found to be within ±25% of the measured value, which is within in the regression error of the Blasius pressure drop correlation (Schlichting and Gersten, 2000) employed.

The current approach is based on the assumption that air flows perpendicularly through the heat exchanger, and there is no maldistribution of air inside the heat exchanger. While this assumption holds true for the current experimental case validated, it might not hold true for highly arbitrary fin sheets which might require computational fluid dynamics (CFD) solution to obtain the air flow through the coil. However, the grid based approach will allow using a CFD velocity distribution within the heat exchanger and apply it to the heat exchanger model. Further, this model provides the capability of carrying out comprehensive optimization of a fin-and-tube heat exchanger (Aute *et al.*, 2004) by coupling this model with an optimizer. Such an optimization would optimize parameters such at tube diameters, locations etc. to

obtain better heat exchanger performance in terms of pressure drop and heat transfer, given constraints such as material used.

# CHAPTER 5. MODELING OF FIN-AND-TUBE HEAT EXCHANGER USING CFD-BASED AIR PROPAGATION

The key to successfully using CFD-based air propagation involves adaptation of CFD results for air flow through a heat exchanger, for a heat exchanger model. This involves processing both heat exchanger geometry data and CFD data, followed by interpretation of CFD results for generation of air propagation sequence for the heat exchanger model. Based on this, the process of employing CFD-based air propagation can be divided into the following steps

1) Processing heat exchanger geometry data

2) Processing CFD data

3) Generating heat exchanger model-CFD hybrid air propagation sequence

## 5.1.1 Processing Heat Exchanger Geometry Data

For the purpose of modeling, a heat exchanger is divided into several fin-and-tube control volumes. These control volumes interact with each other via refrigerant and air flow, as well as tube-to-tube conduction.

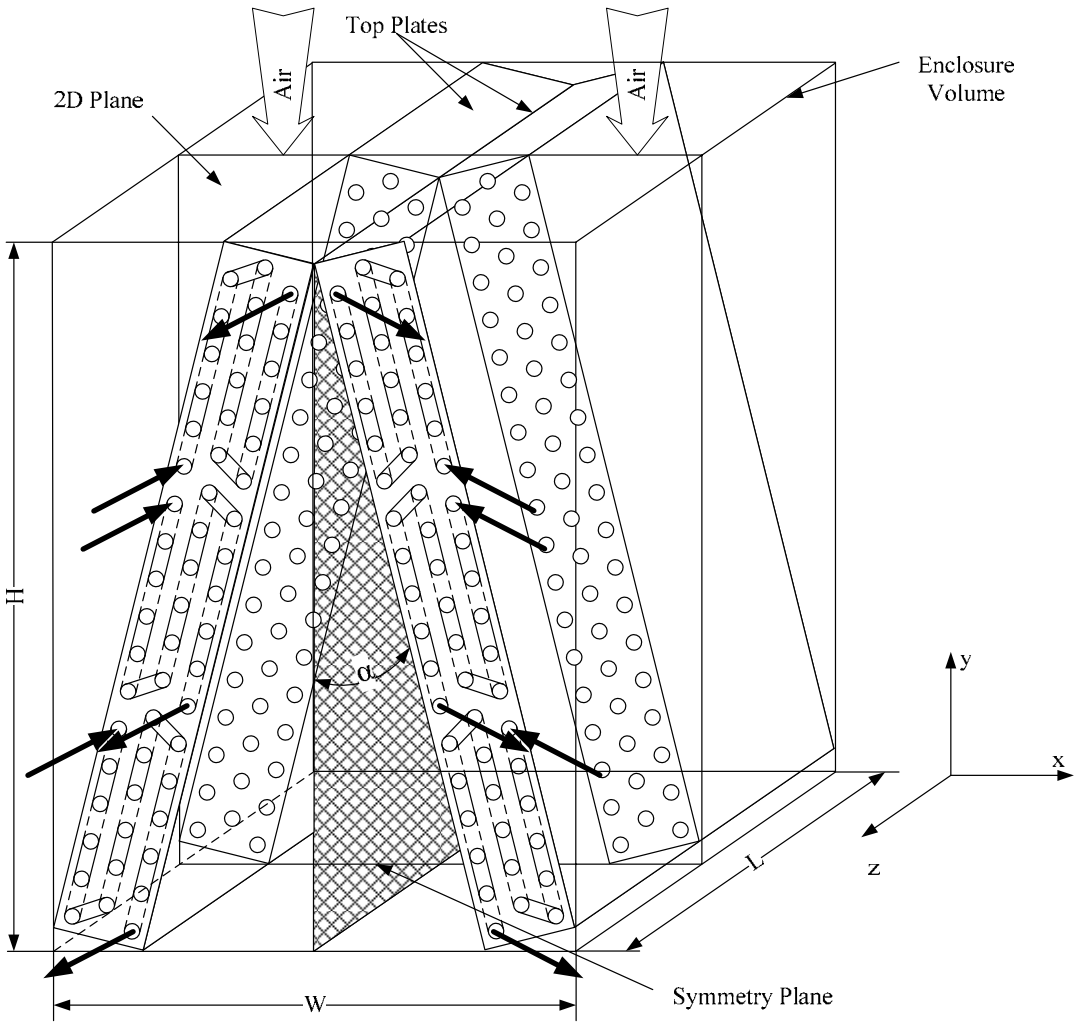


**Figure 5.1: Sample A-Coil**

As shown in Figure 5.1, refrigerant flows into or out of the page, and air flows across tubes, from top to bottom. While refrigerant flow is formalized using the Junction Tube Connectivity Matrix (Jiang *et al.*, 2006), the intent of the CFD-based air propagation is to formalize air flow information through the heat exchanger. For this purpose, all the edges of all control volumes are obtained. An edge is defined as a line segment that separates two neighboring tubes. Through the heat exchanger geometrical information, these edges contain information of the tubes they are separating, as well as their end points in terms of the x and y locations on a Cartesian

grid. The edges near the free stream planes (exit or inlet edges, as well as top and bottom planes) of the heat exchanger represent the neighboring tube number as zero. These edges are further divided into several edge segments, which share the same tube neighbors as their parent edges, but are much smaller in length than the parent edges (see Figure 5.3). The refinement is critical to interpolating CFD results on the heat exchanger Cartesian grid. The extent of heat exchanger grid refinement is determined by the mesh refinement of the CFD solution. This is discussed later in the paper. Once this process (shown in Figure 5.2) is complete, the heat exchanger model is has information regarding the following on its Cartesian grid,

1) Tube center

2) Dimensions of edges as well as interacting tubes

3) Mid-points and lengths of refined edges

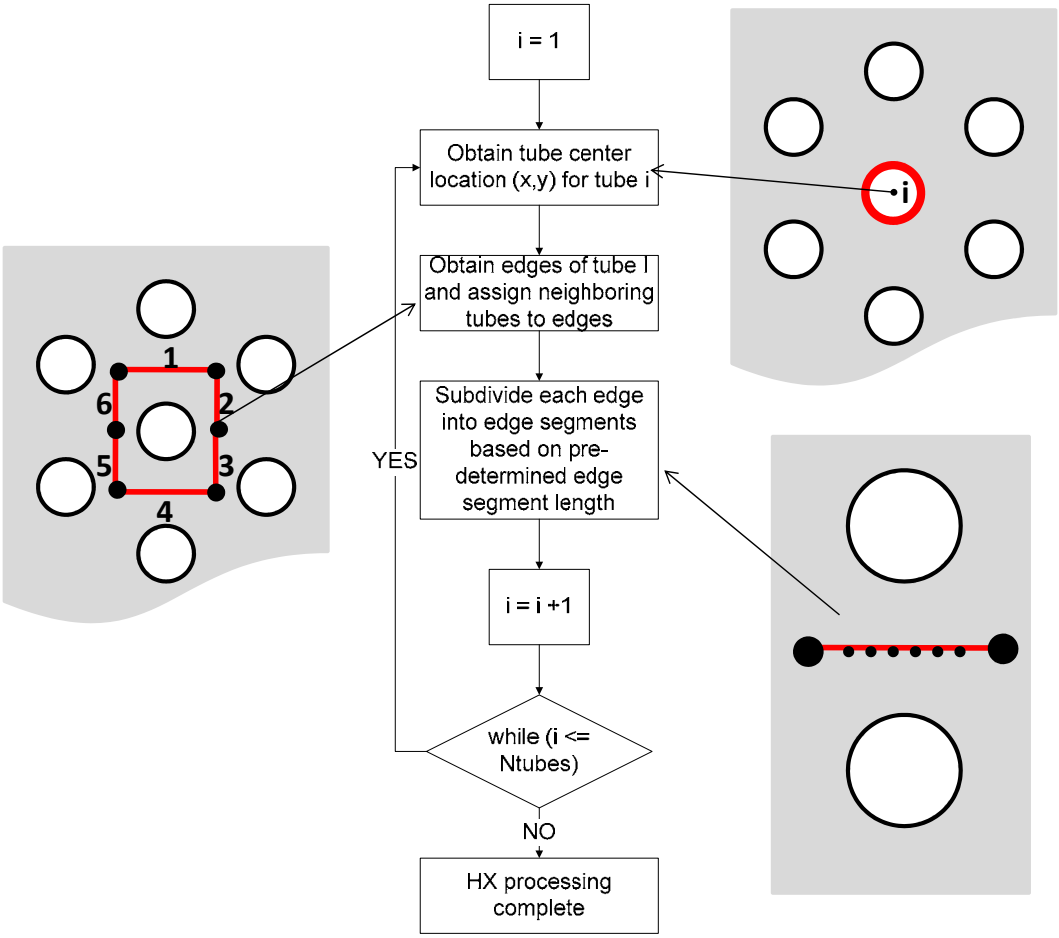


**Figure 5.2: Methodology for processing heat exchanger geometry data**

The definitions used for the heat exchanger grid are described in Figure 5.3.

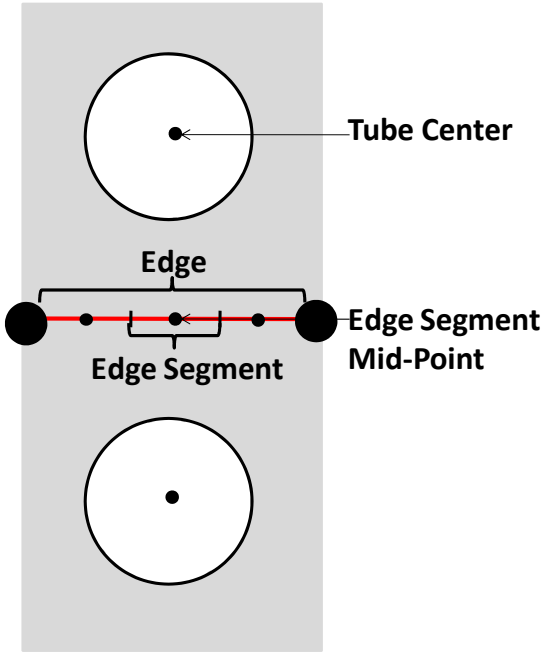


**Figure 5.3: Definitions for heat exchanger grid parameters**

5.1.2 Processing CFD Data

CFD results required for CFD-based air propagation contain the x and y locations of the CFD grid points, as well as the x-component and the y-component of velocities at those points. To utilize 3D CFD results, z location must also be exported in addition to the above mentioned data. The CFD mesh can be either structured or unstructured. Considering the complexity of a fin-and-tube heat exchanger's geometry, most CFD meshes used in simulating a fin-and-tube heat exchanger will likely be unstructured, though it must be noted that the algorithm proposed here is independent of the type of CFD mesh. Overlaying a CFD mesh on the heat exchanger model's Cartesian grid requires interpolation of the CFD results. This interpolated data is used to obtain velocities, u and v, which can be integrated over the edge segments to obtain mass flow rate through the edges around a heat exchanger control volume.

Several interpolation options were investigated. The first method investigated was the simple arithmetic averaging of CFD results within a given radius from the mid points of the edge segments, shown by equation (5.1)

$$\vec{u}\left(x,y\right)=\frac{\sum_{i=1}^{n}\vec{u}\left(xCFD,yCFD\right)}{n}\quad s.t.\ \sqrt{\left(x-xCFD\right)^{2}+\left(y-yCFD\right)^{2}}\leq\left|r\right| \quad (5.1)$$

Though this is a rather straightforward approach, it has two weaknesses which can lead to unrealistic interpolated values of velocity. Firstly, the equal weighting allotted to CFD points, within a prescribed distance, while averaging can lead to spurious velocities. The second weakness stems from an inherent characteristic of CFD simulations. The second weakness arises from an inherent characteristic of CFD itself. To accurately capture the gradients near the wall for viscous flow, CFD meshes are greatly refined. While interpolating such data, the phenomenon of clustering is often encountered. This challenge is illustrated using a simple example in Figure 5.4 . Consider Figure 5.4(a) where an interpolated velocity is obtained at the mid-point of segment AB, and integrated over the AB to obtain mass flow rate through AB. In this case, the clustering of points on the top (near the wall) will weigh greatly towards the top most points.

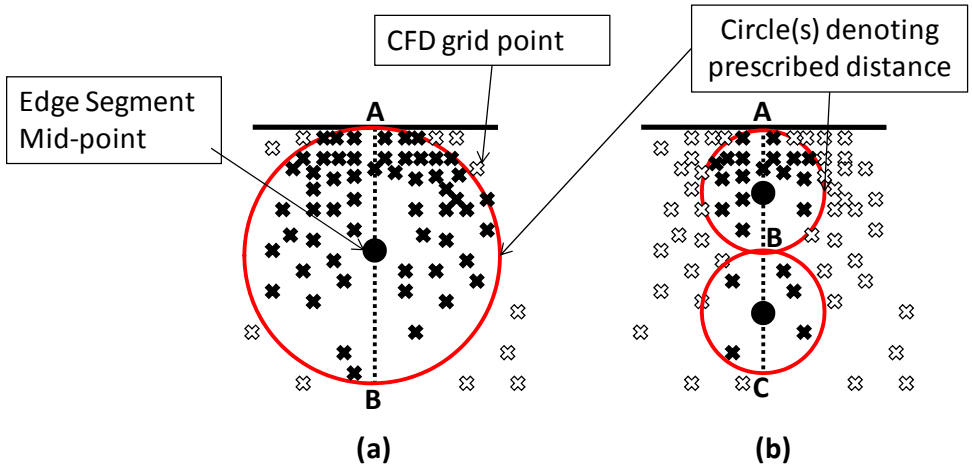


**Figure 5.4: Clustering of points in an unstructured CFD mesh can lead often lead to inaccurate interpolated variables**

To counter the first weakness arising from equal weighting of all points within a prescribed distance, inverse distance averaging (Shepard, 1968) can be employed. This technique provides weights to the actual data points such that data further away from the point of interpolation has less weight, while data with greater proximity to the point of interpolation is assigned higher weight. This is shown in equation (5.2)

$$\vec{u}(x,y) = \begin{cases} \vec{u}(xCFD_i, yCFD_i) & if\ d_i = 0 \\ \left[\sum_{i=1}^{n} d_i^{-1}\vec{u}(xCFD_i, yCFD_i)\right] \Big/ \left[\sum_{i=1}^{n} d_i^{-1}\right] & if\ d_i \neq 0 \end{cases}$$
$$where\ d_i = \sqrt{(x - xCFD_i)^2 + (y - yCFD_i)^2} \qquad (5.2)$$
$$d_i \leq |r|$$

To address the second weakness which arises from clustering, instead of interpolating data using points within a prescribed distance from the segment midpoint, a certain pre-determined number of nearest points can be chosen for interpolation. This modifies the previous equation to equation (5.3)

$$\vec{u}(x,y) = \begin{cases} \vec{u}\left(xCFD_i, yCFD_i\right) & if\ d_i = 0 \\ \left[\sum_{i=1}^{n} d_i^{-1}\vec{u}\left(xCFD_i, yCFD_i\right)\right] \Big/ \left[\sum_{i=1}^{n} d_i^{-1}\right] & if\ d_i \neq 0 \end{cases}$$

$$where\, d_i = \min\left(\sqrt{\left(x - xCFD_i\right)^2 + \left(y - yCFD_i\right)^2}\right) \tag{5.3}$$

$$n \leq N_{prescribed}$$

While this addresses challenges of numerical clustering, inverse distance averaging does not obtain any directional information, which is a shortcoming for unstructured, irregularly-spaced, data interpolation. Consider two different unstructured data sets shown in Figure 5.5 (a) and (b). Each of the data sets has 6 points, denoted by numbers 1 through 6. These data points have the same function values as well. Assuming the number of prescribed points is set to 4, in case (a) and (b), the interpolated result at the edge segment mid-point will be the same, whereas intuitively, in case (b) points 5 and 6 should have a greater influence on the interpolated value than in case (a), because in case (a), they are in the shadow of points 3 and 4. Therefore, a more intuitive interpolation is exhibited by case (c) where points 3, 4, 5 and 6 are used to obtain the interpolated value.

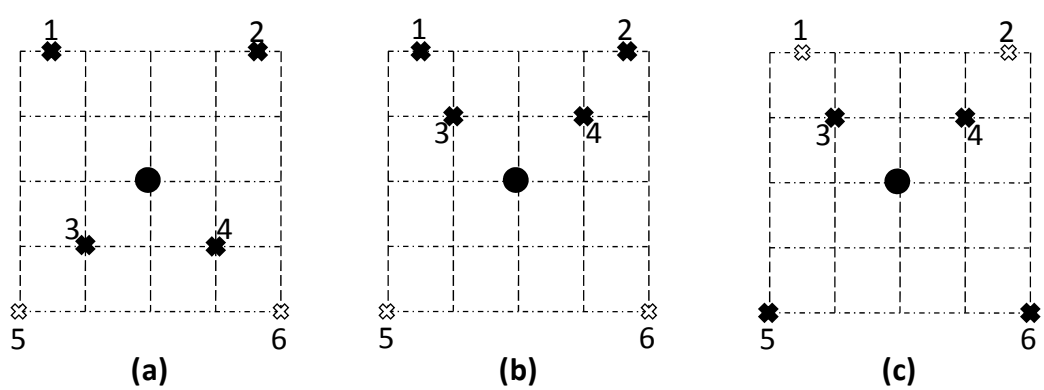


**Figure 5.5: Shortcomings of lack of directional information in inverse distance averaging**

Therefore, the inverse distance interpolation is modified to account for directional information. This is done by applying equation for each quadrant around the edge segment mid-point to obtain one nearest point in each quadrant, for a total of 4 points for 2D CFD results, and then applying inverse distance averaging. For 3D CFD results, a similar approach results in 8 prescribed points, 4 on each side of the z plane. For 3D interpolation, z velocities are ignored because the CFD simulation assumes there is no net mass flowing in the z-direction.

After obtaining velocities at edge segment velocities, they are integrated over the edge segments, to obtain total mass flow rate through each edge using the following equation (5.4) for 2D CFD results.

$$\frac{\dot{m}_{edge}}{l_{cv}} = \sum_{i=1}^{nEdgeSegments} \vec{u} \cdot l_{es} \cdot \rho_{air} \tag{5.4}$$

For 3D CFD results, x and y velocities are integrated over each z segment location using the following equation(5.5).

$$\frac{\dot{m}_{edge}}{l_{cv}} = \sum_{z=1}^{zSegments} \sum_{i=1}^{nEdgeSegments} \vec{u} \cdot l_z \cdot \rho_{air} \tag{5.5}$$

The number of edge segments is determined dividing the length of an edge by the maximum least distance between any two points on the CFD mesh. The expression is rounded up to the nearest integer to obtain the number of edge segments, and edge segment length.

This entire methodology, summed up in Figure 5.6, provides the necessary sources and destination (in terms of tube numbers) and respective mass flow rates to propagate the air through the heat exchanger model.

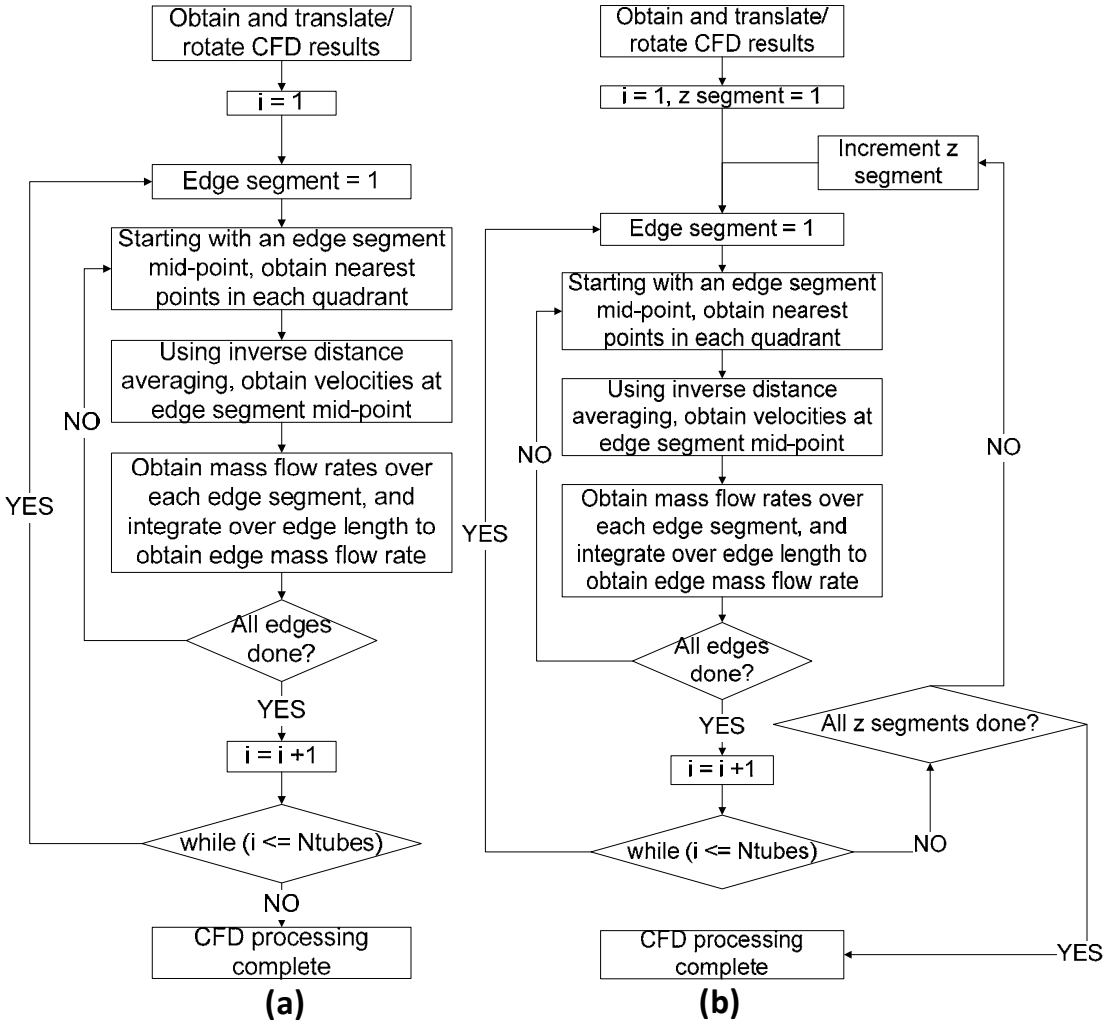


**Figure 5.6: CFD data processing methodologies for (a) 2D-CFD data and (b) 3D-CFD data**

## 5.2 Validation

The CFD-based heat exchanger modeling approach was validated against experiments conducted on an R410A condenser by Wang *et al.* (2009), shown in Figure 5.7.

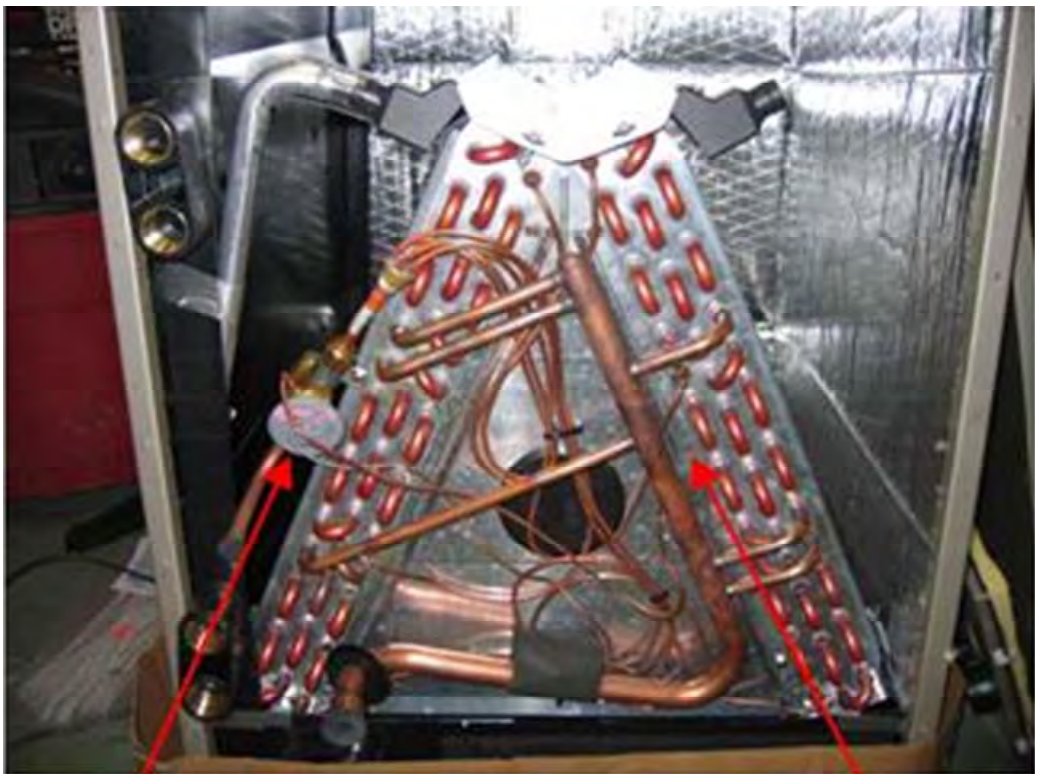

**Figure 5.7: A-shaped coil tested by Wang *et al.* (2009)**

The specifications of single slab, shown in Figure 5.8, are specified in Table 5.1.

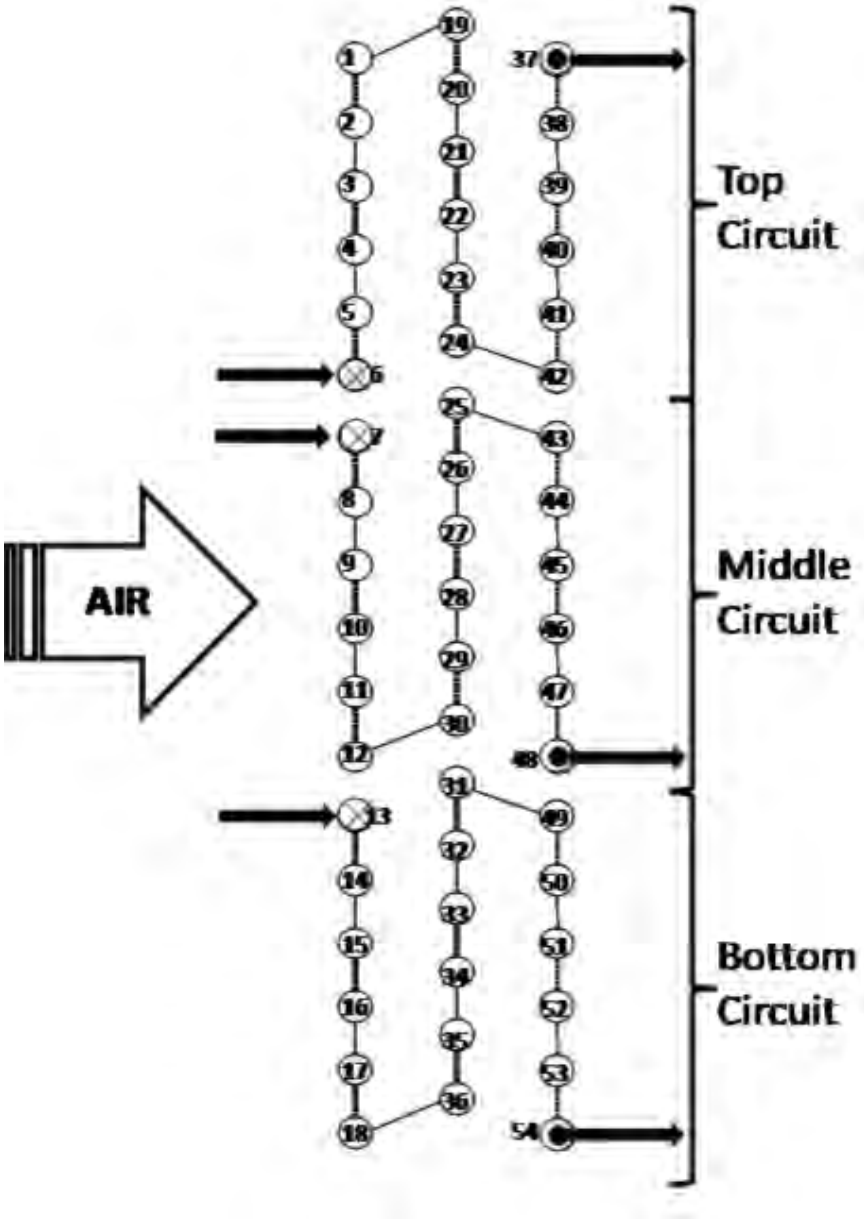


**Figure 5.8: Circuitry of the heat exchanger tested**

Considering the flow and circuit symmetry, only the left bank of the A-coil was simulated.

**Table 5.1: Heat exchanger specifications and correlations used**

| Parameters | | | Correlations | |
|---|---|---|---|---|
| Number of Segments | 10 | --- | Air Side HTC | Chang-Wang |
| Tube Configuration | Staggered | | Refrigerant Side HTC - Liquid | Gnielinski |
| Number of Tubes Per Bank | 18 | --- | Refrigerant Side HTC - Two Phase | Jung-Radermacher |
| Number of Tube Banks | 3 | --- | Refrigerant Side HTC - Vapor | Gnielinski |
| Tube Length | 0.46 | m | | |
| Tube OD | 0.0105 | m | Air Side DP | Chang-Wang |
| Tube Thickness | 0.55 | mm | Refrigerant Side DP - Liquid | Blasius |
| Tube Vertical Spacing | 1.04 | in | Refrigerant Side DP - Two Phase | Jung-Radermacher |
| Tube Horizontal Spacing | 0.8 | in | Refrigerant Side DP - Vapor | Blasius |
| FPI | 14 | fpi | | |
| Fin Thickness | 0.0039 | in | | |
| Fin Type | Louver | --- | | |
| Slab Angle | 18.5 | ° | | |

The condenser performance was measured for six different refrigerant flow conditions, shown in Table 5.2, while air inlet conditions were held constant at 21.15°C and 40% relative humidity, with air volume flow rate for half a slab being 0.283 $m^3s^{-1}$.

**Table 5.2: Test conditions for the heat exchanger**

| Case | Inlet Pressure [Pa] | Inlet Temperature [°C] | Mass flow rate [$gs^{-1}$] |
|---|---|---|---|
| A | 2822282.22 | 69.3 | 66.37 |
| B | 2829701.06 | 70.0 | 66.57 |
| C | 2584393.60 | 67.9 | 50.19 |
| D | 2180680.84 | 66.2 | 28.37 |
| E | 2006091.30 | 69.0 | 19.26 |
| F | 1988625.01 | 68.4 | 18.99 |

## 5.3 CFD Simulation

CFD simulations are based on numerical solutions of the fluid governing equations. The fluid governing equations include the Navier-Stokes equations which describe the flow behaviour (velocity and pressure) as well as other scalar transport equations, e.g. energy, species, and turbulent closure equations. The critical step in CFD simulation is the pressure-velocity coupling. The CFD simulations presented in this paper incorporated the semi-implicit-pressure-linking-equation consistent (SIMPLEC) algorithm (Vandoormal and J. D. Raithby. (1984)). Below is a brief description of the different governing equations involved in the current CFD simulations based on Versteeg and Malalasekera (1995) and Patankar. (1980).

The general form of the continuity equation is shown in equation(5.6). In this equation, the first term can be neglected under the assumptions of incompressible steady state flow. Furthermore, the source term can be neglected since no mass source will be introduced in the current simulations.

$$\frac{\partial \rho}{\partial t} + \nabla \cdot \left( \rho \cdot \vec{v} \right) = S_m \tag{5.6}$$

The conservation of momentum in an inertial (non-accelerating) reference frame may be described by equation(5.7). In this equation, $P$ is the static pressure, $\bar{\bar{\tau}}$ is the stress tensor (described by equation(5.8)), and $\rho\vec{g}$ and $\vec{F}$ are the gravitational body force and external body forces, respectively.

$$\frac{\partial \left( \rho \vec{v} \right)}{\partial t} + \nabla \cdot \left( \rho \cdot \vec{v}\vec{v} \right) = -\nabla P + \nabla \cdot \left( \bar{\bar{\tau}} \right) + \rho \vec{g} + \vec{F} \tag{5.7}$$

$$\bar{\bar{\tau}} = \mu \left[ \left( \nabla \vec{v} + \nabla \vec{v}^T \right) - \frac{2}{3} \nabla \cdot \vec{v} I \right] \tag{5.8}$$

The differential form of the energy equation can be written as shown in equation(5.9), where $\vec{J}_j$ is the diffusion flux of species *j*, and neglected in the proposed analysis. The first three terms on the right-hand side of equation (5.9) represent energy transfer due to conduction, species diffusion, and viscous dissipation, respectively. $S_h$ includes the heat of chemical reaction, and any other volumetric heat sources defined in the flow model – neglected in the current research. $E$ is the total energy of a fluid particle (control volume).

$$\frac{\partial}{\partial t}\left( \rho E \right) + \nabla \cdot \left( \vec{v} \left( \rho E + P \right) \right) = \nabla \cdot \left( k_{\text{eff}} \nabla T - \sum_j h_j \vec{J}_j + \left( \bar{\bar{\tau}}_{\text{eff}} \cdot \vec{v} \right) \right) + S_h \tag{5.9}$$

The CFD commercial package (FLUENT®, 2007) used in the present work neglects the pressure work and kinetic energy in solving incompressible flow using a segregated solver, but they could be included intentionally as per the model requirement. Similarly, the viscous heating is neglected by default when using

segregated solver with incompressible flows as the Brinkman number (Br) will be typically less than unity. In case Br is greater than unity, the viscous heating should be accounted for in the solver settings.

Turbulence state is associated with random flow field properties. This randomness affects all the flow parameters. The velocity fluctuations associated with turbulence add more stresses on the fluid; called the Reynolds stresses. The Reynolds number measures the importance of inertial forces over the viscous forces present in the flow. At values of Re number higher than $Re_{crit}$ the flow amplifies slight unpredictable changes in boundary and initial conditions, such as slight thermal currents, micro-scale surface roughness change, micro-scale input disturbances, to a measurable scale (Bernard and J. Wallace. (2002)).The fluctuated velocity field mixes transported quantities such as momentum, energy, and species concentration, and cause the transported quantities to fluctuate as well. These fluctuations, which can be of small scale and high frequency, are too computationally expensive to be directly simulated in practical engineering calculations. For this reason, the instantaneous governing equations are time-averaged, ensemble-averaged, or otherwise manipulated to remove the small scales, resulting in a modified set of equations that are computationally less expensive to solve. However, the modified equations contain additional unknown variables, and turbulence models are needed to determine these variables in terms of known quantities. FLUENT® offers a variety of RANS turbulence models: Spalart-Allmaras, $k - \varepsilon$ models (standard, Renormalization-Group "RNG", and realizable), $k - \omega$ models (standard and Shear-Stress Transport "SST"), and Reynolds Stress Model "RSM" in addition to Detached and Large Eddy

Simulation models (DES, LES). The realizable $k-\varepsilon$ turbulence model was used in the current CFD simulations with enhanced wall function. Interested reader can refer to Fluent (2007) for further details of the turbulence models and wall function treatment. Both 2D and 3D solution domains were carefully discretized for an improved mesh quality. For the 2D case, 70246 computational face cells were used to represent the computational domain assuming no fin effect. The 3D computational domain was bounded between 2 symmetry planes as shown in Figure 5.9(c). The fin is represented by a plane of zero thickness at the middle of the volume. A total of 1709142 computational volume cells were used for the 3D computational domain.

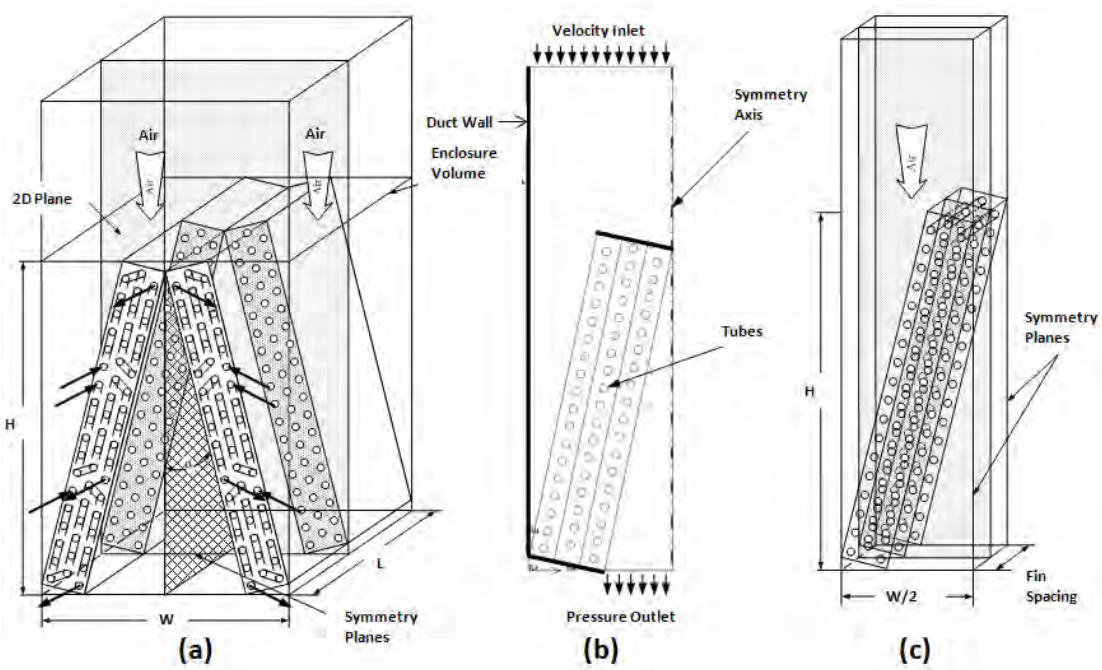


**Figure 5.9: (a) Problem description, (b) 2D computational domain and (c) 3D computational domain**

For the 3D mesh, the 2D mesh, shown in Figure 5.10, was extruded along the z-axis on both sides of the fin. To ensure that the boundary layer was adequately captured, 12 elements were used on each side of the fin.

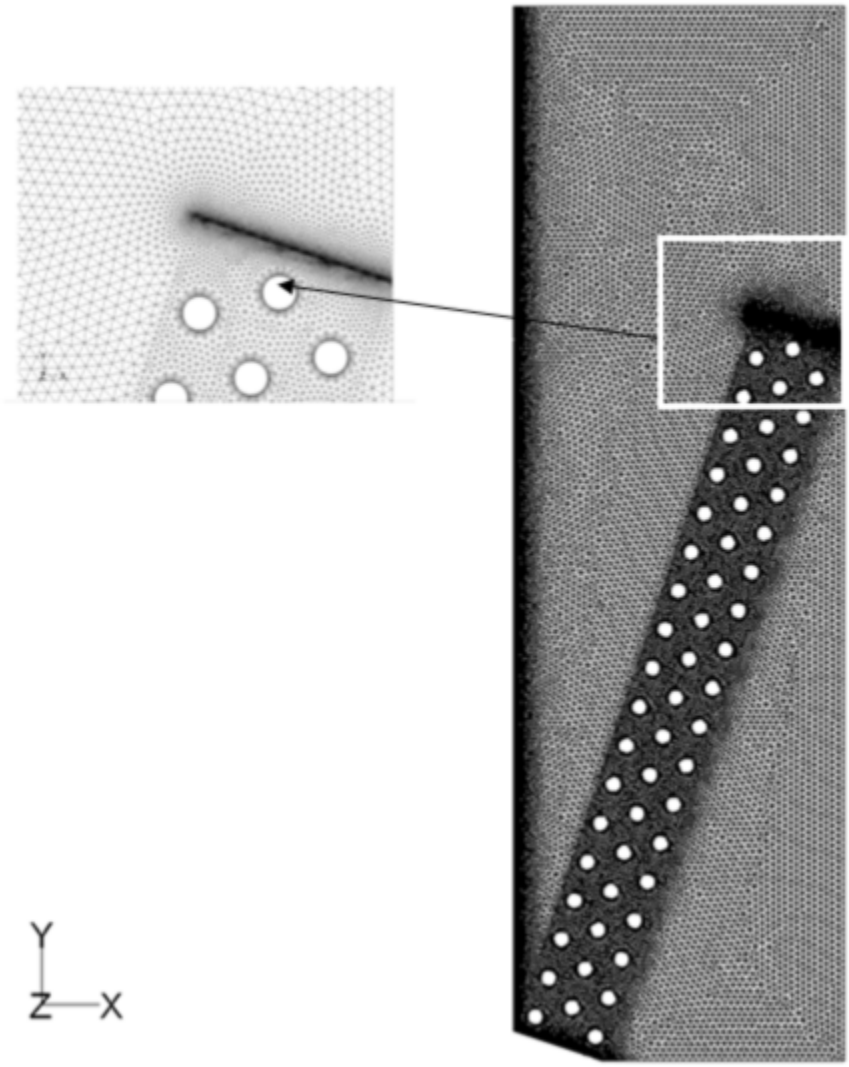


**Figure 5.10: 2D computational domain with a magnified view showing the finer grid resolution near the wall to capture high gradients in flow variables**

CFD simulations were performed with second order upwind discretization scheme. Viscous heat dissipation was accounted for in the energy equation. The no-slip boundary conditions were set for all walls and a pressure outlet condition was used for the air outlet. Symmetry boundary condition was defined along the axis as defined in Figure 5.9(b) and (c). The Green-Gauss Node-Based gradient evaluation was used for a better representation of the unstructured mesh solution. The solver was

allowed to iterate until convergence up to a maximum of 1000 iterations. The few cases which reached the iteration limit employed a relaxed residual of $2 \times 10^{-3}$. The convergence criteria were based on maximum acceptable residuals of $10^{-3}$ for all equations except the energy equation with maximum acceptable residuals of $10^{-5}$.

### 5.4 Results and Validations

Figure 5.11(a) shows the computational domain of the 2D-CFD simulation while velocity vectors from CFD results are shown in Figure 5.11(b). Figure 5.11(c) shows the comparison of u velocities obtained from the interpolation algorithm and the CFD results at the entrance of the heat exchanger, denoted in Figure 5.11(b).

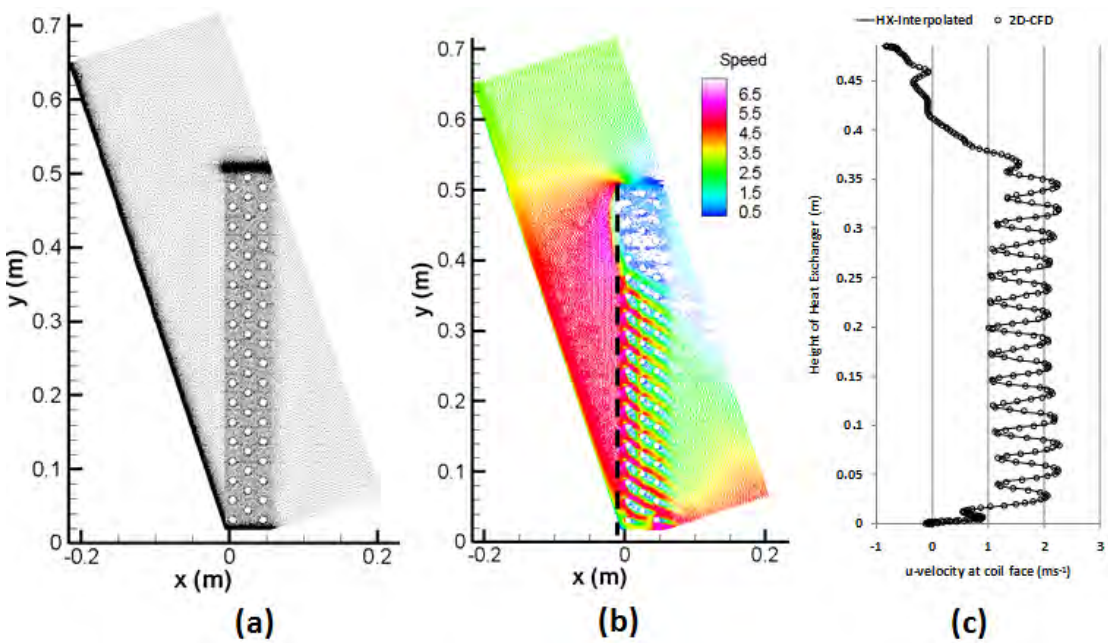


**Figure 5.11: (a) 2D-CFD mesh used to simulate the air flow over the heat exchanger. (b) Velocity vectors in the computational domain, and (c) shows the comparison of interpolated u (x-component) of the velocity on the coil face**

Figure 5.12(a) shows the computational domain at the center-plane, i.e. midway between two consecutive fins, of the 3D-CFD simulation while Figure

5.12(b) displays the velocity vectors from the CFD simulations. Figure 5.12(c) shows the comparison of $u$ velocities obtained from the interpolation algorithm and the CFD results at the entrance of the heat exchanger. Figure 5.12(d) shows the computational domain at 6.9 μm from the wall (or fin), of the 3D-CFD simulation while velocity vectors from CFD results are shown Figure 5.12(e). Figure 5.12(f) shows the comparison of $u$ velocities obtained from the interpolation algorithm and the CFD results at the entrance of the heat exchanger.

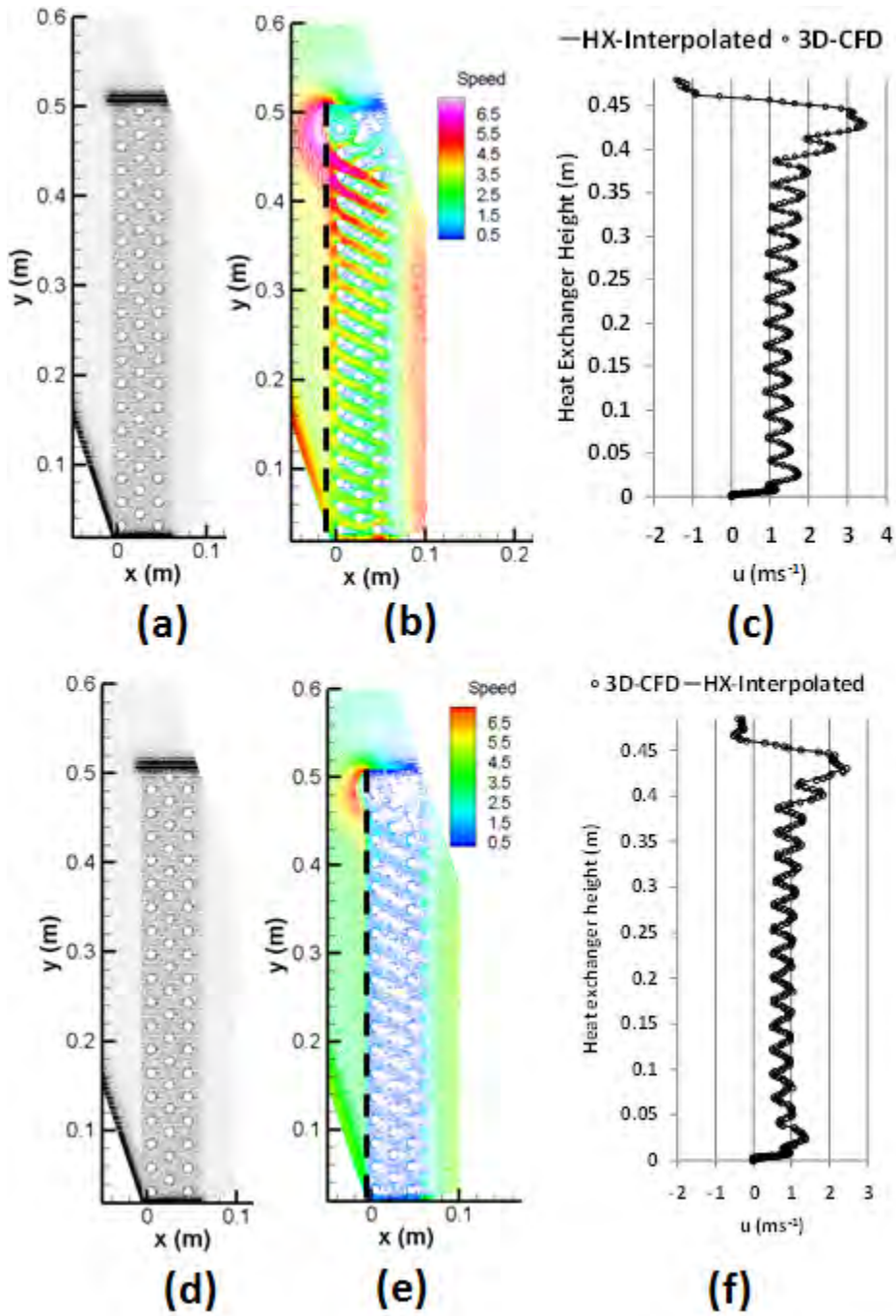


**Figure 5.12: CFD mesh (a) at the centerplane, or the mid-plane between two fins, and the velocity vectors (b) at the centerplane, and (c) shows the comparison of interpolated u velocities at the center inlet plane with the 3D-CFD results. Figures (d) thourgh (f) show the same quantities 6.9e-3 mm from the wall**

For further validation of the interpolation scheme, the centerline u-velocities are compared with the 3D-CFD results, at the inlet plane, the planes after 1st and 2nd

tube banks and the exit plane, in Figure 5.13(a) to (d). Figure 5.13 (e) to (h) show the u-velocity profiles at the same locations at 6.9 μm from the fin surface.

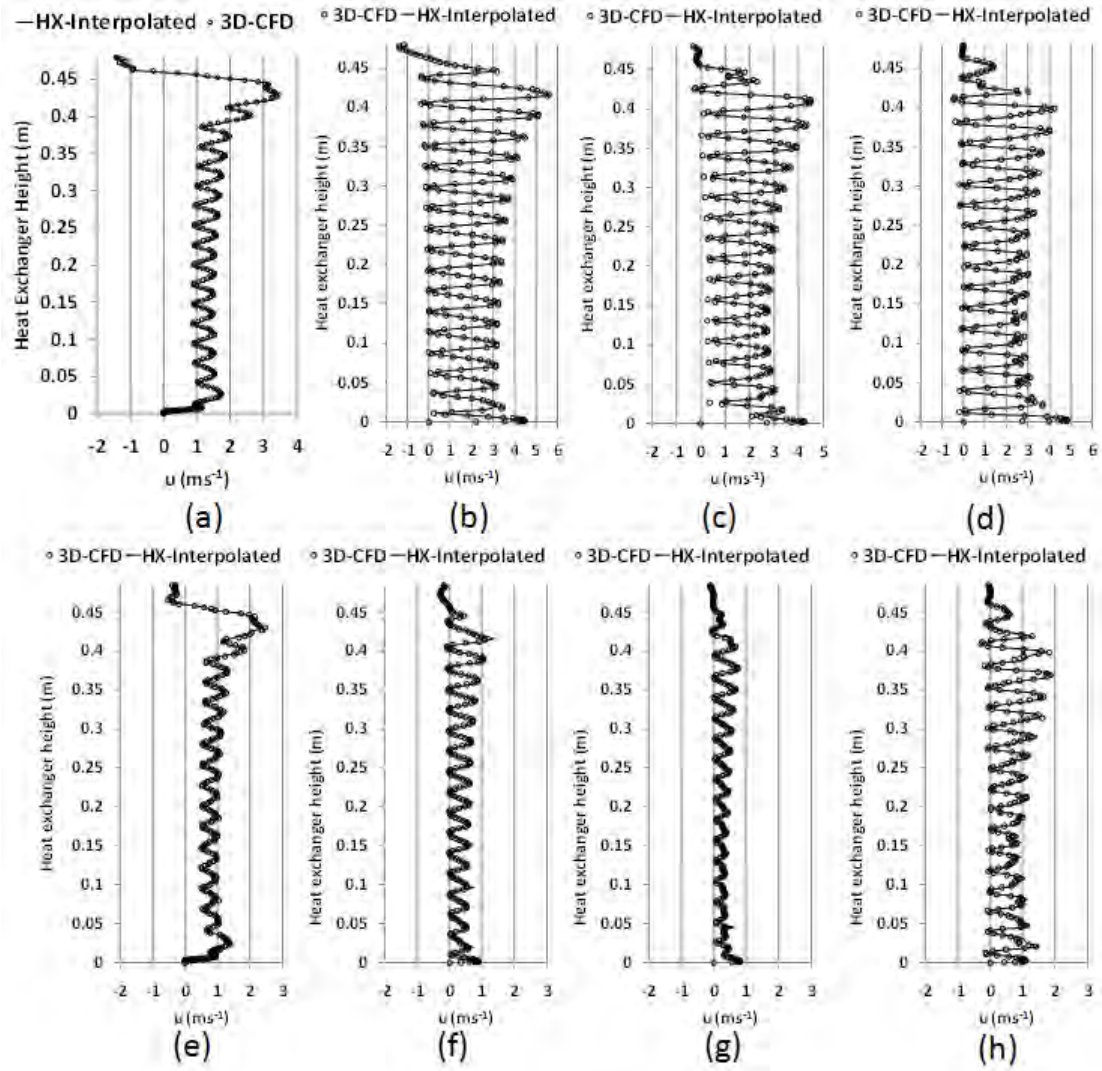


**Figure 5.13: Comparison of 3D-CFD velocities at the centerline at (a) the plane of entry , planes after (b) 1st and (c) 2nd banks, and (d)the plane of exit, and u-velocity profiles (e-h) at 6.9μm from the fin at the same planes as (a) through (d)**

The total incoming mass flow rate measured through 2D-CFD and 3D-CFD results was 0.336 kg-sec$^{-1}$, whereas the total incoming mass flow rate obtained after processing 2D-CFD results was 0.337 kg/sec leading to a difference of +0.2%. The total incoming mass flow rate obtained after processing the 3D-CFD results was 0.335 kg/sec leading to a difference of -0.3%. Both these differences are acceptable,

considering other uncertainties like heat transfer coefficients are comparably larger in magnitude. The difference between the total incoming mass flow rate and the total outgoing mass flow rate for 2D-CFD interpolated data is 0.0002 kg-sec$^{-1}$, which is a 0.05% of the total incoming mass flow rate. The same difference for 3D-CFD results is 0.002 kg-sec$^{-1}$, which is 0.5% of total incoming mass flow rate. The difference is higher for 3D-CFD because the presence of a no-slip boundary at the fin in 3D simulation, leads to high velocity gradients near the wall, which the interpolation scheme is unable to capture in great detail. This can be improved by employing other interpolation schemes (Nina Siu-Ngan Lam. (1983)).

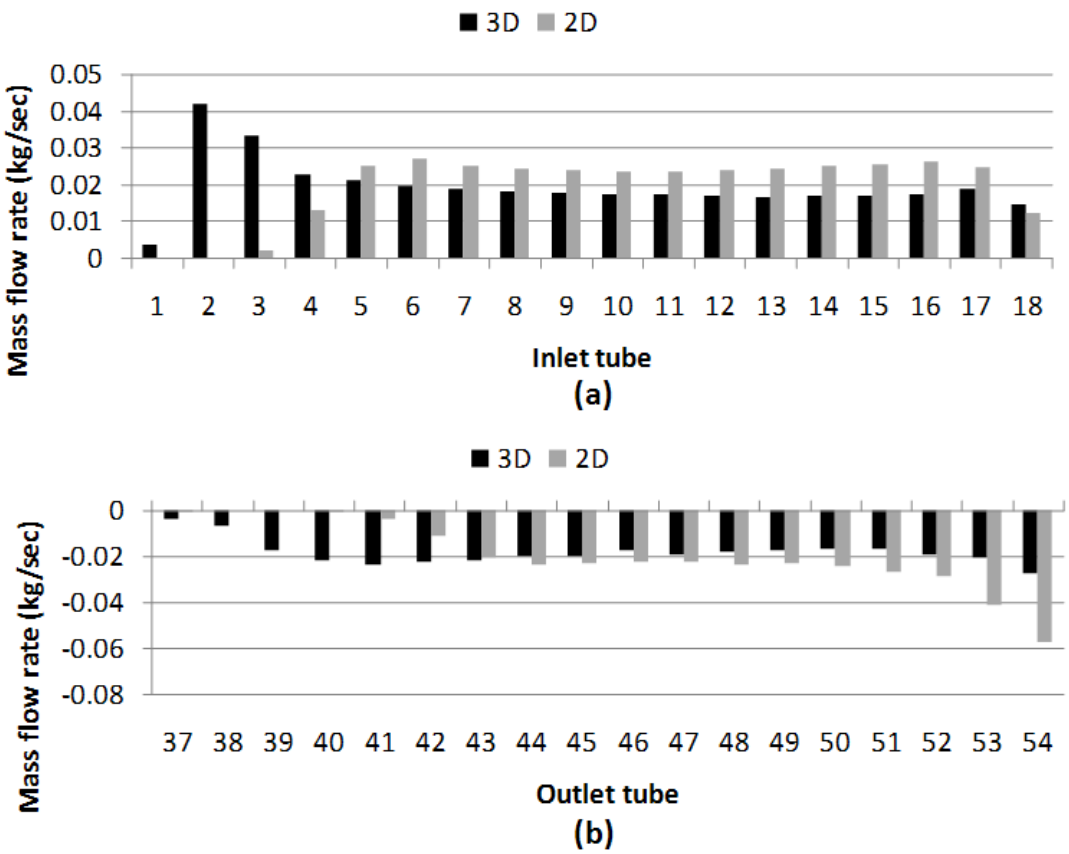


**Figure 5.14: Total air mass flow rate (a) into the heat exchanger and (b) out of the heat exchanger**

Figure 5.14(a) and (b) show the total mass flow rate flowing into (positive) the heat exchanger and out (negative) of the heat exchanger respectively, along with tube numbers. Considering the difference between the two profiles, the results from the 3D-CFD data are used in the proposed heat exchanger model to carry out the validation. This is done because 3D-CFD data accounts for the boundary layer developing on the fin sheet, which is more realistic than the fin-less 2D simulation. 2D-CFD simulations were carried out due to several reasons. While 3D-CFD simulation is more realistic, it is computationally more expensive than 2D-CFD simulations. Often, if the flow field can be accurately simulated using a 2D simulation, it is more desirable in the interest of computational cost and time. Another motivation for conducting 2D-CFD simulations was to understand and show the difference in results between 2D and 3D CFD simulations. In this case, it is evident that the presence of fins with a fin density of 14 fins per inch, the area of recirculation is smaller than 2D-CFD results depict. Further, the focus of the section is on development of a CFD-based air propagation method for a distributed heat exchanger model, which is capable of adapting and processing both 2D and 3D CFD results. One of the key outcomes of this section is to obtain the air flow rate distribution using CFD data.

**Table 5.3: Source tubes (src) and their % contribution of air mass flow rate for each tube, using 3D-CFD data**

| Tube | Src | % | Src | % | Src | % | Src | % | Tube | Src | % | Src | % | Src | % | Tube | Src | % | Src | % | Src | % | Src | % |
|---|---|---|---|---|---|---|---|---|---|---|---|---|---|---|---|---|---|---|---|---|---|---|---|---|
| 1 | 19 | 61.1 | 0 | 22.3 | 2 | 16.5 | 20 | 0.0 | 19 | 37 | 28.0 | 20 | 72.0 | 0 | 0.0 | 37 | 0 | 8.3 | 38 | 88.7 | 20 | 3.0 | | |
| 2 | 0 | 100.0 | | | | | | | 20 | 1 | 20.0 | 21 | 27.3 | 2 | 52.7 | 38 | 20 | 53.2 | 39 | 9.2 | 21 | 37.6 | | |
| 3 | 0 | 58.6 | 2 | 41.4 | | | | | 21 | 2 | 23.3 | 3 | 76.7 | | | 39 | 21 | 39.1 | 22 | 60.9 | 38 | 0.0 | | |
| 4 | 0 | 45.8 | 3 | 54.2 | | | | | 22 | 3 | 10.0 | 21 | 34.2 | 4 | 55.8 | 40 | 22 | 21.5 | 39 | 25.0 | 23 | 53.4 | | |
| 5 | 0 | 48.1 | 4 | 51.9 | | | | | 23 | 4 | 7.7 | 22 | 43.5 | 5 | 48.8 | 41 | 23 | 15.0 | 40 | 36.1 | 24 | 48.9 | | |
| 6 | 0 | 47.8 | 5 | 52.2 | | | | | 24 | 5 | 10.6 | 23 | 41.9 | 6 | 47.5 | 42 | 24 | 17.6 | 41 | 34.2 | 25 | 48.2 | | |
| 7 | 0 | 48.9 | 6 | 51.1 | | | | | 25 | 6 | 9.7 | 24 | 41.6 | 7 | 48.7 | 43 | 25 | 18.6 | 42 | 33.2 | 26 | 48.2 | | |
| 8 | 0 | 49.1 | 7 | 50.9 | | | | | 26 | 7 | 11.7 | 25 | 39.3 | 8 | 48.9 | 44 | 26 | 22.9 | 43 | 28.2 | 27 | 49.0 | | |
| 9 | 0 | 49.5 | 8 | 50.5 | | | | | 27 | 8 | 9.9 | 26 | 38.0 | 9 | 52.1 | 45 | 27 | 23.3 | 44 | 26.9 | 28 | 49.9 | | |
| 10 | 0 | 50.2 | 9 | 49.8 | | | | | 28 | 9 | 11.9 | 27 | 37.3 | 10 | 50.8 | 46 | 28 | 26.7 | 45 | 24.2 | 29 | 49.1 | | |
| 11 | 0 | 50.8 | 10 | 49.2 | | | | | 29 | 10 | 11.6 | 28 | 35.5 | 11 | 52.9 | 47 | 29 | 27.3 | 46 | 22.8 | 30 | 49.9 | | |
| 12 | 0 | 51.0 | 11 | 49.0 | | | | | 30 | 11 | 13.0 | 29 | 34.2 | 12 | 52.8 | 48 | 30 | 34.1 | 47 | 16.8 | 31 | 49.1 | | |
| 13 | 0 | 52.7 | 12 | 47.3 | | | | | 31 | 12 | 11.8 | 30 | 32.1 | 13 | 56.2 | 49 | 31 | 34.4 | 48 | 13.3 | 32 | 52.3 | | |
| 14 | 0 | 52.2 | 13 | 47.8 | | | | | 32 | 13 | 14.4 | 31 | 30.1 | 14 | 55.5 | 50 | 32 | 37.4 | 49 | 13.5 | 33 | 49.1 | | |
| 15 | 0 | 53.4 | 14 | 46.6 | | | | | 33 | 14 | 14.7 | 32 | 29.0 | 15 | 56.3 | 51 | 33 | 36.5 | 50 | 12.6 | 34 | 50.9 | | |
| 16 | 0 | 54.6 | 15 | 45.4 | | | | | 34 | 15 | 17.1 | 33 | 27.4 | 16 | 55.5 | 52 | 34 | 41.1 | 51 | 11.6 | 35 | 47.3 | | |
| 17 | 0 | 58.8 | 16 | 41.2 | | | | | 35 | 16 | 20.1 | 34 | 22.7 | 17 | 57.2 | 53 | 35 | 46.0 | 52 | 5.8 | 54 | 0.4 | 36 | 47.9 |
| 18 | 0 | 54.8 | 17 | 45.2 | | | | | 36 | 17 | 16.2 | 35 | 10.4 | 18 | 73.4 | 54 | 36 | 99.7 | 53 | 0.3 | 0 | 0.0 | | |

Table 5.3 shows the source tubes (src) and the % of air mass flow rate contributed by the sources for each tube, obtained using 3D-CFD data. Source 0 implies inlet or exit plane for first and last bank, or top edge and bottom edge for the heat exchanger.

Results presented in Table 5.3 above depict that, indeed, air propagates within a bank as it propagates across banks. This shows the limitation of the assumption that air propagates normal to the tube banks which is used in earlier heat exchanger models. Furthermore, the above results and Figure 5.15 show that the most significant recirculation effect is experienced at tube 19 as it receives 72% of its air flow rate from Tube 20 and 28% from Tube 38. It should be noted that if a perpendicular flow assumption were applied, Tube 20 won't contribute at all to Tube 19, and Tube 37 would be downstream of Tube 19.

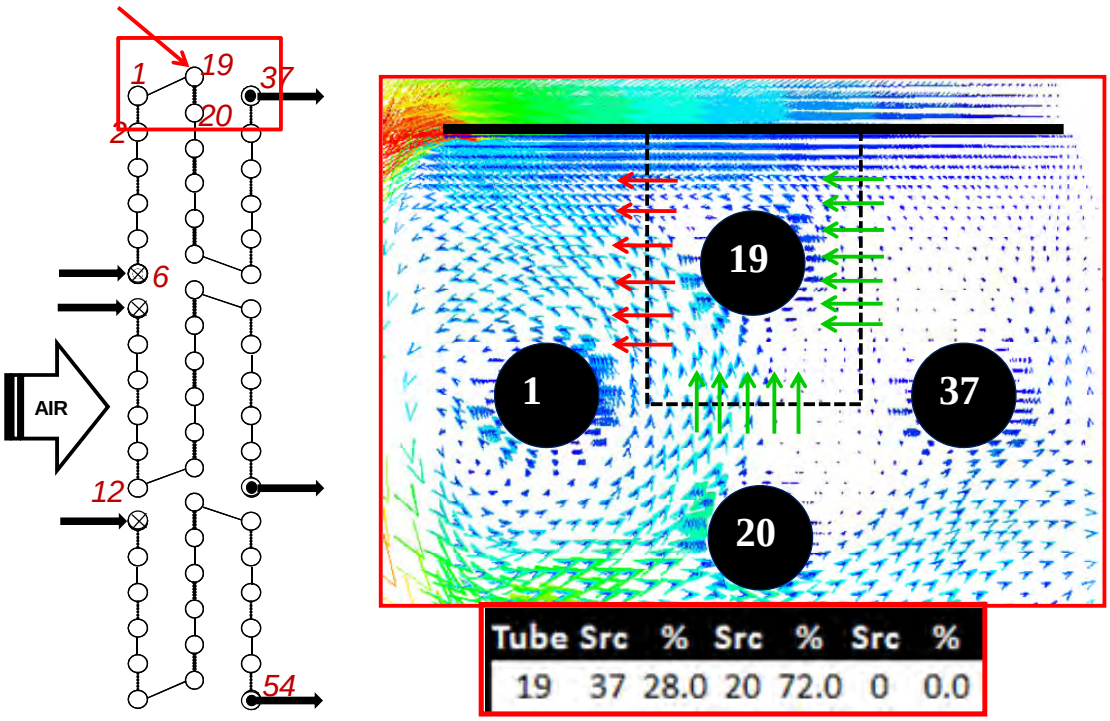


**Figure 5.15: Air velocity vectors for tube 19, with arrows showing control volumes contributing air flow to tube 19**

Analysis of tube-by-tube mass flow rates of air and a closer look at the tubes (Figure 5.16 and Figure 5.17) shows that tubes 37 and 1 are both an inlet and an outlet for air.

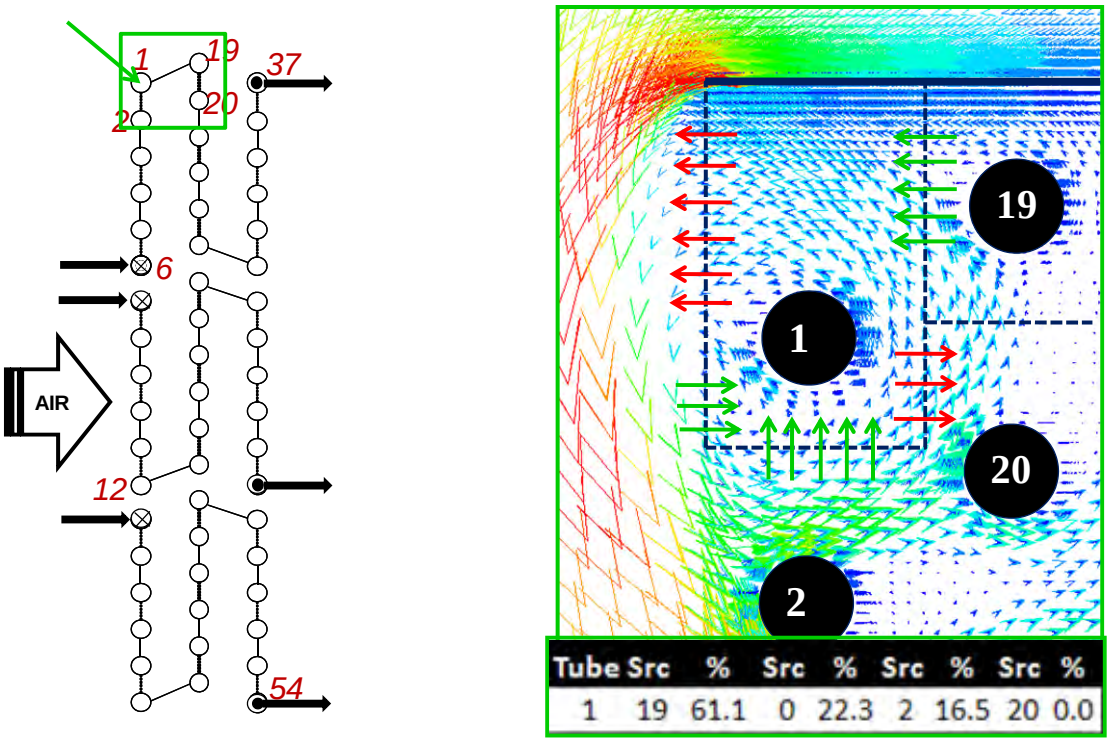


**Figure 5.16: Air velocity vectors for tube 1, with arrows showing control volumes contributing air flow to tube 1**

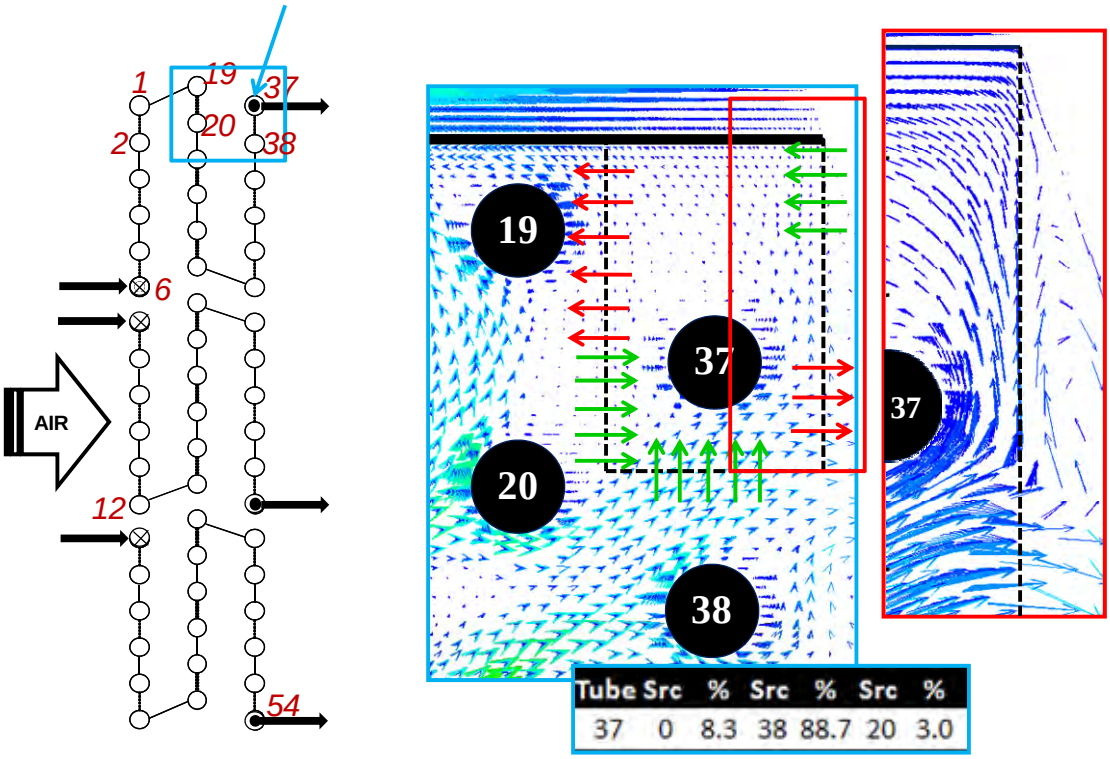


**Figure 5.17: Air velocity vectors for tube 37, with arrows showing control volumes contributing air flow to tube 37 including entrainment of exit flow**

To account for the entrainment of air flow back into the heat exchanger at tube 37, the outlet enthalpy of tube 38 is assigned as the inlet enthalpy for tube 37.

For the purpose of simulation, the Chang-Wang correlation for air side heat transfer (Wang, *et al.* (2001)) was applied, on a control volume basis, by obtaining the average velocity of air per control volume. Chang, *et al.* (2006) was used for calculating air side pressure drop, while Gnielinski (1976) was used for single phase heat transfer coefficient. For two phase heat transfer and pressure drop, the correlation proposed by Jung and Radermacher (1989) was employed, while Blasius type equation (Schlichting and K. Gersten. (2000)) was used for single phase pressure drop. While the model is capable of using air heat transfer coefficients from the CFD results, it was not used here because the emphasis of this paper is on obtaining air maldistribution through CFD results.

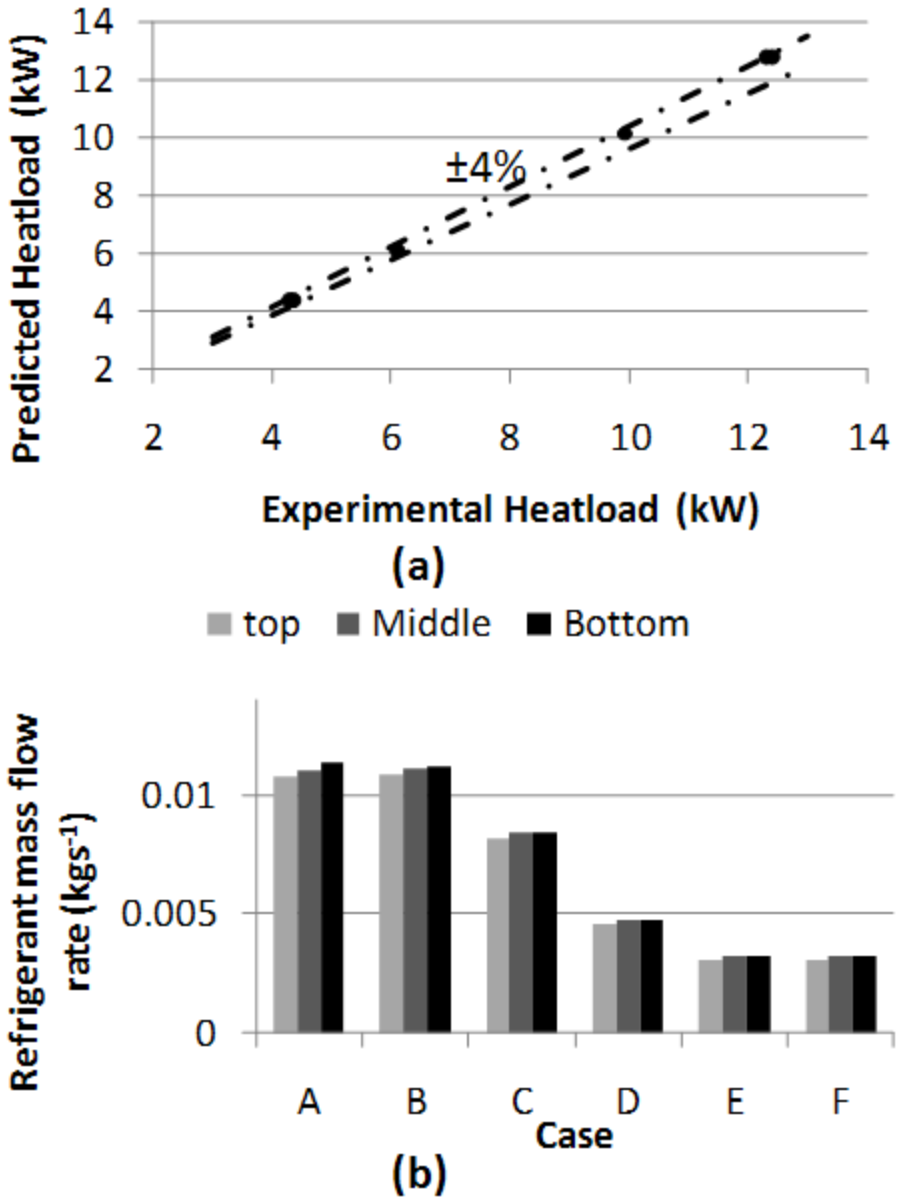


**Figure 5.18: (a) Comparison of predicted heat laod with measured heat capacity and (b) refrigerant mass flow rate distribution through the three circuits**

The overall heat capacity, shown in Figure 5.18(a), agrees within ±4%, without using any correction factors (multipliers) for any correlations, including air side heat transfer. The refrigerant mass flow rate distribution through the circuits is shown in Figure 5.18 (b).

In addition, this hybridization of CFD and a distributed heat exchanger model is capable of providing detailed data which can be used in optimizing existing heat exchangers, as well as designing new heat exchangers.

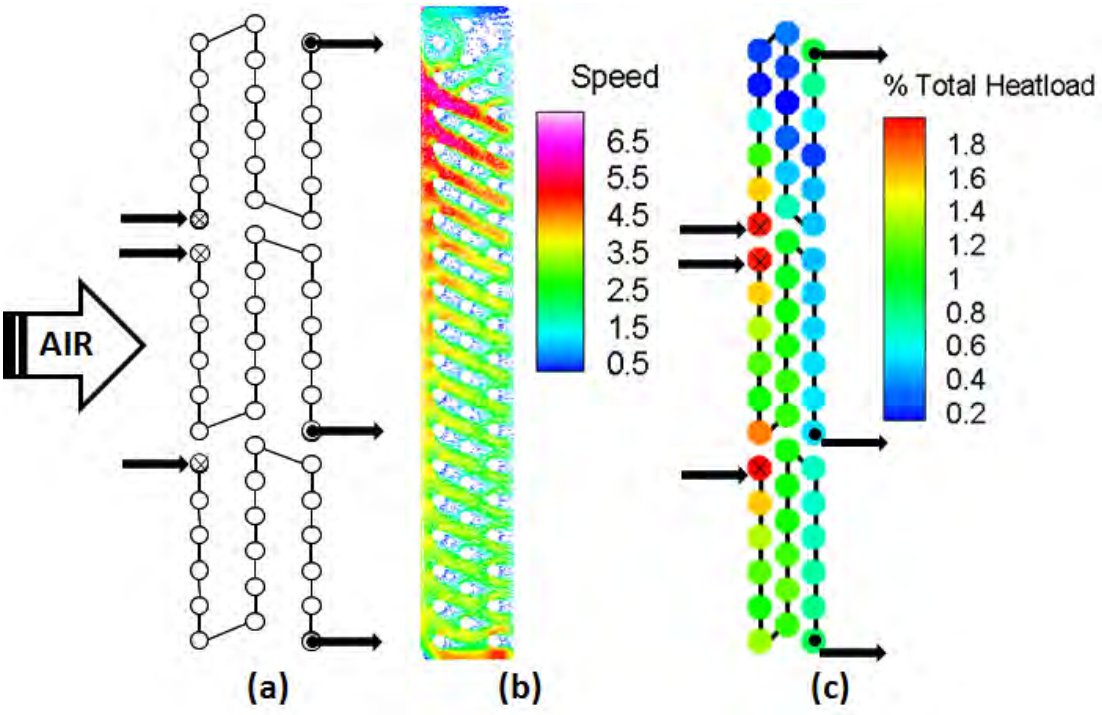


**Figure 5.19: (a) Coil circuitry of the left bank , (b) the 3D-CFD velocity vectors (ms-1) at the center line, and (c) the % heat capacity contribution of each tube to the total heat exchanger heat capacity**

Figure 5.19(c) shows the % heat capacity contribution of each tube to the total heat capacity. The results clearly show that tubes in the top most circuit contribute much less than the tubes in the middle and the bottom circuits. Tubes' airside performance is crucial during circuitry optimization since lower performing tubes should be supplied with less refrigerant flow, to thermally balance the heat exchanger.

### 5.5 Conclusions

A CFD-based air propagation method for fin-and-tube heat exchangers is introduced. The method can use both 2D and 3D CFD results, as well as structured

and unstructured CFD meshes. To interpret and process CFD results, the heat exchanger geometrical information is processed on a Cartesian grid. Using modified inverse distance averaging, the CFD results are interpolated to obtain air flow profiles for the heat exchanger. This information is used to propagate complex air flows through the heat exchanger. While the interpolation scheme leads to an acceptable error (less than 0.5% for 3D-CFD and less than 0.05% for 2D-CFD) in overall mass balance, this can be further improved by employing more advanced interpolation algorithms. Using the CFD-based air propagation, the predicted overall heat capacity for the R410A condenser agrees within ±4% of the experimentally measured values without employing any correction factors or multiplier on air side heat transfer coefficients.

2D (fin-less) and 3D (finned) CFD simulations of the A-coil show significant difference in the air flow profile through the heat exchanger. The 2D flow shows a much larger recirculation zone than the 3D simulation, in the top circuit of the heat exchanger. 2D simulations also show that the top circuit of the heat exchanger is practically starved, with most of the air flowing through the bottom two circuits. These observations show that 2D CFD cannot be used to simulate tube-fin heat exchangers as the presence of fins controls the air flow path through the heat exchanger.

This CFD-based approach for heat exchanger modeling can open new frontiers in the area of heat exchanger design optimization like circuitry optimization, fan-and-heat exchanger coupling, and heat exchanger placement in a duct to name a few. This approach provides coupling of a distributed heat exchanger model with CFD results,

and can provide greater insight into the design and performance prediction of heat exchangers.

# CHAPTER 6. MODELING OF FROST GROWTH AND ACCUMULATION IN FIN-AND-TUBE HEAT EXCHANGERS

This section describes the details of the model for frost growth on fin-and-tube heat exchangers. The overall modeling approach is described in section 2.1.1.

## 6.1.1 Modeling Assumptions

The model for frost growth is based on the following assumptions, in addition to the assumptions described in Section 2.1.2.

1) The process of frost growth is a quasi-steady process. This implies that the air side and refrigerant side conditions relax much faster than the transience of frost growth
2) Frost growth is one-dimensional, i.e. frost always grows perpendicular to the surface
3) Frost layer is homogenous, i.e. the mass of frost that adds to the density of the existing frost layer is distributed evenly throughout the frost thickness.
4) Thermal conductivity of the frost layer is a function of the instantaneous frost density

## 6.1.2 Solution Methodology

As explained in Section 2.1.4, the standard effectiveness-NTU formulae are not valid for conditions where a source or sink of flux is present, as in the case of tube-to-tube conduction. To address this issue, wall temperature linked equations based on the resistance diagram shown in Figure 2.2(c) were proposed. To model frost accumulation, this resistance diagram is modified to Figure 6.1 (a). The thermal conductivity of the frost layer is several orders of magnitude lower than commonly

used fin materials like aluminum, and can be neglected. The modified resistance diagram is shown in Figure 6.1 (b).

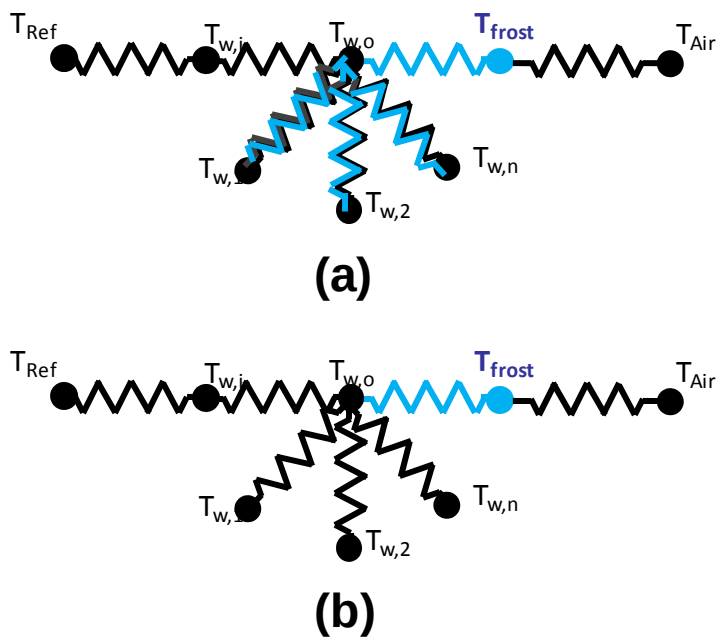


**Figure 6.1: Equivalent resistance diagram for frosting conditions (a), and simplified diagram (b) after ignoring frost layer, indicated by blue lines in (a), present on fins**

The refrigerant side and air side are linked through wall and frost temperature based energy conservation equations. The refrigerant side heat transfer equation based on Log-Mean Temperature Difference calculation is given by equation (6.1)

$$m_{ref,in}(h_{in} - h_{out}) = U_{ref} A_{in} \frac{(\Delta T_{1,r} - \Delta T_{2,r})}{\ln \frac{\Delta T_{1,r}}{\Delta T_{2,r}}} \tag{6.1}$$

The heat conducted through the tube walls, from inner wall to outer wall, is given by equation (6.2)

$$U_{ref} A_{in} \frac{(\Delta T_{1,R} - \Delta T_{2,R})}{\ln \frac{\Delta T_{1,R}}{\Delta T_{2,R}}} = \frac{2\pi kL}{\ln(d_o / d_i)} (Tw_i - Tw_o) \tag{6.2}$$

Now, the heat conducted through the tube walls, is conducted through the frost layer and through the fin sheet to neighboring tubes, given by equation (6.3)

$$\frac{2\pi kL}{\ln(d_o/d_i)}(Tw_o - Tw_i) = \sum_{n=1}^{nMax} k_{fin,eff} \times d_o \times th \times nFin \times \frac{(Tw_n - Tw_o)}{|R_0 - R_n|} + k_{fr} \times (A_{tube} + A_{fin}) \times \frac{(T_{fr} - Tw_o)}{\delta_{fr}} \tag{6.3}$$

The heat conducted through the frost layer is transferred to air, and is given by equation (6.4)

$$k_{fr} \times (A_t + A_{fin}) \times \frac{(T_f - Tw_o)}{\delta_{fr}} = \dot{m}_a c_{pa}\left(T_{a,o} - T_{a,i}\right) + \dot{m}_a i_{fg}\left(\omega_{a,o} - \omega_{a,i}\right) \tag{6.4}$$

Finally, the sensible energy balance on air side is given by equation (6.5)

$$m_a c_{pa}(T_{air,out} - T_{air,in}) = h_a \times (A_{tube} + A_{fin}) \times \frac{(\Delta T_{1,a} - \Delta T_{2,a})}{\ln \frac{\Delta T_{1,a}}{\Delta T_{2,a}}} \tag{6.5}$$

The unknowns and equations associated with the frost model are shown in Figure 6.2.

$$\left\{\begin{matrix} T_{air,out} \\ T_{wall,in} \\ T_{wall,out} \\ T_{frost} \\ h_{ref,out} \end{matrix}\right\} \quad \left\{\begin{matrix} m_{ref,in}(h_{in} - h_{out}) = U_{ref} A_{in} \frac{(\Delta T_{1,R} - \Delta T_{2,R})}{\ln \frac{\Delta T_{1,R}}{\Delta T_{2,R}}} \\ U_{ref} A_{in} \frac{(\Delta T_1 - \Delta T_2)}{\ln \frac{\Delta T_1}{\Delta T_2}} = \frac{2\pi kL}{\ln(d_o/d_i)}(Tw_i - Tw_o) \\ \frac{2\pi kL}{\ln(d_o/d_i)}(T_{wo} - T_{wi}) = \sum_{n=1}^{nMax} k_{fin,eff} \times d_o \times th \times nFin \times \frac{(T_{wn} - T_{wo})}{|R_0 - R_n|} \\ \qquad + k_{fr} \times (A_{tube} + \eta . A_{fin}) \times \frac{(T_{fr} - T_{wo})}{\delta_{fr}} \\ k_{fr} \times (A_t + \eta . A_{fin}) \times \frac{(T_{fr} - T_{wo})}{\delta_{fr}} = \dot{m}_a c_{pa}\left(T_{a,o} - T_{a,i}\right) + \dot{m}_a i_{fg}\left(\omega_{a,o} - \omega_{a,i}\right) \\ m_a c_{pa}(T_{air,out} - T_{air,in}) = h_a \times (A_{tube} + A_{fin}) \times \frac{(\Delta T_{1,a} - \Delta T_{2,a})}{\ln \frac{\Delta T_{1,a}}{\Delta T_{2,a}}} \end{matrix}\right\}$$

**Figure 6.2: Unknowns and equations associated with the frost growth model**

The solution methodology is explained in Figure 6.3.

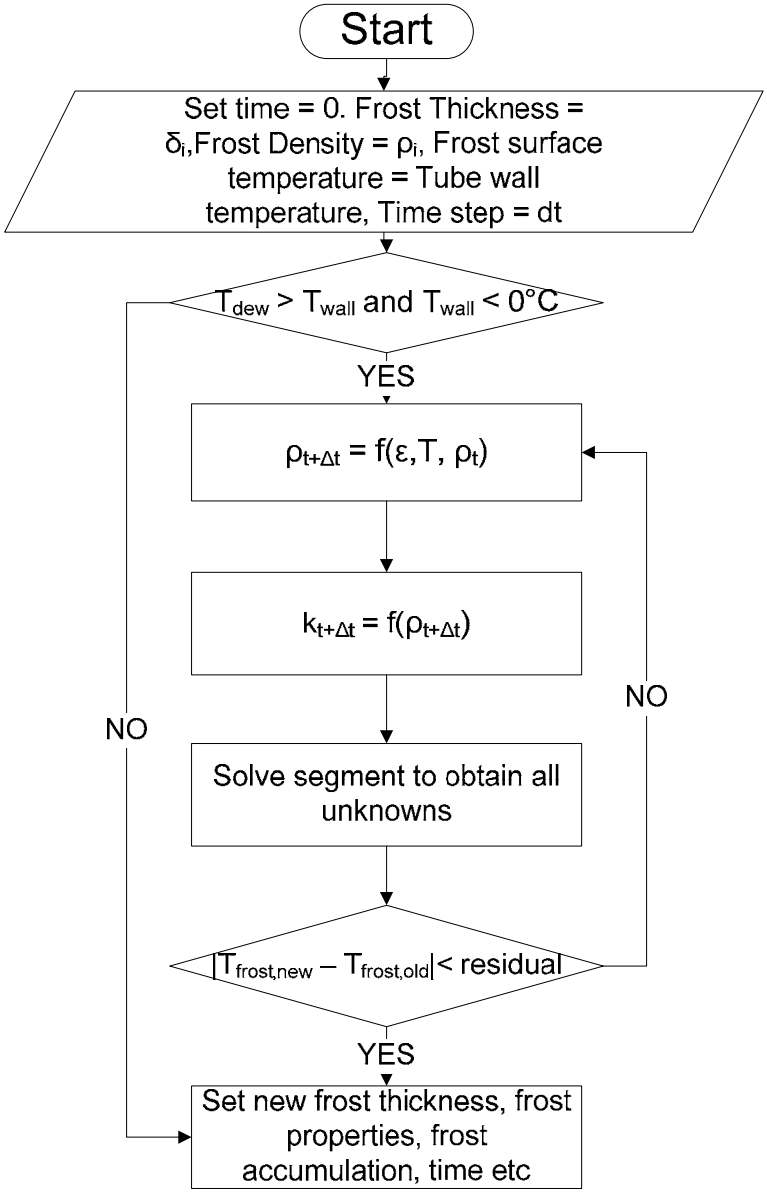


**Figure 6.3: Solution methodology for heat exchanger frost growth model**

The method requires an initial guess value for frost density, which can be assumed to be between 8 and 48 kg-m$^{-3}$, and initial frost thickness is assumed to be 0.02 mm (Na, 2003). These assumptions are essential because the proposed

formulation models the physics of frost growth and accumulation, not of frost incipience modeling of which is beyond the scope of the current research effort. The frost density at subsequent time step is calculated using (Na, 2003) shown in equation (6.6)

$$\rho_{fr,t+\Delta t} = \rho_{fr,t} + \frac{\tau \xi_{fr} D\left(\omega_{f,t} - \omega_{w,t}\right)}{\delta_{fr,t}} \times \frac{\Delta t}{\delta_{fr,t}} \tag{6.6}$$

where frost porosity is given by equation (6.7)

$$\xi_{fr} = \frac{\rho_{ice} - \rho_{fr,t}}{\rho_{ice} - \rho_{a,i}} \tag{6.7}$$

The diffusion coefficient of water is a function of pressure and temperature, and is given by the Sherwood and Pigford (1952) empirical correlation

$$D_v = \frac{9.238e^{-7}}{P} \frac{T_a^{2.5}}{\left(T_a + 245\right)} \tag{6.8}$$

The tortuosity factor, defined as the ratio of the path length for direct straight-line flow through frost to the path length for actual flow through frost, is given by the Prager correlation (Cunningham and Williams, 1980). The total mass of frost accumulated in a given time step is calculated by applying the Colburn analogy (McQuiston and Parker, 1994) to obtain the mass transfer coefficient, $h_d$.

$$Le^{2/3} = \frac{h_{air}}{c_{p,a} h_d} = 1.0^{2/3} \tag{6.9}$$

The equation for mass accumulated is given by equation (6.10)

$$\dot{m}_{fr} = \dot{m}_a \left(\omega_{a,i} - \omega_{a,o}\right) \tag{6.10}$$

Where humidity ratio of air exiting the control volume is given by equation (6.11)

$$\omega_{a,o} = \omega_{fr} + \left(\omega_{a,i} - \omega_{fr}\right) \Big/ e^{\left(h_a\left(A_b + \eta A_f\right)/\left(\dot{m}_a c_{p,a}\right)\right)} \tag{6.11}$$

Using the updated frost density and the total frost mass accumulated, the new thickness of frost is calculated using (6.12)

$$\Delta\delta_{fr} = \left[ \frac{\dot{m}_{fr}}{\left(A_o + \eta A_f\right)} - \left(\rho_{t+\Delta t} - \rho_t\right) \times \frac{\delta_{fr,t}}{\Delta t} \right] \frac{\Delta t}{\rho_{t+\Delta t}} \tag{6.12}$$

Thermal conductivity of frost is calculated using the Sander's correlation (Sanders,1974)

$$k_{fr} = 1.202 \times 10^{-3} \rho_{fr}^{0.963} \tag{6.13}$$

## 6.2 Validation

The model was validated against experiments conducted by Muehlbauer (2004) who tested an R-22 evaporator shown in Figure 6.4.

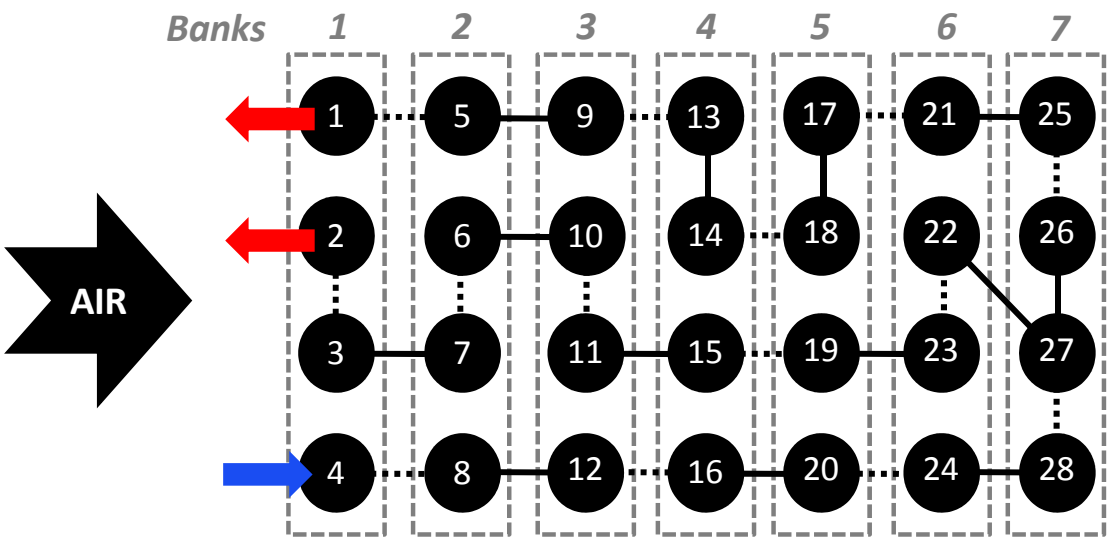


**Figure 6.4: End view of the R-22 evaporator used to validate frost growth model**

The specifications for the evaporator and the correlations employed are specified in Table 6.1. Considering the relatively low fin density of 7 fins per inch, the heat conduction between tubes through fins was neglected for this validation.

**Table 6.1: Heat exchanger specifications and correlations employed for validation**

| Parameters | | | Correlations | |
|---|---|---|---|---|
| Number of Segments | 10 | --- | Air Side HTC | Wang-Chi-Chang |
| Tube Configuration | Inline | | Refrigerant Side HTC - Two Phase | Dobson |
| Number of Tubes Per Bank | 4 | --- | Refrigerant Side HTC - Vapor | Dittus-Boelter |
| Number of Tube Banks | 7 | --- | | |
| Tube Length | 0.54 | m | Air Side DP | Wang-Chi-Chang |
| Tube OD | 0.0095 | m | Refrigerant Side DP - Two Phase | Friedel |
| Tube Thickness | 0.3 | mm | Refrigerant Side DP - Vapor | Blasius |
| Tube Vertical Spacing | 1 | in | | |
| Tube Horizontal Spacing | 1 | in | | |
| FPI | 7 | fpi | | |
| Fin Thickness | 0.005 | in | | |
| Fin Type | Flat | --- | | |
| Coil Face Air Velocity | variable | $ms^{-1}$ | | |

The evaporator was tested over 6 frost-and-defrost cycles. The repeated cycles were aimed at understanding the contribution of condensate retention on successive frost growth periods. However, the first cycle where the coil is completely dry to begin with has been used for the validation here. The coil was tested at two different air flow rates, and for modeling purposes, the air flow rate was fitted to a curve which was used in the model. The curve fits are shown in Figure 6.5 and Figure 6.6. While the model is capable of employing a fan performance characteristics curve and suitable pressure drop correlations to obtain the air flow rate through the heat exchanger for each time step, a curve fit was employed to eliminate the uncertainty associated with a lack of suitable air pressure drop correlations for frosted coils.

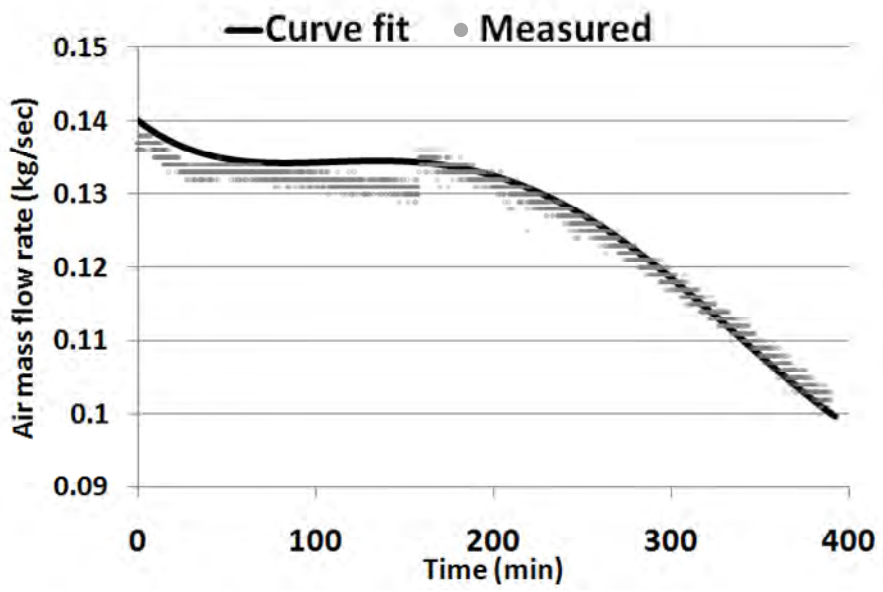


**Figure 6.5: Polynomial curve fit of the inlet air flow rate of 210 cfm used for the simulation**

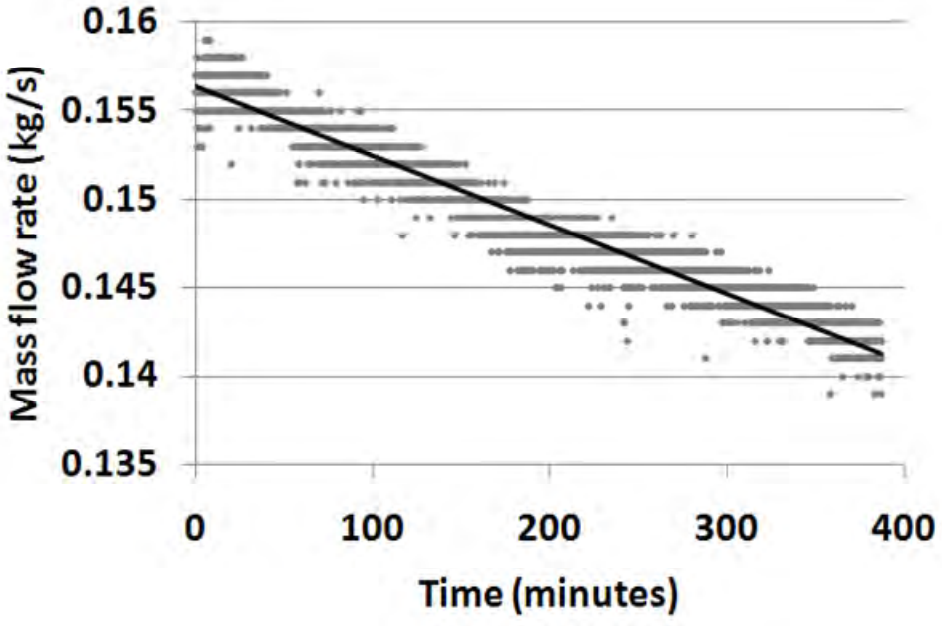


**Figure 6.6: Linear curve fit of air flow rate of 240 cfm used for the simulation**

To ensure time step independence of simulation results, two different time steps of 0.5 and 0.05 seconds were tested for air flow rate of 210 cfm and a time step of 0.5 seconds was chosen. A representative test (growth of frost density with time on

tube 28 for 210 cfm case) for time step independence is shown in Figure 6.7. The highest transients during the frost growth period are in the initial stages. Therefore, only the first 100 seconds of the frost growth period is shown in the figure.

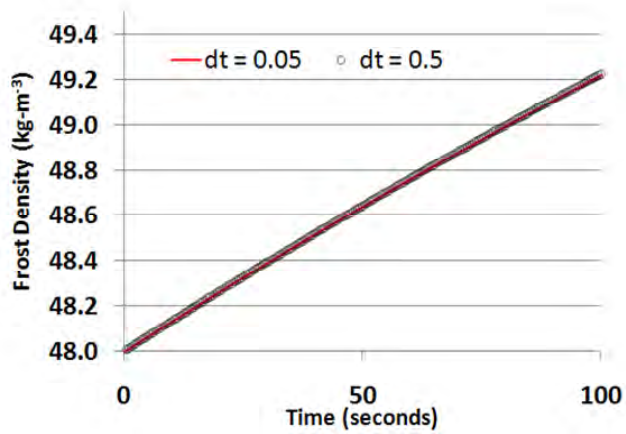


**Figure 6.7: Effect of time step on frost density prediction on Tube 28 illustrates time step independence**

## 6.2.1 Validation results

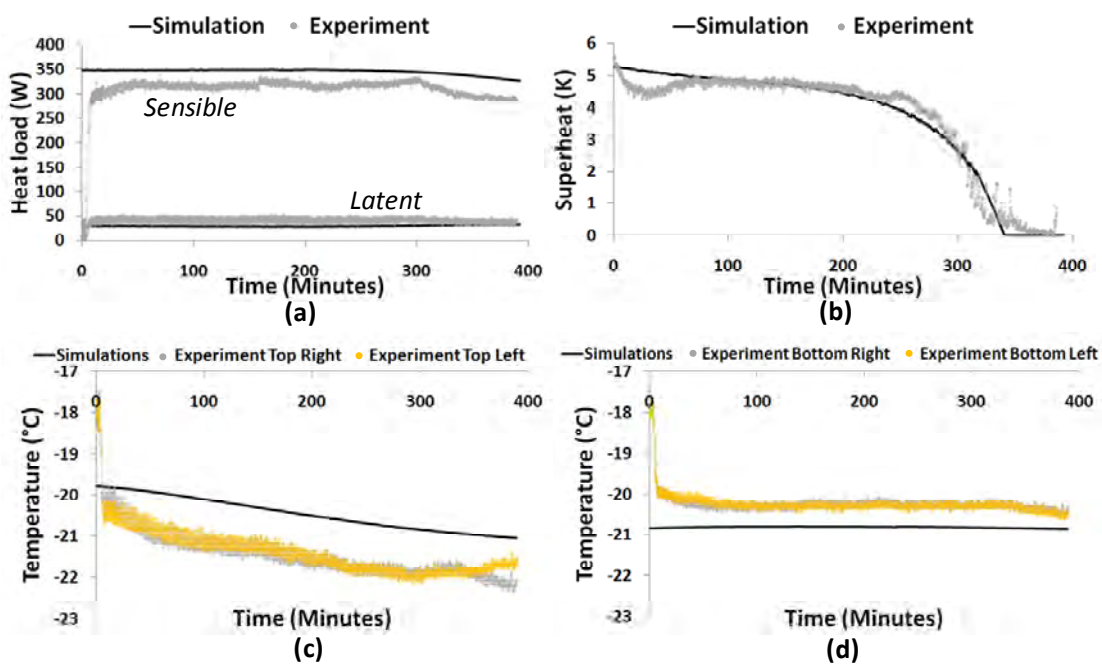


**Figure 6.8: (a) Comparison of simulated and measured sensible and latent heat capacity, (b) comparison of simulation and experimental outlet superheat, (c) comparison of outlet air temperature at the top of the coil and (d) the bottom of the coil.**

Figure 6.8(a) shows the comparison of simulated and measured sensible and latent heat capacities for 210 cfm air flow rate case. The total heat capacity is predicted within 5% of the measured heat capacity. The sensible heat capacity is over predicted 10% whereas the latent heat capacity is under-predicted by 25%. For the 240 cfm case, the sensible heat capacity is over-predicted by 10% on an average over the entire frost growth period, whereas the latent heat capacity is over-predicted by 20% as shown in Figure 6.9 (a).

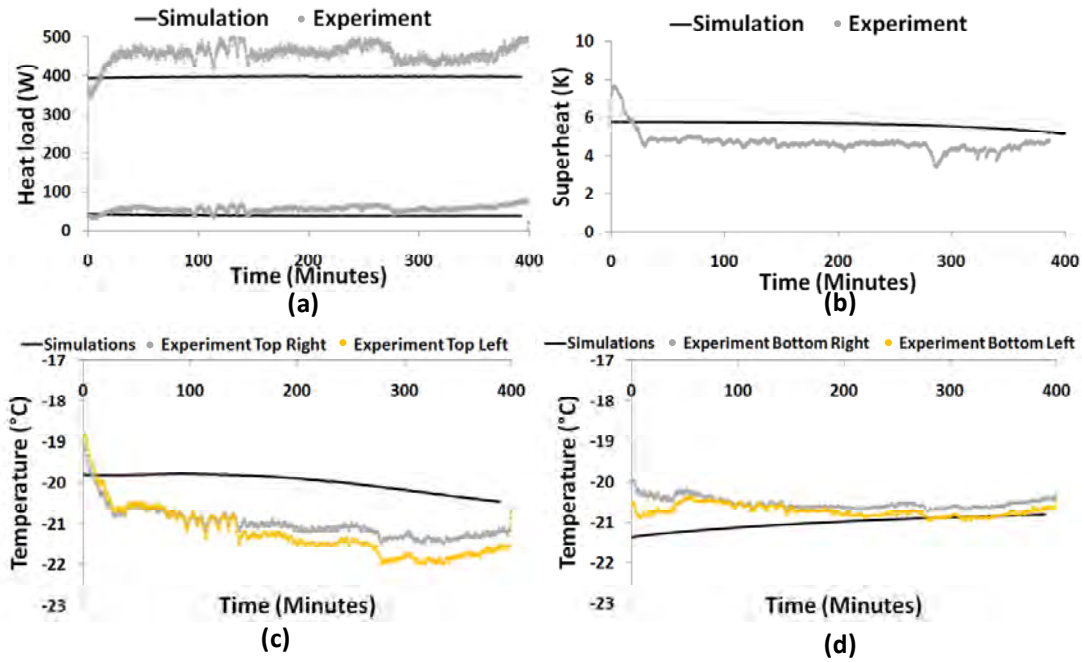


**Figure 6.9: (a) Comparison of simulated and measured sensible and latent heat capacity, (b) comparison of simulation and experimental outlet superheat, (c) comparison of outlet air temperature at the top of the coil and (d) the bottom of the coil.**

It should be noted that the model is aimed at simulating the phenomena of frost growth and accompanying coil performance and does not aim to model the pull down period. While Colburn analogy was employed to calculate dehumidification for these simulations, the results could be improved through the use of multipliers or

correlations for Lewis number. For the 210 cfm case, the predicted time for loss of superheat was 338 minutes, while experiment failed to maintain a steady superheat near 340 minutes, as shown by Figure 6.8(b). The maximum difference between the predicted and the measured superheat values is ±1°C at any time during the frost growth period. For the 240 cfm case, the superheat is predicted within 1.5°C of the measured superheat, as shown in Figure 6.9 (b). For 240 cfm case, the superheat is never lost. The outlet air temperatures were measured at four locations, the two tube ends at the top of the coil and the two tube ends at the bottom of the coil. Figure 6.8(c) and (d) compare the average outlet temperatures at the top tube and the bottom tube with their respective experimental values for the 210 cfm air flow rate case. For 210 cfm, the average outlet temperature at the top tube is over-predicted by a maximum value of 1°C and the bottom is under-predicted within 1°C. Figure 6.9 (c) and (d) compare the average outlet temperatures of the top tube and the bottom tube with the measured values for 240 cfm air flow rate case. For 240 cfm, the average outlet temperature at the top tube is over-predicted by a maximum value of 1.5 °C and the bottom is under-predicted within 1°C. It should be noted that the trends of a relatively flat outlet air temperature profile over the frost growth period at the bottom of the heat exchanger, and decreasing air temperature near the top of the heat exchanger are captured accurately by the model. The bottom part of the coil is predominantly two phase and maintains a near constant temperature, while the top part of the coil is mainly superheated during the initial stages of the frost growth period, and progressively becomes two phase as frost accumulates and air flow drops.

This leads to a lower frost surface temperature over time leading to a constantly reducing outlet air temperature.

### 6.3 Model Verification and Capabilities

The model facilitates the investigation of frost growth on a segment-by-segment basis throughout the frost growth period. As shown in Figure 6.10(e) through (g), all tubes in banks 5, 6 and 7 of the evaporator start accumulating frost from the onset of the frost cycle, while the upper tubes in the rest of the banks accumulate frost as the coil performance starts to degrade due to frost growth and accompanying drop in air flow rate due to blocked passages.

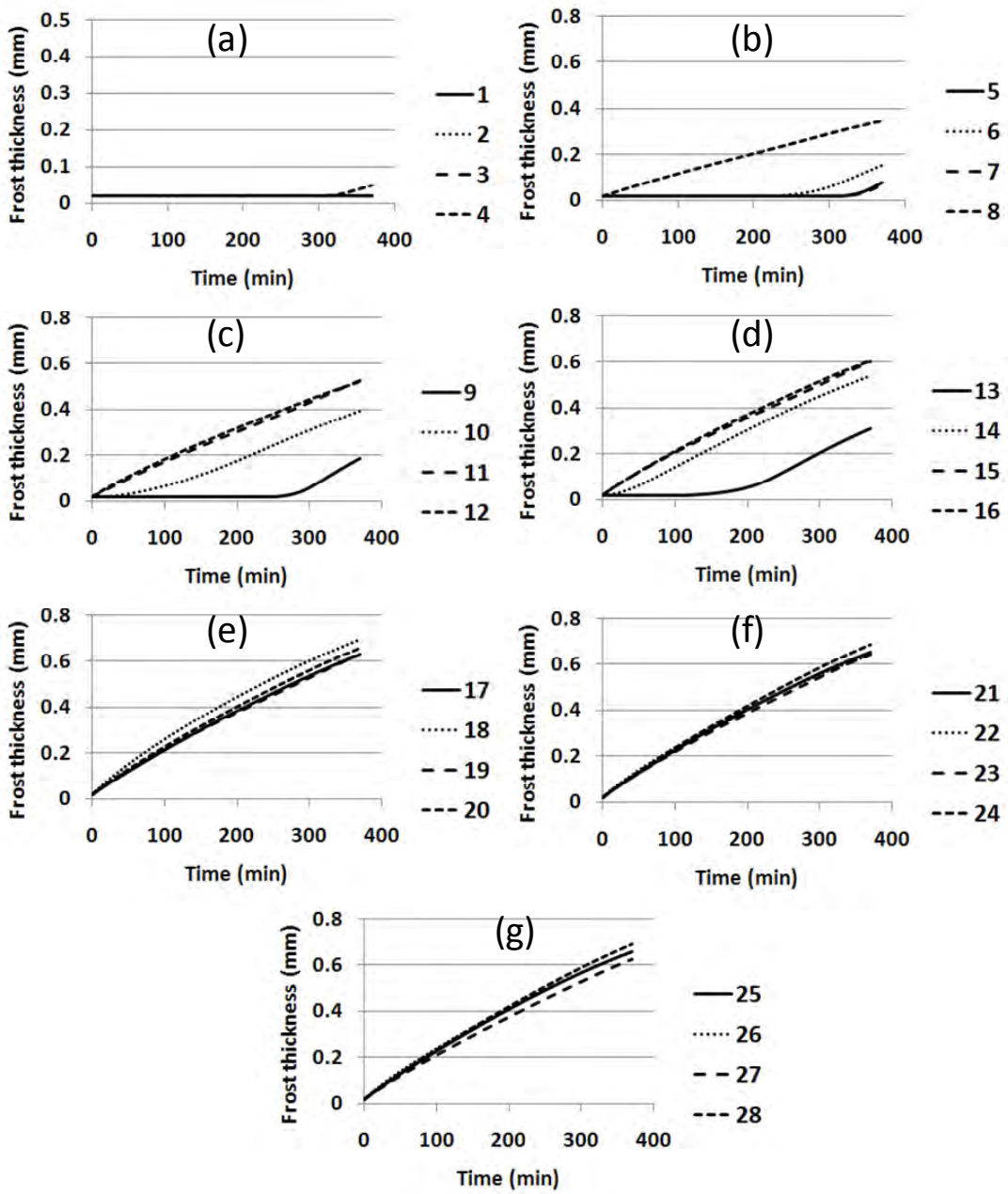


**Figure 6.10: Plots showing growth of frost layer through tubes (a) 1 to 4, (b) 5 to 8, (c) 9 to 12, (d) 13 to 16, (e) 17 to 20, (f) 21 to 24 and (g) 25 to 28.**

Figure 6.11 shows that the tubes in the banks near the exit are nearly 40% blocked by the end of the frost cycle.

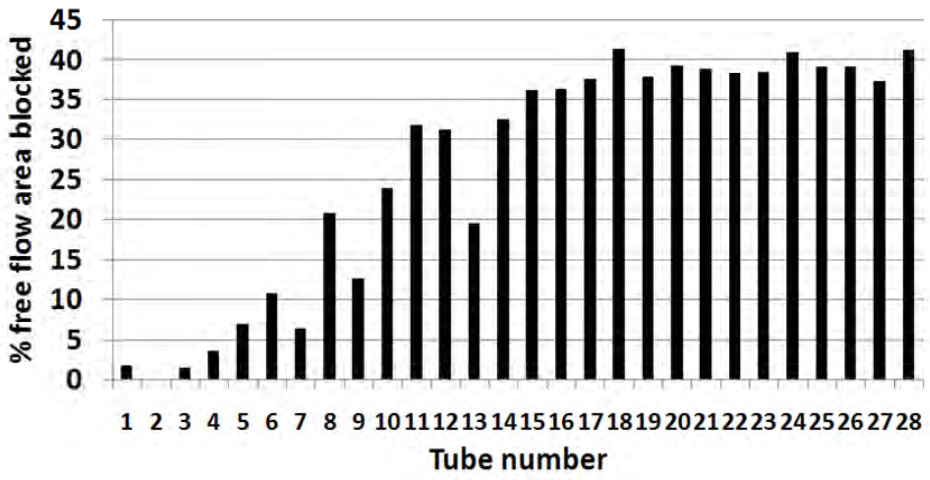


**Figure 6.11: % blockage of free flow area for all tubes at the end of the frost period**

This is a consequence of lower wall temperatures towards the latter banks of heat exchanger, as shown in Figure 6.12 which leads to lower density of frost accumulation shown in Figure 6.13, and therefore greater thickness when it accumulates. The increase in the difference between the two temperatures with time indicates growth of a frost layer on the tube.

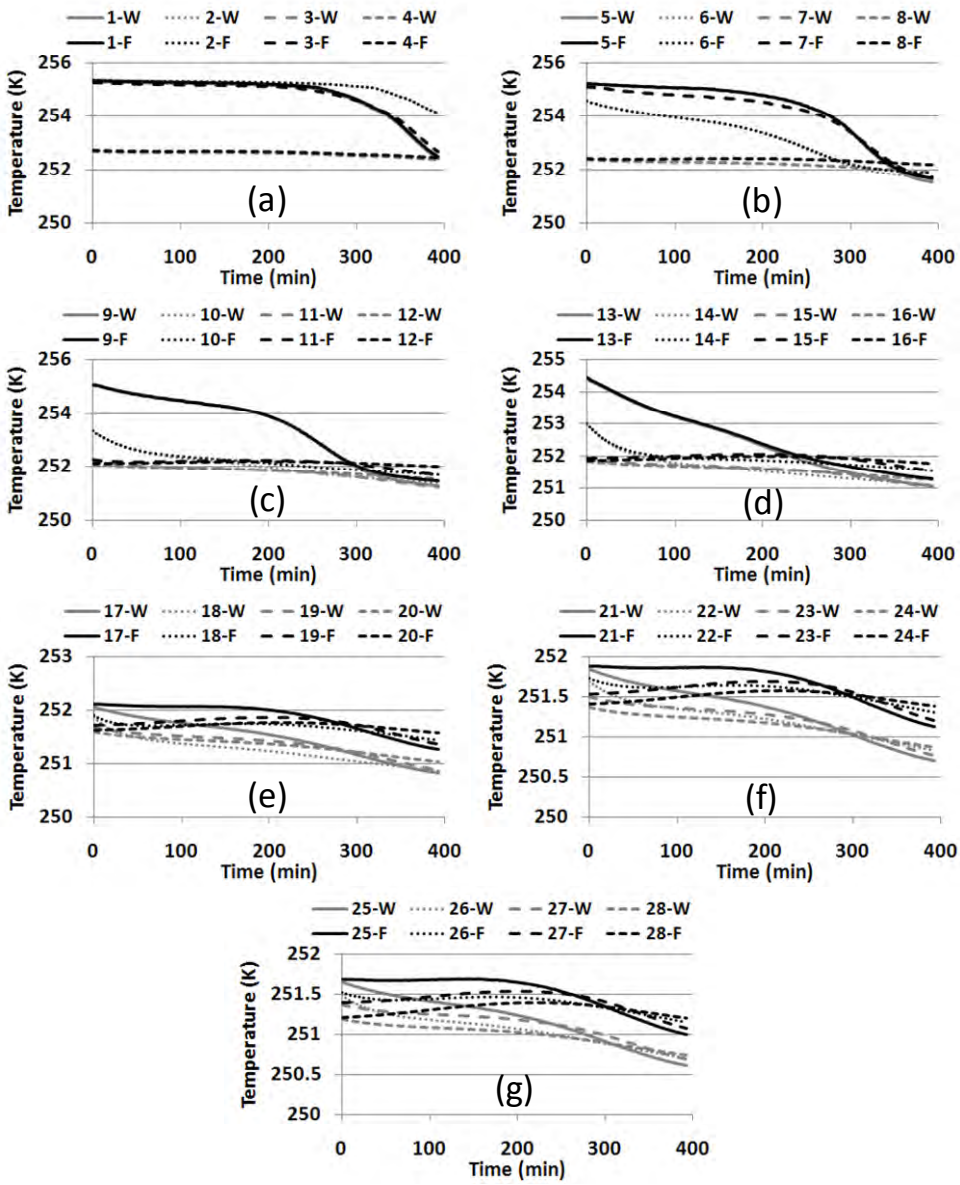


**Figure 6.12: Plots showing time response of tube wall (W) and frost surface (F) temperatures through tubes (a) 1 to 4, (b) 5 to 8, (c) 9 to 12, (d) 13 to 16, (e) 17 to 20, (f) 21 to 24 and (g) 25 to 28.**

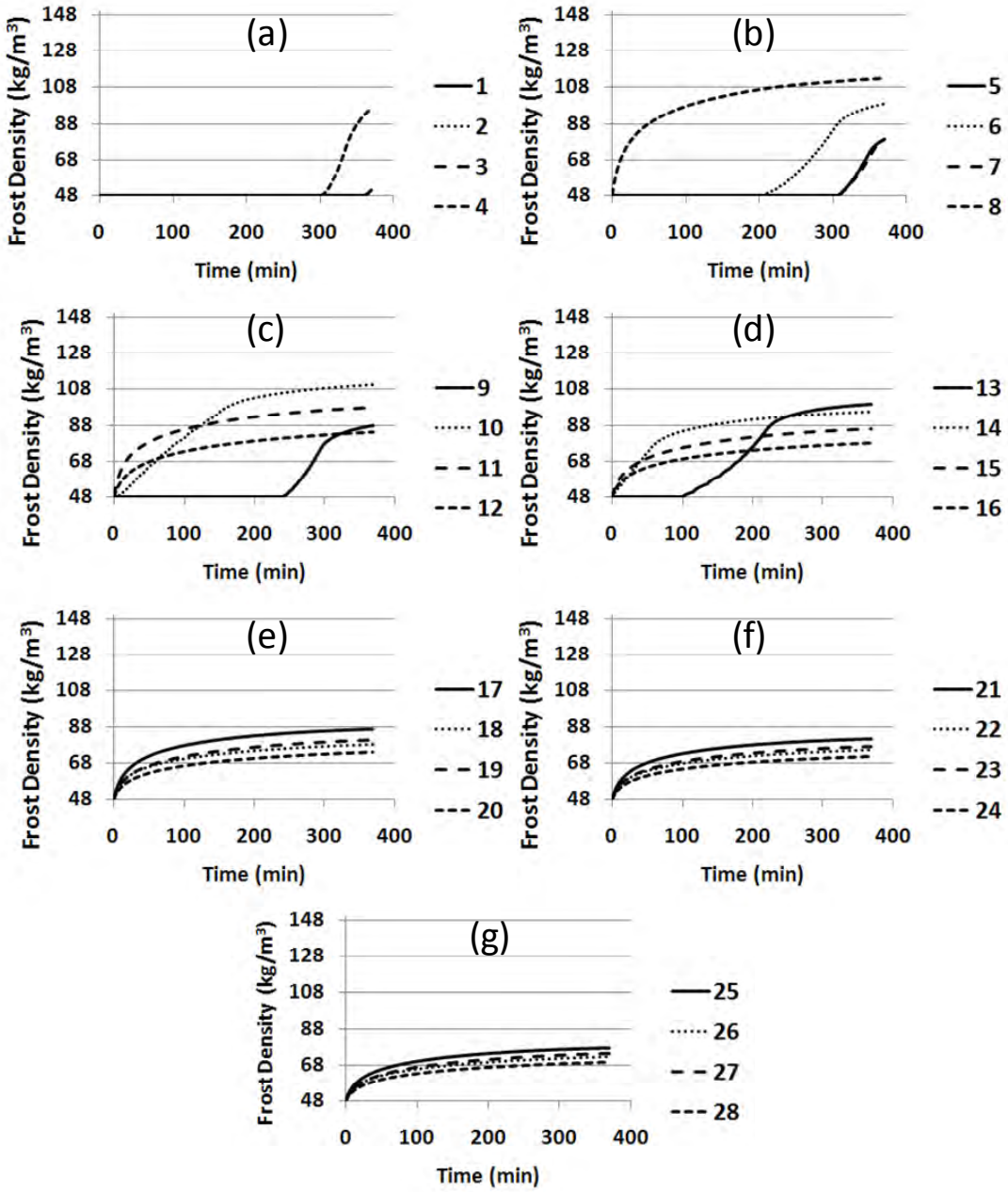


**Figure 6.13: Plots showing time response of frost density through tubes (a) 1 to 4, (b) 5 to 8, (c) 9 to 12, (d) 13 to 16, (e) 17 to 20, (f) 21 to 24 and (g) 25 to 28.**

## 6.4 Conclusions

A quasi-steady state heat exchanger model for simulating frost growth and accumulation on fin-and-tube heat exchangers was developed. The model is capable of simulating frost growth on a heat exchanger on a segment-by-segment basis,

accounting for heat conduction between tubes through fin sheets and it completely models the refrigerant side equations as well which permits prediction of important variables like outlet superheat from the evaporator. The model was validated against frost growth experiments, and the total heat capacity was found to be within 10% of measured values. The superheat was predicted within ±1°C of measured value throughout the frost growth period and the time at which superheat is lost was predicted within 2 minutes of measured value. The air outlet temperatures were predicted within ±1°C of measured values.

The model presented is semi-empirical as it employs correlations for frost density and conductivity but uses physics-based modeling for frost mass accumulation. Considering the purpose of the model, the quasi-steady state assumption facilitates relatively coarse time steps which are critical in curbing the total computational cost of simulations. While most frost evaporators have low fin densities to allow extended periods between defrosting, the ability to model tube-to-tube heat conduction enables the investigation of this on frost growth, if and when desired. The segmented nature of the model allows the study of local variables over the frosting cycle. While a curve fit of varying air flow rate with time was employed, ideally a fan performance characteristic equation should be solved simultaneously with a suitable air side pressure drop equation at every time step to obtain the air flow rate.

# CHAPTER 7. INVESTIGATION OF ENTROPY GENERATION MINIMIZATION IN HEAT EXCHANGER DESIGN

This study investigates the applicability of entropy generation minimization to heat exchanger design in terms of improving heat exchanger performance. Number of entropy generation units describes the irreversibility rate of a heat exchanger using a non-dimensional number. $N_S \rightarrow 0$ implies an almost perfect heat exchanger where both temperature difference and pressure drop losses approach zero. On the other hand, a high $N_S$ implies high losses owing to temperature difference or pressure drop or both. The following section outlines the formulation implemented for the current work, and first developed by Bejan (1978)

## 7.1.1 Entropy Generation

Figure 7.1(a) shows a segment of a heat exchanger of length *dx*. Fluid is flowing from left to right and the fluid control volume is shown by the dashed line. Entropy generated by such a unit of heat exchanger is given by the following equation(7.1).

$$d\dot{S}_{gen} = \dot{m}ds - \frac{q'dx}{T + \Delta T} \tag{7.1}$$

Number of entropy generation units is defined as

$$N_S = \frac{Td\dot{S}_{gen}}{q'dx} \tag{7.2}$$

Given the segmented nature of Jiang *et al.*'s model, it readily facilitates the use of entropy generation units to analyze the irreversibility losses in a heat exchanger. It should be noted that pressure drop is incorporated in the *ds* term.

7.1.2 Effect of Wall-Fluid ΔT on Number of Entropy Generation Units

As shown in Figure 7.1(b), Bejan (1978) illustrated the existence of an optimum ΔT /T where the proper tradeoff between fluid friction losses ($N_{S,\ \Delta P}$) and heat transfer losses ($N_{S,\ \Delta T}$) occurs. When $\Delta T / T < (\Delta T / T)_{opt}$, the heat transfer losses are small compared with the fluid friction losses. When $\Delta T / T > (\Delta T / T)_{opt}$ the number of entropy generation units is dominated by pressure drop losses. However, Bejan assumed that the air side behavior would mimic the refrigerant side behavior in terms of irreversibility. Though this might be true for entropy generated due to heat transfer, it is not necessarily true for entropy generated due to pressure drop. In the current study, authors combine the entropy generated on both sides of the heat exchanger, which is non-dimensionalized based on local flux and local wall temperature, as shown in equation (7.1) to obtain number of entropy generation units.

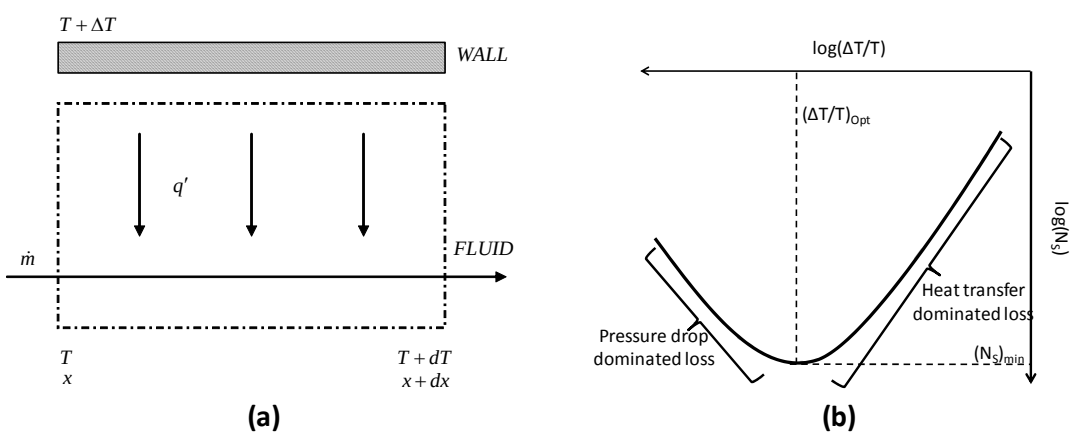


**Figure 7.1: Schematic of entropy generation and optimum point of operation.**

To reduce the irreversibility losses in a heat exchanger, the entropy generated throughout the heat exchanger must be minimized. To evaluate this, a metric as described in equation (7.3) was developed, to obtain the total entropy generated in a

heat exchanger. This was facilitated by the segmented nature of the heat exchanger model.

$$Metric = \sum_{nMax} N_S \tag{7.3}$$

Where, nMax is the total number of segments in the heat exchanger.

7.1.3 Entropy Generation Units and Heat Exchanger Performance

While it is evident that entropy generation units quantify the irreversibility losses in a heat exchanger, it is important to understand the heat capacity and pressure drop performance of a heat exchanger when the entropy generation is minimized. To study this, an R134a condenser, an R134a evaporator, a hot water coil and a chilled water coil were chosen. The evaporator and condenser coil employed is shown in Figure 7.2.

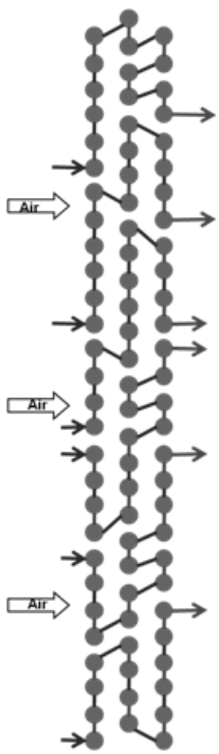


| Parameters | | |
|---|---|---|
| Number of Segments | 10 | --- |
| Tube Configuration | Staggered | |
| Number of Tubes Per Bank | 28 | --- |
| Number of Tube Banks | 3 | --- |
| Tube Length | 0.45 | m |
| Tube OD | 0.01 | m |
| Tube Thickness | 0.3 | mm |
| Tube Vertical Spacing | 0.75 | in |
| Tube Horizontal Spacing | 0.5 | in |
| FPI | 15 | fpi |
| Fin Thickness | 0.0043 | in |
| Fin Type | Louver | --- |
| Coil Face Air Flow Rate | 938 | cfm |

**Figure 7.2: Condenser/Evaporator coil used in entropy study**

The water coil employed in the study is shown in Figure 7.3.

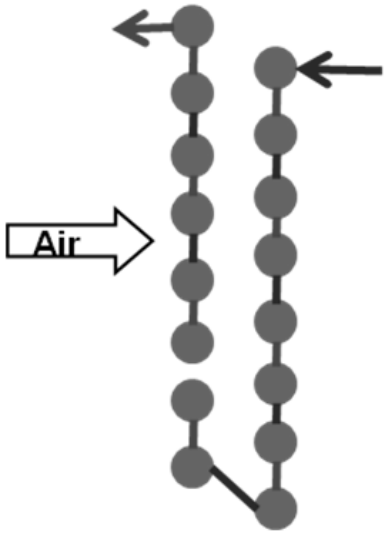


| Parameters | | |
|---|---|---|
| Number of Segments | 10 | --- |
| Tube Configuration | Staggered | |
| Number of Tubes Per Bank | 8 | --- |
| Number of Tube Banks | 2 | --- |
| Tube Length | 0.8 | m |
| Tube OD | 0.0084 | m |
| Tube Thickness | 0.3 | mm |
| Tube Vertical Spacing | 1 | in |
| Tube Horizontal Spacing | 0.625 | in |
| FPI | 22 | fpi |
| Fin Thickness | 0.0043 | in |
| Fin Type | Louver | --- |
| Coil Face Air Flow Rate | 185 | cfm |

**Figure 7.3: Water coil used in entropy study**

A parametric study was performed by varying the tube length while the air flow rate was kept constant. As shown in Figure 7.4 through Figure 7.7, increase in heat capacity flattens out after a certain point due to pinching, but refrigerant side pressure drop continues to increase. When the metric of total entropy generation units is compared with various tube lengths, it is evident that the minimum entropy is generated when the heat capacity gain diminishes but the refrigerant side pressure drop continues to increase. This gives an optimum tube length in terms of minimum entropy generation.

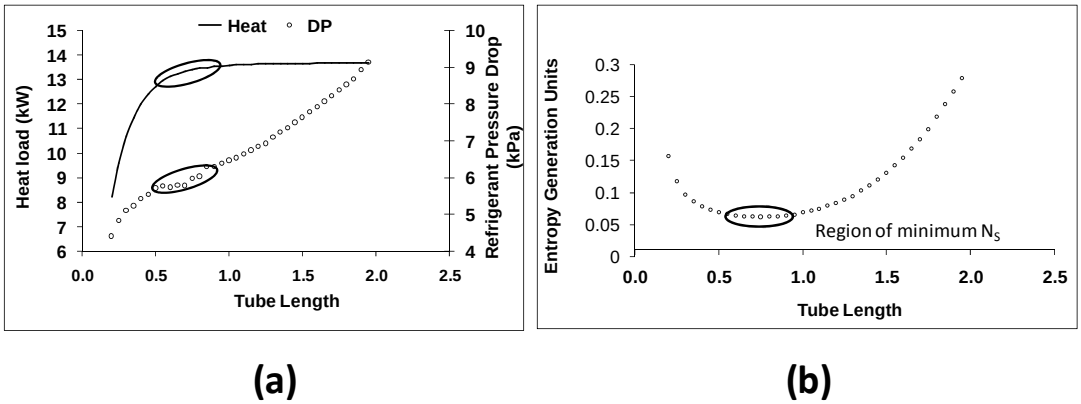


(a) (b)

**Figure 7.4: Effect of varying tube length for R134a condenser on entropy generation, heat capacity and refrigerant pressure drop**

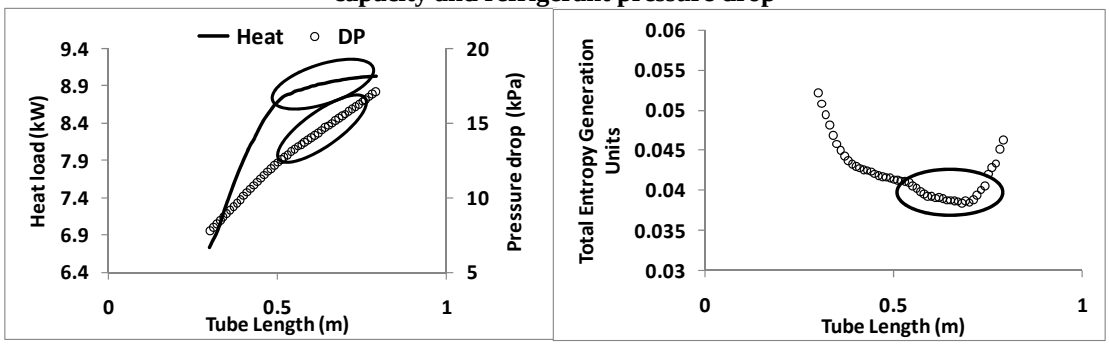


(a) (b)

**Figure 7.5: Effect of varying tube length for R134a evaporator on entropy generation, heat capacity and refrigerant pressure drop**

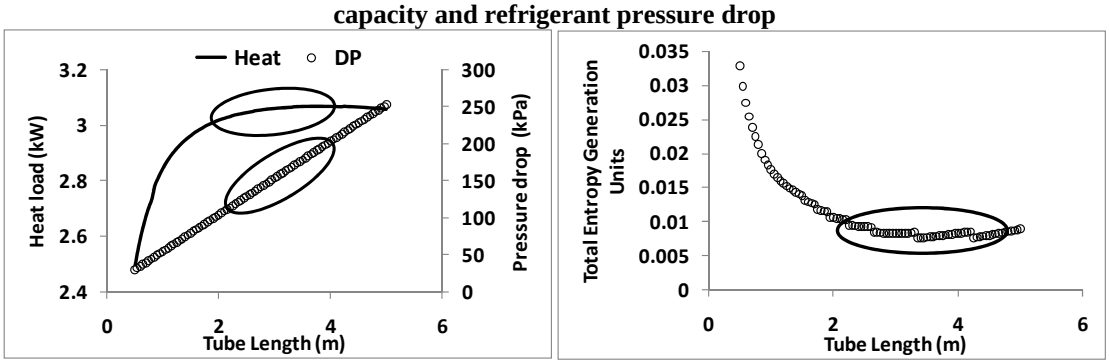


(a) (b)

**Figure 7.6: Effect of varying tube length for a chilled water coil on entropy generation, heat capacity and refrigerant pressure drop**

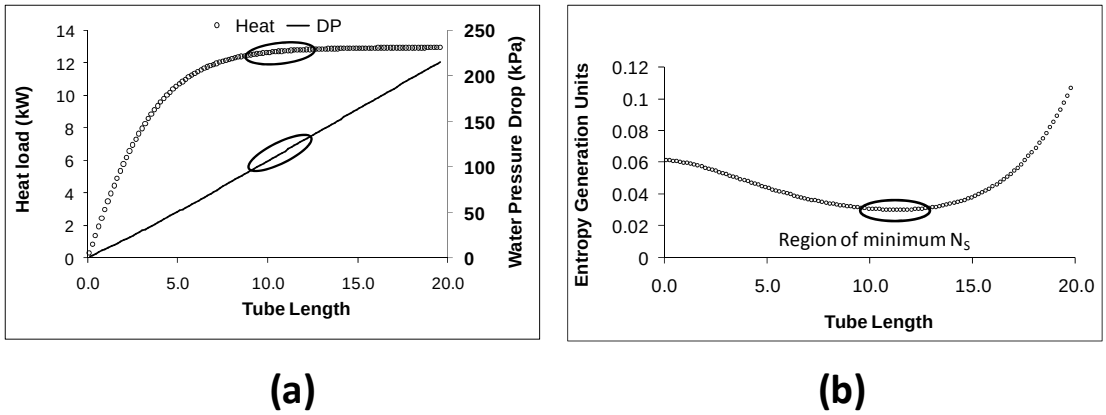


(a) (b)

**Figure 7.7: Effect of varying tube length for hot water coil on entropy generation, heat capacity and refrigerant pressure drop**

Similarly, if a parametric study is conducted with varying fin density, the results as shown in Figure 7.8 through Figure 7.11, show that gain in heat capacity diminishes after a certain point but air side pressure drop continues to increase. At that fin density, the entropy generated in the heat exchanger is minimized.

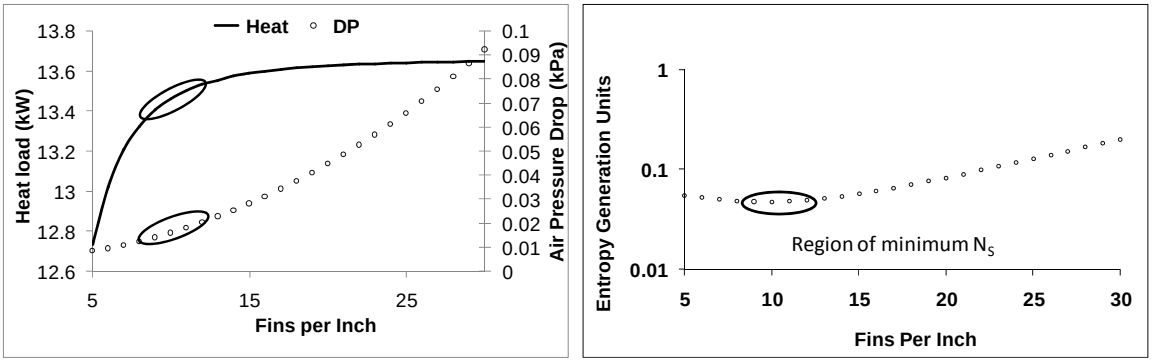


(a) (b)

**Figure 7.8: Effect of varying fin density for R134a condenser on entropy generation a, heat capacity and air pressure drop**

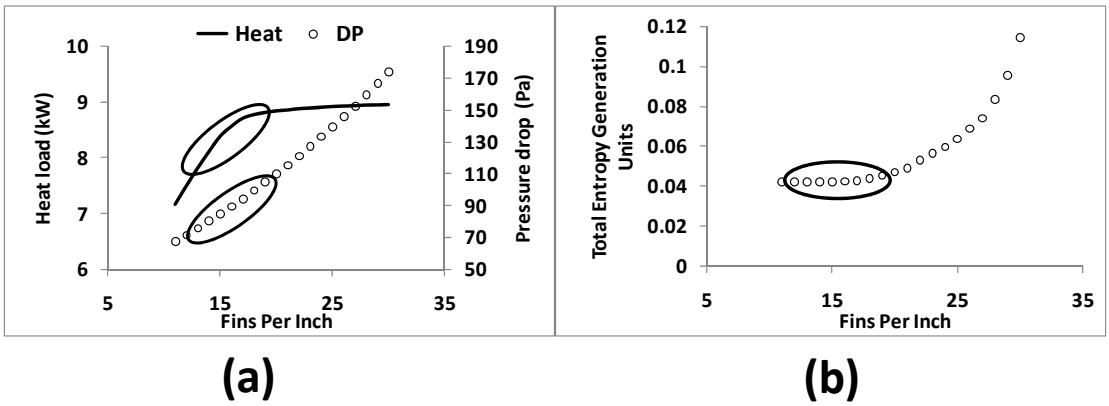


**Figure 7.9: Effect of varying fin density for R134a evaporator on entropy generation a, heat capacity and air pressure drop**

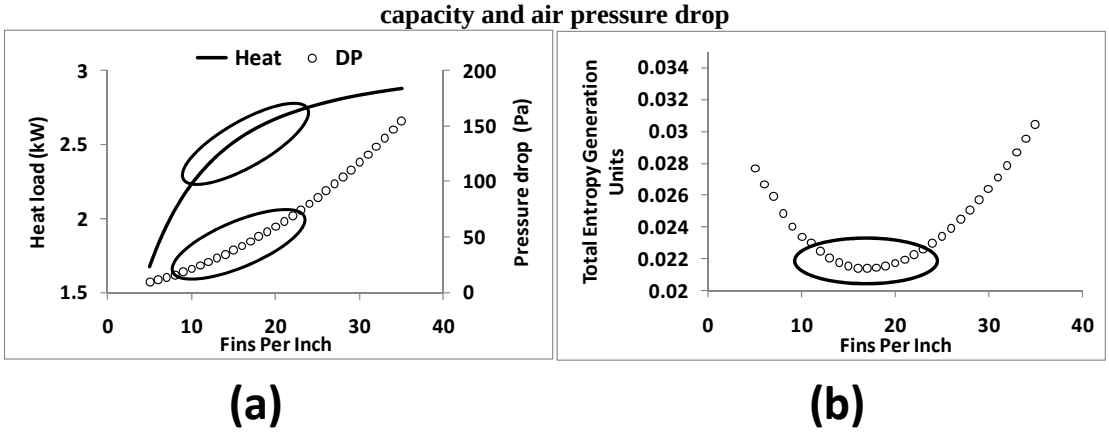


**Figure 7.10: Effect of varying fin density for a chilled water coil on entropy generation a, heat capacity and air pressure drop**

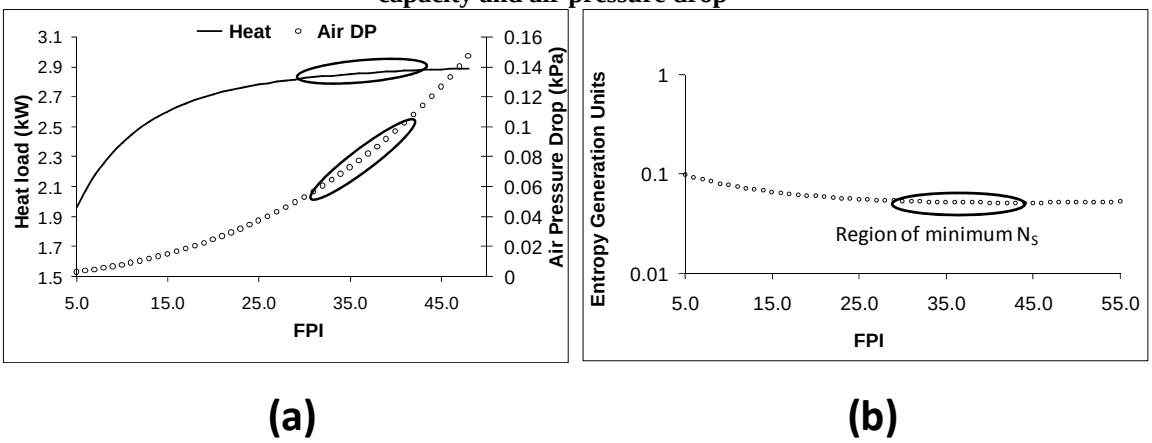


**Figure 7.11: Effect of varying fin density for hot water coil on entropy generation a, heat capacity and air pressure drop**

From these results, it can be inferred that entropy generation is minimized when air pressure drop continues to increase whereas heat capacity gain disappears. It is evident that minimized entropy generation helps quantify the pinch off location in a heat exchanger. It is also clear that in some cases like a study on fins per inch for a hot water coil, minimization of entropy generation might lead to economically expensive designs.

## 7.2 Optimization Study

To better understand the usefulness of entropy generation minimization as a parameter, two optimization problems were set up as shown in Table 7.1. Problem A minimized cost and maximized heat capacity of a given heat exchanger for four variables, viz., tube length, tube vertical spacing, tube horizontal spacing, and fin density. Problem B minimized entropy generation (Total $N_s$) and minimized cost of a given heat exchanger for the same variables as problem A. The optimization process involved a total of 4800 simulations carried out by varying the parameters described in Table 7.1. Using the procedure of non-dominated sorting, the design points were sorted based on the two objectives. Because the optimization was carried out by exhaustive search, the design points for the two problems were same. This allowed the comparison of the solution spaces of the problem A and problem B. This optimization study is carried out for a hot water coil and a condenser.

**Table 7.1: Problem formulation**

| PROBLEM A | PROBLEM B |
|---|---|
| Objectives: minimize material cost<br>maximize heat load | Objectives: minimize material cost<br>minimize entropy generation units |
| Variables: Tube length [0.3m, 0.6m]<br>Tube vertical spacing [19.05mm,38.1mm]<br>Tube horizontal spacing [12.7mm, 25.4mm]<br>Fins per inch [10, 25] | Variables: Tube length [0.3m, 0.6m]<br>Tube vertical spacing [19.05mm,38.1mm]<br>Tube horizontal spacing [12.7mm, 25.4mm]<br>Fins per inch [10, 25] |

7.2.1 Hot Water Coil

The specifications of the hot water coil tested are shown in Table 7.2.

**Table 7.2: Specifications of the hot water coil**

| Parameters | | |
|---|---|---|
| Number of Segments | 10 | --- |
| Tube Configuration | Staggered | |
| Number of Tubes Per Bank | 8 | --- |
| Number of Tube Banks | 2 | --- |
| Tube Length | 0.8 | m |
| Tube OD | 0.0084 | m |
| Tube Thickness | 0.3 | mm |
| Tube Vertical Spacing | 1 | in |
| Tube Horizontal Spacing | 0.625 | in |
| FPI | 22 | fpi |
| Fin Thickness | 0.0043 | in |
| Fin Type | Louver | --- |
| Coil Face Air Flow Rate | 185 | cfm |

For problem A, the number of design points that were Pareto optimal contained 60 points out of a total of 1800 design points evaluated. For problem B, the number of design points on the Pareto optimal front was 63 out of 1800 design points evaluated. Out of 63 points found as a solution for problem B, 55 points were the same as the ones in the solution space for problem A. Figure 7.12 shows the comparison of the two solution spaces. It is evident that even the points that are not present in both the solutions also lie close to the Pareto optimal front. It is important to note that coils with minimum entropy generation units tend to be more costly from a material requirement point of view.

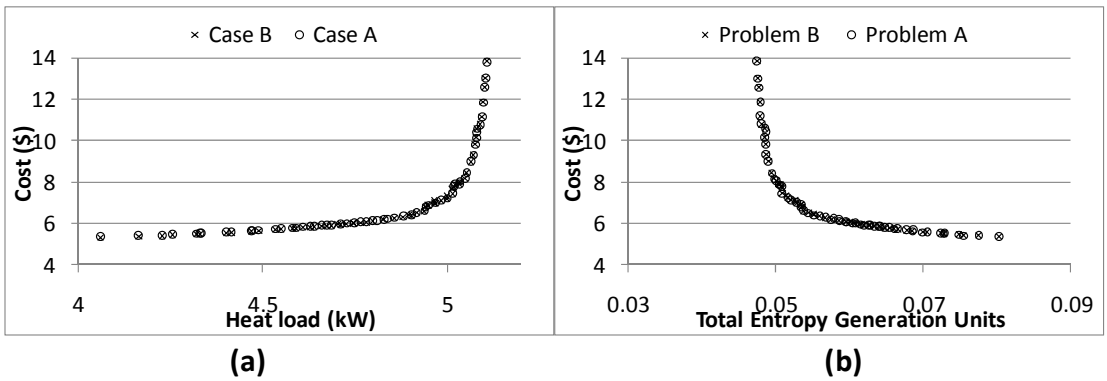


**Figure 7.12: Optimization results for (a) Problem A and (b) for Problem B**

In order to investigate points that are not common to the two solution spaces, it is important to study the refrigerant pressure drop. Comparing cost and heat capacity per unit refrigerant side pressure drop in Figure 7, it is evident that points unique to the solution space of problem B have a higher heat capacity per unit pressure drop performance when compared to solution of problem A. However, 4 out of 5 points unique to the solution space of problem A have equal or lesser cost than the unique solutions of problem B. This implies that using entropy generation units as an objective in problem B has successfully accounted for losses associated with pressure drop as well. This proves the usefulness of entropy generation minimization as an optimization criteria that includes heat transfer as well as pressure drop, for a water coil.

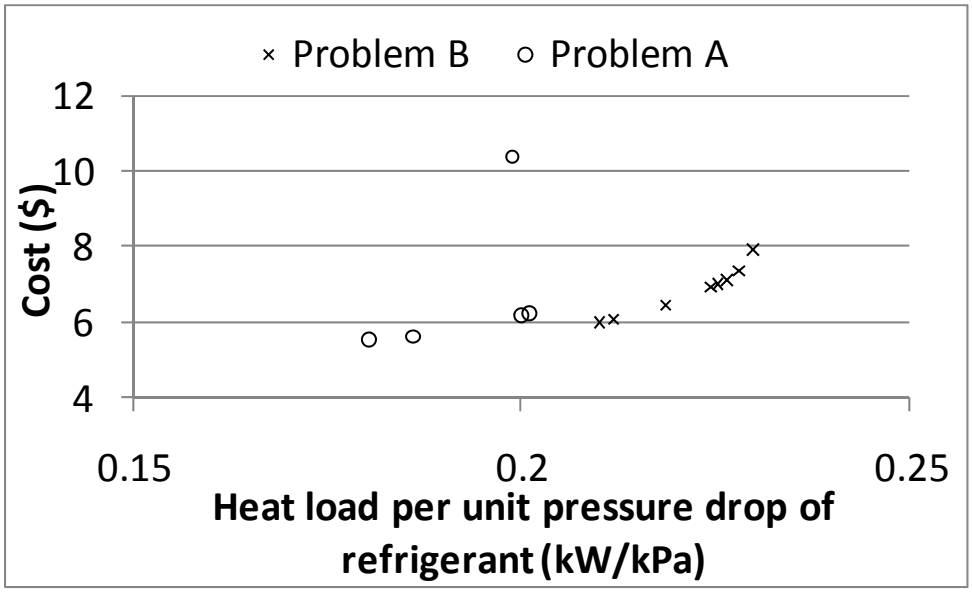


**Figure 7.13: Comparison of unique points in solution spaces of problems A and B, in terms of heat load per unit pressure drop**

7.2.2 Condenser

The specifications of the R134a condenser are shown in Table 7.3

**Table 7.3: Geometry specifications for condenser**

| Parameters | | |
|---|---|---|
| Number of Segments | 10 | --- |
| Tube Configuration | Staggered | |
| Number of Tubes Per Bank | 28 | --- |
| Number of Tube Banks | 3 | --- |
| Tube Length | 0.45 | m |
| Tube OD | 0.01 | m |
| Tube Thickness | 0.3 | mm |
| Tube Vertical Spacing | 0.75 | in |
| Tube Horizontal Spacing | 0.5 | in |
| FPI | 15 | fpi |
| Fin Thickness | 0.0043 | in |
| Fin Type | Louver | --- |
| Coil Face Air Velocity | variable | $ms^{-1}$ |

The mass flow rate of the condenser was chosen such that for all design points evaluated, the entire length of the condenser is two phase. The motivation behind this was to study the usefulness of entropy generation minimization in a two-phase region where refrigerant temperature drop is insignificant but the pressure drop is substantial. The solution for problem A yields 51 points on the Pareto optimal solution, whereas the solution for problem B yielded 72 points. Amongst these solution sets, only 3 points were common. The rest of the solutions in each of the sets were unique. Figure 7.14 shows that solution to problem B yields points with lower total entropy generation but those points don't necessarily have the highest heat capacity. Further, it should be noted that these three points have very low material cost.

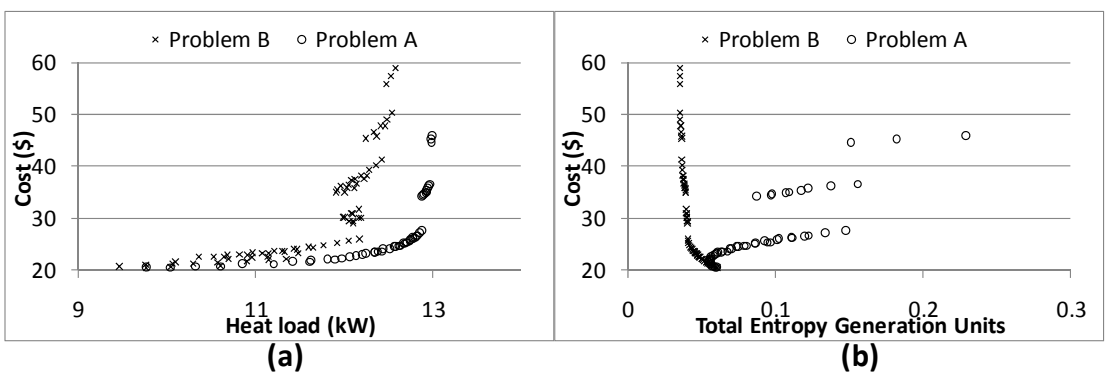


**Figure 7.14: Comparison of solution spaces of problem A and problem B for R134a condenser**

To better understand the reason behind this, it is important to closely examine a design point in each solution which has the same heat capacity but completely different total entropy generation units. For this, the design points with heat capacity closest to 12.5kW were selected from the two solution spaces as shown in Figure 7.15.

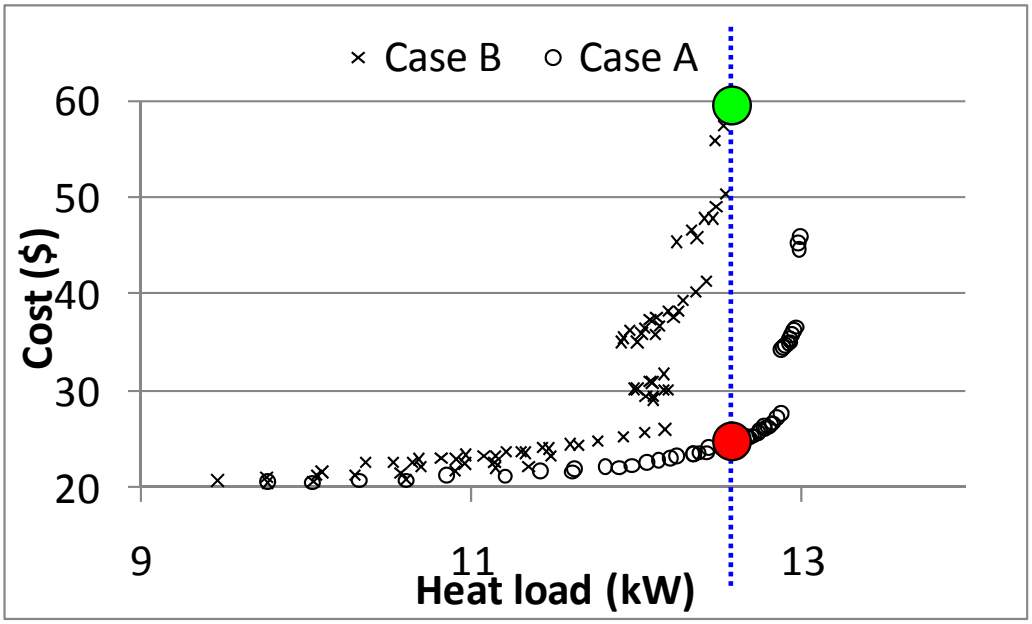


**Figure 7.15: Points chosen to study the cause of divergence of results between problem A and problem B for condenser**

Figure 7.16 shows the entropy generated in every segment of the heat exchanger with respect to local temperature gradient between bulk fluid and the wall. The superimposed curves represent the general shape of the entropy generation units profile as proposed by Bejan and shown here in Figure 7.1. It is evident that the heat exchanger from the solution space of problem B has much lesser number of total entropy generation units, when compared to the point from solution space for problem A. The main reason behind this behavior is the lack of any substantial change in approach temperature over the heat exchanger length, when compared to substantial pressure drop.

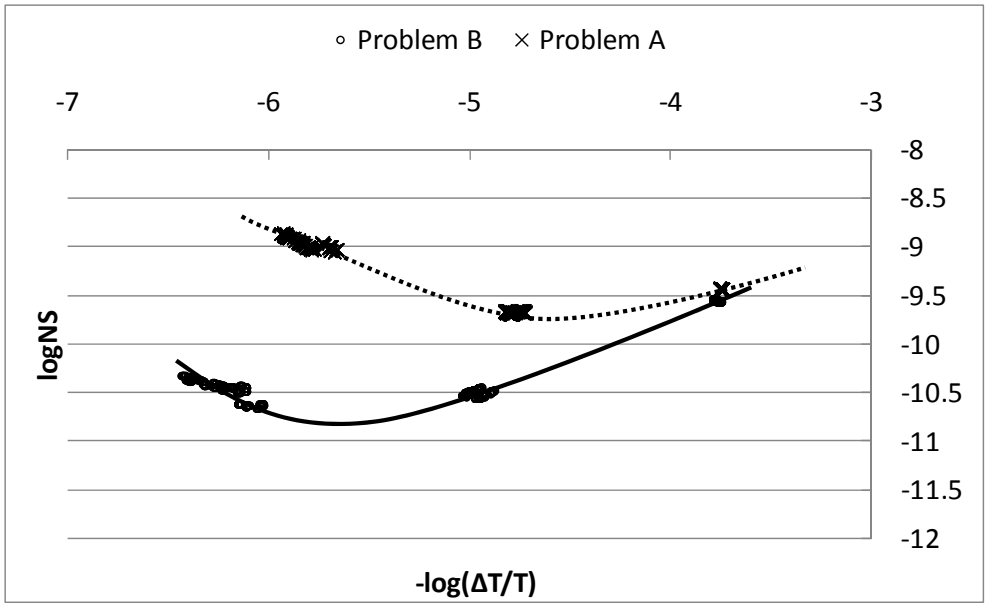


**Figure 7.16: Entropy generation profile for two design points from problem A and problem B for R134a condenser**

## 7.3 Conclusions

The usefulness of entropy generation minimization in the design of a water and R134a condenser and evaporator was examined using a heat exchanger model. It was shown that minimization of entropy generation minimization in water coils, condensers and evaporators yields the same design as maximizing heat capacity and minimizing air side or refrigerant side pressure drop. It was found that for a hot water coil, minimization of entropy generated and minimization of cost yields the same result as maximization of heat capacity and minimization of cost. However, for a completely two-phase condenser, the solution spaces for minimizing entropy generated and cost, and maximizing heat capacity and minimizing cost are almost unique except for a few cases. This result can be explained by examining the formulation of entropy generation units. The premise of entropy generation units is the co-existence of pressure drop and drop in finite temperature difference. However,

this does not occur during phase change heat transfer. Therefore, the technique of entropy generation minimization using entropy generation units represents heat capacity accurately in a single phase flow for the given set of design variables and heat exchanger conditions. For a two-phase heat exchanger, entropy generation units could not be used, instead of heat capacity, for the given set of design variables and flow conditions.

# CHAPTER 8. DESIGN GUIDELINES FOR ENGINEERS

This chapter presents a list of design guidelines for engineers, based on the research presented in this thesis.

- The "thermal resistance model" is fast and the "heat conduction model" is more accurate. When simulating tube-to-tube conduction in a fin-and-tube heat exchanger, the "thermal resistance model" should be used when the air side heat transfer coefficient is less than 1000 $Wm^{-2}K^{-1}$ and computational time is important. For best practice, the "thermal resistance model" should be verified for new designs with the "heat conduction model" by comparing the results including refrigerant temperature profile, to ensure that multipliers used in the "thermal resistance model" are valid.
- Engineers are suggested to employ fin cuts in gas coolers especially when the air speeds are low (~ 1.0 $ms^{-1}$). Studies showed that gains in heat load (given constant material use) and material savings (given targeted heat load) are higher across the board for cases with low air speeds, than for greater air speeds. Engineers should be mindful where the cuts are placed if the cut length is constrained. If the cut length is constrained, the tubes where models show refrigerant gaining heat must be insulated from the surrounding tubes, on a preferential basis. Conversely, when designing circuitry for heat exchangers with high temperature change in the refrigerant (e.g. gas coolers), engineers must try to ensure that the tubes with the highest temperature gradients are as far from each other as permitted within the constrained design space. In case of evaporators, the tubes with superheated vapor must be

insulated from the rest of the heat exchanger to avoid performance degradation.

- When employing the capability of hybridizing CFD simulations with the heat exchanger model, engineers must pay close attention to fin density. For heat exchangers with high number of fins per inch (15 and higher), 3D-CFD simulations become critical in ensuring accuracy of the CFD simulations. The pressure gradients in such a scenario are dominated by the very small spacing between fins, as opposed to tube pitches; and therefore, the maldistribution predicted by 2D-CFD simulations can be unrealistically amplified, as shown

in Figure 8.1.

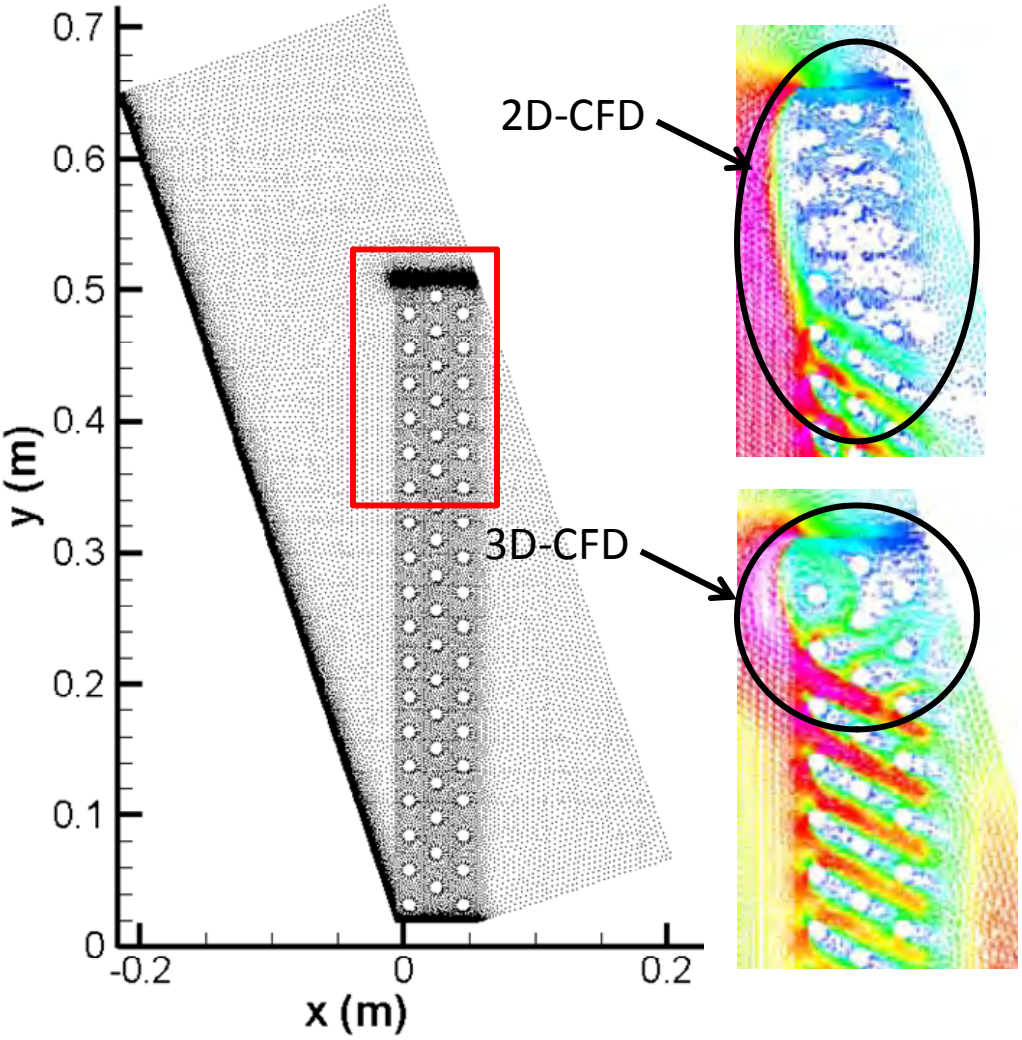


**Figure 8.1: Comparison of air flow maldistribution as predicted using 2D-CFD and 3D-CFD**

This becomes even more critical because air side maldistribution leads to refrigerant side maldistribution, and predictions of refrigerant side maldistribution can be erroneously exacerbated due to an over-predicted air side maldistribution. Figure 8.2 highlights the difference in mass flow rates predicted for the three circuits in the A-coil when 2D-CFD and 3D-CFD air

flow simulations were used.

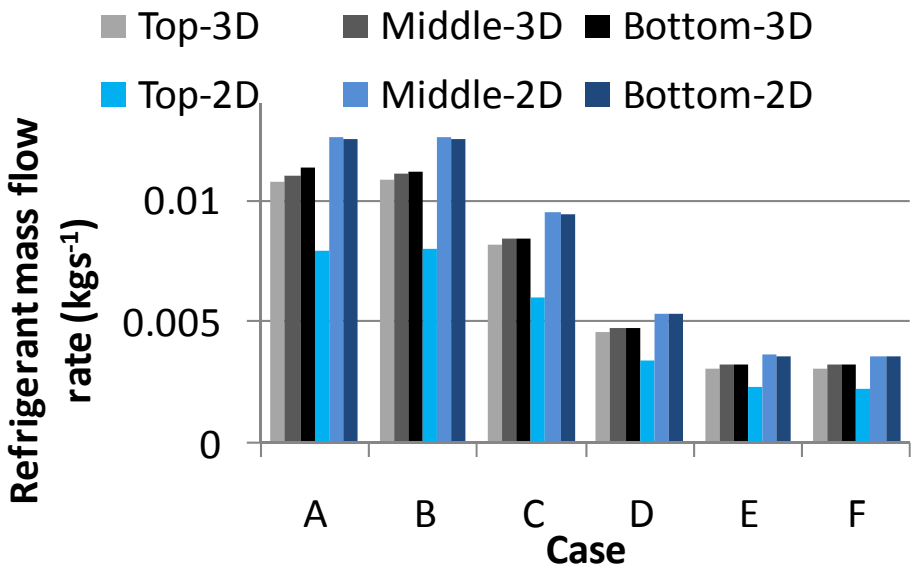


**Figure 8.2: Comparison of refrigerant mass flow rate predicted by the heat exchanger model, when 2D-CFD and 3D-CFD were used for air flow simulation**

When designing circuitry for coils with significant air side maldistribution, engineers must try to make the circuit as ambiguous to the maldistribution as possible.

- When employing the arbitrary fin sheet heat exchanger model, engineers are advised to use visualization studies or CFD studies to ensure that the air flow through the heat exchanger can be considered "normal to the banks"; otherwise CFD simulation must be integrated with the heat exchanger model.
- Engineers must be mindful that simulating frost growth on a heat exchanger is computationally expensive. For instance, even with a relatively coarse time step of 0.5 seconds, a 6 hour (21,600 seconds) cycle requires 43,200 time steps. Given an order of magnitude assessment of calculation time for typical frost heat exchangers (more than 6 banks) without accounting for tube-to-tube

conduction of a minute per time step, leads to a cycle calculation time of 30 days. The "thermal resistance model" takes three times as much time to converge, on an average. Therefore, it is critical that engineers carry out studies in advance to establish whether tube-to-tube conduction plays a significant role in their design. For most frost heat exchangers (< 10 fins per inch, < 10 K superheat at evaporator outlet at rated condition), it doesn't. However, it is suggested that tube-to-tube conduction be incorporated in modeling when fin density and superheat of the evaporator increase beyond traditional design values. By virtue of design, frost evaporators accumulate frost on heat transfer surfaces which block air flow passage. Due to varying local conditions, the degree of accumulation of frost can vary greatly within the heat exchanger. With this in mind, if the frost model predicts vastly varying accumulation along the height of the heat exchanger, the air flow distribution might be significantly impacted. At this point, an engineer is suggested to integrate CFD simulations with the frost model to ensure accuracy of predicted results.

- When considering employing entropy generation minimization as a design objective, engineers must be aware that it can be used as an objective instead of conventional criteria like heat load and pressure drop for single phase heat exchangers where pressure drop is accompanied by a drop in approach temperature of the two fluids. For coils which are predominantly two-phase, engineers are suggested to adhere to conventional design objectives of heat load and pressure drop.

# CHAPTER 9. SUMMARY AND CONCLUSIONS

The primary objective of this work is to develop and validate an advanced heat exchanger model capable of simulating heat exchanger performance under steady state and frosting conditions. Additionally, the heat exchanger model developed was used to investigate performance enhancement of gas coolers as well as to develop insight into 2$^{nd}$ law based heat exchanger performance evaluation criteria. The objectives have been achieved and the conclusions are summarized as follows.

## 9.1 Modeling of Tube-to-Tube Conduction in Fin-and-Tube Heat Exchangers

Two segment-by-segment models that account for fin conduction, the "thermal resistance model" and the "heat conduction model", for refrigerant to air heat transfer in fin-and-tube heat exchangers are developed. The "thermal resistance model" uses Fourier's law of conduction to obtain the heat transferred between neighboring tubes in a heat exchanger, whereas the "heat conduction model" solves the two-dimensional heat diffusion equation on the fin surface to obtain heat transfer between tubes. It is shown that the heat exchanger performance predicted by the "thermal resistance model" is equivalent to the prediction of the "heat conduction model", after using fin conduction multipliers. The proposed models are validated against two sets of experimental data. The "thermal resistance model" is able to predict the overall heat capacity for experiments conducted by Jin *et al.* (2004) within ±3%. It predicts temperatures at 27 tube locations for 36 different test cases within ±3.3°C of the measured values. For experiments conducted by Zilio *et al (*2007)., the "thermal resistance model" predicts all heat capacities within ±5%. All the measured temperatures were predicted within ±8.5°C.

## 9.2 Effect of Fin Cuts on Gas Cooler Performance

A validated heat exchanger model capable of simulating cut and continuous fins, the improvement in heat exchanger performance due to discontinuous fins is shown using wide ranging criteria. To understand effect of cut configurations, two different configurations of cut patterns were studied. It is shown that with increasing cut length, the gain in heat capacity increases in most cases. It was shown that for certain test conditions, the gain in heat capacity can be up to 12% over the baseline. In terms of fin material savings, at lower heat capacities, lower refrigerant and air flow rates, the fin material savings due to the presence of fin cuts can be as high as 45%. Fin material savings are lower at higher air speeds for a given refrigerant mass flow rate, and for a given air speed, lower for higher refrigerant flow rates. For the same heat capacity and constant refrigerant flow rate, the fin material savings are higher for lower air speeds, and decrease with increasing air speed. In terms of evaporator inlet quality, the gains in quality are uniformly higher for lower refrigerant flow rates than those for higher refrigerant flow rates, with % gain in quality as high as 20%. For a given refrigerant flow rate, the gains are higher for higher air speeds, and reduce for lower air speeds. The gains start diminishing with increasing fins per inch, as the specific cases start to approach the pinch-off point. Finally, studies with a fin cut length constraint in place show that, in order to maximize heat capacity, it is suggested that cuts be placed preferentially at locations that ensure the refrigerant doesn’t gain heat.

## 9.3 Modeling of Fin-and-Tube Heat Exchanger with Arbitrary Fin Sheet

A heat exchanger model for fin-and-tube air-to-refrigerant heat exchangers with arbitrary fin sheets was developed. This model is capable of accounting for

several varying parameters, such as tube diameters, tube locations, tube pitches, and internal as well as external jagged edges, variable number of tubes per bank and variable location of fin cuts. A new grid based air propagation algorithm was introduced. The proposed model was validated against experiments, and heat capacity prediction was found to be within ±5% of experimental values. The overall pressure drop for 7 out of 8 cases was found to be within ±25% of the experimental value, which is within the regression error of the pressure drop correlation employed.

### 9.4 Modeling of Fin-and-Tube Heat Exchanger using CFD-based Air Propagation

A CFD-based air propagation method for fin-and-tube heat exchangers is developed. The method can use both 2D and 3D CFD results, as well as structured and unstructured CFD meshes. To interpret and process CFD results, the heat exchanger geometrical information is processed on a Cartesian grid. Using modified inverse distance averaging, the CFD results are interpolated to obtain air flow profiles for the heat exchanger. This information is used to propagate complex air flows through the heat exchanger. While the interpolation scheme leads to an acceptable error (less than 0.5% for 3D-CFD and less than 0.05% for 2D-CFD) in overall mass balance, this can be further improved by employing more advanced interpolation algorithms. Using the CFD-based air propagation, the predicted overall heat capacity for the R410A condenser agrees within ±4% of the experimentally measured values without employing any correction factors or multiplier on air side heat transfer coefficients.

2D (fin-less) and 3D (finned) CFD simulations of the A-coil show significant difference in the air flow profile through the heat exchanger. The 2D flow shows a

much larger recirculation zone than the 3D simulation, in the top circuit of the heat exchanger. 2D simulations also show that the top circuit of the heat exchanger is practically starved, with most of the air flowing through the bottom two circuits. These observations show that 2D CFD cannot be used to simulate tube-fin heat exchangers as the presence of fins controls the air flow path through the heat exchanger.

### 9.5 Modeling of Frost Growth and Accumulation in Fin-and-Tube Heat Exchangers

A quasi-steady state heat exchanger model for simulating frost growth and accumulation on fin-and-tube heat exchangers was developed. The model is capable of simulating frost growth on a heat exchanger on a segment-by-segment basis, accounting for heat conduction between tubes through fin sheets and it completely models the refrigerant side equations as well which permits prediction of important variables like outlet superheat from the evaporator. The model was validated against frost growth experiments, and the total heat capacity was found to be within 10% of measured values. The superheat was predicted within ±1°C of measured value throughout the frost growth period and the time at which superheat is lost was predicted within 2 minutes of measured value. The air outlet temperatures were predicted within ±1°C of measured values.

The model presented is semi-empirical as it employs correlations for frost density and conductivity but uses physics-based modeling for frost mass accumulation. Considering the purpose of the model, the quasi-steady state assumption facilitates relatively coarse time steps which are critical in curbing the total computational cost of simulations. While most frost evaporators have low fin

densities to allow extended periods between defrosting, the ability to model tube-to-tube heat conduction enables the investigation of this on frost growth, if and when desired. The segmented nature of the model allows the study of local variables over the frosting cycle.

### 9.6 Investigation of Entropy Generation Minimization in Heat Exchanger Design

The usefulness of entropy generation minimization in the design of two-phase and single-phase coils was examined using a heat exchanger model. It was shown that for single phase coils as well as two phase coils, the point of minimum entropy generation yields designs where gain in heat capacity flattens and pressure drop continues to increase. It was found that for a hot water coil, minimization of entropy generated and minimization of cost yields the same result as maximization of heat capacity and minimization of cost. However, for a completely two-phase condenser, the solution spaces for minimizing entropy generated and cost, and maximizing heat capacity and minimizing cost are almost unique except for a few cases. This result can be explained by examining the formulation of entropy generation units. The premise of entropy generation units is the co-existence of pressure drop and drop in finite temperature difference. However, this does not occur during phase change heat transfer. Therefore, the technique of entropy generation minimization using entropy generation units represents heat capacity accurately in a single phase flow for the given set of design variables and heat exchanger conditions. For a two-phase heat exchanger, entropy generation units could not be used, instead of heat capacity, for the given set of design variables and flow conditions.

# CHAPTER 10. LIST OF MAJOR CONTRIBUTIONS AND FUTURE WORK

## 10.1 Major Contributions

The advanced heat exchanger model presented in this dissertation provides a significant set of capabilities to enable design and simulation of fin-and-tube heat exchangers. The major contributions are as follows.

- Development of two models for tube-to-tube conduction in fin-and-tube heat exchangers, the "thermal resistance model" and the "heat conduction model" to facilitate simulation of tube-to-tube conduction in heat exchangers, and accompanying performance degradation
- The performance enhancement of gas coolers due to cut fins was quantified as well as a general design guidelines for location of fin cuts on a fin-and-tube heat exchanger were presented
- Development of a heat exchanger model to allow simulation and design of fin-and-tube heat exchangers with arbitrary fin sheets. This allows engineers to study and optimize individual sections of the heat exchanger as a function of local flow conditions, both on the air side as well as refrigerant side
- Development of a heat exchanger model with CFD-based air propagation through the heat exchanger. This facilitates the use of CFD in heat exchanger simulation without the accompanying computational cost of full-scale CFD simulation. Additionally, this allows engineers to study the effect of air maldistribution inside the heat exchanger core, and its effects of performance of local sections of the heat exchanger

- Development of a quasi-steady state heat exchanger model frost growth and accumulation. This provides engineers to study the performance of frost heat exchangers in great detail, including phenomena like diminishing superheat, increasing frost thickness and blockage of air flow passage (including accompanying pressure drop), effect of tube-to-tube conduction on frost accumulation, heat exchanger cycling time and degradation of heat capacity of the heat exchanger
- Investigation of entropy generation minimization for heat exchanger design and optimization. This study provided insight into the strengths and limitations of second law based performance evaluation criteria when compared to conventional criteria of heat capacity and pressure drop

### 10.2 List of Publications

The following peer-reviewed journal papers were published or accepted for publication (pending minor revisions) as an outcome of the research conducted as part of this dissertation.

1) **V.Singh**, V.Aute, R. Radermacher. "*Investigation of Effect of Cut Fins on a Fin-and-Tube Carbon Dioxide Gas Cooler Performance*", Accepted at HVAC&R Research Journal
2) **V.Singh**, O. Abdelaziz, V.Aute, R. Radermacher. "*Simulation of Air-to-Refrigerant Fin-and-Tube Heat Exchanger with CFD-Based Air Propagation*", Accepted at International Journal of Refrigeration

3) **V.Singh**, V.Aute, R. Radermacher. "*Heat Exchanger Model for Air-to-Refrigerant Fin-and-Tube Heat Exchanger with Arbitrary Fin Sheet*", Accepted at International Journal of Refrigeration. doi : 10.1016/j.ijrefrig.2009.05.011

4) **V. Singh**, V. Aute, R. Radermacher. "*Numerical Approach for Modeling Air-to-Refrigerant Fin-and-Tube Heat Exchanger with Tube-to-Tube Heat Transfer*", International Journal of Refrigeration, Volume 31 Issue 8, December 2008, pp. 1414-1425

5) Y. Hwang, **V. Singh**, R. Radermacher, "*Heat Exchanger Design for $CO_2$ Cycle with a Linear Compressor*", HVAC&R Research Journal, Volume 13 Number 3, May 2007

The following peer-reviewed conference papers were published as an outcome of the research conducted for this dissertation

1) **V. Singh**, V.Aute, R. Radermacher. "*Study of Effect of Heat Transfer through Fins in a Fin-and-tube Carbon Dioxide Gas Cooler on its Performance through Numerical Modeling*", Purdue Refrigeration and Air Conditioning Conference, Purdue University, West Lafayette, IN, July 14-17, 2008

2) **V. Singh**, V.Aute, R. Radermacher. "*Usefulness of Entropy Generation Minimization through a Heat Exchanger Modeling Tool*", Purdue Refrigeration and Air Conditioning Conference, Purdue University, West Lafayette, IN, July 14-17, 2008

3) O. Abdelaziz, **V. Singh**, V.Aute, R. Radermacher. "*A-Type Heat Exchanger Simulation Using 2-D CFD for Airside Heat Transfer and Pressure Drop*",

Purdue Refrigeration and Air Conditioning Conference, Purdue University, West Lafayette, IN, July 14-17, 2008

The following papers are currently being developed or undergoing review at CEEE

1) **V.Singh**, V.Aute, R. Radermacher. "*A Quasi-Steady State Frost Growth and Accumulation Model for Fin-and-tube Air-to-Refrigerant Heat Exchangers*", Manuscript under CEEE Review
2) **V.Singh**, V.Aute, R. Radermacher. "*Evaluation of Entropy Generation Minimization as a Design Objective for Fin-and-tube Air-to-Refrigerant Heat Exchangers*", Manuscript under development

### 10.3 Future Work

While this dissertation presents a significant step forward in modeling of fin-and-tube heat exchangers, all advancements open up newer frontiers of research and development. The following items of research could be of significant use to the industry in near future.

- Implement a method for automatic calculation of multipliers for the "thermal resistance model". This will eliminate the tedious task of data fitting when engineers use the faster "thermal resistance model" over the more accurate but computationally expensive "heat conduction model"
- Implement CFD-based air propagation for heat exchanger with arbitrary fin sheets. This will provide researchers the capability of studying an arbitrary fin sheet heat exchanger in detail, once the model developed in this dissertation has provided promising results for a design being considered

- Implement CFD-based calculation of refrigerant side properties. Considering various flow regimes present in flow boiling, heat transfer and pressure drop characteristics for such regimes can be calculated using CFD. To account for transition, a flow regime map can be used. Combining the two in a heat exchanger model can reduce the dependence on correlations for refrigerant side calculations.
- Implement a defrosting model for fin-and-tube heat exchangers. While frost growth is a critical phenomenon, defrosting is equally important. Defrosting presents a challenging tradeoff between energy consumption, which is attributable to the defrosting process itself and introduction of heat into the refrigerated space as well as the duration of defrost cycle. A defrosting model will enable such an investigation
- Extend all capabilities presented in this thesis to a microchannel heat exchanger simulation tool. With increasing move towards microchannel heat exchangers and advancement of manufacturing capabilities, engineers will need an advanced simulation tool to study microchannel heat exchangers.

# CHAPTER 11. APPENDICES

## 11.1 Appendix A: Introduction to Modeling

In the interest of science and technology, it is imperative for computationalists and experimentalists to work in close co-operation. However, this relationship has traditionally been competitive, if not adversarial, as evidenced by a 1975 publication titled "Computers vs. Wind Tunnels". To further and facilitate cooperation, this section is meant to introduce the concept of modeling in a concise and organized manner to novices and experimentalists.

### 11.1.1 Definition

A model can be defined as a formalized interpretation which deals with empirical entities, phenomena and physical processes in a mathematical or logical way.

### 11.1.2 Motivation for modeling

Models strengthen generality and broaden the understanding of original principles and phenomena, through application of quantitative reasoning. Models serve as an aid in visualizing phenomenon that is often difficult to observe directly. Last but not the least, models offer intellectual economy which reduces the lead time in developing and testing newer and better products.

### 11.1.3 Steps in modeling

All modeling involves five key steps as shown in Figure 11.1, even though the focus of computationalists might be on different steps.

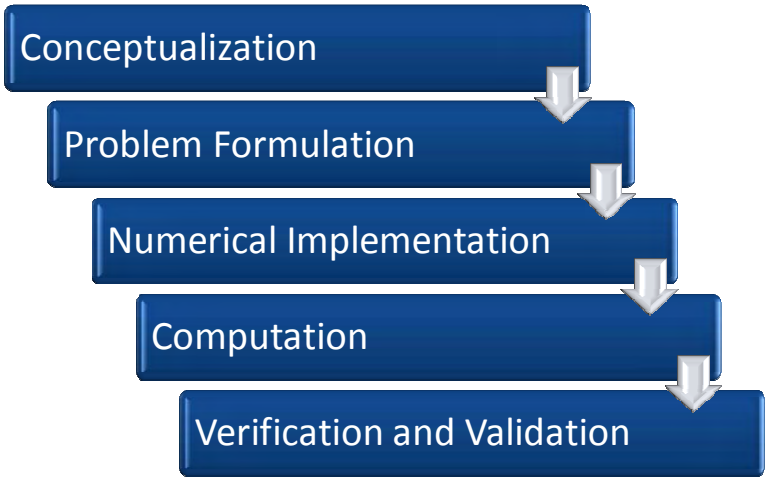


**Figure 11.1: Steps involved in modeling**

The primary objective of conceptualization is to relate observations to relevant physical principles. In this step, it is important to determine the extent of details desired or objectives of the model. Problem formulation involves formulating physical principles in forms of mathematical equations. Numerical implementation involves development of a solution algorithm which is suitable for implementation on a computer. Computation involves coding the solution algorithm using a suitable programming language and the development of pre-processing and post-processing facilities. It is vital to consider issues of computational efficiency during this step. The final stage in modeling is verification and validation. Verification is the assessment of the accuracy of the solution to a computational model by comparison with known solutions. Validation is the assessment of the accuracy of a computational simulation by comparison with experimental data.

## 11.2 Appendix B: Genetic Algorithms

Genetic Algorithms (GAs) are a class of evolutionary algorithms that mimic natural evolutionary principles to constitute search and optimization procedures. Genetic algorithms help overcome or avoid some of the deficiencies of classical optimization algorithms, some of which are as follows.

- Convergence to an optimal solution depends on the chosen initial solution
- Classical algorithms can get “stuck” to suboptimal solutions
- Classic algorithms are not good at handling problems having a discrete search space

The concept of a genetic algorithm was first conceived by John Holland at University of Michigan, Ann Arbor. As the name suggests, GAs borrow their working principle from natural genetics. The steps involved in using GAs for optimization are described in the following sections, using the optimization problem illustrated in Figure 11.2.

- Objectives
  - Minimize the material cost (savings in final product costs)
  - Minimize the enclosure volume (savings in the real-estate footprint)
- Constraints
  - Airside pressure drop ≤100 Pa
  - Heat load within ± 5% of baseline heat load (10874 W)
  - Volume ≤ baseline volume (0.0953 $m^3$)
- Variables
  - Tube length, slab inclination angle, number of fins per inch, tube horizontal spacing and tube vertical spacing

**Figure 11.2: Optimization problem for design optimization of a fin and tube heat exchanger**

11.2.1 Representing a solution

In order to use GAs to find optimal decision variables, variables are first representation as binary strings. The number of bits chosen for each variable depends on the discretization desired in the design space (more bits, more refined design space). Individual strings are then concatenated to create a string that represents the one complete design, as shown in Figure 11.3.

10100101001010100101

**Figure 11.3: Concatenated bit strings which represent one complete design**

Being a population-based method, several such designs are created in this first stage.

### 11.2.2 Assigning fitness to a Solution

After creating of a string representing a design, it is necessary to evaluate the fitness of the solution. This solution fitness is often set to the objective function value(s) of the optimization problem. In this case, it would be material cost and enclosure volume. The steps following fitness assignment are a series of genetic operators, which are Reproduction, Crossover and Mutation.

### 11.2.3 Reproduction operator

The primary objective of the reproduction operator is to make duplicates of good solutions and eliminate bas solutions in a population, while keeping the population size constant. The tasks required to achieve this are a) identify good solutions in a population, (b) make multiple copies of good solutions and (c) eliminate bad solutions from the population to allow multiple solutions of good copies to be placed in the population. There are several ways of creating this mating pool which include tournament selection, proportionate selection and ranking selection amongst others.

### 11.2.4 Crossover operator

A crossover operator is applied to the strings of the mating pool. The crossover operation begins by picking two solutions from the mating pool. A site is chosen along the string length at random and the contents on the right side of this site are exchanged between the two solutions, as shown in Figure 11.4.

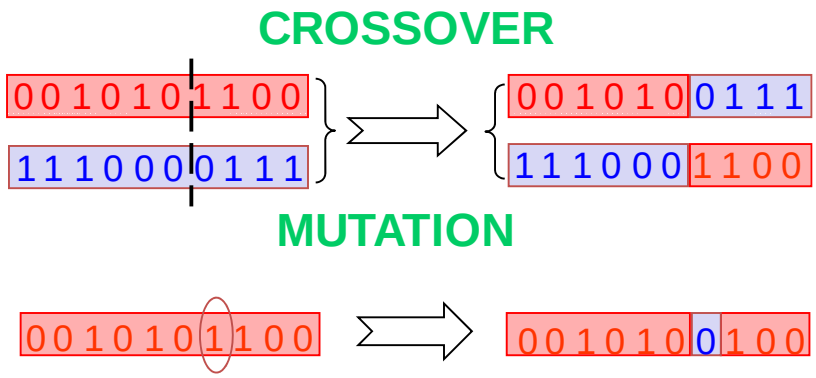


**Figure 11.4: Crossover and mutation operations in GAs**

11.2.5 Mutation operator

The mutation operation involves switching bit in a binary coded genetic algorithm, i.e. 1 to 0 and 0 to 1, as shown in Figure 11.4.

Figure 11.5 sums up the working principle of a GA.

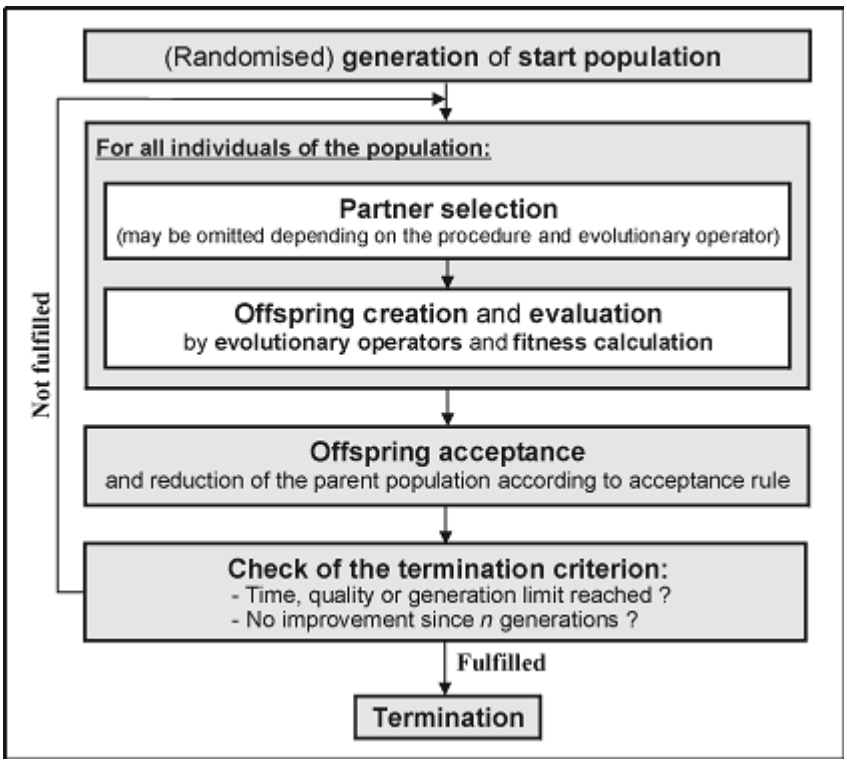


**Figure 11.5: Working principle of a genetic algorithm**

## 11.3 Appendix C: Correlation Applicability Range

**Table 11.1: Air side correlations applicability range**

| Authors (Year) | Fin Type | Dimensions |
|---|---|---|
| Wang, Chang (1999) | Louvered | Tube Outside Diameter = 6.9 - 10.4 mm<br>Tube Horizontal Spacing = 17.7 - 25.4 mm<br>Tube Vertical Spacing = 12.7 - 22.0 mm<br>Fin Pitch = 1.2 - 2.49 mm<br>Louver Height = 0.79 - 1.4 mm<br>Louver Pitch = 1.7 - 3.75 mm |
| Wang, Chi, Chang (2000) | Plain | Number of Columns = 1 - 6<br>Tube Outside Diameter = 6.35 - 12.7 mm<br>Fin Pitch = 1.19 - 8.7 mm<br>Tube Horizontal Spacing = 17.7 - 31.75 mm<br>Tube Vertical Spacing = 12.4 - 27.5 mm |
| Wang, Lee (2001) | Slit | Fin Pitch = 1.20 - 2.50 mm<br>Tube Outside Diameter = 7.52 - 16.4 mm<br>Longitudinal Tube Pitch = 12.7 - 33.0 mm<br>Transverse Tube Pitch = 20.0 - 38.0 mm<br>Fin Thickness = 0.11 - 0.2 mm<br>Number of Longitudinal tube rows = 1 – 6<br>Height of Slit = 0.99 - 2 mm<br>Breadth of a Slit (in the direction of airflow) = 1 - 2.2 mm<br>Number of Slits in an Enhanced Zone = 3 - 7 |
| Wang, Hwang, Lin (2002) | Wavy Herringbone | Number of Columns = 1 – 6<br>Tube Outside Diameter = 7.66 - 16.85 mm<br>Fin Pattern Depth = 0.3 - 1.8 mm<br>Tube Horizontal Spacing = 12 - 33 mm<br>Tube Vertical Spacing = 21-38 mm |
| Wang, Tsai, Lu (1998) | Wavy – Louvered | Number of Columns = 1 – 4<br>Fin Pitch = 1.21 - 2.54 mm<br>Fin Thickness = 0.115 mm<br>Tube Outside Diameter = 8.54 mm<br>Tube Horizontal Spacing = 19.05 mm<br>Tube Vertical Spacing = 25.4 mm |
| Granryd (1965) | Plain | Tube Outside Diameter = 10 - 35 mm<br>Tube Horizontal Spacing = 33.3 - 100 mm<br>Tube Vertical Spacing = 33.3 - 100 mm<br>Fin Spacing = 3 - 16 mm |

| | | |
|---|---|---|
| | | Fin Thickness = 1.2 mm<br>Other comments : No more than 5 banks |
| Kim, Bullard (2002) | Louvered – Microchannel | Flow depth = 16 - 24 mm<br>Fin Pitch = 1.0-1.4 mm<br>Tube Pitch = 10.15 - 11.15 mm<br>Number of Louvers = 8 – 12<br>Louver Angle = 15 - 29 degrees |
| Chang, Wang (1997) | Louvered – Microchannel | Louver Pitch = 0.5 - 3 mm<br>Louver Length = 2.13 - 18.5 mm<br>Louver Angle = 8.43 - 35 degrees<br>Fin Pitch = 0.51 - 3.33 mm<br>Tube Depth = 15.6 - 57.4 mm<br>Fin Depth = 15.6 - 57.4 mm<br>Fin Length = 2.84 - 20 mm<br>Fin Thickness = 0.0254 - 0.16 mm<br>Tube Pitch = 7.51 - 25 mm<br>Rows of Tubes = 1 - 2<br>$100 < Re_{Lp} < 3000$ |

**Table 11.2: Two-phase heat transfer correlation applicability range**

| Authors (Year) | Fluids | Dimensions | Flow Parameters |
|---|---|---|---|
| Kandlikar (1990) | Water, R-11, R-12, R13-B1, R-22, R-113, R-114, R-152a, nitrogen and neon | Diameter = 4 – 32 mm | Mass flux = 0.3 – 8000 $kg/m^2s$ |
| Jung, Radermacher (1989) | R22, R114 | Varying | Mass Flow Rate = 16 - 46 g/s<br>Mass Flux = 250 - 720 $kg/(m^2 s)$<br>Heat Flux = 10 - 45 $kW/m^2$<br>Quality = up to 0.95 |
| Shah-Evaporation (1982) | Verified for 12 fluids | Diameter = 5-15 mm<br>Tube thickness = 1mm to 6mm | Pressures up to reduced pressure of 0.89<br>Mass flux = 70 – 11000 $kg/m^2s$ |

| | | | |
|---|---|---|---|
| Gungor, Winterton (1987) | Water, R-11, R-12, R-13, R-22, R-113, R-114, ethanol, ethylene glycol and n-butanol | Diameter = 2.95 – 32mm | Mass flux = 12 – 61000 $kg/m^2s$ |
| Dobson (1998) | R-12, R-22, R-134a and near-azeotropic blends of R-32/R-125 | Diameter = 3.14 - 7.04 mm | Reduced Pressure = 0.21 - 0.57<br>Saturation Temperature = 35 - 60 °C<br>Quality = 10 - 90 %<br>Mass Flux = 25 - 800 $kg/(m^2s)$<br>Heat Flux = 5 - 15 $kW/m^2$ |
| Shah-Condensation (1979) | Water, R-11, R-12, R-22, R-113, methanol, ethanol, benzene, toluene and trichloroethylene | Diameter = 7 - 40 mm | Reduced Pressure = 0.002 - 0.44<br>Saturation Temperature = 21 - 310 °C<br>Vapor Velocity = 3 - 300 m/s<br>Quality = 0 - 1<br>Mass Flux = 10.8 - 210.5 $kg/(m^2s)$<br>Heat Flux = 158 - 1,893,000 $W/m^2$<br>Liquid Reynolds Number = 100 - 63,000<br>Liquid Prandtl Number = 1 - 13 |
| Traviss, Rohsenow, Baron (1973) | R12, R22 | Diameter = 3.4 – 12mm | Mass Flux = 25- 860 $kg/(m^2s)$ |
| Wojtan, Ursenbacher, Thome (2005) | R22, R410A | Diameter = 8 – 13.84mm | Mass Flux = 70 - 700 $kg/(m^2s)$ |
| Kandlikar, Balasubramaniamn (2004) | R-113, R-141b, HCFC 123 | Diameter = 0.19 - 2.92 mm | Re ranges (used in studies) = 72-2013<br>Quality = 0 - 1 |

| | | | |
|---|---|---|---|
| Yun, Heo, Kim (2006) | R410A | Diameter = 1.36 – 1.44mm | Mass flux: 200 to 400 $kg/m^2s$<br>Heat flux: 10 to 20 $kW/m^2$<br>Saturation temperature: 0-10°C |

**Table 11.3: Two phase pressure drop correlation applicability range**

| Authors (Year) | Fluids | Dimensions | Flow Parameters |
|---|---|---|---|
| Muller-Steinhagen, Heck (1986) | R134a, R123, R402A, R404A, R502 | Diameter = 10 – 12 mm | Mass Flux = 100 - 500 $kg/(m^2s)$<br>Quality = 0.04 to 1.0 |
| Lockhart, Martinelli (1949) | benzene, kerosene, water and various oils | Diameter = 0.0586 - 1.017 inches | |
| Friedel (1979) | R12, Water | Diameter = 17 – 57 mm | Mass Flux = 500 - 4000 $kg/(m^2s)$<br>Quality = 0.01 to 0.4 |
| Cheng, Ribatski, Thome (2008) | Carbon Dioxide | Diameter= 0.6 to 10mm | Mass velocity= 50 to 1500 kg/m2s<br>Heat flux= 1.8 to 46 kW/m2<br>$T_{sat}$ = -28 to 25°C<br>(Reduced pressure: 0.21 to 0.87) |
| Park, Hrnjak (2007) | Carbon Dioxide, R410A, R22 | Diameter = 6.1mm | Tsat = 15 – 30°C<br>Mass flux = 100 – 400 $kg/m^2s$<br>Heat flux = 5 – 15 $kW/m^2$<br>Quality = 0.1 – 0.8 |

## 11.4 Appendix D: Implementation of Alternative Dehumidification Method

An alternative dehumidification method, which accounts for water film thickness on the surface of the heat exchanger, was implemented for fin-and-tube and microchannel air-to-refrigerant heat exchangers. This method is based on the analytical formulation suggested by Domanski (EVSIM, 1999). The water film thickness is given by equation (11.1)

$$\delta_f = 1.082\left[\frac{\mu_w \cdot R'}{g \cdot \rho_w^{\,2}}\right]^{1/3} \tag{11.1}$$

Where R' is condensate removed per unit width of the heat exchanger macrovolume. The existing algorithm is shown in Figure 11.6 (a) and the alternative algorithm is shown in Figure 11.6 (b).

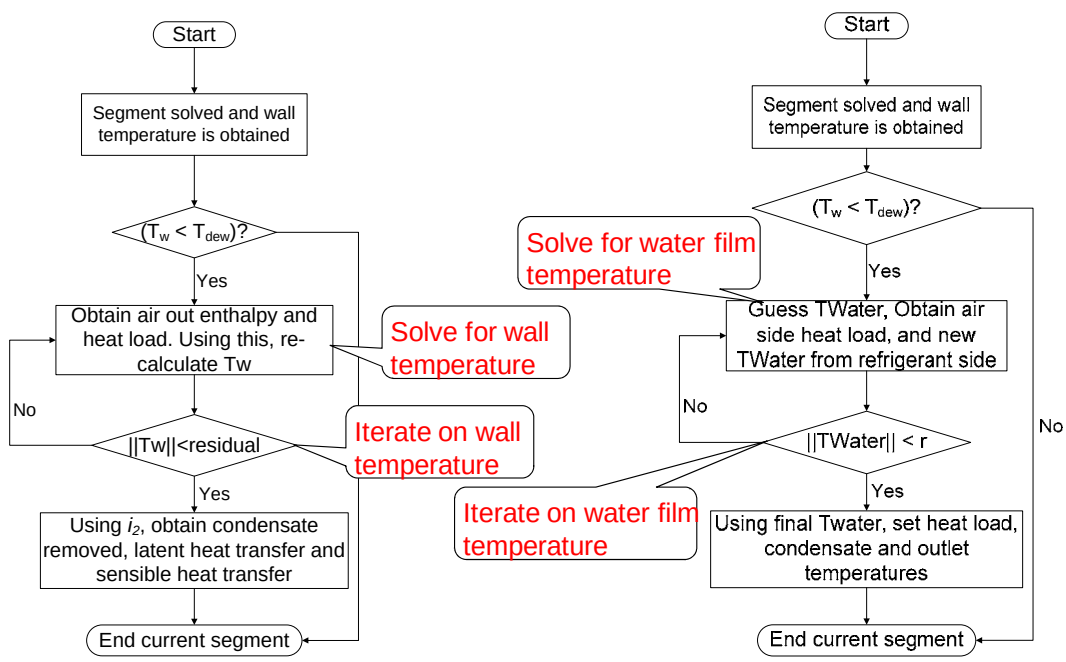


**Figure 11.6: (a) Existing dehumidification method based on enthalpy potential method and (b) alternative dehumidification method based on Domanski's (1999) formulation**

# CHAPTER 12. REFERENCES

[1] Abdelaziz, O., "Development of Multi-scale, Multi-physics, Analysis Capability and its Application to Novel Heat Exchanger Design and Optimization", *Doctoral Thesis, University of Maryland, College Park, 2009*

[2]Abdelaziz, O., Singh, V., Aute, V. and Radermacher, R. "A-Type Heat Exchanger Simulation Using 2-D CFD for Airside Heat Transfer and Pressure Drop" *12th International Refrigeration and Air Conditioning Conference at Purdue,*2008,

[3] Aute, V.A., Radermacher, R., Naduvath, M.A., "Constrained Multi-Objective Optimization of a Condenser Coil Using Evolutionary Algorithms", *10th International Refrigeration and Air Conditioning Conference at Purdue, 2004*

[4]Aceves-Saborio, S., Ranasinghe, J. and Reistad, G.M. "An Extension to the Irreversibility Minimization Analysis Applied to Heat Exchangers" *ASME Journal of Heat Transfer,*1989, 11, 129

[5]Auracher, H. "Fundamental Aspects of Exergy Application to the Analysis and Optimisation of Energy Processes"*Journal of Heat Recovery Systems,*1984, 45, 323-327

[6]Bahnke, G.D. and Howard, C.P. "The Effect of Longitudinal Heat Conduction on Periodic-Flow Heat Exchanger Performance"*ASME Journal of Engineering for Power,*1964, 86, 105-120

[7]Bejan, A. "The Concept of Irreversibility in Heat Exchanger Design: Counterflow Heat Exchangers for Gas-to-Gas Applications"*Transactions of ASME,*1977,9(9),374

[8]Bejan, A. "General criterion for rating heat-exchanger performance"*International Journal of Heat and Mass Transfer,*1978,21(5), 655-658

[9]Bennett, I. J. D., Besant, R. W., Schoenau, G. J. and Johnson, A. B."*Procedure for optimizing coils in a run-around heat exchanger system*", 1st ed., translated by New Orleans, LA, USA: ASHRAE, 442-451,1994

[10]Bernard P., Wallace J.,Turbulent flow, analysis, measurement and prediction, 2002, John Wiley and Sons.

[11]Brosky, A.F. "Pre-heat air at Glen Rogers mine chiefly to prevent ice formation in Wet Shaft"*Coal Age,*1926,29(25), 901-903

[12]Brown, J.S., Kim, Y. and Domanski, P.A. "Evaluation of Carbon Dioxide as R-22 Substitute for Residential Air Conditioning"*ASHRAE Transactions,*2002,1082

[13]Cavazzuti, M. and Corticelli, M.A. "Optimization of heat exchanger enhanced surfaces through multiobjective genetic algorithms" *Numerical Heat Transfer-Part A*, 2008, 54, 603-628

[14]Chen, H., Thomas, L. and Besant, R.W. "Fan supplied heat exchanger fin performance under frosting conditions"*International Journal of Refrigeration,* 2003, 26(1), 140-149

[15]Chen, H., Thomas, L. and Besant, R.W. "Modeling frost characteristics on heat exchanger fins: Part I. Numerical model"*ASHRAE Transactions,*2000a,106,357-367

[16]Chen, H., Thomas, L. and Besant, R.W. "Modeling frost characteristics on heat exchanger fins: Part II. Model validation and limitations"*ASHRAE Transactions,*2000b,106,368-376

[17] Cheng, L., Ribatski, G., Quiben, J.M., Thome, J.R., "A two-phase flow pattern map and a flow pattern based phenomenological model for two-phase flow frictional pressure drops", *International Journal of Heat and Mass Transfer, 2008, 51, 111-124*

[18]Cheng, C. and Cheng, Y. "Predictions of frost growth on a cold plate in atmospheric air" *International communications on heat and mass transfer,* 2001, 28(7), 953-962

[19]Cheng, L., Ribatski, G. and Thome, J.R. "New prediction methods for CO2 evaporation inside tubes: Part II—An updated general flow boiling heat transfer model based on flow patterns"*International Journal of Heat and Mass Transfer,*2008, 5(11), 2125-135

[20]Chiou, J.P. "The Effect of Longitudinal Heat Conduction on Crossflow Heat Exchanger"*Transactions of ASME,*1978,100, 346-351

[21]Chu, W., "Development of a general finite difference approximation for a general domain - part 1: Machine transformation", *Journal of Computational Physics*, 1971, 8, 392-408

Chwalowski, M., Didion, D.A. and Domanski, P.A. "Verification of Evaporator Computer Models and Analysis of Performance of an Evaporator Coil"*ASHRAE Transactions,*1989,951

[22]Clausius, R. "On the Motive Power of Heat and on the Laws which can be deduced from it for the Theory of Heat."*Philosophical Magazine and Journal of Science,*1851,24

[23]Cornelissen, R.L. and Hirs, G.G. "Thermodynamic Optimisation of a Heat Exchanger"*International Journal of Heat and Mass Transfer,*1999,42, 951-959

[24]Cornelissen, R.L. and Hirs, G.G. "Exergetic Optimisation of a Heat Exchanger"*Energy Conservation and Management,*1997, 1567-1576

[25]Cox, E.R. "Heat Exchanger"1925,Patent number : 5116021542613

[26]Cunningham, R.E. and Williams, R.J.J. "Diffusion in Gases and Porous Media"1980, Plenum press New York

[27]DeJong, N.C., Gentry, M.C. and Jacobi, A.M. "An Entropy-Based, Air-Side Heat Exchanger Performance Evaluation Method: Application to Condenser"*HVAC&R Research Journal,*1997,33, 185-196

[28]Dittus, F.W. and Boelter, L.M.K. " Heat Transfer in Automobile Radiators of the Tubular Type" *International Communications in Heat and Mass Transfer,*1985,1213-22

[29]Dobson, M.K., Chato, J.C., Condensation in Smooth Horizontal Tubes, *ASME Journal of Heat Transfer,* 1998, 120, 193-213.

[30]Domanski, P.A. and Yashar, D. "Application of an Evolution Program for Refrigerant Circuitry Optimization" *Challenges to Sustainability: ACRECONF Proceedings,*2007

[31]Domanski, P.A. "EVAP-COND, simulation models for finned tube heat exchangers"2003, NIST Building and Fire Research Laboratory Report

[32]Domanski, P.A. "Finned-tube evaporator model with a visual interface"*20th International Congress of Refrigeration,*1999

[33]Fagan, T.J. "The effects of air maldstribution on air-to-refrigerant heat exchanger performance"*ASHRAE Transactions,*1980,862

[34]Fluent I., 2007.FLUENT 6.3 .

[35]Friedel, L., "Improved friction pressure drop correlations for horizontal and vertical two phase pipe flow". *Paper E2. European Two Phase Flow Group Meeting,* Ispra, Italy, 1979

[36]Gnielinski, V. "New equations for heat and mass transfer in turbulent pipe and channel flow"*International Chemical Engineering,*1976,16(2), 359

[37]Granryd, E., "Fin coil heat transfer and pressure drop" *KULDE* 1965

[38]Groll, E.A. and Kim, J. "Review of Recent Advances toward Transcritical $CO_2$ Cycle Technology"*HVAC&R Research JournalR Res,*2007,13(3), 499

[39]Gungor, K.E., Winterton,"Simplified General Correlation for Saturated Flow Boiling and Comparisons of Correlations with Data", *Transactions of the Institute of Chemical Engineers, Chemical Engineering Research and Design* 65 (1987) 148-156.

[40]Hermann, P.J. "Simulation of Steam Generation in a Heat Exchanger"*Institute of Radio Engineers Transactions on Electronic Computers,*1962,11, 153-57

[41]Heun, M.K. and Crawford, R.R. "Longitudinal fin conduction in multipass cross-counterflow finned-tube heat exchangers"*ASHRAE Transactions,*1994,100(11), 382-389

[42]Hwang, Y., Singh, V. and Radermacher, R. "Heat Exchanger Design for $CO_2$ cycle with a Linear Compressor"*HVAC&R Research Journal,*2007,13(3), 471-483

[43]Incropera, F.P. and DeWitt, D.P. "Fundamentals of Heat and Mass Transfer"1996, Wiley and Sons

[44]Iragorry, J., Tao, Y. and Jia, S. "A critical review of properties and models for frost formation analysis"*HVAC&R Research,*2004,10(4), 393-420

[45]Jiang, H., Aute, V. and Radermacher, R. "CoilDesigner: a general-purpose simulation and design tool for air-to-refrigerant heat exchangers"*International Journal of Refrigeration,*2006,29, 601-610

[46]Jin, D.H., Hwang, Y. and Radermacher, R. "The Performance of a Carbon Dioxide Gas Cooler"April 2004, CEEE Report to the US Army

[47]Jung, D.S., Radermacher, R.,"A study of flow boiling heat transfer with refrigerant mixtures", *International Journal of Heat and Mass Transfer,* 1989, 32 (9) 1751-1764.

[48]Kandlikar, S.G.,"A General Correlation for Saturated Two-Phase Flow Boiling Heat Transfer Inside Horizontal and Vertical Tubes", *Transactions of the ASME, Journal of Heat Transfer,* 1990, 112, 219-228.

[49]Kandlikar, S.G., Balasubramanian, P.,"An extension of the flow boiling correlation to transition, laminar, and deep laminar flows in minichannels and microchannels", *Heat Transfer Engineering,* 2004, 25(3): 86-93

[50]Kandlikar, S.G., Grande, W.J., "Evolution of Microchannel Flow Passages: Thermohydraulic Performance and Fabrication Technology", *ASME International Mechanical Engineering Congress and Exposition*, 2002

[51]Katz, D.L. and Briggs, D.E. "A bright future for computers in heat transfer"*Chemical Engineerings Progress,*1965,6(11),91-96

[52]Kays, W.M. and London, A.L. "Compact Heat Exchangers"1998, Krieger Publishing Company

[53]Kim, N.H., Yun, J.H., Webb, R.L., "Heat Transfer and Friction Correlations for Wavy Plate Fin-and-Tube Heat Exchangers", *Transactions of the ASME, Journal of Heat Transfer,* 1997, 119, 560-567.

[54]Kim, N.H., Youn, J.H. and Webb, R.L. "Air-side heat transfer and friction correlations for plain fin-and-tube heat exchangers with staggered tube arrangements"*ASME Journal of Heat Transfer,*1999,121, 662-667

[55]Kramer, W., Eitel, J., "Application of advanced engineering tools to the performance improvement of a radiator in a cooling system", *Vehicle Thermal Management Systems*, 2003

[56]Kreyszig, E. "Advanced Engineering Mathematics"2005,Wiley and Sons.

[57]Lee, J. and Domanski, P.A. "Impact of Air and refrigerant Maldistributions on the Performance of Finned-Tube Evaporators with R-22 and R-407C"July, 1997,DOE/CE/23810-81

[58]Liang, S.Y., Wong, T.N. and Nathan, G.K. "Numerical and experimental studies of refrigerant circuitry of evaporator coils"*International Journal of Refrigeration,* 2001, 24, 823-833

[59]Litinetski, V. V. and Abramzon, B. M. "Mars - a multistart adaptive random search method for global constrained optimization in engineering applications", *Engineering Optimization,* 1998, 30(2), 125-154.

[60]Liu, J., Wei, W., Ding, G., Zhang, C., Fukaya, M., Wang, K. and Inagaki, T. "A general steady state mathematical model for fin-and-tube heat exchanger based on graph theory"*International Journal of Refrigeration,* 2004, 27(8), 965-973

[61]Lockhart, R.W., Martinelli, R.C.,"Proposed Correlation of Data for Isothermal Two-Phase, Two-Component Flow in Pipes", *Chemical Engineering Progress,* 1949, 45 (1),39-48.

[62]McClintock, F.A. "Design of heat exchangers for minimum irreversibility", *ASME Journal of Heat Transfer,*1951, 35

[63]McQuiston, F. and Parker, J. "Heating, Ventilation, and Air Conditioning, Analysis and Design"1994, Wiley and Sons

[64]Mitsubishi Electric. "Mitsubishi Electric Air-Conditioning Systems"2008, 200812/91, Company website

[65]Mondt, J.R. "Correlating the Effects of Longitudinal Heat Conduction on Exchanger Performance"*American Society of Mechanical Engineers, Heat Transfer Division, (Publication) HTD,*1979,10, 123-134

[66]Na, B. "Analysis of Frost Formation In An Evaporator"2003, *PhD Dissertation*, The Pennsylvania State University

[67]Nina Siu-Ngan Lam, "Spatial Interpolation Methods: A Review", *American Cartographer,* 1983, 10(2),129-50

[68]Ogulata, R.T., Doba, F. and Yilmaz, T. "Irreversibility Analysis of Cross Flow Heat Exchangers"*Energy Conversion and Management,*2000, 41, 1585 - 1599

[69]Ogulata, R.T. and Doba, F. "Experiments and Entropy Generation Minimization Analysis if a Cross-flow Heat Exchanger"*International Journal of Heat and Mass Transfer,*1998,41(2), 373-381

[70]Oliet, C., Perez-Segarra, C.D., Danov, S. and Oliva, A. "Numerical simulation of dehumidifying finand-tube heat exchangers: modeling strategies and experimental comparisons" *10th International Refrigeration Engineering Conference at Purdue,*2002

[71] Oliet, C., Perez-Segarra, C.D., Oliva, A. and Castro, J. "Multidimensional and unsteady simulation of fin and tube heat exchangers", 2009, *Numerical Heat Transfer - Part A*, 56, 193-200

[72]O'Neal, D.L. and Tree, D.R. "A Review of Frost Formation in Simple Geometries" *ASHRAE Transactions,*1985,267

[73]Ould Didi,Kattan, N., Thome, J.R., "Prediction of two-phase pressure gradients of refrigerants in horizontal tubes", *International Journal of Refrigeration,* 2002*,* 25, 935-947.

[74]Ozkol, I. and Komugoz, G. "Determination of optimum geometry of a heat exchanger body via a genetic algorithm", *Numerical Heat Transfer - Part A,* 2005, 48, 283-296

[75]Park, Y., Hrnjak,P.,"$CO_2$ and R410A flow boiling heat transfer, pressure drop, and flow pattern at low temperatures in a horizontal smooth tube", *International Journal of Refrigeration,*2007, 30, 166-178

[76]Park, Y. and Jacobi, A.M. "A Second-Law Based Comparison of the Air-Side Thermal-Hydraulic Performance of Flat-Tube and Round-Tube Heat Exchangers"*International Congress of Refrigeration,*2003,Washington, DC

[77]Patankar, S.V. "Numerical Heat Transfer and Fluid Flow"1980, Taylor and Francis

[78]Payne, W.V. and Domanski, P.A. "Potential Benefits of Smart Refrigerant Distributors"January 2003,ARTI-21CR/605-200-50-01

[79]Peng, H. and Ling, X.,"Optimal design approach for the plate-fin heat exchangers using neural networks cooperated with genetic algorithms", *Applied Thermal Engineering*, 28(5-6), 642-650, 2008

[80]Perrotin, T., Clodic, D., " Thermal-hydraulic CFD study in louvered fin-and-flat-tube heat exchangers", *International Journal of Refrigeration*, 2004, 27, 422-432

[81]Poulikakos, D. and Bejan, A. "Fin Geometry for Minimum Entropy Generation in Forced Convection"*Heat Transfer Division of Transactions of the ASME,*1982

[82]Queipo, N., Devarakonda, R. and Humphrey, J. A. C. "Genetic algorithms for thermosciences research: Application to the optimized cooling of electronic components", *International Journal of Heat and Mass Transfer*, 1994, 37(6), 893-908

[83]Romero-Mendez, R., Sen, M., Yang, K.T. and McClain, R.L. "Effect of tube-to-tube conduction on plate-fin and tube heat exchanger performance"*International Journal of Heat and Mass Transfer,*1997,40(1), 3909-3916

[84]Rossi, T.M. and Braun, J.E. "Computer Models for the Development, Evaluation, and Implementation of Fault detection and Diagnostic Methods for HVAC Equipment"*Report No. : HL95-13(A),*1995,

[85]Sami, S.M. and Duong, T. "Mass and heat transfer during frost growth"*ASHRAE Transactions,*1989,95(1),158-165

[86]Sanders, C.T. "The Influence of Frost Formation and Defrosting on the Performance of Air Coolers"1974, Ph. D. Thesis Technische Hogeschool, Delft

[87]Schlichting, H. and Gersten, K. "Boundary Layer Theory"2000,Springer

[88]Schropp, K. "Untersuchungen ueber die Tau- und Reifbildung an Kuehlrohren in ruhender Luft, etc"*Zeitschrift fuer das Gesamte Kaelte-Industrie,*1935,428151-154

[89]Schmit, T. S., Dhingra, A. K., Landis, F. and Kojasoy, G.,"Genetic algorithm optimization technique for compact high intensity cooler design", *Journal of Enhanced Heat Transfer*, 1996,3(4), 281-290.

[90]Seker, D., Karatas, H. and Egrican, N. "Frost formation on fin-and-tube heat exchangers. Part II - Experimental investigation of frost formation on fin-and-tube heat exchangers"*International Journal of Refrigeration,*2004a,27(4), 375-377

[91]Seker, D., Karatas, H. and Egrican, N. "Frost formation on fin-and-tube heat exchangers. Part I - Modeling of frost formation on fin-and-tube heat exchangers"*International Journal of Refrigeration,*2004b,27(4), 367-374

[92]Sekulic, D.P. "The Second Law Quality of Energy Transformation in a Heat Exchanger"*ASME Journal of Heat Transfer,*1990,112, 295

[93]Sekulic, D.P. "Entropy Generation in a Heat Exchanger"*Heat Transfer Engineering,*1986,71, 283

[94]Shah, M.M.,"Chart Correlation for Saturated Boiling Heat Transfer: Equations and Further Study" *ASHRAE Transactions,* 1982, 88 (1), 185-196.

[95]Shah, M.M.,"A General Correlation for Heat Transfer During Film Condensation Inside Pipes", *International Journal of Heat and Mass Transfer,* 1979, 22, 547-556.

[96]Shah, R.K. and Sekulic, D.P. "Fundamentals of Heat Exchanger Design"2003,1941

[97]Shah, R.K. and Mueller, A.C. "Heat Exchangers"1985

[98]Shen, B., Groll, E.A. and Braun, J.E. "ACMODEL - A Steady-State System Simulation Model for Unitary Air Conditioners and Heat Pumps"*UNSC/IIR Short Course on "Simulation Tools for Vapor Compression Systems and Component Analysis", West Lafayette, IN,*2004,

[99]Shepard, D. "A two-dimensional interpolation function for irregularly-spaced data"*ACM National Conference,*1968,517

[100]Sherwood, T.K. and Pigford, R.L. "Absorption and Extraction"1952, McGraw Hill

[101]Singh, V., Aute, V. and Radermacher, R. "Usefulness of Entropy Generation Minimization Through a Heat Exchanger Modeling Tool" *12th International Refrigeration and Air Conditioning Conference, Purdue University,* July, 2008,

[102]Singh, V., Aute, V. and Radermacher, R. "Study of Effect of Heat Transfer through Fins in a Fin-and-tube Carbon Dioxide Gas Cooler on its Performance through Numerical Modeling"*12th International Refrigeration and Air Conditioning Conference at Purdue,*2008a,West Lafayette, IN

[103]Singh, V., Aute, V. and Radermacher, R. "Numerical approach for modeling air-to-refrigerant fin-and-tube heat exchanger with tube-to-tube heat transfer"*International Journal of Refrigeration,*2008b,31(8),1414-1425

[104] Singh, V., Aute, V. and Radermacher, R. "A heat exchanger model for a fin-and-tube heat exchanger with an arbitrary fin sheet"*International Journal of Refrigeration,*doi: 10.1016/j.ijrefrig.2009.05.011

[105]Sunden, B., "Computational fluid dynamics in research and design of heat exchangers",*Heat Transfer Engineering*, 2007, 28(11), 898-910

[106]Traviss, D.P., Rohsenow, W.M., Baron, A.B., "Forced convection condensation inside tubes: A heat transfer equation for condenser design", *ASHRAE Transactions*, 1973, 79, 157-165

[107]Vandoormal J.P., Raithby J.D., "Enhancement of SIMPLE method for predicting incompressible fluid flows", *Numerical Heat Transfer,* 1984, 7,147-163

[108]Versteeg H.K., Malalasekera W., "An Introduction to Computational Fluid Dynamics, The Finite Volume Method", 1995, Prentice Hall

[109]Wang, C.C.,Lee, C.J, Chang, C.T., Lin, S.P., "Heat transfer and friction correlation for compact louvered fin-and-tube heat exchangers", *International Journal of Heat and Mass Transfer,* 1999, 42, 1945-1956.

[110]Wang, C.C., Chi, K.Y., Chang, C.J.,"Heat transfer and friction characteristics of plain fin-and-tube heat exchangers, part II: Correlation", *International Journal of Heat and Mass Transfer,* 2000, 43, 2693-2700.

[111]Wang, C.C., Lee, W.S., Sheu, W.J., "A comparative study of compact enhanced fin-and-tube heat exchangers", *International Journal of Heat and Mass Transfer* , 2001, 44, 3565-3573.

[112]Wang,C.C., Hwang, Y.M., Lin, Y.T.,"Empirical Correlations for Heat Transfer And Flow Friction Characteristics of Herringbone Wavy Fin and Tube Heat Exchangers", *International Journal of Refrigeration,* 2002, 25 ,673-680

[113]Wang, C.C, Tsai, Y.M., Lu, D.C.,"Comprehensive Study of Convex-Louver and Wavy Fin-and-Tube Heat Exchangers", *Journal of Thermophysics and Heat Transfer*, 1998, 12(3)

[114]Wang CC, Lee W, Sheu W. "A comparative study of compact enhanced fin-and-tube heat exchangers." *International Journal of Heat and Mass Transfer*. 2001, 44, 3565-3573.

[115] Wang, X., Hwang, Y., Radermacher, R., "Two-stage heat pump system with vapor-injected scroll compressor using R410A as a refrigerant", International Journal of Refrigeration, doi:10.1016/j.ijrefrig.2009.03.004, 2009

[116]Witte, L.C. and Shamsundar, N. "A Thermodynamic Efficiency Concept for Heat Exchange Devices"*Journal of Engineering for Power,*1983,105, 199

[117]Yang, D., Lee, K. and Song, S. "Fin spacing optimization of a fin-tube heat exchanger under frosting conditions"*International Journal of Heat and Mass Transfer,*2006a, 49(15), 2619-2625

[118]Yang, D., Lee, K. and Song, S. "Modeling for predicting frosting behavior of a fin–tube heat exchanger"*International Journal of Heat and Mass Transfer,*2006b, 49 (7), 1472-1479

[119]Yang, D., Lee, K. and Song, S. "Modeling for predicting frosting behavior of a fin-tube heat exchanger"*International Journal of Heat and Mass Transfer,*2006c,49(7),1472-1479

[120] Yuan, P. and Kou, H-K. "The effect of longitudinal wall conduction in a three-fluid cross flow heat exchanger", *Numerical Heat Transfer - Part A*, 1998, 34, 135-150

[121]Yun, R., Heo, J.H., Kim, Y.,"Evaporative heat transfer and pressure drop of R410A in microchannels", *International Journal of Refrigeration*, 29, 2006, pp. 92-100

[122]Zhang, M., Dahl, S.D., "Computational study of heat transfer and friction characteristics of a smooth wavy fin heat exchanger", *Annual Meeting of the American Society of Heating, Refrigerating and Air-Conditioning Engineering,2000*

[123]Zilio, C., Cecchinato, L., Corradi, M. and Schiochet, G. "As Assessment of Heat Transfer through Fins in a Fin-and-Tube Gas Cooler for Transcritical Carbon Dioxide Cycles"*HVAC&R Research Journal,*2007,133457-469